Department of Pharmacology

University College London

Gower Street

London WC1E 6BT

Calcium Homeostasis in Rat Sympathetic Neurones: A Primary Role for the Plasma Membrane Calcium ATPase

by

Nicolas Jean Wanaverbecq

2001

A thesis submitted for the Degree of

Doctor of Philosophy

University of London

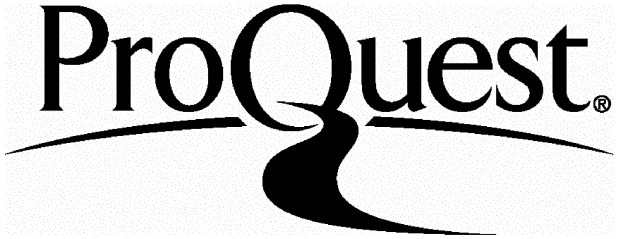

Pour

Angie, Jo et Christiane

Abstract

Patch-clamp experiments combined with indo-1 measurement of free intracellular Ca^{2+} concentration ($[Ca^{2+}]_i$) were used to determine the homeostatic systems involved in the maintenance of resting $[Ca^{2+}]_i$ and the clearance of Ca^{2+} transients following activation of voltage-gated Ca^{2+} channels in neurones from rat superior cervical ganglion (SCG).

In these neurones, the Ca^{2+} buffering capacity was estimated to be $\approx$ 1000 at $[Ca^{2+}]_i$ close to rest and $\approx$ 250 at $[Ca^{2+}]_i \approx 1$ μM and to involve at least two buffering systems with different affinities for Ca^{2+}.

Removal of extracellular Ca^{2+} led to a decrease in $[Ca^{2+}]_i$ that was mimicked by the addition of La^{3+}. This decrease in $[Ca^{2+}]_i$ was more pronounced after inhibition of the endoplasmic reticulum Ca^{2+} uptake system (SERCA) and subsequent depletion of the intracellular stores. Inhibition of the plasma membrane Ca^{2+} pump (PMCA) by intracellular carboxyeosin or extracellular alkalisation (pH 9) both increased resting $[Ca^{2+}]_i$ and prolonged the recovery of Ca^{2+} transients at peak $[Ca^{2+}]_i \leq 500$ nM.

For $[Ca^{2+}]_i$ loads > 500 nM, recovery showed an additional plateau phase that was abolished in carbonyl cyanide *m*-chlorohydrazone (CCCP) or on omitting Na^+ from the intracellular solution. Inhibition of the plasma membrane Na^+/Ca^{2+} exchanger (NCX) and of SERCA had a small but significant effect on the rate of decay of these larger Ca^{2+} transients. However, neither of these mechanisms appeared to contribute substantially to the recovery from rises in $[Ca^{2+}]_i$ below 1 μM.

In conclusion, resting $[Ca^{2+}]_i$ is maintained as the result of a passive Ca^{2+} influx regulated by a large Ca^{2+} buffering system, Ca^{2+} extrusion *via* a PMCA and Ca^{2+} transport from the intracellular stores. PMCA is also the principal Ca^{2+} extrusion system at low Ca^{2+} loads, with additional participation of the NCX and intracellular organelles at high $[Ca^{2+}]_i$.

Acknowledgements

The submission of the PhD thesis represents both the fulfilment of one's study and the first step into the scientific world. In my case the journey has been rather long (1996-2001) and complicated. It would have been certainly even more difficult without the help and assistance of several people to whom I am grateful and that I would like to thank.

My recognition goes first to *Professor Paul Feltz* who welcomed me in his laboratory and, unlike other members of University Louis Pasteur in Strasbourg, trusted my ability to succeed in research. My thanks go also to members of Paul's lab (*Dr. Pascale Pigue, Professor Remy Schlichter and Dr. Jerome Trouslard*) who helped me during my Master degree that, in other circumstances, would have led to the PhD.

I would also like to thank *Dr. Malcolm P. Caulfield* formerly at the Neurosciences institute in the University of Dundee and now enjoying the sunny weather in Australia! Malcolm offered me a fresh start after the loss of Paul Feltz and more importantly gave me the possibility to join University College of London.

I am finally particularly grateful to *Professor David A. Brown* to have accepted my transfer from Dundee and to have given me the possibility to reach the final stage of my PhD in his group. I would like to thank *Dr. Steve J. Marsh* for his help, advice, patience and many other things during the last three years. I wish also to acknowledge all the members of David's lab past and present that I met during my stay at UCL with a particular attention to Alex (*Dr. Alexander A. Selyanko*) who died at the end of September 2001.

Of course, I could not have accomplished any of this without the continuous support and attention of my parents and family and some close friends here in United Kingdom, in Italy and back in France.

Publications and Communications

Delmas, P., **Wanaverbecq, N.**, Abogadie, Fe C., Mistry, M. and Brown, D.A. Microdomains shape receptor-mediated PLC signalling pathways in sympathetic neurons. *Neuron* (in press).

Marsh, S.J., **Wanaverbecq, N.**, Selyanko, A.A., & Brown, D.A. (2000). Calcium signalling in neurons exemplified by rat sympathetic ganglion cells. pp 27-44 in *Calcium: the molecular basis of calcium action in biology and medicine*, ed. Pochet, R., Donato, R., Haiech, J., Heizman, C. and Gerke, V.

Fernandez-Fernandez, J. M., **Wanaverbecq, N.**, Halley, P., Caulfield, M. P., & Brown, D. A. (1999). Selective activation of heterologously expressed G protein-gated K^+ channels by M2 muscarinic receptors in rat sympathetic neurones. *J. Physiol. Lond.* **515(3),** 631-637.

Jan. 2002: XIIth International Symposium on Calcium-Binding Proteins and Calcium Function in Health and Disease – Cavalese, Italy.
Wanaverbecq, N., Marsh, S.J. & Brown, D.A. (2002). Calcium Homeostasis in Rat Sympathetic Neurones: A Primary Role for the Plasma Membrane Calcium ATPase. (Poster, P171).

Nov. 2001: Society for Neuroscience 31st Annual Meeting – San Diego, USA.
Wanaverbecq, N., Marsh, S.J. & Brown, D.A. (2001). Dominant role for the plasma membrane calcium pump in calcium extrusion from rat sympathetic neurons. (P707.13).

Sept. 2001: British Pharmacological Society and the Physiological Society – Bristol, UK.
Wanaverbecq, N., Marsh, S.J. & Brown, D.A. (2001). Maintenance of resting intracellular calcium concentration in rat sympathetic neurones. *J. Physiol. Lond.* **536.P**, p 103P.

June 2000: 6th European Symposium on Calcium Binding Protein in Normal and Transformed Cells – Paris, France.
Wanaverbecq, N., Marsh, S.J. and Brown, D.A. (2000) Calcium sequestration and buffering capacity in rat sympathetic neurones. (Poster).

Dec. 1999: The Physiological Society – Birmingham, UK.
Brown, D.A., Marsh, S.J., **Wanaverbecq, N.** and Selyanko, A.A. (2000) Regulation of neuronal ion channels by intracellular calcium (exemplified in sympathetic ganglion cells). *J. Physiol. Lond.* **523.P**, p 91S .

June 1998: European Neuroscience Association meeting – Berlin, Germany.
Fernandez-Fernandez, J.M., **Wanaverbecq, N.**, Halley, P., del Rio, E. and Caulfield, M.P. (1998) Muscarinic activation of GIRK channels heterologously expressed in rat SCG neurones. *Eur. J. Neurosc.* **10 (10),** p180 (Poster)

List of Figures

CHAPTER II MATERIALS AND METHODS

2. Electrophysiological recordings

3. Monitoring free intracellular calcium concentration

4. Monitoring intracellular pH

6. Data analysis

7. Immunocytochemistry

CHAPTER III RESULTS

1. Calcium currents and changes in intracellular calcium

2. Endogenous calcium buffering capacity

3. Mitochondrial regulation of the intracellular calcium

4. Endoplasmic reticulum and regulation of intracellular calcium

5. Plasma membrane calcium ATPase and intracellular calcium

6. Sodium/calcium exchanger and intracellular calcium

7. Control of resting calcium concentration at rest

CHAPTER IV GENERAL DISCUSSION AND CONCLUSION

2. Regulation of resting intracellular calcium

3. Mechanisms involved in the clearance of calcium

4. Clearance of depolarisation-induced calcium transients

List of Tables

CHAPTER II MATERIALS AND METHODS

2. Electrophysiological recordings

3. Monitoring free intracellular calcium concentration

4. Monitoring intracellular pH

7. Immunocytochemistry

8. Molecular biology

CHAPTER III RESULTS

2. Endogenous calcium buffering capacity

3. Mitochondrial regulation of the intracellular calcium

4. Endoplasmic reticulum and regulation of intracellular calcium

5. Plasma membrane calcium ATPase and intracellular calcium

6. Sodium/calcium exchanger and intracellular calcium

List of Abbreviations

$[Ca^{2+}]_i$: intracellular free Ca^{2+} concentration

$[Ca^{2+}]_L$: free Ca^{2+} concentration of the ER lumen

$[Ca^{2+}]_m$: free Ca^{2+} concentration of the mitochondrial matrix

BCECF: 2',7'-bis-(2-carboxyethyl)-5-(and -6)-carboxyfluorescein

CaBP: Ca^{2+} binding protein

cADPr: cyclic adenosine diphosphosphate ribose

CaM: calmodulin

CCCP: carbonyl cyanide *m*-chlorophenyl hydrazone

CE: 5,6-succinylmidyl carboxyeosin

CGP: benzothiazepine CGP-37157

CICR: Ca^{2+}-induced Ca^{2+} release

CPA: cyclopiazonic acid

CRAC: Ca^{2+} release activated Ca^{2+} (channel)

ER: endoplasmic reticulum

FCCP: carbonyl cyanide *p*-trifluromethoxy-phenylhydrazone

IP_3: inositol 1,4,5-triphosphate

IP_3R: inositol 1,4,5-triphosphate receptor

*m*CU: mitochondrial Ca^{2+} uniporter

*m*NCX: mitochondrial Na^+/Ca^{2+} exchanger

MPTP: mitochondrial permeability transition pore

NAADP: nicotinic acid adenine dinucleotide phosphate

nAChR: nicotinic cholinergic receptor

NCX: Na^+/Ca^{2+} exchanger

NMDG: N-methyl D glucamine

PKA: protein kinase A

PKC: protein kinase C

PLC: phospholipase C

PMCA: plasma membrane Ca^{2+}-ATPase

RuR: ruthenium red

RyR: ryanodine receptor

SCG: superior cervical ganglion

SERCA: sarco/endoplasmic Ca^{2+}-ATPase

SOCC: store operated Ca^{2+} channels

TG: thapsigargin

TRP: transient receptor potential

VACC: voltage-activated Ca^{2+} channel

Publications and Communications

Delmas, P., **Wanaverbecq, N.**, Abogadie, Fe C., Mistry, M. and Brown, D.A. Microdomains shape receptor-mediated PLC signalling pathways in sympathetic neurons. *Neuron* (in press).

Marsh, S.J., **Wanaverbecq, N.**, Selyanko, A.A., & Brown, D.A. (2000). Calcium signalling in neurons exemplified by rat sympathetic ganglion cells. pp 27-44 in *Calcium: the molecular basis of calcium action in biology and medicine*, ed. Pochet, R., Donato, R., Haiech, J., Heizman, C. and Gerke, V.

Fernandez-Fernandez, J. M., **Wanaverbecq, N.**, Halley, P., Caulfield, M. P., & Brown, D. A. (1999). Selective activation of heterologously expressed G protein-gated K^+ channels by M2 muscarinic receptors in rat sympathetic neurones. *J. Physiol. Lond.* **515(3),** 631-637.

Jan. 2002: XIIth International Symposium on Calcium-Binding Proteins and Calcium Function in Health and Disease – Cavalese, Italy.
Wanaverbecq, N., Marsh, S.J. & Brown, D.A. (2002). Calcium Homeostasis in Rat Sympathetic Neurones: A Primary Role for the Plasma Membrane Calcium ATPase. (Poster, P171).

Nov. 2001: Society for Neuroscience 31st Annual Meeting – San Diego, USA.
Wanaverbecq, N., Marsh, S.J. & Brown, D.A. (2001). Dominant role for the plasma membrane calcium pump in calcium extrusion from rat sympathetic neurons. (P707.13).

Sept. 2001: British Pharmacological Society and the Physiological Society – Bristol, UK.
Wanaverbecq, N., Marsh, S.J. & Brown, D.A. (2001). Maintenance of resting intracellular calcium concentration in rat sympathetic neurones. *J. Physiol. Lond.* **536.P**, p 103P.

June 2000: 6th European Symposium on Calcium Binding Protein in Normal and Transformed Cells – Paris, France.
Wanaverbecq, N., Marsh, S.J. and Brown, D.A. (2000) Calcium sequestration and buffering capacity in rat sympathetic neurones. (Poster).

Dec. 1999: The Physiological Society – Birmingham, UK.
Brown, D.A., Marsh, S.J., **Wanaverbecq, N.** and Selyanko, A.A. (2000) Regulation of neuronal ion channels by intracellular calcium (exemplified in sympathetic ganglion cells). *J. Physiol. Lond.* **523.P**, p 91S .

June 1998: European Neuroscience Association meeting – Berlin, Germany.
Fernandez-Fernandez, J.M., **Wanaverbecq, N.**, Halley, P., del Rio, E. and Caulfield, M.P. (1998) Muscarinic activation of GIRK channels heterologously expressed in rat SCG neurones. *Eur. J. Neurosc.* **10 (10),** p180 (Poster)

List of Figures

CHAPTER II MATERIALS AND METHODS

2. Electrophysiological recordings

3. Monitoring free intracellular calcium concentration

4. Monitoring intracellular pH

6. Data analysis

7. Immunocytochemistry

CHAPTER III RESULTS

1. Calcium currents and changes in intracellular calcium

2. Endogenous calcium buffering capacity

3. Mitochondrial regulation of the intracellular calcium

4. Endoplasmic reticulum and regulation of intracellular calcium

5. Plasma membrane calcium ATPase and intracellular calcium

6. Sodium/calcium exchanger and intracellular calcium

7. Control of resting calcium concentration at rest

CHAPTER IV GENERAL DISCUSSION AND CONCLUSION

2. Regulation of resting intracellular calcium

3. Mechanisms involved in the clearance of calcium

4. Clearance of depolarisation-induced calcium transients

List of Tables

CHAPTER II MATERIALS AND METHODS

2. Electrophysiological recordings

3. Monitoring free intracellular calcium concentration

4. Monitoring intracellular pH

7. Immunocytochemistry

8. Molecular biology

CHAPTER III RESULTS

2. Endogenous calcium buffering capacity

3. Mitochondrial regulation of the intracellular calcium

4. Endoplasmic reticulum and regulation of intracellular calcium

5. Plasma membrane calcium ATPase and intracellular calcium

6. Sodium/calcium exchanger and intracellular calcium

List of Abbreviations

$[Ca^{2+}]_i$: intracellular free Ca^{2+} concentration

$[Ca^{2+}]_L$: free Ca^{2+} concentration of the ER lumen

$[Ca^{2+}]_m$: free Ca^{2+} concentration of the mitochondrial matrix

BCECF: 2',7'-bis-(2-carboxyethyl)-5-(and -6)-carboxyfluorescein

CaBP: Ca^{2+} binding protein

cADPr: cyclic adenosine diphosphosphate ribose

CaM: calmodulin

CCCP: carbonyl cyanide *m*-chlorophenyl hydrazone

CE: 5,6-succinylmidyl carboxyeosin

CGP: benzothiazepine CGP-37157

CICR: Ca^{2+}-induced Ca^{2+} release

CPA: cyclopiazonic acid

CRAC: Ca^{2+} release activated Ca^{2+} (channel)

ER: endoplasmic reticulum

FCCP: carbonyl cyanide *p*-trifluromethoxy-phenylhydrazone

IP_3: inositol 1,4,5-triphosphate

IP_3R: inositol 1,4,5-triphosphate receptor

*m*CU: mitochondrial Ca^{2+} uniporter

*m*NCX: mitochondrial Na^+/Ca^{2+} exchanger

MPTP: mitochondrial permeability transition pore

NAADP: nicotinic acid adenine dinucleotide phosphate

nAChR: nicotinic cholinergic receptor

NCX: Na^+/Ca^{2+} exchanger

NMDG: N-methyl D glucamine

PKA: protein kinase A

PKC: protein kinase C

PLC: phospholipase C

PMCA: plasma membrane Ca^{2+}-ATPase

RuR: ruthenium red

RyR: ryanodine receptor

SCG: superior cervical ganglion

SERCA: sarco/endoplasmic Ca^{2+}-ATPase

SOCC: store operated Ca^{2+} channels

TG: thapsigargin

TRP: transient receptor potential

VACC: voltage-activated Ca^{2+} channel

Chapter I

General Introduction

Chapter I

General Introduction

1. Why is intracellular calcium so precisely controlled?

An abundance of calcium-containing minerals are present in the earth's crust and, because of their high solubility in water, Ca^{2+} is also present in high concentrations in the biological environment (see Kretsinger, 1990 for review). One of the possible ways to control Ca^{2+} and protect arising life would have been to develop biological systems and macromolecules insensitive to all Ca^{2+} sources. Instead, the omnipresence of this metal ion has been used to the benefit of biological processes and has been integrated to relay signals between the extracellular environment and the intracellular machinery.

Several arguments offer an explanation to why Ca^{2+} was preferred as an intracellular messenger over other ions such as Na^{+}, K^{+} or Mg^{2+}. Firstly, to enable the role of an ionic messenger, intracellular systems capable of detection, control and regulation had to be developed. All these processes required a selective and tight binding with the intracellular ligand and that could only be provided by protein macromolecules because of the specialisation and diversity required. Monovalent cations and polyatomic anions have large ionic radii and low charge that therefore makes them unsuitable for forming stable complexes with proteins. Since the protein backbones are generally insufficiently flexible to offer regular and small cavities, small ions like Mg^{2+} often need to form complexes with the oxygen atoms of water molecules to successfully bind to proteins. These oxygen bonds weaken the binding strength and tend to make small ions unsuited for tight binding (see Carafoli, 1987 and Kretsinger, 1990 for review). In contrast, the larger ionic radius and the greater versatility of Ca^{2+} ions (flexible coordination geometry, lower charge density and slow dissociation rate - see Kretsinger, 1990 for review) make this metal ion more adapted than other ions to complex tightly to protein while imposing smaller physical constraints to the protein.

Secondly, cellular metabolism relies on phosphate-containing compounds to provide the necessary energy to cellular activity. As these compounds are continuously degraded to liberate energy and re-synthesised to store it, large amounts of inorganic phosphate are present in cells. A high concentration of free Ca^{2+} would be incompatible with a phosphate-based metabolism as Ca^{2+} would bind to phosphate and form insoluble complexes (see Carafoli, 1987 and Kretsinger, 1990 for review).

In all animal cells, intracellular Ca^{2+} is maintained at a low concentration (50-100 nM) and therefore a large Ca^{2+} gradient exists across the plasma membrane. In response to depolarisation or receptor activation, Ca^{2+} enters the cytoplasm through Ca^{2+} permeable channels located in the plasma membrane and/or on intracellular organelles. As a consequence, the intracellular Ca^{2+} concentration ($[Ca^{2+}]_i$) is rapidly increased and triggers numerous and various biological responses depending on the cell type. Thus, a rise in $[Ca^{2+}]_i$ leads to muscle contraction, to disaggregation of microtubules, exocytosis in exocrine and endocrine cells and neurotransmitter release in nerve terminals (see Verkhratsky & Toescu, 1998 for review). Changes in $[Ca^{2+}]_i$ also modulate DNA replication and protein synthesis, stimulate metabolic pathways and activate specific enzymes (see Verkhratsky & Toescu, 1998 for review). On the other hand, long exposure to high $[Ca^{2+}]_i$ has been shown to be cytotoxic and to induce apoptosis and cell death. Therefore cells need efficient systems to sequester, buffer and/or extrude Ca^{2+} and restore resting $[Ca^{2+}]_i$ after a period of cellular activity.

2. Calcium enters the cytosol through specialised channels

In excitable cells, voltage-activated Ca^{2+} channels (VACC) represent the most important Ca^{2+} influx pathway and, following depolarisation of the plasma membrane, they induce a rapid and large rise in $[Ca^{2+}]_i$ (see Hille, 1992 and Kostyuk & Verkhratsky, 1995a for review). Ligand-operated receptors are an alternative pathway allowing Ca^{2+} entry. These receptors incorporate cationic channels that are permeable to Ca^{2+} and open following the binding of a specific ligand (see Miller, 1991 and Kostyuk & Verkhratsky, 1995a for review). Intracellular messengers following the activation of membrane receptors and/or depletion of intracellular stores activate an additional set of channels, which is generally described as capacitative or store-operated Ca^{2+} channels (SOCC - see Miller, 1991; Kostyuk & Verkhratsky, 1995a and Putney & McKay, 1999 for review).

2.1. Voltage-activated calcium channels

The VACC are heteroligomeric complexes formed by 5 subunits (α_1, β, α_2-δ and γ) and the channel properties mainly depend on the pore forming α_1-subunit (De

Waard *et al.*, 1996; Dunlap *et al.*, 1995 and Dolphin, 1998 for review). Ten different isoforms of the α_1-subunit have been cloned and lead to the formation of channels with different biophysical and pharmacological properties as well as different tissue distribution (Snutch & Reiner, 1992 and Birnbaumer *et al.*, 1994; Ertel *et al.*, 2000 for review).

Traditionally the VACC were divided in two groups based on their voltage dependency: the low voltage activated (LVA) and the high voltage activated (HVA) Ca^{2+} channels (see Bean, 1989; Carbone & Swandulla, 1989 and Dunlap *et al.*, 1995). More recently, a new nomenclature for VACC has been introduced both to regroup channels formed by α_1-subunit with structural similarities under a same class and to avoid the confusion of the former alphabetical nomenclature (see Ertel *et al.*, 2000 for review). By analogy with the voltage-gated potassium channels, the VACC have been renamed Ca_V where Ca and the subscript V represent the permeating ion and the principal physiological regulator (voltage), respectively. Three main groups have therefore been proposed: (1) $Ca_V1.1$ to 1.4 corresponding to the former L-type VACC comprising of α_{1S}-, α_{1C}-, α_{1D}-, and α_{1F}-subunit, respectively; (2) $Ca_V2.1$ to 2.3 corresponding to the former P/Q- (α_{1A}), N- (α_{1B}) and R-type (α_{1E}) VACC, respectively and (3) $Ca_V3.1$ to 3.3 representing the former T-type VACCs with three different α_1-subunits (G, H and I) (see Ertel *et al.*, 2000 for review).

The different members of the HVA or Ca_V1 and 2 groups are characterised by the variety of the α_1-subunit isoforms that form channels with different electrophysiological and pharmacological properties. However, the common property of these channels is a selective block by cadmium at low concentrations ($\approx$ 100 μM, see Bean, 1989; Carbone & Swandulla, 1989; Scott *et al.*, 1991 and Hille, 1992 for review).

The first HVA channel type that was isolated on the basis of its sensitivity to dihydropyridines (DHP) was the L-type channel (Ca_V1) which specificity was further confirmed by the cloning of particular α_1-subunits (see above and Birnbaumer *et al.*, 1994; Ertel *et al.*, 2000 for review). Channels of the Ca_V1 group are characterised by a long lasting current, which slowly inactivates in a Ca^{2+}-dependent manner (see Bean, 1989; Scott *et al.*, 1991 and Hille, 1992 for review). A major role attributed to L-type channels is the involvement in the excitation-contraction coupling in muscle cells, in the secretion mechanism of endocrine cells and some neurones (see Bean, 1989 for review)

and the stimulation of Ca^{2+}-activated potassium channels (*e.g.* BK channels see Marrion *et al.*, 1987; Smart, 1987; Davies *et al.*, 1996 and Selyanko, 1996).

In cerebellar Purkinje cells, a VACC largely insensitive to both DHP and ω-Conotoxin GVIA has been characterised: the P/Q-type Ca^{2+} channel or $Ca_V2.1$ (Mintz *et al.*, 1991 and see Birnbaumer *et al.*, 1994; Ertel *et al.*, 2000 for review). This channel is formed by a α_{1A}-subunit and is selectively blocked by ω-Agatoxin IVA (see Tsien *et al.*, 1991; Birnbaumer *et al.*, 1994 and Dunlap *et al.*, 1995 for review). The Q-type channel, which exhibits similar properties to the P-type, is thought to have a lower sensitivity to ω-Agatoxin IVA and to be more potently blocked by ω-Conotoxin MVIIC (EC_{50} below 500 nM - see Nooney *et al.*, 1997 for review). The activation of P/Q-type channels by depolarisations above -50 mV elicits a sustained current that exhibits little inactivation during long depolarising pulse (see Nooney *et al.*, 1997 for review).

The $Ca_V2.2$ (formerly N-type Ca^{2+}) channel is characterised by a selective irreversible block by ω-Conotoxin GVIA (see Bean, 1989 ; Scott *et al.*, 1991; Hille, 1992 and Williams *et al.*, 1992 for review) and is activated by depolarisation above -20 mV. The elicited current exhibit a moderate inactivation rate during the depolarising pulse (see Scott *et al.*, 1991; Hille, 1992 and Nooney *et al.*, 1997 for review).

Calcium channels of the N- and P/Q-type are mostly expressed in neurones and although they display different properties, their main function is the regulation of neurotransmitter release at the nerve terminal (see Dunlap *et al.*, 1995; Nooney *et al.*, 1997 for review) as well as the modulation of ionic conductances in the soma (Ca^{2+}-activated chloride or potassium currents – see Hille, 1992 for review).

The last member of the Ca_V2 group corresponds to the former R-type ($Ca_V2.3$) channel, which is mainly expressed in brain and heart and selectively blocked by nickel at a concentration of 100 μM (see Ertel *et al.*, 2000 for review). Although, R-type channels have specific characteristics, they also exhibit biophysical properties similar to both LVA (voltage range for steady-state inactivation) and HVA channels (selective block by cadmium).

Calcium channels of T-type currently represent the only member of the LVA or Ca_V3 group and three different isoforms of the α_1-subunit have been cloned (see above and Ertel *et al.*, 2000). The activation of channels from the Ca_V3 group elicits a transient current for membrane potentials more positive than -70 mV

characterised by a rapid voltage-dependent inactivation and an efficient block by nickel (≈ 30 μM - see Bean, 1989; Carbone & Swandulla, 1989; Scott *et al.*, 1991 and Hille, 1992 for review). The low threshold of T-type channel activation makes them well suited for participating in pacemaker activity and in repetitive firing of neurones (see Bean, 1989 for review). The T-type VACC is largely distributed in neuronal as well as non-neuronal cells, especially in embryonic and immature cells raising the possibility of a role in developmental functions (see Bean, 1989).

2.2. Ligand-operated calcium-permeable channels

Ligand-operated receptors are divided, from a conceptual point of view, into 'ionotropic' (coupled with the activation of ionic transport) and 'metabotropic' (leading to the formation of an intracellular messenger) receptors and belong to several gene families, which encode glutamate, acetylcholine, adenosine nucleotide, serotonine, glycine and γ-aminobutyric acid receptors. The ionotropic receptors of excitatory neurotransmitters (*e.g.* glutamate, adenosine nucleotides and acetylcholine) represent an important additional pathway for Ca^{2+} entry into nerve cells and this section will focus on the cholinergic subtype (nicotinic receptors), which is functionally expressed in rat sympathetic neurones (Trouslard *et al.*, 1993). On the other hand, following activation of metabotropic receptors, intracellular messengers can also induce changes in $[Ca^{2+}]_i$ either by acting on Ca^{2+} permeable channels in the plasma membrane or by stimulating Ca^{2+} release from intracellular stores.

2.2.1. Calcium influx through ionotropic receptors

The ionotropic form of acetylcholine receptors, which is selectively activated by nicotine (nicotinic receptor - nAChR), was extensively studied in the peripheric nervous system (neuro-muscular junction and synapses between neurones throughout the autonomic system). Molecular cloning has shown that nAChR are formed by the association of four subunits (α, β, γ and δ) organised in a pentamere and numerous nAChR subunits have been characterised. The different combinations of nAChR subunits lead to receptors functionally distinct with mainly one muscular and two neuronal types. The muscular nAChR is composed by α2, β, γ and δ subunits (see Karlin, 1993 for review). Seven different α subunits (α2 to α9) and three β subunits (β2

to β4) are thought to be involved in the formation of the neuronal nAChR but the precise molecular composition of the neuronal pentamer is not certain (Luetje & Patrick, 1991; Vernallis *et al.*, 1993; Covernton *et al.*, 1994; McGehee & Role, 1995 and Sivilotti *et al.*, 1997). The activation of nAChR generates a cationic current carried by the flux of K^+, Na^+ and Ca^{2+} ions and induces a rapid plasma membrane depolarisation (Fieber & Adams, 1991; Trouslard *et al.*, 1993 and Rogers & Dani, 1995). The nAChR are Ca^{2+} permeant with 4.4 % of the nicotinic inward current carried by Ca^{2+} ions (at 2.5 mM external [Ca^{2+}], Fieber & Adams, 1991; Trouslard *et al.*, 1993 and Rogers & Dani, 1995) and therefore the activation of nAChR induces a substantial Ca^{2+} influx. However, it is unlikely that sufficient Ca^{2+} enters during a single excitatory post-synaptic potential to raise $[Ca^{2+}]_i$ by more than a few nanomolar, which is probably negligible compared with that entering through VACC. Nevertheless, experiments on frog sympathetic neurones suggested that the sub-membrane rise in $[Ca^{2+}]_i$ might be sufficient to activate Ca^{2+}-dependent K^+ channels and accelerate recovery of the depolarisation (Tokimasa *et al.*, 1983 and Tokimasa & North, 1984).

In the brain, the major excitatory neurotransmission is mediated through glutamate receptors (GluRs) and numerous studies have demonstrated the Ca^{2+} permeability of their ionotropic subtypes (*e.g.* Westbrook & Mayer, 1984; Keinanen *et al.*, 1990; Pellegrini-Giampietro *et al.*, 1992; Jonas *et al.*, 1994 and see Kohler *et al.*, 1993; Wisden & Seeburg, 1993; Kostyuk & Verkhratsky, 1995a for review). The Ca^{2+} influx through GluRs will depend on the subunit composition of a particular receptor isoform which in turn will depend on the stage of the development and on the neuronal subpopulation (see Kohler *et al.*, 1993; Wisden & Seeburg, 1993 and Kostyuk & Verkhratsky, 1995a for review). Another source of Ca^{2+} influx is through ionotropic ATP or 'purinergic' receptors (P_2 subtype - see Dubyak & el-Moatassim, 1993 and Edwards, 1994 for review). These receptors were shown to display a substantial permeability to Ca^{2+} and to induce membrane depolarisation and VACC activation (Dubyak & el-Moatassim, 1993 and see Edwards, 1994 for review).

2.2.2. Capacitative and store-operated calcium influx

The activation of membrane receptor from a variety of hormones, growth factors and neurotransmitters produces intracellular second messenger that have been

shown to induce a Ca^{2+} influx either through the activation of Ca^{2+} permeable channels in the plasma membrane or as a result of Ca^{2+} release from intracellular stores (see also below section 4.2.4). In this section, the attention will be focused on the activation of membrane conductance following Ca^{2+} release from intracellular stores.

Several experiments suggested that depletion of the intracellular stores by phospholipase C (PLC)-linked agonist (Putney, 1986 and see Putney, 1997 for review) or inhibition of the Ca^{2+} uptake into the endoplasmic reticulum induced a sustained elevation of the $[Ca^{2+}]_i$ due to a Ca^{2+} influx that could be block by lanthanum (La^{3+}) (see Putney, 1997 for review). In fact, the PLC activation induces the formation of inositol (1,4,5)-triphosphate (IP_3) and diacylglycerol (DAG). The liberation of IP_3 in turn activates Ca^{2+} release from intracellular stores (see below section 4.2.4.1) and a subsequent Ca^{2+} influx across the plasma membrane (see Putney & Bird, 1993; Putney & McKay, 1999; Putney, 1999a and Berridge *et al.*, 2000 for review). It was suggested that the secondary Ca^{2+} influx through the plasma membrane was not due to the activation of the receptor or the associated G-protein nor from the IP_3 liberation but was a consequence of the intracellular store depletion (Putney, 1986 and see Putney & McKay, 1999; Putney, 1999a and Berridge *et al.*, 2000 for review). As a result, the induced Ca^{2+} influx was termed Ca^{2+} release activated Ca^{2+} (CRAC) influx or capacitative Ca^{2+} influx (see Putney & McKay, 1999; Putney, 1999a and Berridge *et al.*, 2000 for review).

To explain the activation of the capacitative Ca^{2+} influx, three main processes have been proposed: liberation of a diffusible intracellular messenger (Ca^{2+} influx factor, CIF), conformational coupling between intracellular Ca^{2+} store and plasma membrane channels (Kiselyov *et al.*, 1999, 2000 and Yue *et al.*, 2001) and through vesicular fusion with the plasma membrane (see Putney & McKay, 1999; Putney, 1999b and Berridge *et al.*, 2000 for review).

The nature of the channel mediating the Ca^{2+} influx is still unclear however much interest has been focused on the transient receptor potential (TRP) channel first described in *Drosophila* photoreceptors. Subsequently, TRP channels were found in mammalian cells and they now represent a family of at least 20 different members (see Clapham *et al.*, 2001 for review). The TRP channels are permeable to cations including Ca^{2+}, blocked by La^{3+} and activated by various signals such as DAG, IP_3,

phosphorylation, changes in temperature or osmolarity, cyclic nucleotide and also depletion of the intracellular Ca^{2+} stores (see Clapham *et al.*, 2001 for review). Among these channels, the TRP3-type appears to be the most promising candidate for capacitative Ca^{2+} entry (see Putney, 1999b; Putney & McKay, 1999 and Berridge *et al.*, 2000 for review). Thus, when expressed in cell lines, TRP3 is activated by store depletion but is also gated by direct physical connection to either IP_3R (Kiselyov *et al.*, 1998; Boulay *et al.*, 1999 and Ma *et al.*, 2000) or ryanodine receptors (RyR - Kiselyov *et al.*, 2000 and see Putney, 1999b; Putney & McKay, 1999; Berridge *et al.*, 2000 for review). Furthermore, Boulay and colleagues demonstrated that in native HEK-293T cells Ca^{2+} influx after stores depletion involved a TRP channel (see Boulay *et al.*, 1999 and see Putney, 1999b; Berridge *et al.*, 2000 for review). These authors, in agreement with Irvine (1990), suggested that the simplest mechanism by which depleted Ca^{2+} stores might activate the TRP channels was through a Ca^{2+}-dependent conformational change of the IP_3R. This concept was further supported by the fact that depletion of intracellular stores has been shown to modulate IP_3R (Missiaen *et al.*, 1994; Taylor, 1998 and see Putney, 1999b for review).

Although, the mechanism of the capacitative Ca^{2+} influx activation has recently become clearer, there are still several unresolved issues (see Putney, 1999b and Berridge *et al.*, 2000). Firstly, the exact role of IP_3 is still unclear, as TRP channels require IP_3 to be activated (Vaca & Kunze, 1994; Kiselyov *et al.*, 1998, 1999 and Zubov *et al.*, 1999) whereas there is clear evidence for a PLC-independent (*i.e.* without IP_3 production) activation of capacitative Ca^{2+} influx (see Putney, 1997 for review). Secondly, none of the members of the TRP family is *stricto sensu* a SOCC because they are activated not only by store depletion but also by several other messengers (see Clapham *et al.*, 2001 for review).

3. Intracellular calcium buffering

After entering the cell through Ca^{2+}-permeable channels, Ca^{2+} ions are immediately confronted by a complexity of mechanisms that will bind or try to exclude them from their physiological activity. As a consequence the major part of Ca^{2+} ions entering the cells is rapidly buffered by intracellular Ca^{2+} binding protein (CaBPs) and only a small fraction remains in the free ionic form.

3.1. Some general aspects about calcium buffering

The plasma membrane, which is formed by a phospholipid bilayer with inserted or associated proteins, has long been known to extensively bind Ca^{2+} (Guillemette *et al.*, 1988). Several elements of the cytoskeleton have been shown to also bind Ca^{2+} and to acquire their function in a Ca^{2+}-dependent manner (Keith *et al.*, 1983). Furthermore, microfilaments are often associated to subcortical regions of the plasma membrane and may be anchored through annexins or calpactins, which become active following Ca^{2+} binding (Glenney & Glenney, 1985). The CaBPs are found in a variety of tissues, have affinities for Ca^{2+} ranging from micromolar (*e.g.* calpain) to submicromolar (*e.g.* parvalbumin) and have been shown to play various roles in cell physiology (*e.g.* cell migration, neurites outgrowth, vesicles movement and cytoskeleton reorganisation - see van Rossum, 1998 for review).

According to the similarities in the structure of their binding domains, three main groups of CaBPs have been identified (Baimbridge *et al.*, 1992). The first group, which includes annexins, spectrin and fodrin, is characterised by repeat domains enabling the CaBPs to bind to phospholipids and to connect cytoskeletal elements in a Ca^{2+}-dependent manner (see Heizmann & Hunziker, 1990 for review). The second group contains sequences homologous to the C2-domain of the protein kinase C (PKC). This C2-domain is involved in a Ca^{2+}-dependent enzyme activation and translocation from the cytosol to the membrane (see Heizmann & Hunziker, 1990 for review). The third group, which will be detailed below, is characterised by EF-hand regions and exhibit high affinity for Ca^{2+} (see Chin & Means, 2000 and Toutenhoofd & Strehler, 2000 for review). Finally, in addition to these CaBPs, inorganic compounds like ATP have been shown to bind Ca^{2+} (Zhou & Neher, 1993).

3.2. Calcium binding proteins with a 'E-F hand' motif

This group of CaBPs share a common structural motif, the EF-hand, which consists of a pair of α helices joined by a Ca^{2+} binding loop (Heizmann & Berchtold, 1987; Kretsinger, 1987 and Persechini *et al.*, 1989). A CaBP can contain up to 6 Ca^{2+} binding loops, which bind Ca^{2+} with a high affinity (10^{-8} to 10^{-5} M) generally in a co-operative way (Heizmann & Berchtold, 1987; Baker & Umbach, 1987; Donahue &

Abercrombie, 1987 and Persechini *et al.*, 1989). These proteins are thought to rapidly bind Ca^{2+} and therefore to be capable of terminating the Ca^{2+} response by acting as a buffering system. However, the major role of CaBPs does not appear to be the buffering of Ca^{2+} but the processing of its signal. In fact, intracellular Ca^{2+} mostly acts as a second messenger when bound to an effector. Thus, Ca^{2+} binding to CaBPs induces a conformational change of the protein, which then acquire the ability to interact with target enzymes and therefore to induce a cellular response (Dedman *et al.*, 1977; Richman & Klee, 1978; Kretsinger, 1980 and see Carafoli, 1987; Heizmann & Hunziker, 1990; Miller, 1991; Chin & Means, 2000 for review). The CaBPs represent a superfamily of over 150 members including calmodulin, parvalbumin, and calbindin (Heizmann & Berchtold, 1987; Persechini *et al.*, 1989 and see Carafoli, 1987; Heizmann & Hunziker, 1990; Miller, 1991 for review).

3.2.1. Calmodulin

Calmodulin (CaM) is a highly acidic protein (16.5 kDa) and represents the prototypical Ca^{2+}-sensor containing four Ca^{2+} binding sites. The C-terminal pair of E-F hands exhibits a three- to five-fold higher affinity for Ca^{2+} than the N-terminal pair of sites (K_d for CaM ranging from 5.10^{-7} to 5.10^{-6} M). The binding of a target protein by CaM raises its affinity for Ca^{2+} by approximately 10-fold and sensitises the CaM-effector complex to changes in $[Ca^{2+}]_i$ (Peersen *et al.*, 1997). Calmodulin was originally described as an activator of brain cAMP phosphodiesterase (Kakiuchi & Yamazaki, 1970 and Cheung, 1970). It was subsequently shown to belong to the CaBPs family and to have multiple roles in the cellular activity (England, 1986; Heizmann & Berchtold, 1987 and see Chin & Means, 2000; Toutenhoofd & Strehler, 2000 for review). Calmodulin was shown to activate adenylyl cyclases, phosphodiesterases, protein kinases and the protein phosphatase calcineurin. All of these enzymes have been shown to be involved directly or indirectly in protein phosphorylation (see Chin & Means, 2000 for review). Calmodulin also regulates the activity of various ionic channels such as the ryanodine and inositol (1,4,5)-triphospate (IP_3) receptors and also the plasma membrane Ca^{2+}-ATPase (see below section 5.1.3 and Carafoli, 1987; Carafoli & Stauffer, 1994 and Chin & Means, 2000 for review).

3.2.2. Parvalbumin

Parvalbumins are a family of acidic proteins (MW ≈ 11.5 kDa) that bind 2 Ca^{2+} ions with a high affinity ($K_d \approx 10^{-8}$ M). Effects of Ca^{2+} buffers are determined by their affinity for Ca^{2+} ions and by the kinetics (on and off rates) of Ca^{2+} binding and release. In this regard, parvalbumin is an interesting molecule because it has a slow dissociation rate ($\approx 1\ s^{-1}$) and a slow apparent association constant ($\approx 10^7\ M^{-1}\ s^{-1}$), due to Mg^{2+} competition with Ca^{2+} for the binding sites (Heizmann, 1984 and England, 1986). For these reasons, parvalbumin is considered as a slow Ca^{2+} buffer and it has been suggested to be able to affect the characteristics of transient rise in $[Ca^{2+}]_i$ (Celio, 1990 and Chard *et al.*, 1993). Parvalbumin was first described in fast-twitch skeletal muscles where it is thought to play a role in the relaxation of muscle fibres by temporarily binding Ca^{2+} before it is pumped back into the sarcoplasmic reticulum (Gerday & Gillis, 1976; Thatcher & Pechere, 1977 and Birdsall *et al.*, 1979). Similarly, parvalbumin is thought to buffer Ca^{2+} entering neurones and to play a role in some form of synaptic plasticity (Blaustein, 1988a; Caillard *et al.*, 2000 and see Miller, 1991 for review). Parvalbumin was also suggested to have a tissue-specific distribution. Thus, this CaBP was found to be largely expressed in GABAergic neurones from the central nervous system particularly in the cerebellum and the hippocampus (Kawaguchi *et al.*, 1987; Sloviter, 1989; Celio, 1990; and Yoshida *et al.*, 1990). However, other authors found that parvalbumin was also present in non-GABAergic neurones (Jones & Hendry, 1990 and Nitsch *et al.*, 1990). Furthermore, neuronal excitability is often regulated by Ca^{2+} activated conductance such as Ca^{2+}-dependent potassium currents (*e.g.* $I_{K(Ca)}$). It was proposed that the presence of parvalbumin could underlie particular electrophysiological properties of neurones. Thus, parvalbumin was suggested to strongly buffer rises in $[Ca^{2+}]_i$ during neuronal activity and therefore to reduce the level of activation of $I_{K(Ca)}$ resulting in a lower spike accommodation (Kawaguchi *et al.*, 1987). The fact that parvalbumin-containing neurones in the hippocampus have been found to be 'fast spiking' while neurones without parvalbumin had a different firing pattern supported this idea. So far, the only well agreed role for parvalbumin is Ca^{2+} buffering as no definitive evidence has been provided to link its expression to a particular cell function.

3.2.3. Calbindin D_{28k}

Calbindin D_{28k} is present in many vertebrate tissues where it was shown to be α,25-dihydroxyvitamin-D_3-dependent in several tissues including kidney and pancreas (Norman *et al.*, 1982 and Bruns *et al.*, 1989) but not in neurones (Hall & Norman, 1991). Calbindin D_{28k} is unique among CaBPs because it has a larger molecular weight (≈ 30 kDa) and 6 Ca^{2+} binding sites (Fullmer & Wasserman, 1987; Hunziker & Schrickel, 1988 and Minghetti *et al.*, 1988). Although the precise role of calbindin D_{28k} is poorly understood, several observations are consistent with a protective role of this CaBP in neurotoxicity and neurodegenerative diseases. Calbindin D_{28k} expression and *m*RNA levels are decreased in brain area affected in ageing (Iacopino & Christakos, 1990; Krzywkowski *et al.*, 1996; Molinari *et al.*, 1996; Potier *et al.*, 1994) and Parkinson's, Huntington's and Alzheimer's diseases (Ichimiya *et al.*, 1989 and Iacopino & Christakos, 1990). Finally, calbindin D_{28k} is strongly expressed in cerebellar Purkinje neurones where it acts as a strong Ca^{2+} buffering system (Baimbridge *et al.*, 1992; de Talamoni *et al.*, 1993 and Fierro & Llano, 1996). A similar role in Ca^{2+} buffering was observed in hippocampal neurones in culture (Mattson *et al.*, 1991).

3.3. *Endogenous calcium buffering properties*

A comparison of the Ca^{2+} entry and the subsequent elevation in $[Ca^{2+}]_i$ suggest that more than 99% of the Ca^{2+} that enters a neurone does not remain in the free ionic form in the cytoplasm (Neher & Augustine, 1992; Belan *et al.*, 1993a, b; Muller *et al.*, 1993; Tse *et al.*, 1994 and Vanselow & Keller, 2000). The exact nature of the cellular components that are responsible for the Ca^{2+} buffering has not been conclusively identified. However, it appears reasonable to suggest that proteins binding Ca^{2+} with a high affinity would have the ability to act, at least temporarily, as endogenous buffer systems and therefore shape Ca^{2+} responses (Neher & Augustine, 1992 and Neher, 1995). The sum of all Ca^{2+} binding sites in the cytoplasm has been defined as 'endogenous Ca^{2+} buffer' and has led to the concept of endogenous buffering capacity (Neher & Augustine, 1992 and Neher, 1995). The Ca^{2+} buffering capacity

represents the cell's ability to bind Ca^{2+} ions entering the cytosol during the activation of Ca^{2+} channels and therefore to limit the extent of the increase in $[Ca^{2+}]_i$.

In living cells, several approaches were used to determine the Ca^{2+} binding ratio or the Ca^{2+} buffering capacity. The first one, is the 'buffer added' method whereby an exogenous buffer (fluorescent Ca^{2+} dye), with a high affinity for Ca^{2+} and at a known maximal concentration, is dialysed through a patch pipette into the cell and Ca^{2+} transients are elicited by depolarisation-induced activation of VACC. With dialysis, the buffering capacity of the exogenous buffer increases and causes concentration-dependent changes in the properties of depolarisation-induced Ca^{2+} transients *i.e.* decreasing their amplitude and slowing their recovery time. Since both the endogenous and exogenous buffers compete for Ca^{2+}, the changes in the Ca^{2+} transients' properties represent the buffering effects of the added exogenous buffer (Neher & Augustine, 1992; Neher, 1995 and Palecek *et al.*, 1999). Therefore, the endogenous Ca^{2+} binding ratio can be estimated in terms of added buffer from the changes in the Ca^{2+} transient's amplitude as well as from the changes in its recovery time and extrapolated to a situation without exogenous buffer (Neher & Augustine, 1992; Neher, 1995 and Palecek *et al.*, 1999).

Another method is the 'Ca^{2+}-clamp' technique (Ahmed & Connor, 1988 and Belan *et al.*, 1993a, b) and consists of measuring the changes in $[Ca^{2+}]_i$ induced by injection through a iontophoresis electrode of a known concentration of Ca^{2+}. The injection of Ca^{2+} will induce a transient rise in $[Ca^{2+}]_i$, which represents the filling of a fast cytosolic buffer, before reaching a new increased level of $[Ca^{2+}]_i$. The Ca^{2+} binding ratio can then be calculated as the ratio between the change in total $[Ca^{2+}]$ over the change in $[Ca^{2+}]_i$. A variation of this method consists of injecting increasing concentration of Ca^{2+} indicator (fura-2) and inducing changes in $[Ca^{2+}]_i$ either by iontophoretic injection of Ca^{2+} (Muller *et al.*, 1993) or by depolarisation and activation of VACC (Tse *et al.*, 1994). The Ca^{2+} binding ratio was calculated at different concentrations of the exogenous buffer and the endogenous buffer was then determined by extrapolating the Ca^{2+} binding ratio to a situation without dye (Tse *et al.*, 1994).

Finally, the last method consists of a direct measurement of the Ca^{2+} buffering properties in cell loaded with a low concentration of the Ca^{2+} indicator. The changes in the total Ca^{2+} are calculated from the integral of the Ca^{2+} current or from a calibrated

flash photolysis of caged Ca^{2+} and the changes in free intracellular Ca^{2+} measured using the fluorescent probe (Maeda *et al.*, 1999). Knowing the total amount of Ca^{2+} entering a cell or released in the cytoplasm upon photolysis as well as the amount of free Ca^{2+}, it is possible to determine the amount of Ca^{2+} bound to the buffer and to subsequently calculate the endogenous Ca^{2+} binding ratio (Ca^{2+} bound over Ca^{2+} free).

All the methods presented above have advantages and disadvantages. With the 'added buffer' technique, it is only possible to estimate Ca^{2+} buffering ratio but not the 'apparent' affinity and concentration of the endogenous buffer. Such parameters could be obtained from measurements of free Ca^{2+} changes with a low affinity dye, providing that $[Ca^{2+}]_i$ can be increased sufficiently to produce at least partial saturation of the buffer (Maeda *et al.*, 1999). However, the comparison of changes in free Ca^{2+} with changes in total Ca^{2+} requires knowledge of the accessible volume, which is not easy to measure precisely.

Measurements of the Ca^{2+} binding ratio have demonstrated notable heterogeneity in excitable cells ranging from 40 in adrenal chromaffin cells (Zhou & Neher, 1993) to 100-130 in other preparations such as gonadotrophs (Tse *et al.*, 1994) and GH3 cells (Lledo *et al.*, 1992) and up to $\approx$ 2000 in rat and mouse cerebellar Purkinje neurones (Fierro & Llano, 1996 and Maeda *et al.*, 1999, respectively). Evidence for low Ca^{2+} binding ratio values in neurones were obtained for recordings from the soma, dendrites and presynaptic terminals in a variety of preparations (see Regehr & Tank, 1994; Borst *et al.*, 1995 and Regehr & Atluri, 1995 for review). Using the 'added buffer' approach, Ca^{2+} binding ratio values of $\approx$ 174 were obtained for neurohypophysal nerve ending (Stuenkel, 1994), of $\approx$ 126 for neurones from the nucleus basalis (Tatsumi & Katayama, 1993). Helmchen and colleagues reported Ca^{2+} binding ratio values in the range of 100-135 for cortical layer V pyramidal cells and of 168-207 for hippocampal CA1 pyramidal cells (Helmchen *et al.*, 1996).

The large variations in the Ca^{2+} buffering properties observed among different cell types may be the result of the properties of the expressed CaBPs as well as of their level of expression. Firstly, the nature of CaBPs expressed in different neuronal population is highly variable and correlates with the variability in the observed Ca^{2+} binding ratio (see Baimbridge *et al.*, 1992; Regehr & Tank, 1994; Borst *et al.*, 1995 and Regehr & Atluri, 1995 for review). Secondly, changes in the buffering properties have been reported

during cell development and ageing. A substantial reduction in the expression level of calbindin D_{28k} and calretinin was accompanied by a decrease in the buffering capacity in hippocampal neurones (Villa *et al.*, 1994). In contrast, in cerebellar Purkinje neurones an increase in the buffering capacity was observed during neuronal maturation (Ca^{2+} binding ratio of ≈ 900 for 6-day-old and ≈ 2000 for 15-day-old rat – Fierro & Llano, 1996). Finally, the endogenous Ca^{2+} buffering capacity was proposed to have a protective role against pathology and neurodegenerative diseases. Thus, in mice, oculomotor neurones have a higher Ca^{2+} binding ratio (≈ 265 – Vanselow & Keller, 2000) than motoneurones from the spinal cord (≈ 50 Palecek *et al.*, 1999) and oculomotor neurones are particularly resistant during amyotrophic lateral sclerosis-related motoneurone disease (Palecek *et al.*, 1999 and Vanselow & Keller, 2000).

4. Intracellular organelles and calcium regulation

Although CaBPs efficiently buffer Ca^{2+} and take part in the regulation of the Ca^{2+} signal, they correspond to a temporary buffering system, which is limited and saturable (see General Introduction section 3). Therefore, intracellular organelles are required to sequester Ca^{2+} until it can be extruded across the plasma membrane (see below section 5). The early studies on the mitochondrial role in the regulation of $[Ca^{2+}]_i$ were carried out on isolated mitochondria in the presence of high extra-mitochondrial $[Ca^{2+}]$ and therefore the physiological relevance of Ca^{2+} handling by mitochondria was questioned. However, in the last two decades data have been produced that now support the idea of mitochondrial Ca^{2+} uptake and release during physiological cellular activity (see below section 4.1). The endoplasmic reticulum (ER) has been shown to contain specialised structures that enable it to act both as a Ca^{2+} sink and a Ca^{2+} source (see below section 4.2). Depending on its Ca^{2+} content, the ER was also proposed to stimulate Ca^{2+} influx through the plasma membrane (see above General Introduction section 2.2.2 and section 4.2).

4.1. The mitochondria

4.1.1. Some general aspects about mitochondria

Mitochondria are thought to be derived from prokaryotic micro organisms, which have developed a symbiotic relationship with their eukaryotic host (see Margulis *et al.*, 1996 and Gray & Lang, 1998 for review). The intra-mitochondrial matrix is isolated from the cytoplasm by two membranes, an outer membrane, which is permeable to most cations and small molecules (≤ 1 kDa), and an inner membrane mainly permeable to Ca^{2+} (see Frey & Mannella, 2000 for review). The major role of mitochondria is the production of the ATP necessary for cellular activity (tricarboxylic acid cycle and respiratory chain). During this process protons are translocated across the inner mitochondrial membrane generating a membrane potential of ≈ -150 to -200 mV (Mitchell & Moyle, 1967 and see Duchen, 1999 for review). According to the chemiosmotic model (Mitchell & Moyle, 1967), this 'protonmotive force' is used to drive, *via* protons re-uptake, the ATP-synthase (a proton channel associated to an ATP synthase) (see Duchen, 1999 for review). Several pharmacological agents are currently used to block one of the complexes of the respiratory chain (rotenone, cyanide), to inhibit the ATP synthesis (oligomycin) or to short-circuit the membrane potential and uncouple respiration from phosphorylation (protonophores such as carbonyl cyanide *m*-chlorophenyl hydrazone, CCCP and carbonyl cyanide *p*-trifluromethoxy-phenylhydrazone, FCCP). Although, these inhibitors have different functional consequences, their action results in the uncoupling of mitochondria , which are then unable to function normally.

4.1.2. Mitochondrial calcium transport mechanisms

In 1955, Chance demonstrated that mitochondria were able to sequester large amount of Ca^{2+} in parallel with their better-known role in ATP synthesis (Chance, 1955 and see Carafoli, 1982, 2002 for review). Moreover, it was suggested that Ca^{2+} accumulation by mitochondria might take precedence over ATP synthesis and uncouple oxidative phosphorylation (see Carafoli, 1982, 2002 and Duchen, 1999 for review). Calcium influx was shown to be mediated through a Ca^{2+} uniporter (see below section 4.1.2.1), whereas Na^{+}-dependent and independent mechanisms were proposed to

underlie the Ca^{2+} efflux (see below section 4.1.2.2; Lehninger *et al.*, 1967 and see Carafoli, 1982, 1987 and Duchen, 1999 for review). Finally, recent studies now support the involvement of a mitochondrial permeability transition pore (MPTP see below section 4.1.2.3) in Ca^{2+} efflux (Babcock *et al.*, 1998; Duchen, 1999; Murchison & Griffith, 2000 and Montero *et al.*, 2000).

4.1.2.1. Mitochondrial calcium uniporter

Evidence that Ca^{2+} was transported into the mitochondrial matrix through a mitochondrial Ca^{2+} uniporter (*m*CU) came from the demonstration that Ca^{2+} influx was driven by the mitochondrial membrane potential (-150 to -200 mV, mainly set by the proton gradient), that it followed the Ca^{2+} electrochemical gradient and that it was not coupled to the transport of any other ion (see Carafoli, 1982, 1987; Gunter & Pfeiffer, 1990; Budd, 1998 and Duchen, 1999 for review). It was therefore suggested that Ca^{2+} influx was a 'simple' electrophoretic process and was mediated through a specialised structure, the mitochondrial Ca^{2+} uniporter (*m*CU), which was activated by an increase in $[Ca^{2+}]_i$ (see Carafoli, 1982, 1987; Gunter & Pfeiffer, 1990; Budd, 1998 and Duchen, 1999 for review). Finally, the Ca^{2+} uptake through the *m*CU ($K_d \approx$ 1-5 μM) was shown to vary with the 3rd power of $[Ca^{2+}]_i$, a characteristic that would allow for amplification of mitochondrial Ca^{2+} uptake at higher cytoplasmic $[Ca^{2+}]_i$ (Zoccarato & Nicholls, 1982; Hansford, 1985; Nicholls, 1986; Crompton & Roos, 1985 and Crompton & Costi, 1990).

Calcium uptake strictly depends on the Ca^{2+} electrochemical gradient (see above) and therefore if Ca^{2+}could reach equilibrium, the amount of free Ca^{2+} sequestered into the mitochondria would be $10^5 - 10^6$ (0.1-1 M at 25°C) higher than in the cytosol. This Ca^{2+} uptake would lead to a depolarisation of the mitochondrial membrane potential because of the difference in net charges transfer (accumulation of positive charge into the mitochondria). In turn, an alkalisation of the mitochondrial matrix would be observed as protons are translocated through the respiratory chain process to maintain the mitochondrial membrane potential constant. The changes in pH and in the net charge in the mitochondrial matrix would, in the long term, impair mitochondrial function and therefore they need to be compensated. The symport of anions, such as phosphate (HPO_3^{2-}), with Ca^{2+} will serve both to dissipate the Ca^{2+}-induced alkalisation

and to allow the restoration of the mitochondrial membrane potential (see Nicholls & Ferguson, 1992 for review). Besides compensating pH changes and net charge accumulation in the mitochondrial matrix, phosphate uptake appears to have another important role. Thus phosphate was shown both to accelerate Ca^{2+} uptake and to allow larger Ca^{2+} amount to be sequestered (see Carafoli, 1982, 2002 for review). In fact, Ca^{2+} was shown to precipitate with phosphate and to form hydroxylapatite ($Ca_3(PO_4)_2$) an insoluble but osmotically inactive complex (see Carafoli, 1982, 2002 for review). Therefore, the formation of hydroxylapatite would enable the mitochondria to sequester larger amount of Ca^{2+} without perturbation of their normal activity.

Ruthenium red (RuR) and its analogues have been shown to block with some specificity the *m*CU ($K_i \approx 30$ nM – Moore, 1971; Reed & Bygrave, 1974a and Crompton & Andreeva, 1994). Unfortunately, although these compounds are the most commonly used *m*CU inhibitors, they are membrane non-permeant and, at higher concentrations, they also inhibit the VACC and Ca^{2+} release from the ER. Lanthanum has been shown to inhibit the *m*CU but in a less specific manner as it also affects the Na^+-dependent and independent Ca^{2+} efflux (Reed & Bygrave, 1974b). On the other hand, polyamines such as spermine are known to activate *m*CU; however they may also act as inhibitor at higher concentrations (≈ 500 µM – Jensen *et al.*, 1990 and Lenzen *et al.*, 1992).

Attempts to isolate the *m*CU produced a variety of protein fractions binding Ca^{2+} with a high affinity. One of these fractions is a 30 kDa glycoprotein, which was found inserted in both the outer and inner mitochondrial membranes but was not present in the matrix (Sottocasa *et al.*, 1972 and Carafoli & Sottocasa, 1974a). This molecule binds Ca^{2+} at two sites with different affinities for Ca^{2+} and is inhibited by both La^{3+} and RuR (see Carafoli, 1982 and Carafoli, 1987 for review). A second fraction was found to be a 3 kDa protein termed calciphorin that also binds Ca^{2+} with a high affinity and is inhibited with low concentration of RuR (Jeng & Shamoo, 1980a, b and see Carafoli, 1982, 1987 for review). It was suggested that these two proteins might interact to form the *m*CU. However for the moment no evidence is available to confirm this hypothesis (Carafoli, 1975 and see Carafoli, 1982, 1987 for review).

4.1.2.2. Calcium efflux mechanisms

In 1974, Carafoli and colleagues showed that, following Ca^{2+} uptake into energised heart mitochondria, addition of Na^+ induced a rapid Ca^{2+} efflux that was RuR-insensitive. This observation was confirmed by later experiments, which showed that the rate of Ca^{2+} efflux from the mitochondria exhibits a strong dependence on $[Na^+]$ (Carafoli *et al.*, 1974b; Crompton *et al.*, 1976 and see Carafoli, 1982, 1987; Gunter & Pfeiffer, 1990; Pozzan *et al.*, 1994; Duchen, 1999 for review). It was therefore suggested that Ca^{2+} would be released from the mitochondria *via* a Na^+-dependent mechanism that was independent and separated from the one used for the electrophoretic uptake. This Na^+-dependent Ca^{2+} release system has been observed in mitochondria from most tissues and proposed to be mediated *via* a specific Na^+/Ca^{2+} exchanger (*m*NCX, Mitchell & Moyle, 1967; Crompton *et al.*, 1976, Crompton *et al.*, 1978a, b; Nicholls, 1978b; Al Shaikhaly *et al.*, 1979 and see Carafoli, 1982, 1987; Gunter & Pfeiffer, 1990 for review). By contrast, in mitochondria from liver and part of the kidney, the Ca^{2+} efflux was found to be practically Na^+-independent, and it was suggested to be mediated through a Ca^{2+}/H^+ exchanger with $1Ca^{2+}$ being transported in exchange of $2H^+$ (Puskin *et al.*, 1976; Crompton *et al.*, 1978a, b; Akerman, 1978; Fiskum & Cockrell, 1978; Brand, 1985 and Fiskum & Lehninger, 1979). However, even if a Ca^{2+} efflux through a Na^+-independent mechanism cannot be ruled out, the Na^+-dependent system appears to be the major mitochondrial extrusion system, particularly in excitable cells, and as such has retained the most attention. (Bernardi & Azzone, 1979; Beatrice *et al.*, 1982; Gunter *et al.*, 1983; Jurkowitz *et al.*, 1983; Saris, 1987 and see Carafoli, 1982, 1987 ; Gunter & Pfeiffer, 1990 for review).

The Na^+/Ca^{2+} exchanger (*m*NCX) has been shown to be different from that present in the plasma membrane and to exhibit a sigmoidal dependence on the logarithm of cytoplasmic $[Na^+]$ with a half maximal activity at 4-5 mM Na^+ and a Hill coefficient of 2-3 (Crompton & Heid, 1978; Nicholls, 1978a, b and see Carafoli, 1982, 1987; Gunter & Pfeiffer, 1990; Pozzan *et al.*, 1994; Duchen, 1999 for review). It was proposed that the exchanger works in an asymmetric way to optimise Ca^{2+} efflux with a high affinity for Ca^{2+} at the matrix side ($\approx$ 3 to 6 μM see Hansford & Castro, 1981; Coll *et al.*, 1982 and Jung *et al.*, 1995) and a higher affinity for Na^+ at the external side

(Crompton & Roos, 1985 and see Carafoli, 1982, 1987; Gunter & Pfeiffer, 1990 for review).

Several antagonists of the VACC, such as diltiazem, clonazepan or diazepam exhibit an inhibitory effect on *m*NCX. The benzothiazepine CGP-37157 (CGP) has been shown to selectively and reversibly inhibit the *m*NCX in isolated cardiac mitochondria with a K_i in the range of 360 to 800 nM (Chiesi *et al.*, 1988 and Cox *et al.*, 1993) and is commonly used to inhibit mitochondrial Ca^{2+} release (Colegrove *et al.*, 2000 and Montero *et al.*, 2000). Finally, because of the high Na^+ dependence of *m*NCX another efficient way to inhibit the exchanger is to remove intracellular Na^+ (see Gunter & Pfeiffer, 1990 and Colegrove *et al.*, 2000).

4.1.2.3. Mitochondrial permeability transition pore

From studies on the swelling of isolated mitochondria, it was shown that the permeability of the mitochondrial inner membrane could suddenly increase. This phenomenon, which was termed 'permeability transition', allows fluxes of small ions and molecules up to 1.5 kDa and subsequently the collapse of the mitochondrial membrane potential (Massari *et al.*, 1972, Haworth & Hunter, 1979; Hunter & Haworth, 1979a, b and see Crompton *et al.*, 1999; Bernardi, 1999 for review). First thought to be the consequence of 'unspecific membrane damage', this phenomenon was then shown to be mediated through a channel: the mitochondrial permeability transition pore (MPTP). The MPTP can be defined as a Ca^{2+}- and voltage-dependent channel of the inner mitochondrial membrane that is blocked by cyclosporine A (see Zoratti & Szabo, 1995; Crompton *et al.*, 1999 and Bernardi, 1999 for review). Although the exact nature of this channel is still controversial it was proposed to be part of or associated with the mitochondrial ATP/ADP carrier (Brustovetsky & Klingenberg, 1996) and functionally reminiscent of the ryanodine-receptor channel of the endoplasmic reticulum (Bernardi & Petronilli, 1996). Electrophysiological recordings suggested that MPTP has a maximal conductance $\approx$ 1.5 nS and would operate under two main modes (Crompton & Costi, 1990 and see Zoratti & Szabo, 1995; Crompton *et al.*, 1999 and Bernardi, 1999 for review). Firstly, a high conductance state was proposed to be associated with a persistent pore opening and thought to be involved in the intracellular cascade leading to oxidative cell death (Crompton & Costi, 1990; Griffiths & Halestrap, 1995;

Nieminen *et al.*, 1995 and see Kroemer *et al.*, 1998 for review). Secondly, a low conductance state associated with transitory pore openings has also been observed but its functional significance remains unclear. Nevertheless, in non-excitable cells, the MPTP has been implicated in the release of Ca^{2+} under non-toxic conditions (Cassarino *et al.*, 1998) and increasing evidence is available for excitable cells suggesting its involvement under physiological conditions (Petronilli *et al.*, 1999; Murchison & Griffith, 2000 and Montero *et al.*, 2000).

4.1.3. Physiological role of the mitochondrial calcium transport

4.1.3.1. Calcium cycling in mitochondria

Since Ca^{2+} uptake and release systems are mediated through two separate processes both operative under physiological conditions, the concept of Ca^{2+} cycling across the inner mitochondrial membrane was proposed (Carafoli, 1979). While the Ca^{2+} efflux is essentially constant, the Ca^{2+} uptake is determined by the cytosolic $[Ca^{2+}]_i$. Therefore, for high cytosolic $[Ca^{2+}]_i$, Ca^{2+} will be predominantly transported into the mitochondria and when $[Ca^{2+}]_i$ decreases to a value where Ca^{2+} efflux and influx balance each other the net mitochondrial Ca^{2+} flux will be equal to zero (Nicholls, 1978a). Having reached this steady-state, the mitochondria would be able to respond to any $[Ca^{2+}]_i$ changes by either taking up or releasing Ca^{2+}. This $[Ca^{2+}]_i$ has been defined as the 'set-point' of the Ca^{2+} cycle and will determined the direction of the net Ca^{2+} flux. Values for the set-point have been reported between 0.3 and 3 μM that would depend on the level of activation of Ca^{2+} uptake and/or Ca^{2+} release systems (Nicholls, 1978a; Nicholls & Scott, 1980 and Brand & de Selincourt, 1980). Thus, above the set-point there will be a net Ca^{2+} uptake whereas below the set-point a net Ca^{2+} efflux will be observed. Under these conditions, if $[Ca^{2+}]_i$ remains below the set-point value, then a depletion of the total matrix Ca^{2+} is expected.

4.1.3.2. Mitochondrial role in calcium homeostasis

The development of fluorescent Ca^{2+} probes enabled the measurement of $[Ca^{2+}]_i$ in most cells, including neurones, with minimum disruption of the plasma membrane. Cytoplasmic Ca^{2+} could be monitored and when cells were depolarised with KCl, activation of VACC or by neurotransmitters, a rise in $[Ca^{2+}]_i$ in the micromolar

range was observed. Typically, the rise in $[Ca^{2+}]_i$ is transient and shows a multiphasic recovery with a fast initial decay followed by a characteristic secondary slow phase that could last for tens of seconds (*e.g.* Thayer & Miller, 1990; Werth & Thayer, 1994; Friel & Tsien, 1994; Herrington *et al.*, 1996; Babcock *et al.*, 1997 and Colegrove *et al.*, 2000). The inhibition of the mitochondrial Ca^{2+} uptake, with protonophores or RuR, generally induced a prolongation of the initial recovery sometimes associated with an increase in the amplitude of the Ca^{2+} transient and abolished the slow secondary phase. Similar results were obtained from smooth muscle cells (Drummond & Fay, 1996), chromaffin cells (Herrington *et al.*, 1996 and Babcock *et al.*, 1997), anterior pituitary cells (Hehl *et al.*, 1996) and neurones (Thayer & Miller, 1990; Werth & Thayer, 1994; Friel & Tsien, 1994 and Colegrove *et al.*, 2000). A major argument against the direct involvement of the mitochondria in the regulation of $[Ca^{2+}]_i$ was the possibility that mitochondrial inhibition would cause ATP depletion impairing the activity of ATP-dependent Ca^{2+} clearance mechanisms (endoplasmic reticulum and plasma membrane Ca^{2+}-ATPases see below section 4.2.2 and 5.1, respectively). However, three experimental observations argued against that possibility and confirmed a mitochondrial role in the regulation of $[Ca^{2+}]_i$. Firstly, the effects of protonophores were evident in less than 5s, before any substantial ATP depletion could occur. Secondly, prolongation of the early Ca^{2+} clearance phase could still be induced by protonophores in the presence of oligomycin to minimise mitochondrial ATP consumption of cytosolic ATP. Finally, the same results were observed in voltage-clamped experiments where patch-clamp electrodes, filled with an intracellular solution containing ATP, would provide a supply of energy (see Babcock *et al.*, 1997).

Uncoupling of the mitochondria during the slow secondary phase of a Ca^{2+} transient causes a large rise in $[Ca^{2+}]_i$ suggesting Ca^{2+} release from Ca^{2+} loaded mitochondria (Hehl *et al.*, 1996; Herrington *et al.*, 1996 and Babcock *et al.*, 1997). On the other hand, the slow secondary phase could also be abolished using selective inhibitor of the *m*NCX such as diltiazem and CGP (White & Reynolds, 1997; Babcock *et al.*, 1997 and Colegrove *et al.*, 2000). The effect of CGP was shown to be concentration-dependent and consistent with a single binding site model and an $IC_{50} \approx$ 560 nM (Colegrove *et al.*, 2000 and see above section 4.1.2.2). Similarly, in voltage-clamped cells, the removal of intracellular Na^+ was shown to abolish the slow secondary

recovery phase and to occlude the CGP effect (Colegrove *et al.*, 2000 and see above section 4.1.2.2). It was generally believed that mitochondria only participate in the regulation of large rises in $[Ca^{2+}]_i$ because of the properties of the mitochondrial Ca^{2+} cycling and the set-point value (see above section 4.1.3.1). However, several observations suggested that mitochondria could play a role in $[Ca^{2+}]_i$ regulation at $[Ca^{2+}]_i$ as low as 200-300 nM (Zhou *et al.*, 1998 and Colegrove *et al.*, 2000). Thus, mitochondrial Ca^{2+} transport was shown to occur in neurones and cardiac cells during 'weak' depolarisation and rise of $[Ca^{2+}]_i$ to low levels ($\approx$ 300 nM).

Miyata and colleagues (1991) suggested that Ca^{2+} uptake into mitochondria is rapid and followed by a slow re-equilibration of $[Ca^{2+}]_m$. However, direct measurements of the Ca^{2+} content of the mitochondrial matrix using site-directed aequorin or rhod-2, a fluorescent Ca^{2+} indicator selectively targeted into the mitochondria, demonstrated that in fact both the Ca^{2+} uptake and release processes were fast (< 5 seconds and tens of seconds, respectively - Rizzuto *et al.*, 1992, 1994; Babcock *et al.*, 1997 and Robb-Gaspers *et al.*, 1998). These same experiments also suggested several important new features of the mitochondrial regulation of $[Ca^{2+}]_i$. Firstly, they showed that the resting mitochondrial free Ca^{2+} concentration ($[Ca^{2+}]_m$) was around 80-200 nM suggesting that under resting condition the mitochondria are in a steady state where Ca^{2+} influx and efflux balance each other (Rizzuto *et al.*, 1992, 1994 and Babcock *et al.*, 1997). Secondly, following Ca^{2+} influx through the plasma membrane or release from intracellular stores, the $[Ca^{2+}]_i$ is increased to micromolar range (1-2 μM) and $[Ca^{2+}]_m$ increases in parallel to concentration generally higher (1-5 μM measured with targeted Ca^{2+} probes - Rizzuto *et al.*, 1992, 1994 and Babcock *et al.*, 1997). Finally, because mitochondrial Ca^{2+} uptake is large and fast, these organelles have been suggested to act as a fixed buffering system that would play an important role in the endogenous Ca^{2+} buffering capacity and as such would shape the overall Ca^{2+} signal (Coll *et al.*, 1982; Lukacs & Kapus, 1987 and Babcock *et al.*, 1997). Babcock and colleagues (1997) suggested that in chromaffin cells the Ca^{2+} taken up into the mitochondria would bind quickly and reversibly to Ca^{2+} binding sites in the matrix and these authors estimated a Ca^{2+} binding ratio of $\approx$ 4000 (see also Coll *et al.*, 1982; Lukacs & Kapus, 1987), which is about 100 times higher than the cytoplasmic Ca^{2+} binding ratio (see General Introduction section 3.3).

Over the years, evidence has been collected that supports the idea of an important mitochondrial role in the regulation of $[Ca^{2+}]_i$ under physiological conditions. Firstly, mitochondria are the 'energy factory' of the cell and key rate-limiting enzymes of the tricarboxylic acid cycle have been shown to be upregulated by Ca^{2+} either directly or through Ca^{2+}-dependent phosphorylation (Fein & Tsacopoulos, 1988; Duchen, 1992; Di Lisa *et al.*, 1993; Hajnoczky *et al.*, 1995 and Robb-Gaspers *et al.*, 1998). Therefore, it appears likely that mitochondrial Ca^{2+} uptake serves not only to upregulate ATP synthesis in anticipation to an increased energy demand during cellular activity, but also to actively regulate and propagate Ca^{2+} signal (Ichas *et al.*, 1994, 1997; Jouaville *et al.*, 1995; Tang & Zucker, 1997; Hoth *et al.*, 1997; David *et al.*, 1998; Rizzuto *et al.*, 1998 and Montero *et al.*, 2000).

4.2. The endoplasmic reticulum

4.2.1. Some general aspects about the endoplasmic reticulum

The endoplasmic reticulum (ER) is present in all eukaryotic cells as a vast network of cistern-like stacks and primarily acts as a factory for storage, folding and transport of proteins (see Ashby & Tepikin, 2001 for review) but also as an important Ca^{2+} store. This dual role of the ER is reflected in the functions of individual proteins of the ER such as CaBPs (ER-CaBPs), which firstly handle and buffer Ca^{2+} but, more importantly, act as molecular chaperones for the folding and quality control of proteins (see Ashby & Tepikin, 2001 for review). Interestingly, many processes involved in protein synthesis have been shown to be Ca^{2+}-dependent (*e.g.* protein synthesis, folding and maturation are affected by Ca^{2+} depletion of the ER – see Ashby & Tepikin, 2001 for review).

In neurones, the endoplasmic reticulum has been shown to spread throughout the cell and to represent a highly structurally organised system of tubules and cisternae with regional specialisation (see Pozzan *et al.*, 1994 and Berridge, 1998 for review). Originating around the nucleus with the nuclear envelope, the ER network extends up into the dendrites and down the axon. In the soma and the proximal dendrites, portions of the ER have been shown to be in the vicinity of the plasma membrane and to form sub-surface cisternae classified as type I, II and III depending on how close to the plasma membrane they are located (see Berridge, 1998 for review). Along the axon, the

ER can form structures similar to sub-surface cisternae and ends in the synapse where it can be found associated to mitochondria (see Berridge, 1998 for review). On the dendritic side, the ER follows the dendritic tree and terminates as a stack of tubules sometimes in the vicinity of the postsynaptic density (see Berridge, 1998 for review). Along all this network of cisternae and tubules, sarco/endoplasmic Ca^{2+}-ATPases (SERCA) are expressed next to clusters of inositol (1,4,5) triphosphate (IP_3R) and/or ryanodine receptors (RyR). This particular organisation of the Ca^{2+} stores and of their different components enable a highly localised and precise Ca^{2+} handling as well as the propagation of Ca^{2+} signal throughout the neurones (see Berridge, 1998 and Usachev & Thayer, 1999a for review).

4.2.2. Calcium sequestration into intracellular stores

4.2.2.1. Structure of the sarco/endoplasmic calcium ATPase

The observation, in the early 1960s, that vesicles isolated from the sarcoplasmic reticulum were able to sequester Ca^{2+} *via* an ATP-dependent mechanism represented the first step in the demonstration of the role of the ER as Ca^{2+} store (Ebashi, 1961; Hasselbach & Makinose, 1961 and Ebashi & Lipmann, 1962). About 10 years later, McLennan purified a 110 kDa protein (McLennan, 1970) that was shown to belong to the P-type ATPases family characterised by the formation of a phosphoenzyme intermediate. This Ca^{2+}-ATPase represents a large asymmetrical protein inserted in the membrane of the ER this protein was therefore named the sarco/endoplasmic Ca^{2+}-ATPase or SERCA (see Lee & East, 2001 for review). Following the cloning of the skeletal muscle Ca^{2+}-ATPase (McLennan *et al.*, 1985 and see Lee & East, 2001) and more recently, the determination of the crystal structure of SERCA it has been shown that this protein is formed by three cytoplasmic domains (A, P and N) connected to 10 transmembrane α-helices (M1-M10) and terminated by a small luminal region (Toyoshima *et al.*, 2000 and see Lee & East, 2001 for review).

Several pharmacological agents that inhibit SERCA have been isolated. The most commonly used is thapsigargin (TG), which has proved to be a highly selective and potent inhibitor (EC_{50} between 0.2 and 50 nM – Lytton *et al.*, 1991 and see Treiman *et al.*, 1998; Andersen & Vilsen, 1998; Taylor & Broad, 1998 for review). Cyclopiazonic acid (CPA) and 2,5-di-*t*-butyl-hydroquinone also selectively inhibit SERCA but they

appear less potent than thapsigargin (Demaurex *et al.*, 1992; Wictome *et al.*, 1992 and see Pozzan *et al.*, 1994; Taylor & Broad, 1998 for review).

4.2.2.2. SERCA isoforms and tissue specific expression

Three main isoforms of SERCA have been characterised who share a common overall structure and sensitivity to inhibitors but differ in their tissue distribution and biochemical properties (see Pozzan *et al.*, 1994 for review). The expression of distinct isoforms with different properties (rate of Ca^{2+} transport, regulatory pathways) would enable a fine modulation of the Ca^{2+} uptake in different cell types or even in different region of a cell. SERCA-1 exist as two isoforms (SERCA-1a and 1b) and has been shown to be exclusively present in fast twitch skeletal muscle (Brandl *et al.*, 1986 and see Pozzan *et al.*, 1994 for review). The isoform 2 of SERCA ($\approx$ 84 % homology with SERCA-1) also exists as two splice variants (SERCA-2a and 2b) and differ from the other SERCA pumps by its lower turnover rate and a longer C-terminal tail (Gunteski-Hamblin *et al.*, 1988; Lytton & McLennan, 1988 and see Pozzan *et al.*, 1994 for review). Finally, SERCA-3, which is mainly found in intestine, lymphatic tissues and neuronal cells (Burk *et al.*, 1989 and see Pozzan *et al.*, 1994; Treiman *et al.*, 1998 for review), only shares $\approx$ 75% homology with SERCA-1 or SERCA-2 and has been shown to have a lower affinity for Ca^{2+} (K_d of 1.1 *vs.* 0.4 μM) than the other members (see Pozzan *et al.*, 1994 for review).

4.2.2.3. Regulation of SERCA activity

The SERCA are characterised by a high affinity for Ca^{2+} with a half maximal rate of transport at $[Ca^{2+}]_i \approx$ 0.1-1 μM and it was suggested that at rest SERCA would pump Ca^{2+} at 50% of their maximal rate (Pozzan *et al.*, 1994). The activity of SERCA is regulated by several mechanisms among them are the regulation by Ca^{2+} itself, by phosphorylation and by ER-CaBPs (Pozzan *et al.*, 1994). Following an increase in $[Ca^{2+}]_i$ after membrane depolarisation or receptor activation and Ca^{2+} release from the ER, Ca^{2+} uptake into the stores is activated. Thus, it has been shown that SERCA activation depends on the $[Ca^{2+}]_i$ and that the rate of Ca^{2+} uptake increases with $[Ca^{2+}]_i$ (Favre *et al.*, 1996 and Mogami *et al.*, 1998). However, although Ca^{2+} uptake into the ER is activated by a rise in $[Ca^{2+}]_i$, the Ca^{2+} transport itself does not need

elevated $[Ca^{2+}]_i$ as when $[Ca^{2+}]_i$ is clamped close to its resting value, Ca^{2+} transport into the ER is still observed (Mogami *et al.*, 1998). More interestingly, the free luminal Ca^{2+} concentration ($[Ca^{2+}]_L$) acts as a negative feedback and the rate of Ca^{2+} uptake decreases with the rise in $[Ca^{2+}]_L$ (Inesi & de Meis, 1989; Favre *et al.*, 1996 and Mogami *et al.*, 1998). The mechanism by which this feedback inhibition occurs is unclear but it was suggested that it could be mediated by direct interaction between SERCA and ER-CaBPs such as calreticulin (John *et al.*, 1998) or the phosphorylated form of calnexin (Roderick *et al.*, 2000) as both proteins have been shown to interact with SERCA-2 and to inhibit its activity.

Another regulatory pathway of the SERCA activity occurs by direct phosphorylation of the SERCA protein and appears to be isoform specific (see Pozzan *et al.*, 1994 for review). This phosphorylation process can involve CaM-dependent protein kinase, which was suggested to stimulate Ca^{2+} uptake and to accelerate the relaxation of cardiac and skeletal muscle (Narayanan & Xu, 1997).

Phospholamban (PLB) is coexpressed (1:1 ratio) and interacts with SERCA (Wegener *et al.*, 1989 and Pozzan *et al.*, 1994). The PLB is the substrate of two protein kinases, a cAMP-dependent protein kinase (PKA) and a CaM-activated one (CaM-kinase). It was suggested that in its unphosphorylated form, PLB is attached to SERCA and inhibits the Ca^{2+} pump (Simmerman *et al.*, 1986 and Toyofuku *et al.*, 1993). The phosphorylation of PLB, which appears to be Ca^{2+}-dependent, induces a conformational change of the protein and relieves SERCA inhibition (see Carafoli, 1987 and Pozzan *et al.*, 1994 for review). A similar process has been characterised for PMCA where the activation of CaM leads to the activation of the Ca^{2+}-ATPase by unmasking the active site (see below General Introduction section 5.1.3). The PLB phosphorylation was shown to occur following activation of β-adrenergic receptors in cardiac myocytes and to participate in muscle relaxation by stimulating SERCA (see Pozzan *et al.*, 1994 for review).

4.2.3. Calcium binding proteins of the endoplasmic reticulum

From measurements with Ca^{2+} microelectrodes or targeted Ca^{2+} probes, the ER Ca^{2+} content was estimated in the millimolar range (2-10 mM) of which ≈ 100-300 μM is in the free ionic form ($[Ca^{2+}]_L$, *e.g.* see Pozzan *et al.*, 1994 and Mogami *et al.*,

1998). Therefore, by analogy with the cytosol, the ER exhibits a large buffering capacity mediated by ER-CaPBs that can be divided in two groups. The first ER-CaBPs group (*e.g.* reticuloplasmins - see Pozzan *et al.*, 1994 for review) posses a high affinity for Ca^{2+} and because of the high Ca^{2+} content of the lumen they are thought to be permanently occupied and to have a minor role in Ca^{2+} storage. In contrast, the other group is thought to correspond to a high capacity Ca^{2+} storage system as well as a rapidly releasable Ca^{2+} pool. Calsequestrin and calreticulin are two well-studied examples. These proteins are expressed at high level, exhibit a large binding capacity (≈ 25-50 mol of Ca^{2+}/mol of protein) and low Ca^{2+} affinity ($K_d \approx 1$ mM) (see Pozzan *et al.*, 1994).

4.2.4. Main routes for calcium release into the cytosol

Calcium release is mediated through specialised channels inserted in the ER membrane that belong to the ligand-operated Ca^{2+} permeable channels: the inositol (1, 4, 5)-triphosphate (IP_3 - see below section 4.2.4.1) and the Ca^{2+} activated or ryanodine receptors (RyR - see below section 4.2.4.2). Although these two receptors are activated by different agonist and through different pathways, they share a homologous general structure and a coincidental activation by Ca^{2+} and a second messenger, which leads to Ca^{2+}-dependent stimulation of the release (Ca^{2+} induced Ca^{2+} release, CICR see below section 4.2.5 - see Pozzan *et al.*, 1994 and Kostyuk & Verkhratsky, 1995b for review).

4.2.4.1. Inositol triphosphate receptors

Inositol (1,4,5)-triphosphate receptors (IP_3R) are characterised by a N-terminal IP_3 binding site and a C-terminal Ca^{2+} binding site separated by a transmembrane region (see Pozzan *et al.*, 1994 and Kostyuk & Verkhratsky, 1995b for review). The transmembrane region carries several key features for the activity of the IP_3R as it forms the channel of the receptor but also corresponds to the coupling region between IP_3 binding and channel opening (Mignery *et al.*, 1990; Miyawaki *et al.*, 1991 and see Pozzan *et al.*, 1994 and Kostyuk & Verkhratsky, 1995b for review). This same domain contains also the modulatory sites of the receptor (phosphorylation sites, ATP, CaM and Ca^{2+} binding sites - see Pozzan *et al.*, 1994 and Kostyuk & Verkhratsky, 1995b for review). The C-terminal region binds Ca^{2+} and is thought to be involved in

the modulation of the channel opening (Nakade *et al.*, 1991; Miyawaki *et al.*, 1991 and see Pozzan *et al.*, 1994; Kostyuk & Verkhratsky, 1995b for review).

At least three main IP_3R isoforms, referred as type 1, 2 and 3 IP_3R, have been isolated and found to share ≈ 60-70 % sequence homology (see Pozzan *et al.*, 1994 and Kostyuk & Verkhratsky, 1995b for review). Apart from cerebellar Purkinje cells, which almost exclusively express IP_3R-1, most of the other cell types express at least two different isoforms of the IP_3R (Bush *et al.*, 1994 and see Pozzan *et al.*, 1994 and Kostyuk & Verkhratsky, 1995b for review). It was suggested that IP_3R could be formed by the association of subunits from different isoforms, which would increase the diversity of the expressed receptors (Joseph *et al.*, 1995 and Monkawa *et al.*, 1998).

The IP_3Rs were found to be synergistically activated by IP_3 and low $[Ca^{2+}]_i$ (< 1 μM) and to exhibit a 'bell-shaped' dependence on $[Ca^{2+}]_i$ (Bezprozvanny *et al.*, 1991; Iino & Tsukioka, 1994 and Adkins & Taylor, 1999). Recently, Adkins & Taylor (1999) suggested that the effect of $[Ca^{2+}]_i$ would depend on the concentration of IP_3 and, more importantly, on the order of application of Ca^{2+} and IP_3. Thus, the binding of IP_3 to the receptor was suggested to occlude an inhibitory Ca^{2+} binding site and at the same time to unmasks the activatory Ca^{2+} binding site (Adkins & Taylor, 1999; Taylor, 1998; Bootman & Lipp, 1999). Several studies have indicated that IP_3R activity is regulated by $[Ca^{2+}]_L$, (Nunn & Taylor, 1992; Taylor & Marshall, 1992; Oldershaw & Taylor, 1993 and Missiaen *et al.*, 1992), by phosphorylation processes through cAMP-dependent protein kinase (PKA) (Berridge, 1993; Joseph & Ryan, 1993 and Haug *et al.*, 1999), *via* PKC (Mironov & Hermann, 1996 and Haug *et al.*, 1999) and by CaM-dependent protein kinase (Ferris & Snyder, 1992; Marshall & Taylor, 1993 and see Pozzan *et al.*, 1994; Kostyuk & Verkhratsky, 1995b; Berridge, 1998 for review). Finally, heparin represents the most commonly used but not specific antagonist of IP_3R (Hill *et al.*, 1987; Ehrlich *et al.*, 1994 and see Kostyuk & Verkhratsky, 1995b for review).

4.2.4.2. Ryanodine receptors

The ryanodine receptor (RyR), which resembles in many respects the IP_3R, has been shown to belong to a receptor family with three main members (≈ 65% homology): skeletal type 1 (RyR-1), cardiac type 2 (RyR-2), which is also considered as the major neuronal subtype and brain type 3 (RyR-3) (Takeshima *et al.*, 1989; Zorzato

et al., 1990; McPherson & Campbell, 1993 and see Pozzan *et al.*, 1994; Kostyuk & Verkhratsky, 1995b for review). These receptors share a general common tetrameric structure consisting of a transmembrane region, yielding the channel pore, a small C-terminal domain that anchors the receptor into the ER membrane and a large N-terminal cytoplasmic loop (Otsu *et al.*, 1990; Chen *et al.*, 1992 and see Pozzan *et al.*, 1994; Kostyuk & Verkhratsky, 1995b for review). Regulatory and binding sites for CaM, ATP and Ca^{2+} have been describe in this N-terminal region (Otsu *et al.*, 1990; Chen *et al.*, 1992 and see Pozzan *et al.*, 1994; Kostyuk & Verkhratsky, 1995b for review). Although RyR are typically gated by Ca^{2+}, in skeletal muscle, RyR-1 are activated by the membrane depolarisation transmitted through a direct coupling to L-type VACC (Rios & Pizarro, 1991; Rios *et al.*, 1992 and see Pozzan *et al.*, 1994 for review).

Ryanodine receptors are cation-selective channels characterised by a high conductance for Ca^{2+} and recordings in the single-channel configuration have indicated that RyR can be opened as single event or as burst of openings (Rousseau *et al.*, 1987; Stein & Palade, 1988; Ashley, 1989 and Liu *et al.*, 1989). The activation of RyR exhibits a bell-shaped dependence on $[Ca^{2+}]_i$ (Bezprozvanny, 1994 and see Kostyuk & Verkhratsky, 1995b for review). Similarly to IP_3Rs, RyRs are modulated by the state of filling of the Ca^{2+} stores and it was suggested that calsequestrin might interact with the channel (Gilchrist *et al.*, 1992). On the other hand, depletion of the Ca^{2+} stores was suggested to reduce the sensitivity of the RyR to $[Ca^{2+}]_i$ and therefore to increase the threshold for their activation (Valdivia *et al.*, 1995; Usachev & Thayer, 1997 and see Sitsapesan & Williams, 1997; Usachev & Thayer, 1999a and Sitsapesan & Williams, 2000 for review).

Adenosine nucleotides (*e.g.* AMP, ADP and ATP) have been shown to strongly potentiate the Ca^{2+}-dependent activation of RyRs presumably through binding to a specific regulatory site located in the N-terminal region (Otsu *et al.*, 1990; Meissner, 1994 and see Pozzan *et al.*, 1994; Kostyuk & Verkhratsky, 1995b; Sitsapesan & Williams, 1997, 2000 for review). In addition, CaM was shown to bind to RyR and to exhibit an activatory effect in its Ca^{2+}-free form while CaM-Ca^{2+} had an inhibitory effect on RyR-1 and RyR-2 (Yamaguchi *et al.*, 2001 and Balshaw *et al.*, 2001). It was further suggested that CaM would inhibit Ca^{2+} release by decreasing the open probability of the RyR (Suko *et al.*, 2000). Finally, CaM has been proposed to activate

the RyR-2 through phosphorylation *via* a CaM-dependent kinase (see Henzi & McDermott, 1992 and Sorrentino & Volpe, 1993).

Until recently, RyR were thought to be exclusively activated by Ca^{2+}. However, the newly discovered endogenous cyclic ADP ribose (cADPr) has been suggested to be the counterpart of IP_3 for the activation of RyR (see Sitsapesan *et al.*, 1995a, b for review). There is evidence for a cADPr-dependent and ryanodine-sensitive Ca^{2+} release in urchin eggs and similar results were observed in neurones, heart, pancreatic and pituitary cells (Currie *et al.*, 1992; Meszaros *et al.*, 1993; Hua *et al.*, 1994; White *et al.*, 1993; Galione, 1994; Lee *et al.*, 1994 and see Pozzan *et al.*, 1994; Sitsapesan & Williams, 1995a, b for review). Many cells contain cADPr and the enzymes capable of producing and hydrolysing cADPr were found in neurones (Verkhratsky & Shmigol, 1996). Moreover, injection of cADPr in neurones failed to elicit Ca^{2+} release by itself but appeared to increase the Ca^{2+} sensitivity of RyR (Hua *et al.*, 1994). However, evidence for a direct binding of cADPr to RyR is still missing, there are only few reports for a cADPr production in response to the stimulation of physiological pathways and so far only the RyR-2 was shown to respond to the cADPr activation (Galione *et al.*, 1993; Takasawa *et al.*, 1993 and see Pozzan *et al.*, 1994; Sitsapesan & Williams, 1995a, b for review).

Caffeine (< 5 mM) was shown to activate RyR by shifting the RyR activation curve towards lower $[Ca^{2+}]_i$ and therefore sensitising RyR to $[Ca^{2+}]_i$ (see Kostyuk & Verkhratsky, 1995b and Zucchi & Ronca-Testoni, 1997 for review). At higher concentrations (>5 mM), caffeine was shown to activate RyR in a Ca^{2+}-independent manner and to induce Ca^{2+} release in several cell types (*e.g.* Thayer *et al.*, 1988; Sitsapesan & Williams, 1990; Usachev *et al.*, 1993; Shmigol *et al.*, 1994a, b and Hernandez-Cruz *et al.*, 1995).

Ryanodine, which was the first described selective agonist for RyR, is well known to activate the channel at low concentrations (< < 10 μM see Pozzan *et al.*, 1994 for review). Ryanodine increases the channel open probability to ≈ 1 and also potentiates the Ca^{2+}-dependent release (Rousseau *et al.*, 1987; Nagasaki & Fleischer, 1988). However, at higher concentrations (>10 μM), ryanodine locks the RyR into a low conductance open state and causes inhibition of both Ca^{2+}- and caffeine-induced Ca^{2+} release (Rousseau *et al.*, 1987 and Nagasaki & Fleischer, 1988 and McPherson *et al.*,

1991). This dual effect of ryanodine was suggested to be due to two different binding sites: a high affinity ($K_d \approx$ 5-10 nM) that promotes channel opening and a low affinity ($K_d \approx$ 3 μM) that inhibits the receptor (McGrew *et al.*, 1989 and see Kostyuk & Verkhratsky, 1995b for review). Finally, other compounds like dantrolene, procaine and RuR were also shown to inhibit RyR and the Ca^{2+} release from intracellular stores (see Kostyuk & Verkhratsky, 1995b for review).

4.2.4.3. New calcium-releasing messenger

Until the late 1980s, the general idea was that Ca^{2+} could be released *via* the activation of either IP_3R or RYR. However, an important experiment carried out by Lee and colleagues in 1987 demonstrated that a substrate of β-nicotinamide adenine dinucleotide (β-NAD^+), now identified as cADPr (Lee *et al.*, 1989), had Ca^{2+}-releasing activity by sensitising RyR to Ca^{2+} (see above section 4.2.4.2 and Galione, 1992; Patel *et al.*, 2001 for review). It was later demonstrated that nicotinic acid adenine dinucleotide phosphate (NAADP) is also able to induce Ca^{2+} release in a wide range of cell types (see Table 1 in Patel *et al.*, 2001). The NAADP-dependent Ca^{2+} release is thought to be mediated by a release mechanism distinct from both IP_3 and ryanodine (or cADPr) stores and several arguments support this observation (see Genazzani & Galione, 1997 and Patel *et al.*, 2001 for review). Firstly, the NAADP-induced Ca^{2+} release undergoes homologous desensitisation but does not affect Ca^{2+} release induced by either IP_3 or ryanodine/cADPr (Lee & Aarhus, 1995; Chini *et al.*, 1995; Genazzani *et al.*, 1996a and see Genazzani & Galione, 1997; Patel *et al.*, 2001 for review). Secondly, NAADP-induced Ca^{2+} release is insensitive to inhibitor of both IP_3 and ryanodine channels (Lee & Aarhus, 1995; Chini *et al.*, 1995; Lee *et al.*, 1996 and see Genazzani & Galione, 1997; Patel *et al.*, 2001 for review). On the other hand, the phenomenon of Ca^{2+}-induced Ca^{2+}-release (CICR) does not appear to be activated by NAADP, NAADP-dependent Ca^{2+} release is not sensitive to divalent cations (Ca^{2+}, Mg^{2+} or Sr^{2+} - Graeff *et al.*, 1995; Chini *et al.*, 1996; Genazzani & Galione, 1996) but was mostly inhibited by thio-NADP and L-type channel blockers (Genazzani *et al.*, 1996a and see Genazzani & Galione, 1997; Patel *et al.*, 2001 for review). Finally, in contrast to the IP_3- and ryanodine-induced Ca^{2+} responses, the NAADP-dependent Ca^{2+} release is not

modulated by $Ca^{2+}$and does not show a biphasic activation relationship (Chini *et al.*, 1996; Genazzani *et al.*, 1996b and see above section 4.2.4.1 and 4.2.4.2).

Although increasing evidence supporting a role for NAADP as a new Ca^{2+} releasing mechanism have been collected in recent years, some important issues are still unresolved. Thus, it has been demonstrated that low sub-threshold concentration of NAADP are able to inactivate a subsequent Ca^{2+} release that would normally be observed in the presence of a high NAADP concentration (Genazzani *et al.*, 1996a; Navazio *et al.*, 2000; Aarhus *et al.*, 1996 and see Patel *et al.*, 2001 for review). This observation therefore suggests that NAADP has to be synthesised or liberated in a high concentration very quickly in order to be able to activate Ca^{2+} release before it becomes inactivated. Moreover, although NAADP has been shown to be synthesised and to induce Ca^{2+} release in numerous tissues neither the localisation of the NAADP-sensitive store nor the NAADP receptor have been clearly identified (see Patel *et al.*, 2001 for review).

4.2.5. Role of intracellular stores in shaping calcium signals

The ER acts as a Ca^{2+} sequestration system through SERCA activation and accelerates the recovery from rises in $[Ca^{2+}]_i$ following Ca^{2+} influx through the plasma membrane (Kuba, 1980; Neering & McBurney, 1984; Thayer *et al.*, 1988 and Usachev *et al.*, 1993). However, the main role for Ca^{2+} stores appears to be the CICR process (see Usachev & Thayer, 1999a and Bootman *et al.*, 2001 for review). This phenomenon involves the amplification of a modest rise in $[Ca^{2+}]_i$ into a secondary larger Ca^{2+} release from the intracellular stores. The level of activation and the characteristics of the Ca^{2+} release system(s) will determine the shape of the overall Ca^{2+} signal, which could remain localised or spread throughout the cell as a regenerative Ca^{2+} wave. Calcium induced Ca^{2+} release can be generated by both IP_3 (see Berridge, 1998; Taylor, 1998 and Bootman *et al.*, 2001; for review) and ryanodine (Usachev & Thayer, 1999a for review) systems following related activation mechanisms.

Evidence for CICR in neurones came from the observations that caffeine could induce Ca^{2+} release from the ER and that this release was inhibited by ryanodine and dantrolene (Kuba, 1980; Neering & McBurney, 1984; Thayer *et al.*, 1988 and Usachev *et al.*, 1993). Later, CICR was directly demonstrated in voltage-clamped neurones from

both the central (Llano *et al.*, 1994) and peripheral (Hua *et al.*, 1993 and Shmigol *et al.*, 1995) nervous system. Following depolarisation of the plasma membrane, the increase in $[Ca^{2+}]_i$ was larger than predicted from the transmembrane Ca^{2+} current (Llano *et al.*, 1994) and both ryanodine or dantrolene could inhibit the amplification of the Ca^{2+} response (Shmigol *et al.*, 1995).

Calcium-induced Ca^{2+} release was proposed to be a all-or-none process in that $[Ca^{2+}]_i$ needed to reach a threshold value to successfully stimulate the release from the stores. However, the Ca^{2+} influx was suggested to only act as a trigger for the CICR but not to be required for the regenerative process (Friel & Tsien, 1992; Usachev & Thayer, 1997 and see Usachev & Thayer, 1999a for review). Generally a refractory phase followed CICR that was suggested to be primarily caused by the depletion of the stores and the increase in the activation threshold of RyR (Usachev & Thayer, 1997). The bell-shaped Ca^{2+} dependence of the RyR was also proposed to underlie this refractory phase presumably due to Ca^{2+} binding to a low affinity inhibitory binding site present on RyR. This site would require the $[Ca^{2+}]_i$ to return close to rest in order to remove the Ca^{2+}-dependent inhibition (Fabiato, 1983; Bezprozvanny *et al.*, 1991 and Hernandez-Cruz *et al.*, 1995). Finally, a phenomenon of Ca^{2+}-dependent desensitisation of the RyR was described in cardiac muscles (Gyorke & Fill, 1993) and was supported by experiments where a rapid time-dependent decrease in the open probability of RyR-2 was observed in the presence of activating $[Ca^{2+}]_i$ (Valdivia *et al.*, 1995). Since the Ca^{2+}-bound form of CaM was shown to inhibit the activity of RyR, this mechanism was also proposed to underlie the inhibition of Ca^{2+} release from the ER (Rousseau *et al.*, 1987 and Suko *et al.*, 2000).

The elaborate organisation of the Ca^{2+} stores and the distribution of Ca^{2+} uptake and release systems will determine the complex spatio-temporal pattern of cytosolic Ca^{2+} responses known as Ca^{2+} sparks, puffs, and Ca^{2+} waves (see Berridge, 1993 and Clapham & Sneyd, 1995 for review). These complex Ca^{2+} signals are mainly the results of the Ca^{2+} uptake systems being stimulated by a rise in $[Ca^{2+}]_i$ and located next to Ca^{2+} release pathways that exhibit a 'bell-shape' Ca^{2+} dependence (see Berridge, 1993 and Clapham & Sneyd, 1995 for review). In fact, if one considers a moderate stimulation of a neurone, the $[Ca^{2+}]_i$ elevation will be strongly attenuated by the buffering and extrusion mechanisms and therefore remains localised under the plasma membrane

(Hernandez-Cruz *et al.*, 1990). In contrast, with the increase of the Ca^{2+} influx, the rise in $[Ca^{2+}]_i$ may reach threshold and trigger a chain reaction that generates a saltatory activation of RyR deeper into the cytoplasm leading to a more global response (Kuwajima *et al.*, 1992 and Korkotian & Segal, 1998). As RyR are distributed in the whole somata and in neurites, for large enough rise in $[Ca^{2+}]_i$, this saltatory activation of RyR could generate a Ca^{2+} wave that would propagate throughout the cell (Lechleiter & Clapham, 1992; Usachev & Thayer, 1997 and Berridge, 1998). In this situation the cytoplasm could act as an 'excitable medium' and Ca^{2+} waves might travel considerable distance from the soma to distal parts of the apical dendrites (Jaffe & Brown, 1994) or from the growth cone back into the soma (Gomez *et al.*, 1995).

The induction of CICR would depend on the amplitude and duration of the Ca^{2+} influx and on the nature of the Ca^{2+} channels, which are highly regulated by phosphorylation processes and the activation of G protein-coupled receptors (*e.g.* Llano *et al.*, 1994; Dolphin, 1996; Moore *et al.*, 1998 and see Hille, 1994; Usachev & Thayer, 1997 for review). Since, co-agonists, protein-protein interactions and phosphorylation/ dephosphorylation processes as well as the Ca^{2+} content of the ER have been shown to modulate RyR, all these regulatory mechanisms would activate or inhibit RyR as well as determine the sensitivity of the RyR to Ca^{2+} and therefore determine the development or not of CICR (Thayer *et al.*, 1988 and Hua *et al.*, 1993 and Usachev *et al.*, 1993 and see Pozzan *et al.*, 1994; Usachev & Thayer, 1997 for review).

One of the major questions that arise from the demonstration of a CICR mechanism is certainly the physiological significance of such a phenomenon. Voltage-activated Ca^{2+} channels are well suited to induce Ca^{2+} influx into the cytosol and therefore to link changes in cell excitability to changes in $[Ca^{2+}]_i$. However, because of the regulation of $[Ca^{2+}]_i$ mainly through buffering and extrusion system the response induced by VACC is proposed to be localised and limited. Therefore, the major role of CICR is thought to act as a relay and amplification system of the Ca^{2+} influx and to transform a localised rise in $[Ca^{2+}]_i$ into a cellular global response. Thus the induction of CICR was shown to promote gene transcription and protein synthesis (Kuwajima *et al.*, 1992; Bading *et al.*, 1993; Hardingham *et al.*, 1997 and Korkotian & Segal, 1998). It was also suggested that CICR might enhance neurotransmitter release (Peng, 1996; Reyes & Stanton, 1996; Smith & Cunnane, 1996; Wang *et al.*, 1997 and Cochilla &

Alford, 1998) and might modulate neuronal excitability by acting on several Ca^{2+}-dependent channels (Kuba, 1980; Nishimura *et al.*, 1991; Sah, 1996 and Sah & Bekkers, 1996).

4.3. Interactions between mitochondria and calcium stores

In recent years, evidence has suggested that there may be cross-talk between mitochondria and the ER (Rizzuto *et al.*, 1993, 1998 and see Rutter & Rizzuto, 2000 for review). Thus three-dimensional reconstruction suggested that mitochondria could form a network of interlinked structures and close contacts with the ER cisternae and mitochondria were also observed (Bakeeva *et al.*, 1978; Mannella *et al.*, 1998; Rizzuto *et al.*, 1998 and see Rutter & Rizzuto, 2000 for review). Furthermore, using aequorin, a fluorescent Ca^{2+} indicator, targeted to the mitochondrial matrix or intermembrane space, Rizzuto and colleagues (1993, 1998) showed that mitochondria were also functionally 'connected' to the ER and that both organelles rapidly exchanged Ca^{2+} (see Rizzuto *et al.*, 1999 and Rutter & Rizzuto, 2000 for review). Thus, in HeLa cells histamine or ATP-dependent Ca^{2+} release from 'IP_3 Ca^{2+} stores' induced a strong increase in the $[Ca^{2+}]_m$ and the rise in $[Ca^{2+}]_i$ was far larger in the vicinity of the mitochondria than in the rest of the cytoplasm (Rizzuto *et al.*, 1993, 1998; Wang *et al.*, 2000 and see Rutter & Rizzuto, 2000 for review). These results suggested that mitochondria and ER might be both physically and functionally interconnected and that Ca^{2+} released from the ER would locally expose mitochondria to microdomains of high $[Ca^{2+}]_i$ (Rizzuto *et al.*, 1993, 1998; Csordas *et al.*, 1999 and Wang *et al.*, 2000). These close contacts and rapid exchanges of Ca^{2+} between ER and mitochondria could serve several purposes. Firstly, they would enable localised increase in $[Ca^{2+}]_i$ and site targeted stimulation of the mitochondrial function therefore locally priming the organelle to increased metabolic demand. Secondly, this interaction between ER and mitochondria would also influence the shape and velocity of Ca^{2+} waves as mitochondrial Ca^{2+} uptake could promote Ca^{2+} release from the stores by buffering Ca^{2+} close to the channel mouth and reducing the Ca^{2+}-dependent channel inhibition (Jouaville *et al.*, 1995). On the other hand, mitochondria could take part in the propagation of Ca^{2+} waves (see Kostyuk & Verkhratsky, 1995b and Rutter & Rizzuto, 2000 for review).

5. Calcium extrusion through the plasma membrane

Two major systems for Ca^{2+} extrusion are present in most eukaryotic cells. The first one is the plasma membrane Ca^{2+}-ATPase (PMCA, see below section 5.1), which hydrolyses ATP to transport Ca^{2+}, and the second one is the Na^+/Ca^{2+} exchanger (NCX, see below section 5.2) that uses the energy of the inwardly directed Na^+ gradient to export Ca^{2+}.

5.1. The plasma membrane calcium ATPase

The earlier works, mainly on red blood cells and dialysed squid giant axon, suggested the involvement of an ATP-dependent Ca^{2+} extrusion mechanism especially at low $[Ca^{2+}]_i$ (Schatzmann, 1966; Schatzmann & Vincenzi, 1969; Sarkadi *et al.*, 1978; Baker & DiPolo, 1984 and see Schatzmann, 1982; Carafoli, 1987 for review). This result was confirmed with the isolation of the plasma membrane Ca^{2+}-ATPase (PMCA, Schatzmann, 1966; Schatzmann & Vincenzi, 1969; Baker & Glitsch, 1973; DiPolo, 1974, DiPolo, 1978; Baker & DiPolo, 1984 and see Schatzmann, 1982; Garraham & Rega, 1990; Carafoli, 1994 for review). Since its discovery, PMCA has been shown to belong to a large family of proteins encoded by four main isogenes and to be expressed in almost all cell types, where it plays a major role in Ca^{2+} homeostasis (see Schatzmann, 1982; Miller, 1991, Carafoli, 1994 and Guerini *et al.*, 1998 for review).

5.1.1. PMCA function

The PMCA, which is related to SERCA pumps (see above section 4.2.2.1 and Carafoli, 1994; Carafoli & Stauffer, 1994; Guerini *et al.*, 1998 for review), is activated by an elevation in $[Ca^{2+}]_i$ (apparent $K_{Ca} \leq 1\mu M$, see Downes & Michell, 1981) and extrudes Ca^{2+} out of the cytosol upon ATP hydrolysis with a stoichiometry of 1:1 (see Schatzmann, 1982 for review). The rate of Ca^{2+} transport through PMCA is a saturable function of $[Ca^{2+}]_i$ with an EC_{50} between 0.1 and 30 μM depending on the cell type, the pH and the CaM content (see Table I in Garraham & Rega, 1990). An excess of extracellular Ca^{2+} has been shown to have an inhibitory effect on PMCA activity presumably through a low affinity binding to the site where Ca^{2+} leaves the pump after translocation (see Schatzmann, 1982 and Garraham & Rega, 1990 for review). Among the P-type pumps, PMCA exhibits a unique feature in that multiple pathways,

particularly a direct interaction with CaM (see below section 5.1.3), regulate its activity (see Carafoli, 1994 and Carafoli & Stauffer, 1994 for review).

Experiments using purified PMCA inserted in liposome and whole erythrocytes demonstrated that the pump is an obligatory exchanger for proton (Waisman *et al.*, 1981a, b, c; Rossi & Schatzmann, 1982; Niggli *et al.*, 1982; Smallwood *et al.*, 1983 and Milanick, 1990). Although early results suggested that the transport was electroneutral (exchange ratio of $1Ca^{2+}:2H^{+}$ - Niggli *et al.*, 1982) further experiments demonstrated that in fact the exchange was electrogenic *i.e.* 1 proton was transported in exchange of 1 Ca^{2+} (Rossi & Schatzmann, 1982; Gassner *et al.*, 1988; Romero & Ortiz, 1988; Salvador *et al.*, 1998 and see Carafoli, 1994 for review). The necessity for proton as counter-ions in the Ca^{2+} transport was further supported by experiments where the activity of PMCA was tested against the extracellular pH (*e.g.* DiPolo & Beauge, 1982; Niggli *et al.*, 1982; Yu *et al.*, 1994 and Xu *et al.*, 2000). These experiments suggested that extracellular alkalisation decreases the rate of Ca^{2+} transport through PMCA with a half maximal inhibition for a pH value of 8.5-8.8 (Niggli *et al.*, 1982 and Xu *et al.*, 2000). More recently, direct measurements of the proton concentration either at the surface of the plasma membrane or in the cytoplasm confirmed the involvement of protons as counter-ions in the Ca^{2+} extrusion and suggested that PMCA activation resulted in an acidification of the cytosol (Chesler & Kaila, 1992; Schwiening *et al.*, 1993; Daugirdas *et al.*, 1995; Khodorov *et al.*, 1995 and Trapp *et al.*, 1996).

Following its activation by CaM (see below section 5.1.3), PMCA exhibits a high affinity for Ca^{2+}, which enables it to work efficiently at low $[Ca^{2+}]_i$ and therefore most authors agree that PMCA plays a role in the regulation of resting $[Ca^{2+}]_i$ and the extrusion of small rises in $[Ca^{2+}]_i$ (DiPolo & Beauge, 1982, 1983, 1984; Benham *et al.*, 1992; Schwiening *et al.*, 1993; Trapp *et al.*, 1996; Fierro *et al.*, 1998 and see Carafoli, 1987, 1994; Miller, 1991 for review). It was suggested that Ca^{2+} extrusion *via* PMCA would start in parallel with the rise in $[Ca^{2+}]_i$ and that during $[Ca^{2+}]_i$ rises from 0.2 to 0.5 μM, the extrusion rate would increase from ≈ 0.3 to 5 μM s^{-1} per cell volume (see Tepikin *et al.*, 1991 and see Kostyuk & Verkhratsky, 1995c for review). In most neurones, because of its high affinity for Ca^{2+} and saturable transport capacity, PMCA was suggested to play only a minor role in the clearance of Ca^{2+} and to be inoperative in the extrusion of micromolar rise in $[Ca^{2+}]_i$ (DiPolo & Beauge, 1983, 1984; Benham *et*

al., 1992; Schwiening *et al.*, 1993; Trapp *et al.*, 1996; Fierro *et al.*, 1998 and see Miller, 1991 for review). Finally, it was proposed that Ca^{2+} extrusion through PMCA was fast with kinetics comparable to those of the Ca^{2+} transient suggesting that PMCA activation could substantially influence the characteristics of a Ca^{2+} response.

5.1.2. PMCA structure

The primary structure of PMCA (130 to 150 kDa) was originally deduced from the *c*DNA isolated from rat brain (Shull & Greeb, 1988 and Greeb & Shull, 1989) and human teratoma cell (Verma *et al.*, 1988). From the cloning studies, PMCA was predicted to contain 10 transmembrane domains, three main cytosolic regions representing the major part of the protein (80%) and C- and N-terminal regions oriented in the cytosol (see Carafoli, 1994; Carafoli & Stauffer, 1994; Guerini *et al.*, 1998 for review). The first cytosolic domain contains one of the two sequences that bind acidic phospholipids (Zvaritch *et al.*, 1990), however its function remains unclear. The second cytosolic region represents the largest domain of the protein and consists of a ATP/FITC binding site and the active site with the aspartic residue involved in the phosphoenzyme formation (see Carafoli, 1994 and Carafoli & Stauffer, 1994 for review). The third region, the C-terminal tail, is characteristic of PMCA and corresponds to the major 'regulatory domain'. It consists of consensus sites for phosphorylation by PKA and PKC and contains binding sites for Ca^{2+}, phospholipids and CaM (see Carafoli, 1994; Carafoli & Stauffer, 1994; Guerini *et al.*, 1998 for review). The CaM binding region, which consists of two domains (A and B), was shown to interact with a region close to the active site in the large central loop and to be involved in the autoinhibition of the protein (see below section 5.1.3 and Carafoli, 1994; Carafoli & Stauffer, 1994 and Guerini *et al.*, 1998 for review). Several sites of proteolysis by calpain have also been identified in the C-terminal region and were linked to the cleavage, in a CaM-dependent and independent manner, of part of the C-terminal tail. The C-terminal region contains several acidic residues that have been shown to retain PMCA in the ER when they are exposed by proteolysis of the protein (Zvaritch *et al.*, 1995 and see Carafoli, 1994; Guerini *et al.*, 1998 for review). Finally, there are several reports suggesting that PMCA can form oligomers that might be of relevance for PMCA function *in vivo* (Cavieres, 1984; Kosk-Kosicka & Bzdega, 1988;

Vorherr *et al.*, 1991) and more recent studies suggested that PMCA might be found as a CaM-dependent monomer or as a CaM-independent oligomer (Sackett & Kosk-Kosicka, 1996).

5.1.3. Isoform specific regulation and tissue distribution of PMCA

Molecular studies have demonstrated that PMCA is encoded by four main isogenes (pmca-1 to -4) (Verma *et al.*, 1988; Shull & Greeb, 1988; Greeb & Shull, 1989; Strehler *et al.*, 1990; Burk & Shull, 1992; Keeton *et al.*, 1993 and see Carafoli, 1994, 1996; Guerini *et al.*, 1998 for review). Through alternative splicing of the primary transcripts, these isogenes produce more than 20 additional isoforms resulting in a complex nomenclature (see Carafoli, 1994 for review). A comparison of the isoform sequences has demonstrated that PMCA isoforms are highly homologous (≈ 75 %) except in their N- and C-terminal regions.

The site in the central domain interacting with the CaM binding site has been shown to differ between isoforms resulting in variations in the interaction with the 'inhibitory' domain and therefore in an isoform-specific level of activation (Falchetto *et al.*, 1991 and see Carafoli, 1994; Carafoli & Stauffer, 1994; Guerini *et al.*, 1998 for review).

The most important feature of PMCA activity is its regulation by CaM, which has formal similarities with the SERCA-phosholamban interaction (see above section 4.2.2.3 and see Schatzmann, 1982; Carafoli, 1987, 1994; Garraham & Rega, 1990 for review). In the resting state PMCA is characterised by a low affinity for Ca^{2+} ($K_m \approx$ 10-20 μM). In contrast, PMCA activation by CaM has been shown to increase both the Ca^{2+} affinity ($K_m \approx 0.5$ μM) and the maximal velocity of the Ca^{2+} transport (≈ 10-fold - Gopinath & Vincenzi, 1977; Jarrett & Penniston, 1977; Gmaj *et al.*, 1982 and see Schatzmann, 1982; Carafoli, 1987, 1994 and Garraham & Rega, 1990 for review). In fact, CaM activates PMCA by direct interaction with a stoichiometry of 1:1 and in a Ca^{2+}-dependent way (Ca^{2+}-CaM, $K_d \approx 1$ nM - Niggli *et al.*, 1979 ; Graf & Penniston, 1981; Hinds & Andreasen, 1981 and see Schatzmann, 1982; Carafoli, 1987, 1994 and Strehler *et al.*, 1991 for review). Extensive studies have suggested that in the resting state (low $[Ca^{2+}]_i$) the CaM binding site interacts with the active site and reduces PMCA activity (see Carafoli, 1994 for review). When $[Ca^{2+}]_i$ is increased, CaM binds Ca^{2+} and

subsequently interact with its binding site on the Ca^{2+} pump. The Ca^{2+}-CaM/PMCA complex will induce a conformational change of the protein and the C-terminal tail will swing away from the centre of the protein, unmask the active site and therefore relieve the autoinhibition (see Carafoli, 1994 for review).

This CaM binding site corresponds to a region of high isoform variability and following alternative splicing the subdomain B (see above section 5.1.2) has either a different sequence or is absent (Strehler *et al.*, 1989 and Heim *et al.*, 1992). The variability in the CaM binding site would result in changes of PMCA affinity for CaM and therefore different level of modulation could be observed. Thus, some isoforms exhibit a very high affinity (*e.g.* PMCA-2) for CaM and are thought to be permanently associated to CaM and constitutively active (see Carafoli, 1994 for review). The activation of calpain, an intracellular protease, has been shown to cleave at several sites the CaM binding domain and therefore to affect the CaM-dependent activity of PMCA (Wang *et al.*, 1988 and see Carafoli & Stauffer, 1994 and Carafoli, 1994). At least in the erythrocytes, calpain was shown to selectively target PMCA and was therefore suggested to be an irreversible PMCA activator (Salamino *et al.*, 1994 and see Carafoli & Stauffer, 1994 for review).

The Ca^{2+} pump also contains amino acid residues (in the central cytosolic domain and next to the CaM binding site - see Strehler *et al.*, 1991 for review) that are phosphorylated by PKA (Caroni & Carafoli, 1981 and see Carafoli & Stauffer, 1994 and Carafoli, 1994 for review). The phosphorylation sites for PKA have been shown to be differently located or even absent depending on the isoform resulting in a differential regulation of the protein isoforms (James *et al.*, 1989 and Strehler *et al.*, 1989).

Protein kinase C activates PMCA in a similar way to CaM with the only difference that the removal of the autoinhibition results from the phosphorylation of amino acid residues within the CaM binding site (Wang *et al.*, 1991 and see Carafoli, 1994 for review). The effect of PKC was suggested to be smaller, competitive to that of CaM and more importantly to dependent on the PKC isoform and on the lipids associated with the pump (Wang *et al.*, 1991 and see Carafoli, 1994 for review). Although, PKA or PKC appear to have different sites of action and mechanisms of activation, they both induce an increase of the Ca^{2+} affinity and of the maximal rate of Ca^{2+} transport but to a lower extent than CaM (see Carafoli, 1994 for review).

The N-terminal region is poorly conserved and of different length among PMCA isoforms. This region was suggested to be implicated in the phospholipid sensitivity of the Ca^{2+} pump (Zvaritch *et al.*, 1990 and see Carafoli, 1994). In the absence of CaM, PMCA is activated (increase in Ca^{2+} affinity and pump rate) by acidic phospholipids and long-chain polyunsaturated fatty acid (Ronner *et al.*, 1977 and see Carafoli, 1987, 1994; Carafoli & Stauffer, 1994 for review). Since PMCA is embedded in the plasma membrane, which contains high concentrations of acidic phospholipids, the Ca^{2+} pump would be, at least partially, in a permanent active state. In fact, experiments on the reconstituted pump have suggested that the phospholipid environment would account for 50% of the enzyme maximal stimulation (Niggli *et al.*, 1981 and see Carafoli, 1987, 1994 and Carafoli & Stauffer, 1994 for review). The phospholipid composition of the plasma membrane varies between cell types and during cellular activity. One can therefore suppose that such variations in the phospholipid content would have an effect on the PMCA activity. However, so far the exact mechanism by which phospholipids activate the Ca^{2+} pump remains unclear (see Carafoli, 1987, Carafoli, 1994 and Carafoli & Stauffer, 1994 for review).

The different isoforms were shown to have a tissue-specific expression. Thus, PMCA-1 and 4 are thought to be expressed in almost all tissues in equivalent amount whereas isoform 2 and 3 expression was only observed in specialised tissues (muscle and brain - Stauffer *et al.*, 1993 and see Carafoli, 1994 and Carafoli & Stauffer, 1994; Guerini *et al.*, 1998 for review). Therefore PMCA-1 and 4 are often considered as the 'house-keeping' isoforms for general Ca^{2+} pumping functions and PMCA-2 and 3 as specialised Ca^{2+} pumps. Moreover, the expression pattern in neuronal and non-neuronal cells shows remarkable differences. Firstly, while neurones express almost all splice forms in non-neuronal cells only the main splice variants are expressed (see Carafoli & Stauffer, 1994 for review). Secondly, along with the 'house-keeping' isoform, specific regions of the brain express either PMCA-2 or PMCA-3 (Borke *et al.*, 1989; Brandt & Neve, 1992; Stauffer *et al.*, 1995, Stauffer *et al.*, 1997; Filoteo *et al.*, 1997). Finally, in neurones, PMCA isoforms are not only expressed in the soma, but also in the dendrites and nerve terminals (Stauffer *et al.*, 1997 and Juhaszova *et al.*, 2000).

Although no selective inhibitor for PMCA has been isolated, several pharmacological tools are available to inhibit its activity. Similarly to all P-type pumps,

orthovanadate and lanthanides inhibit PMCA (Karlish *et al.*, 1979; Luterbacher & Schatzmann, 1983 and Garraham & Rega, 1990 for review). Fluorescein and its analogues (*e.g.* eosin, carboxyeosin) have been shown to be potent inhibitors of PMCA (Bassani *et al.*, 1995; Park *et al.*, 1996 and Fierro *et al.*, 1998) by interacting with the ATP/FITC binding site of the protein (Gatto & Milanick, 1993, 1995 and see Schatzmann, 1982; Garraham & Rega, 1990 for review). Unfortunately, the inhibition of the ATPase activity with vanadate or lanthanum is not selective and fluorescein analogues have been shown to also inhibit SERCA (Bassani *et al.*, 1995). Calmodulin inhibitors (*e.g.* calmidazolium, trifluoperazine) have also been proposed to inhibit PMCA but only partially and with numerous secondary effects (Vincenzi *et al.*, 1982; Adunyah *et al.*, 1982; Gietzen, 1983 and Benham *et al.*, 1992). Finally, another commonly used way to inhibit the Ca^{2+} pump is extracellular alkalisation (*i.e.* reduction in the availablity of protons - $IC_{50} \approx 2$ nM - Xu *et al.*, 2000). This process takes advantage of the obligatory counter-transport of proton during Ca^{2+} extrusion (see above section 5.1.1 and Niggli *et al.*, 1982; Carafoli, 1988; Benham *et al.*, 1992; Park *et al.*, 1996 and Xu *et al.*, 2000). In most of the cell types where the role of PMCA in $[Ca^{2+}]_i$ regulation was tested, the inhibition of the Ca^{2+} pump resulted in delays in the recovery of induced Ca^{2+} transients (*e.g.* Benham *et al.*, 1992; Schwiening *et al.*, 1993; Daugirdas *et al.*, 1995; Park *et al.*, 1996; Herrington *et al.*, 1996; Khodorov *et al.*, 1995; Trapp *et al.*, 1996 and Fierro *et al.*, 1998) and some authors also reported a rise in resting $[Ca^{2+}]_i$ (*e.g.* Benham *et al.*, 1992).

5.2. The sodium/calcium exchanger

The Na^+/Ca^{2+} exchanger (NCX) represents another major Ca^{2+} extrusion system and was first described in cardiomyocytes (Reuter & Seitz, 1968) and shortly after in squid giant axon (Baker *et al.*, 1969 and see Blaustein & Lederer, 1999; Philipson & Nicoll, 2000 for review). Following the cloning of NCX (Nicoll *et al.*, 1990), extensive studies, mainly in excitable cell, have determined the structure of the protein, identified several isoforms with various tissue distribution and characterised different regulatory pathways of NCX activity (see Blaustein & Lederer, 1999 for review).

5.2.1. NCX structure

The primary structure of NCX (≈ 110 kDa) has been deduced based on the hydropathy profil of the protein sequence and was initially thought to have 11 transmembrane domains (TM) with short extracellular N-terminal and intracellular C-terminal domains and a large cytoplasmic loop representing about half of the whole protein (Nicoll *et al.*, 1990 and see Blaustein & Lederer, 1999 for review). However, more recent experiments using cysteine mutation suggested that NCX would rather consist of 9 TM with a large intracellular loop between TM 5 and 6 (Cook *et al.*, 1998; Iwamoto *et al.*, 1999; Nicoll *et al.*, 1999 and see Philipson & Nicoll, 2000; Shigekawa & Iwamoto, 2001 for review). Both the C- and N-terminal halves of the membrane domains contain repeat sequences (α1 and α2, respectively) conserved in all NCX isoforms and forming reentrant membrane loops (Schwarz & Benzer, 1997 and see Shigekawa & Iwamoto, 2001 for review). The intracellular loop contains the regulatory sites for NCX, particularly the Na^+-dependent inactivation site, the Ca^{2+} regulatory site and consensus phosphorylation sequences (see Blaustein & Lederer, 1999; Philipson & Nicoll, 2000; Shigekawa & Iwamoto, 2001 for review). Finally, NCX has been proposed to contain a binding site for an 'exchanger inhibitory peptide' (XIP), which is thought to induce a conformational change of the protein and the inhibition of the Ca^{2+} transport (see Blaustein & Lederer, 1999 and Philipson & Nicoll, 2000 for review).

To date, three isoforms of NCX (NCX-1 to -3) with different tissue distribution and high sequence homology have been isolated and cloned (Philipson *et al.*, 1988; Nicoll *et al.*, 1990, Li *et al.*, 1994 and Nicoll *et al.*, 1996). The main region of divergence is the regulatory intracellular loop suggesting that the different isoforms will exhibit differential modulation. The NCX-1 isoform was first cloned from canine cardiac myocytes (Philipson *et al.*, 1988 and Nicoll *et al.*, 1990). The NCX-2 and NCX-3 isoforms are more ubiquitously expressed with the isoform 2 being mainly neuronal (Nicoll *et al.*, 1990; Li *et al.*, 1994; Nicoll *et al.*, 1996 and see Blaustein & Lederer, 1999 for review). More recently, a new protein involved in the transport of Ca^{2+} has been isolated from retinal and brain tissues and was shown to depend on both the Na^+ and K^+ gradient (Schnetkamp *et al.*, 1989; Reilander *et al.*, 1992; Tsoi *et al.*, 1998 and see Blaustein & Lederer, 1999; Philipson & Nicoll, 2000 for review).

The NCX has been shown to be as largely expressed in muscular cells and in neurones however these two tissues exhibit very different Ca^{2+} signalling. Regarding NCX, the explanation for these differences in the $[Ca^{2+}]_i$ regulation might arise from the expression of different isoforms especially if one considers that, so far, more than 30 members of the NCX family have been identified and that these differ mainly in the structure of their regulatory intracellular loop (see Blaustein & Lederer, 1999 for review).

5.2.2. NCX function

The NCX transports Ca^{2+} in exchange of Na^+ using the energy of the Na^+ gradient set by the ATP-dependent Na^+/K^+-pump and transports 1 Ca^{2+} for at least 3 Na^+ (Baker & DiPolo, 1984; Reeves & Sutko, 1983; Reeves & Hale, 1984; Wier, 1990 and see Blaustein & Lederer, 1999 for review). The activity of NCX is thought to be determined by the transmembrane Na^+ and Ca^{2+} gradients and the membrane potential of the cell (Baker & DiPolo, 1984; Reeves & Sutko, 1983; Reeves & Hale, 1984; Wier, 1990 and see Blaustein & Lederer, 1999 for review). Since, Ca^{2+} transport through NCX is thought to induce the net movement of one positive charge (+ve), NCX was proposed to be electrogenic (Baker & DiPolo, 1984; Reeves & Sutko, 1983; Reeves & Hale, 1984; Wier, 1990 and see Blaustein & Lederer, 1999 for review). Finally, another key feature of NCX is its ability to transport Ca^{2+} either out of or into a cell depending on the ionic gradients and the membrane potential.

From the earlier studies (Baker & Glitsch, 1973 and DiPolo, 1973, 1974), it has been suggested that NCX activity is regulated by ATP through a Ca^{2+}-dependent phosphorylation (DiPolo & Beauge, 1987) resulting in an increase in the affinity for internal Ca^{2+} and external Na^+ (Blaustein & Santiago, 1977 and see Blaustein & Lederer, 1999; Philipson & Nicoll, 2000 for review). Thus in the presence of ATP, the half maximal activity of NCX was observed for a $[Ca^{2+}]_i \approx 0.75$ μM instead of 8 μM and for 50 mM instead of ≈ 140 mM extracellular Na^+. It was further suggested that Ca^{2+} itself could also regulate NCX activity by binding (not transport) to a high affinity regulatory site and that this binding was necessary for the Ca^{2+} transport and resulted in an increased turn-over of the exchanger (DiPolo, 1979; Allen & Baker, 1985; Condrescu *et al.*, 1995 and see Blaustein & Lederer, 1999 for review). NCX exhibits a

strict dependence on $[Na^+]$ and especially on the Na^+ gradient. Thus a decrease in the extracellular $[Na^+]$ impairs Ca^{2+} extrusion while an increase in intracellular $[Na^+]$ would induce Ca^{2+} influx (see Blaustein & Lederer, 1999 and Philipson & Nicoll, 2000 for review). Intracellular sodium was proposed to elicite dual effects either Ca^{2+} extrusion (*i.e.* Na^+ influx) or time dependent-inactivation of NCX depending on the intracellular $[Na^+]$ and the level of regulatory Ca^{2+} (Hilgemann *et al.*, 1992; Matsuoka & Hilgemann, 1994 and see Blaustein & Lederer, 1999; Philipson & Nicoll, 2000 for review). This difference in the effects of intracellular Na^+ was suggested to underlie two different Na^+ binding sites. Thus, Na^+ binding to its transport site on NCX would initiate the Na^+/Ca^{2+} exchange whose direction will depend on the respective $[Ca^{2+}]_i$ and $[Na^+]$ whereas, Na^+ has been suggested to bind to a site on the large intracellular loop and thereby to induce an inhibitory conformational change of the protein structure (see Blaustein & Lederer, 1999 and Philipson & Nicoll, 2000 for review). Finally, the activity of NCX is also modulated by phosphorylation processes involving protein kinases (DiPolo & Beauge, 1991; DiPolo & Beauge, 1998; Iwamoto *et al.*, 1995, 1996; Fan *et al.*, 1996 and see Blaustein & Lederer, 1999 for review).

So far no specific inhibitor for NCX has been isolated, although compounds known to affect the activity of other proteins have been shown to posses inhibitory activity (*e.g.* amilorides analogues, general anaesthetics and verapamil). However, because of the high dependence of the Ca^{2+} transport on $[Na^+]$ (K_d = 2-50 mM - Allen & Baker, 1986 and DiPolo & Beauge, 1988) the most effective way to inhibit NCX is the substitution of extracellular Na^+ with non transported ions like lithium, choline or N-methyl D-glucamine (NMDG).

5.2.3. NCX regulation of intracellular calcium in neurones

The importance of NCX, as a regulatory mechanism for resting $[Ca^{2+}]_i$ and for Ca^{2+} extrusion after neuronal excitation, appears to vary depending on the cell type. Thus, in peripheral neurones, Na^+ removal from the extracellular medium did not appreciably affect the regulation of $[Ca^{2+}]_i$ (dorsal root ganglion neurones - Thayer & Miller, 1990; Duchen *et al.*, 1990 and Benham *et al.*, 1992), whereas in central neurones it was shown both to significantly perturb the recovery phase from depolarisation-induced Ca^{2+} transient and sometimes to increase resting $[Ca^{2+}]_i$ (rat brain synaptosomes

- Taglialatela *et al.*, 1990a, b; cultured hippocampal neurones - Segal & Manor, 1992; cultured cerebellar granule cells - Kiedrowski *et al.*, 1994). Most authors agree that, because of its low affinity for Ca^{2+}, NCX would mainly be active in the Ca^{2+} extrusion of large rise in $[Ca^{2+}]_i$ (>1μM - Benham *et al.*, 1992 and Fierro *et al.*, 1998) and it was suggested that NCX and PMCA might work in a complementary way. Thus, PMCA would control resting $[Ca^{2+}]_i$ and extrude Ca^{2+} during rises in $[Ca^{2+}]_i$ too low to activate NCX, while NCX would be responsible for the extrusion of larger $[Ca^{2+}]_i$ when PMCA is saturated. Some interesting aspects of NCX activity were observed in cerebellar granule cells where the inhibition of NCX was shown to potentiate glutamate-induced neurotoxicity (Mattson *et al.*, 1989 and Andreeva *et al.*, 1991). On the other hand, because of the reversibility of the Na^+/Ca^{2+} exchange, NCX could transiently amplify the rise in $[Ca^{2+}]_i$. Thus, during glutamate exposure, Na^+ influx through NMDA receptor was suggested to increase the intracellular $[Na^+]$ to value as high as 60 mM close to the membrane at which concentration NCX could function in the reverse mode (Kiedrowski *et al.*, 1994). Finally, Blaustein (1988b) suggested that, in nerve terminals, NCX could potentiate Ca^{2+} influx during the rising phase of an action potential while it would promote Ca^{2+} extrusion during the repolarisation and afterhyperpolaristion phase (Blaustein, 1988b and see Miller, 1991 for review).

6. Rat sympathetic neurones and intracellular calcium

The superior cervical ganglion (SCG) is part of the sympathetic chain of paravertebral ganglia. Neurones within SCG receive cholinergic inputs from the cervical region of the spinal cord and the noradrenergic postganglionic fibres inervate viscera such as the heart, abdominal organs and structures in the head such as eyes, salivary glands and blood vessels. In rat sympatheic neurones, the stimulation of nAChR following synaptic input would generate excitatory postsynaptic potential that in turn might induce plasma membrane depolarisation and lead to the activation of VACC.

In rat SCG neurones, nAChR have been demonstrated to be permeable to Ca^{2+} (Trouslard *et al.*, 1993; Rogers & Dani, 1995 and Rogers *et al.*, 1997) and their activation was shown to induce a substantial rise in $[Ca^{2+}]_i$ (Trouslard *et al.*, 1993). On

the other hand, SCG neurones express both on the soma and dendrites mainly N-type Ca^{2+} channels (Regan *et al.*, 1991; Plummer *et al.*, 1989; Hirning *et al.*, 1988 and Delmas *et al*, 2000) but L-type Ca^{2+} channels along with other channel subtypes (P-, Q- and R-types) have also been shown to be present (Delmas *et al*, 2000). Numerous studies carried out on SCG neurones have demonstrated that N-type Ca^{2+} channels are modulated by G-protein coupled receptors such as mACh and α_2-adrenergic receptors (see Hille, 1994; Dolphin *et al.*, 1998 for review). Both the characteristics of N-type Ca^{2+} channels and their modulation have been shown to be different in the soma and dendrites of SCG neurones (Delmas *et al.*, 2000) and one would expect different Ca^{2+} signals depending on the site of the Ca^{2+} entry.

An elevation of $[Ca^{2+}]_i$ in SCG neurones was shown to activate two classes of Ca^{2+}-dependent K^+ channels (large 'BK' and small 'SK' conductances, Smart, 1987 and Selyanko, 1996, respectively), a Ca^{2+}/PKC-dependent Cl^- channels (Marsh *et al.*, 1995) and to inhibit the M-type voltage-activated K^+ channels (Selyanko & Brown, 1996). By modulating these ionic conductances, intracellular Ca^{2+} was shown to have significant effects on the excitability of SCG neurones (Tokimasa & North, 1984; Smart, 1987; Brown, 1990; Davies *et al.*, 1996; Selyanko, 1996 and see Marsh *et al.*, 2000 for review). Although, the mechanisms underlying neuronal excitability in SCG have been extensively studied and the involvement of intracellular Ca^{2+} as a regulatory factor demonstrated, little is known about the processes responsible for the control of $[Ca^{2+}]_i$ in these neurones. The few studies on the regulation of $[Ca^{2+}]_i$ focused on the role of the ER and it has been demonstrated that SCG neurones posses Ca^{2+} stores that were both sensitive to caffeine and selectively blocked by high ryanodine concentrations (Thayer & Miller, 1988 and Hernandez-Cruz *et al.*, 1995). It was further demonstrated that Ca^{2+} influx through VACC was not amplified or at least to a low degree by Ca^{2+} release from ryanodine stores (Thayer & Miller, 1988 and Hernandez-Cruz *et al.*, 1995, 1997).

Since Ca^{2+} represents a key element in cellular physiology and particularly appears to modulate the excitability of SCG neurones, it was important to understand how $[Ca^{2+}]_i$ is controlled and which systems are involved in its regulation. The aim of the present study was to determine which Ca^{2+} homeostatic systems are functional in SCG neurones and how they might interact to regulate $[Ca^{2+}]_i$.

Variations in $[Ca^{2+}]_i$ were mainly induced by membrane depolarisation and the activation of VACC. The first step was therefore to determine the type of VACC responsible for the Ca^{2+} influx (see Results section 1). The properties of the depolarisation-induced Ca^{2+} transients, including their dependence on Ca^{2+} influx and the kinetics of their recovery, were then determined (see Results section 1) along with the Ca^{2+} buffering capacity in the soma of sympathetic neurones (see Results section 2). Since in most cell types, intracellular stores have been shown to participate in the control of $[Ca^{2+}]_i$, the next step was to investigate the role of mitochondria (see Results section 3) and the of ER (see Results section 4) as regulatory systems for $[Ca^{2+}]_i$. Ultimately, Ca^{2+} is extruded from the cytoplasm and PMCA and NCX, the two major Ca^{2+} extrusion systems, have been shown to be involved in this process. Thus, the role of PMCA (see Results section 5) and of NCX (see Results section 6) in the clearance of Ca^{2+} transients was determined. Finally, between periods of cellular activity, $[Ca^{2+}]_i$ is tightly maintained at a low level (50-100 nM). Therefore, the last section of the work presented here investigates which mechanisms are involved in the maintenance of resting $[Ca^{2+}]_i$ (see Results section 7).

Chapter II

Materials and Methods

1. Tissue Culture

Superior cervical ganglion (SCG) neurones were isolated from Sprague-Dawley rats and cultured following a method described by Fernandez-Fernandez *et al.* (1999).

1.1. Dissection of rat superior cervical ganglion

15- to 17-day-old male Sprague-Dawley rats were killed by CO_2 asphyxiation and decapitated. The SCG were removed and bathed in Leibovitz L15 medium. The ganglia, cleaned from the conjunctive tissue, were washed several times in modified Hank's balanced salt solution (mHBSS; see Methods section 1.3 for details) and chopped into $\approx 1mm^2$ pieces.

The ganglion fragments were then incubated at 37°C initially with collagenase (500 U ml^{-1} for 15 min) and, after several washes in mHBSS, with trypsin type XIIs (1 mg ml^{-1} for 30 min). The enzymes were dissolved in mHBSS supplemented with bovine serum albumin (BSA, 6 mg ml^{-1}).

The digested tissue fragments were transferred into a modified L15 medium (m-L15; see Methods section 1.3 for details), washed several times with m-L15 to stop the enzymatic digestion, and mechanically dissociated using a fire-polished Pasteur pipette (internal diameter ≈1 mm) until the medium appeared cloudy. The cell suspension was finally centrifuged at 800-1000 rpm at room temperature for 5 minutes. The supernatant was decanted and the pellet re-suspended in fresh SCG growth medium (≈ 250 µl m-L15 per ganglion).

1.2. Culture of rat sympathetic neurones

Sterile culture chambers were coated with a laminin substrate (10 µg ml^{-1} in mHBSS; see Methods section 1.3 for details) and incubated at 37°C until plating the cell suspension. These chambers, which were also used as recording chambers, consisted of glass rings (diameter 16 mm; height 3 mm; ≈ volume 500 µl) attached to borosilicate glass coverslips (BDH, 22 x 22 mm, thickness 0.13-0.17 mm) with silicone elastomer (Sylgard®, *Dow Corning*; cured at 180°C for 2 hours). Just before use, the laminin was washed with m-L15 and the cell suspension plated on to the coverslips. The chambers

were then placed into 35 mm Petri dishes and incubated at 37°C under an atmosphere of 95% O_2/5% CO_2 for 4 hours to allow the cells to adhere to the coverslip. After this time, fresh growth medium was added to the dishes up to 500 µl. The day after the culture, the growth medium was replaced with fresh medium and, generally, the cultures were used for recordings within 3 days.

1.3. Culture solutions and growth medium

The modified Hank's balanced salt solution (mHBSS) consisted of a $Ca^{2+}$and Mg^{2+}-free solution supplemented with 10 mM HEPES. The laminin substrate was stored at -20°C in stock aliquots (50 µg ml^{-1}) and diluted with mHBSS to the final concentration (10 µg ml^{-1}) the day of the culture. The SCG growth medium, or modified L-15 medium (m-L15), was prepared from Leibovitz L-15 medium supplemented with 2 mM L-glutamine, 38 mM glucose, 24 mM $NaHCO_3$, 10% heat inactivated foetal calf serum, 50 ng ml^{-1} nerve growth factor (NGF), and 50 U ml^{-1} penicillin/streptomycin. All culture reagents were supplied from *Gibco BRL* except laminin, collagenase, trypsin (*Sigma*) and NGF (*Tocris*).

2. Electrophysiological recordings

2.1. Recording apparatus

The recording chamber was transferred on to the microscope stage and superfused with external solution (see Methods section 2.4.1, *Table 1*). Electrophysiological experiments were conducted under voltage-clamp conditions, using an axopatch 200A patch-clamp amplifier (*Axon Instruments*), both in the perforated patch configuration (Horn & Marty, 1988; Methods section 2.2.1 and *figure 1*) and in the whole-cell recording mode (Hamill *et al.*, 1981; Methods section 2.2.2 and *figure 1*). Electrophysiological experiments were carried out simultaneously with measurements of the intracellular Ca^{2+} concentration ($[Ca^{2+}]_i$, see Methods section 3) unless otherwise stated.

Recording electrodes were pulled on a vertical pipette puller (PC-10, *Narishige*) using thin-walled filamented borosilicate glass (TF150, *Clark Biomedical*). The electrode tips were fire-polished with a microforge (MF-830, *Narishige*) and, when

filled with the internal pipette solution (see Methods section 2.4.3, *Table 2*), had a 2-3 MΩ nominal resistance. The series resistance and cell capacitance were compensated prior to the recordings.

For the study of whole-cell currents, experiments were carried out in the whole-cell configuration and no Ca^{2+} indicator was added to the intracellular solution. Whole-cell currents were filtered at 1 kHz and sampled at 40 kHz using a Digidata 1200 interface (analogue-to-digital converter; *Axon Instruments*) driven by the pClamp 8 software package (*Axon Instruments*) installed on a pentium II *DELL* personal computer. Data were acquired using the pClampex 8 software and recorded on to the computer as well as with an analogue chart recorder (*Gould 2400S*).

2.2. Recording configurations

2.2.1. Perforated patch configuration

Using the whole-cell recording mode (see *figure 1*), it was not possible to carry out stable recording of $[Ca^{2+}]_i$ for more than 15-20 minutes. In this configuration, resting $[Ca^{2+}]_i$ increased and the recovery time of any changes in $[Ca^{2+}]_i$ became slower over this recording duration (see Results section 5.2). This phenomenon was certainly due to the characteristics of the whole-cell recording *i.e.* dialysis of the intracellular compartment with the pipette solution and loss of soluble components. Therefore recordings were preferably carried out in the perforated patch mode where the antibiotic amphotericin B (Rae *et al.*, 1991 and see *figure 1*) was added to the pipette solution. This compound forms pores in the plasma membrane enabling the flow of monovalent ions and therefore electrical continuity between the recording pipette and the intracellular environment. A stock solution at a concentration of 100 mg ml^{-1} was prepared daily by dissolving, through sonication (20-40 seconds), the amphotericin B in dimethylsulphoxide (DMSO). Amphotericin B was added (final concentration of 0.1-0.15 mg ml^{-1}) to the filtered (*Gelman*, 0.2 μm) pipette solution and dissolved through sonication. As DMSO perturbs the seal formation, the electrode's tip was first dipped in an antibiotic-free solution for 15-20 seconds and then the electrode was back-filled with the pipette solution containing the amphotericin B. After the formation of a 'giga-ohm seal' (>1 GΩ), the cell was kept in the cell-attached configuration (*figure 1*)

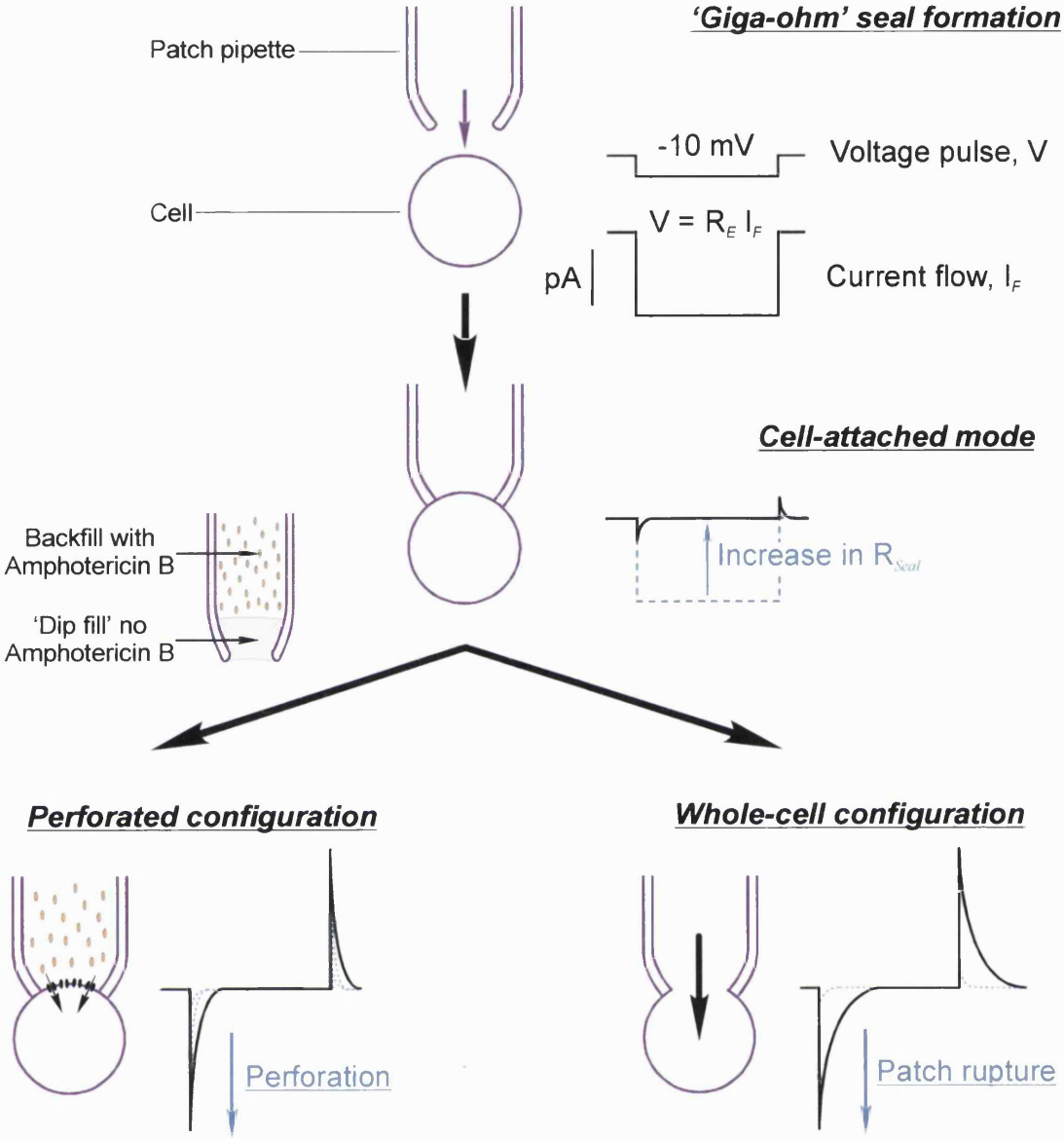

Figure 1: Patch-clamp recording configurations

A patch electrode (resistance R_E) filled with the intracellular solution is approached in contact with a cell (top panel). To follow the formation of a tight seal, a 10 mV hyperpolarising pulse (V - top panel, right) is applied using the patch amplifier and the current flowing through the electrode's tip monitored (I_F in pA - top panel, right). The current is visualised as a square signal and is based on the Ohm's law (I_F =V / R_E). As the contact between the cell and the electrode's tip become stronger (middle panel), the seal resistance increases and therefore I_F decreases (middle panel, right). A tight seal is achieved when the seal resistance reaches at least 1 giga-ohm (>1 GΩ, 'giga-ohm seal') and the recording is in the cell-attached configuration (middle panel). In the perforated patch mode (bottom panel, left), amphotericin B is added to the intracellular solution and, by the time the cell-attached mode is obtained, has diffused to the tip of the electrode. The amphotericin B molecules get progressively inserted in the membrane patch and form pores enabling electrical continuity. With time, the number of formed amphotericin pores increases and the electrical access improves (*i.e.* the resistance decreases) resulting in a larger current flow (Perforation, left panel, bottom). At the perforation equilibrium, the current flow is maximal and constant generally ≈ 1000 pA (*i.e.* the resistance is ≈ 10 MΩ). In the whole-cell configuration (bottom panel, right), a strong and short suction is applied in the cell-attached mode and the membrane patch ruptured. The electrical access is obtained by the sudden drop in the resistance (<5 MΩ) and visualised by the increase in the current flow (>1000 pA). In this configuration, there is a complete dialysis of the cell content with the intracellular solution and equilibrium is generally reached in less than 10 minutes. When relevant, the recording configuration will be illustrated by an inset in the figures of the Results Chapter.

and the membrane potential hold at -60 mV until the permeabilization reached a steady state (*figure 1*). The progress in the perforation was monitored by the slow increase in the amplitude of the transient capacity current in response to a 10 mV hyperpolarizing voltage step (*figure 1*). Usually after 10-20 minutes, a final access resistance of 10-15 MΩ was obtained. A sudden change in the size of the capacity transients normally represented the rupture of the cell membrane and therefore such cells were discarded.

2.2.2. The whole-cell configuration

After the formation of a 'giga-ohm seal' in the cell-attached mode (*figure 1*), the whole-cell configuration was obtained by applying a short and strong suction to rupture the membrane patch (*figure 1*). With this method, low resistance pathway was obtained (access resistance ≈ 5 MΩ), and therefore an improved voltage-clamp and a nearly complete dialysis of the intracellular compartment could be achieved. However, this meant also that soluble endogenous components could be lost due to dialysis. Therefore, this recording configuration was rarely used except for whole-cell currents recordings, when it was necessary to apply membrane non-permeant pharmacological agents (buffers or blockers) or to carry out the Ca^{2+} indicator calibration (see Methods section 3). In order to allow full equilibration of the intracellular content, experiments in the whole-cell mode were always started 10-15 minutes after rupture of the membrane patch.

2.3. Voltage protocols

SCG neurones were voltage-clamped at -60 mV and specific voltage protocols were designed to induce Ca^{2+} influx of different amplitude and duration. Typically, Ca^{2+} currents were elicited with a single depolarising step from the holding potential of -60 mV to +0 mV for 60 and 500 ms. Calcium currents were also elicited from -60 mV to various test potentials (between -40 and +30 mV in 10 mV increments), to determine the voltage dependence of the Ca^{2+} influx (current/voltage relationship). Depolarisation steps from -60 mV to +0mV of various durations were used as well, to induce increasing Ca^{2+} influx.

In the whole-cell configuration, the same voltage protocols as in the perforated patch-clamp mode were used. For the experiments where an accurate measurement of

the Ca^{2+} charges transfer was necessary, the amplitude of the generated Ca^{2+} currents were measured after digital subtraction of the outward current remaining during the same voltage protocol in the presence of 100 µM cadmium (a blocker VACCs).

2.4. Perfusion media and intracellular solutions

2.4.1. Composition of the extracellular solutions

Experiments were performed at 33°C and cells were continuously superfused with the extracellular medium. The standard perfusion solution (A) was a modified Krebs' solution, whose pH was buffered with HEPES and adjusted to 7.4 with sodium hydroxide (NaOH). The osmolarity of the extracellular solution was determined by the freezing point depression method using an automatic osmometer (*CamLab*) and set at ≈ 285 mosmol l^{-1} by adding mannitol when necessary (see *Table 1*).

Table 1: Composition of the extracellular solutions

	A	B	C	D	E	F	G
	Standard pH 7.4	Na^+ - free pH 7.4	Na^+ - free pH 9	Ca^{2+}-free pH 7.4	Ca^{2+}-free pH 9	Alkaline pH 9	High KCl
Na^+	140	0	0	140	140	140	90
NMDG	0	130	130	0	0	0	0
K^+	3	3	3	3	3	3	50
Mg^{2+}	1.5	1.5	1.5	6	6	1.5	1.5
Ca^{2+}	2.5	2.5	2.5	0	0	2.5	2.5
Cl^-	137	139	139	142	142	137	134
Cs^+	0	0	2	0	2	2	0
Mannitol	0	14	26	0	24	0	0
EGTA	0	0	0	0.2	0.2	0	0

All solutions contained 11 mM glucose, 10 mM HEPES, the pH and osmolarity were adjusted as mentioned in the text. The concentrations mentioned in mM take into account the ionic addition due to pH adjustment.

Generally, tetrodotoxin (TTX, *Tocris*) was added at 0.5 µM (final concentration) to eliminate the sodium currents. For the sodium-free solution (B and C), the extracellular sodium chloride (NaCl) was replaced by N-methyl D-glucamine (NMDG) and the pH adjusted with hydrochloride acid (HCl). For the Ca^{2+}-free solutions (D and E), the extracellular Ca^{2+} was omitted and the extracellular magnesium chloride ($MgCl_2$) added increased from 1.5 to 6 mM. To buffer any Ca^{2+} contamination, 200 µM EGTA was

added to the solution. For the alkaline solutions (C, E and F), the pH was adjusted to 7.4 with NaOH and then to pH 9 using caesium hydroxide (CsOH) except in solution C where the pH was adjusted to 9 with HCl. The addition of extracellular Cs^+ was without effect on membrane currents since most of the potassium currents were already blocked by the caesium-based intracellular solutions (see below Methods section 2.4.3 and *Table 2*). In solution G, used to depolarised neurones in experiments monitoring the variations in intracellular pH (see Results section 5.3), the KCl concentration was increased from 3 mM to 50 mM and the NaCl concentration reduced accordingly. The extracellular solutions were prepared to maintain as much as possible equivalent ionic concentrations. The detailed composition of the perfusion solutions is listed in *Table 1* (see previous page).

2.4.2. Perfusion system and fast application

The recording chamber was gravity fed at 10-15 ml min^{-1} with the extracellular solutions contained in 50 ml syringes. The perfusion solution was preheated to 35°C with a heating device (thermistor probe and temperature controller; *Mr. C. Courtice, School of Pharmacy, University of London*) prior to entering the recording chamber. With this system, the temperature of the bath was maintained constant at 33 ± 0.5°C. Generally, changes of the extracellular medium and drug applications were realised by switching between syringes. Thus, because of the small volume of the recording chamber (≈ 500 µl), the bath solution could be completely exchanged within 15-20 seconds. However, in some experiments a pressure ejection system or puffer (Neurophore BH-2, *Medical System Corporation*) was used to accelerate drug application or medium changes and limit the exposure to the recorded cell. Under these conditions, the perfusion medium was not recycled.

2.4.3. Composition of the intracellular solutions

The intracellular solutions were mainly caesium-based to block most of the potassium currents and therefore unmask Ca^{2+} currents and improve the space-clamp. The pH of the pipette solutions was adjusted to 7.3 with CsOH and the osmolarity set at ≈ 280 mosm l^{-1} with caesium acetate (CsAc). In the perforated patch configuration, two solutions were used with (H) or without (I) sodium to investigate the role of the

intracellular sodium in Ca^{2+} homeostasis. For the experiments carried out in the whole-cell configuration, a NMDG-based intracellular solution (J) was used and supplemented with ATP, GTP and phosphocreatine (see *Table 2* below). In this mode, 100 µM indo-1 acid (see Methods section 3.3.4 for details) was added to the pipette solution to perform measurement of $[Ca^{2+}]_i$ (see Methods section 3). Some experiments were carried out with a solution containing high intracellular Na^+ (solution K, see *Table 2*) to study the Na^+/Ca^{2+}exchanger properties and its involvement in the regulation of $[Ca^{2+}]_i$. The composition of the intracellular solutions used in the different experiments is described in more detail in *Table 2*:

Table 2: Composition of the intracellular solutions

	H	I	J	K
	Standard Cs^+-based	**Na^+ - free Cs^+-based**	**Whole-cell Cs^+-based**	**High Na^+-based**
Na^+	10	0	3.3*	140
NMDG	-	-	125	-
Mg^{2+}	3	3	3	3
Cl^-	26	26	26	28
Cs^+	133	133	30	-
Ac^-	120	110	10	115

All solutions contained 10 mM HEPES, the pH and osmolarity were adjusted as mentioned in the text. The concentrations are mentioned in mM. * Final sodium concentration after addition of (mM) 3 Na_2ATP, 0.15 Na_3GTP and 0.15 Na_2Phosphocreatine.

3. Monitoring free intracellular calcium concentration

Most of the work presented in this thesis was carried out using electrophysiological technique combined with simultaneous photometric measurements of $[Ca^{2+}]_i$. This type of experiments was carried out using indo-1 as Ca^{2+} indicator (see Methods section 3.1) and the ratiometric method (see Methods section 3.3.1) described by Grynkiewicz *et al.* (1985).

3.1. Indo-1 as a calcium indicator

Indo-1 is a dual emission fluorescent Ca^{2+} indicator, which is excited at 349 nm (peak excitation wavelength) and whose emission wavelength is dependent on the

binding of Ca^{2+}. Thus the peak emission wavelengths are 410 nm when indo-1 is saturated with Ca^{2+} and 485 nm in the absence of Ca^{2+} (Grynkiewicz *et al.*, 1985). As both the Ca^{2+}-free and Ca^{2+}-bound forms of the fluorophore emit fluorescence at different wavelengths, it is possible to use a ratiometric method to monitor $[Ca^{2+}]_i$ independently from the dye concentration and any instrumental or optical factors (see Methods section 3.3.1).

3.2. Experimental apparatus

The apparatus used to monitor intracellular Ca^{2+} is illustrated in *figure 2*. Briefly, an inverted microscope (*Nikon Diaphot*) was fitted with ultraviolet (UV) epifluorescence illumination system (75 W xenon arc lamp, *Osram*). The emitted light travelled through a quartz collector lens and a 360 nm filter (330-380 nm bandwidth). A manual shutter (Sh.) was inserted in the light path to limit the excitation of the dye to the recording periods and a field aperture (FA.) was set to reduce the excitation field to a single cell (diameter of 20 μm). Neutral density (ND.) filters were also positioned in the light pathway to reduce the intensity of the excitation light. All these precautions were taken to limit the photobleaching or denaturation of the fluorescent probe upon too long exposure to UV light and therefore to maximise the duration of the experiments. The excitation light was reflected by a 400 nm dichroic mirror (DM.) and passed through an oil-immersion fluorescent objective (UV fluor x40, numerical aperture, NA. 1.3; *Nikon*) on to the cell. The light emitted from the cell travelled back through the 400 nm dichroic mirror before being reflected by a normal mirror to the side port of the microscope where a x1 relay lens and a diaphragm, with a pinhole just greater than the cell area, were positioned. An additional 430 nm dichroic mirror split the emitted light on to two photomultipliers (PMT, *Thorn EMI QL 30*) with input filter at 407 (396-414 nm bandwidth) and 480 nm (474-487 nm bandwidth). The 407 and 480 output currents from each photomultiplier tube were converted into voltage by a home-build ratiometric amplifier (*Mr. N. Gill, UCL*), filtered at 1.6 Hz and then the 407/480 emission ratio was generated. The 407/480 ratio output (1 ratio per Volt) was acquired on to a computer using the Digidata 1200 interface (200 Hz acquisition rate) and the pClampex 8 software. However, to evaluate possible artefacts due to dye quenching, the 407 and 480 nm emission fluorescence could also be acquired.

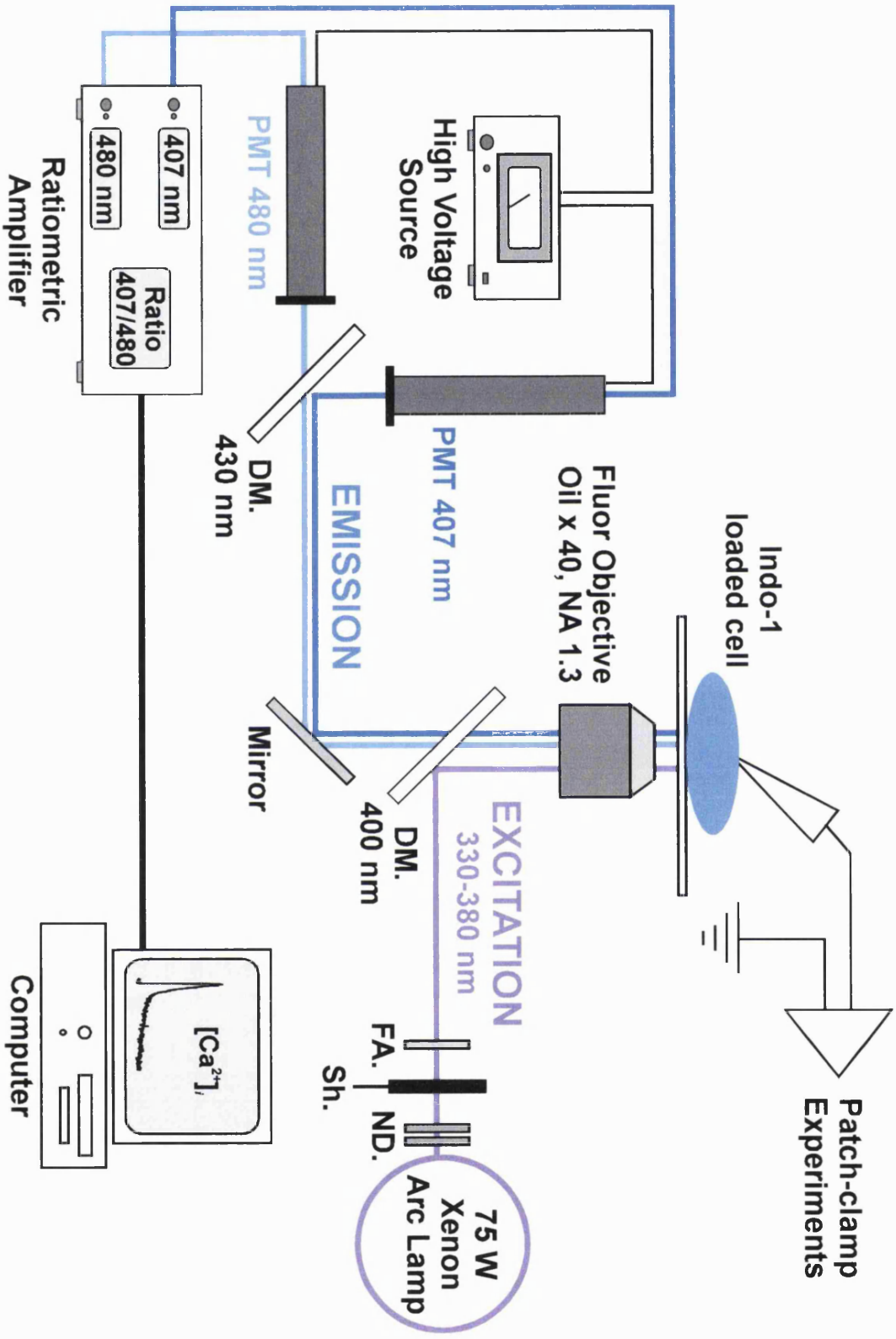

Figure 2: Experimental apparatus for calcium imaging with indo-1

Fluorescence at 407 nm and 480 nm was monitored using photomultiplier tubes. The ratiometric amplifier converted the output currents from each photomultiplier tube into voltage and subsequently into the 407/480 ratio. This fluorescence ratio was then directly recorded onto the computer and converted into $[Ca^{2+}]_i$ using the calibration parameters (full detail in the text).

The 407/480 ratio was converted online into $[Ca^{2+}]_i$ using the parameters obtained from the *in situ* calibration and the built-in equation of the Camplex 8 'Math channel' (see Methods section 3.3.1, *Equation 4*).

3.3. Measurement of intracellular calcium

3.3.1. The ratiometric method for calcium measurement

Due to the properties of indo-1 (see Methods section 3.1), it is possible to convert an emission fluorescence ratio into a $[Ca^{2+}]_i$ using the equation described by Grynkiewicz *et al.* (1985):

$$[Ca^{2+}]_i = K_d \times \left(\frac{F_o}{F_s}\right) \times \left(\frac{R - R_{min}}{R_{max} - R}\right) \quad \textit{Equation 1}$$

where R is the measured 407/480 fluorescence ratio, R_{min} is the ratio at zero Ca^{2+}, R_{max} is the ratio for a saturating $[Ca^{2+}]$, K_d is the dissociation constant for Ca^{2+} binding to indo-1 and F_o / F_s is the maximal excursion measured at 480 nm. In fact:

$$K_d \times \left(\frac{F_o}{F_s}\right) = K_d^* \quad \textit{Equation 2}$$

and *Equation 1* can be simplified as follow:

$$[Ca^{2+}]_i = K_d^* \times \left(\frac{R - R_{min}}{R_{max} - R}\right) \quad \textit{Equation 3}$$

where K_d^* represents the *apparent* dissociation constant for Ca^{2+} binding to indo-1. To be able to estimate $[Ca^{2+}]_i$, the free $[Ca^{2+}]$ needs to be related to a value of the 407/480 fluorescence ratio. To do so, it is necessary to undergo a calibration procedure (see Methods section 3.3.2) in order to determine the parameters of *Equation 3*. In the protocol designed with pClampex 8, a modified version of *Equation 3* was used and enabled the online conversion of ratio values into $[Ca^{2+}]_i$:

$$[Ca^{2+}]_i = \frac{(K_d^* \times R + K_1)}{(K_2 \times R + R_{max})} \quad \textit{Equation 4}$$

$$\text{with } K_1 = -R_{min} \times K_d^* \text{ and } K_2 = -1$$

3.3.2. Indo-1 calibration

It is easy to calibrate indo-1 *in vitro*, but as the biochemical environment may affect the properties of fluorophores, especially the ionic strength (Williams and Fay, 1990) and the protein binding characteristics (Baker *et al.*, 1994), an *in situ* calibration is far more accurate. Thus, the indo-1 fluorescence ratios were calibrated in cells using a modified "calcium calibration kit" (*Molecular Probes*). It consisted of 12 solutions of 100 mM KCl, 10 mM 3-[N-Morpholino]propane sulfonic acid (MOPS) to buffer the pH, and 0-10 mM Ca-EGTA so that the total free $[Ca^{2+}]$ ranged between 0 and 1 mM. The free $[Ca^{2+}]$ in these solutions was estimated using the published dissociation constants of H^+ and Ca^{2+} binding to EGTA (see Methods section 3.3.3). The pH and the osmolarity were adjusted to 7.2 with KOH and to 280 mosm l^{-1} with KAc, respectively. Solutions, supplemented with 100 µM indo-1 acid, were introduced into single cell under whole-cell patch-clamp configuration *via* dialysis of the cytoplasm. The cells were bathed in a Ca^{2+}-free extracellular solution (see Methods section 2.4.1, *Table 1* - solution D) at 33°C and voltage-clamped at -60 mV. For each of the 12 'Ca^{2+} solutions', the 407/480 ratio was monitored every 5 minutes until no further change was observed (30-50 minutes). The final ratio values are summarised in *Table 3* and were plotted *versus* $[Ca^{2+}]_i$ in *figure 3* (with $[Ca^{2+}]_i$ calculated in Methods section 3.3.3). The parameters R_{min}, R_{max}, and K_d^* from *Equation 3* were determined by fitting the following curve to the data points:

$$R = \left[\frac{R_{min} - R_{max}}{1 + \left(\frac{[Ca^{2+}]_i}{K_d^*} \right)^n} \right] + R_{max} \quad \textit{Equation 5}$$

with R, R_{min} , R_{max}, $[Ca^{2+}]_i$ and K_d^* as defined for *Equation 3* and *n*, the Hill slope, constrained to 1 (*i.e.* binding ratio of 1:1).

Table 3: Indo-1 407/480 emission ratio obtained for various $[Ca^{2+}]_i$

Free Ca^{2+} (μM)	Mean Ratio	n
0	0.23 ± 0.025	5
0.015	0.26 ± 0.032	6
0.034	0.29 ± 0.015	4
0.058	0.35 ± 0.031	6
0.090	0.40 ± 0.024	5
0.134	0.48 ± 0.030	7
0.2	0.50 ± 0.020	4
0.32	0.65 ± 0.035	5
0.52	0.95 ± 0.030	5
1.12	1.52 ± 0.030	6
12.2	3.30 ± 0.023	6
901.5	3.45 ± 0.032	5

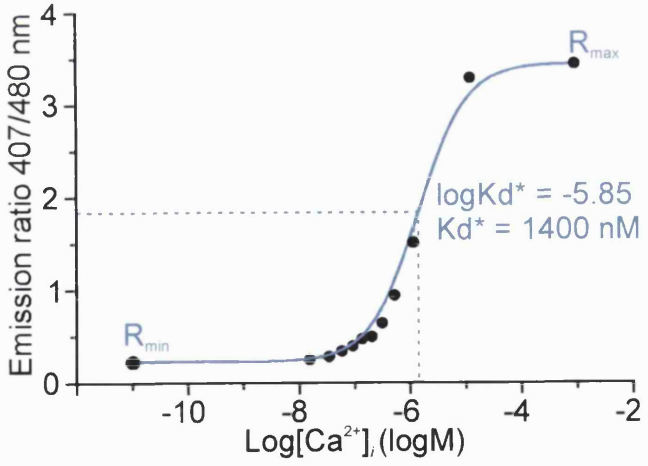

Figure 3: Calibration curve for the determination of the free intracellular Ca^{2+} concentration ($[Ca^{2+}]_i$) using the indo-1 fluorescence ratio (data as mean ± S.E.M included in the data points, see *Table 3*).

The fitted curve is illustrated in *figure 3* (previous page) and the best fit is obtained with the following parameters:

$$R_{min} = 0.23,\ R_{max} = 3.45 \text{ and } K_d^* = 1400 \text{ nM}$$

3.3.3. Calculation of free intracellular calcium

The calibration solutions contained 10 mM EGTA and increasing concentration of Ca^{2+} to produce calculated $[Ca^{2+}]$. These concentration were determined using the dissociation constant of Ca^{2+} binding to EGTA ($K_{d(EGTA)}$ = 55.8 nM) at the temperature, pH and ionic strength of the experimental conditions. The free $[Ca^{2+}]$ could then be calculated using the equation:

$$[Ca^{2+}]_{free} = K_{d(EGTA)} \times \frac{[Ca - EGTA]}{[EGTA]_{free}} \quad \textit{Equation 6}$$

Indo-1 also binds Ca^{2+} and can act as a Ca^{2+} buffer, especially at $[Ca^{2+}]$ where EGTA starts to be saturated. The $[Ca^{2+}]_i$ are then overestimated and therefore, these concentrations have to be re-calculated taking into account the presence of 100 µM indo-1. The calibration curve presented in *figure 3* uses the re-calculated values for $[Ca^{2+}]_i$.

3.3.4. Cell loading with indo-1

Indo-1 is a charged molecule and is therefore membrane non-permeant. Thus, in the whole-cell configuration, indo-1 was simply added to the intracellular solution at a concentration of 100 µM (see Methods section 2.4.3 and *Table 2* - solution J). However, indo-1 is also available as an acetoxymethyl (AM) ester form (indo-1-AM), which is able to cross the plasma membrane. Once in the cytoplasm, the ester moiety is cleaved by endogenous esterases into the anionic form, which is then retained in the cell. Indo-1-AM was prepared in a solution of pluronic acid F127/20% DMSO (*Molecular Probes*) at a concentration of 5 mM and used to load the cells for experiments in the perforated patch configuration. Thus 0.5 µl of the stock solution (final concentration at 5 µM) was added to the culture medium (≈ 500 µl) directly in the

recording chamber and incubated for 30-40 minutes at 37°C. The chamber was then transferred on to the microscope's stage, and superfused for ≈ 20 minutes at 33°C with the standard perfusion medium to remove any excess of indo-1-AM and allow the ester to hydrolyse

3.3.5. Recording of the free intracellular calcium

Cells contain many substances that are fluorescent when excited within the UV spectrum (*e.g.* NADH). However, under the experimental condition the cell auto-fluorescence is negligible compared to the fluorescence emitted by indo-1.

Prior to recording of indo-1 fluorescence the background light had to be subtracted. In the whole-cell configuration, with indo-1 included in the patch solution, the amplifier outputs were adjusted to zero whilst in the cell-attached mode. In the perforated patch mode, the amplifier outputs were reset to zero over a 'cell-free' field of view. Then, the chosen cell (≈ 20 μm diameter) was placed in the centre of the view field and the field aperture (see Methods section 3.2) closed around its soma before being patch-clamped. To ensure the quality of the seal and the healthiness of the cell during recordings in the perforated patch configuration, resting $[Ca^{2+}]_i$ was always monitored before and after the seal formation. Only cells with similar resting ratio values (± 0.01 ratio units) were used for the rest of the experiment.

4. Monitoring the intracellular pH

Experiments to monitor variations in the intracellular pH (pH_i) were carried out using 2',7'-bis-(2-carboxyethyl)-5-(and -6)-carboxyfluorescein (BCECF) a dual excitation fluorophore (Rink *et al.*, 1982). Thus, at 470 nm the absorbance of BCECF is decreased upon the binding of H^+ (*i.e.* acidification) whilst at 445 nm (isosbestic point) it is not affected. The emitted fluorescence was monitored at 535 nm. These characteristics of BCECF are taken advantage of in the ratiometric method and allow a calibration of the pH indicator (see Methods section 4.2.1).

4.1. Experimental apparatus

The apparatus used to monitor the pH_i of single cells is illustrated in *figure 4*. Briefly, an inverted fluorescent microscope (*Nikon Diaphot 200*) was used and excitation light provided by a monochromator (Polychrome II, *T.I.L.L. Photonics GmbH.*). This device was attached to the microscope through an epifluorescence condenser (*T.I.L.L. Photonics GmbH.*) via a light guide (quartz fibre optic, 1.5 mm diameter; *T.I.L.L. Photonics GmbH.*). The monochromator system allowed computer-controlled regulation of the excitation wavelength and a fast switching between wavelengths. A set of neutral density filters (ND.) and an electronically controlled shutter (Sh.) were placed in the light pathway to limit photobleaching of the fluorophore by controlling light intensity and exposure duration, respectively. The excitation wavelengths (445 and 470 nm) were reflected by a 510 nm dichroic mirror (DM.) and passed through a glycerine-immersion fluorescent objective (UV fluor x100, NA. 1.3, *Nikon*) on to the cell. The emitted light was then passed through a 535 nm DF35 bandpass filter (*Omega*) before being captured on to a 12-bit grey-scale computer-controlled digital (CCD) camera (*Hamamatsu 4880*). The Openlab 2.2.4 software (*Improvision*), installed on to a G4 *Apple MacIntosh* computer, controlled all the hardware (shutter, monochromator and camera) and the 'in house' designed automations (software routines).

4.2. Measurement of intracellular pH

4.2.1. The ratiometric method for intracellular pH measurement

For BCECF, the ratiometric method was used and based on the following equation:

$$\left[H^+\right] = K_a^* \times \left(\frac{R - R_A}{R_B - R}\right) \quad \textit{Equation 7}$$

where $[H^+]$ is the concentration of proton, R the measured 445/470 fluorescence ratio. R_A and R_B represent the limiting values at the acidic and basic endpoints of the

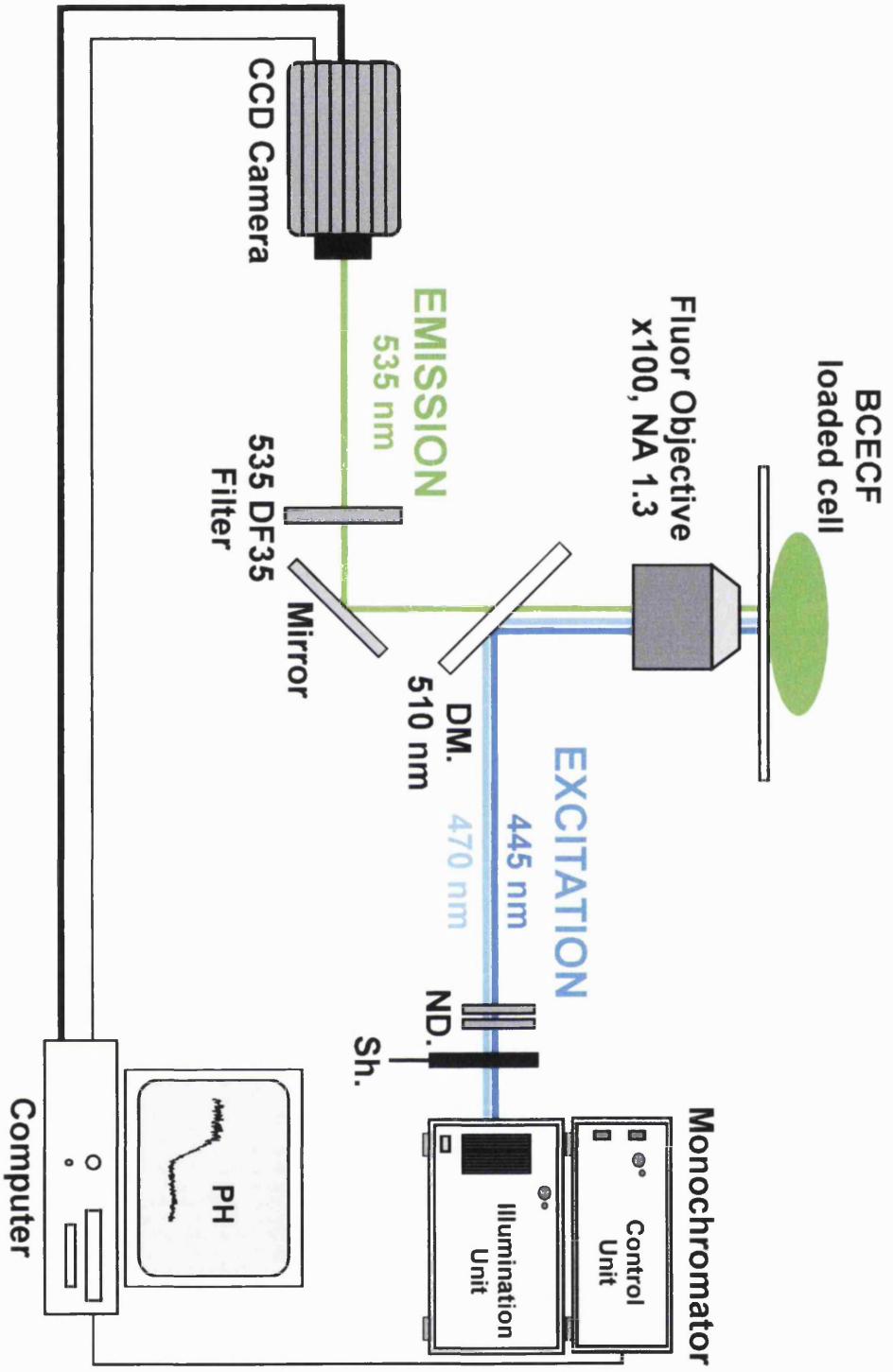

Figure 4: Experimental apparatus for intracellular pH (pH_i) imaging with BCECF
Fluorescence emitted (535 nm) after excitation at 445 nm and 470 nm was acquired using a CCD camera. From the recorded images the 445/470 fluorescence ratio was calculated using the Openlab 2.2.4 software. This ratio was subsequently displayed as pH_i values using the calibration parameters (full details in the text).

calibration, respectively and K_a^* corresponds to the *apparent* dissociation constant for proton binding to BCECF. As the pH corresponds to the logarithm of $[H^+]$, *Equation 7* can be expressed as follow:

$$pH = pK_a^* + \log\left(\frac{R - R_A}{R_B - R}\right) \quad \textit{Equation 8}$$

4.2.2. BCECF calibration for intracellular pH measurement

The calibration was carried out *in situ* using BCECF-AM (see Methods section 4.2.3) to load the cells. Cells were then superfused at 33°C with Ca^{2+}-free and symmetric KCl solutions (in mM: 130 KCl, 4 $MgCl_2$, 20 HEPES adjusted to ≈ 285 mosm l^{-1} with KAc and to the various pH values with either KOH or HCl) containing the protonophore *m*-chlorophenylhydrazone (CCCP, 20 μM). The 445/470 fluorescence ratio was then measured at 5 different pH values. The final ratio values obtained at each pH are summarised below in *Table 4*:

Table 4: BCECF 445/470 excitation ratio obtained for various $[H^+]$

Free H^+ (M)	pH	Mean Ratio	n
$5x10^{-12}$	11.3	3.92 ± 0.02	7
$5x10^{-9}$	8.3	3.66 ± 00.2	6
$6.3x10^{-8}$	7.2	2.83 ± 0.02	6
$6.3x10^{-6}$	5.2	1.77 ± 0.02	5
$6.3x10^{-5}$	4.2	1.64 ± 0.02	5

The plots of the ratio values *versus* $[H^+]$ and pH_i are illustrated in *figure 5-A* and *5-B*, respectively. The parameters R_A, R_B, and K_a^* (*i.e.* pK_a^*) from *Equation 7 and 8* were determined by fitting a curve to the data points using the equation below.

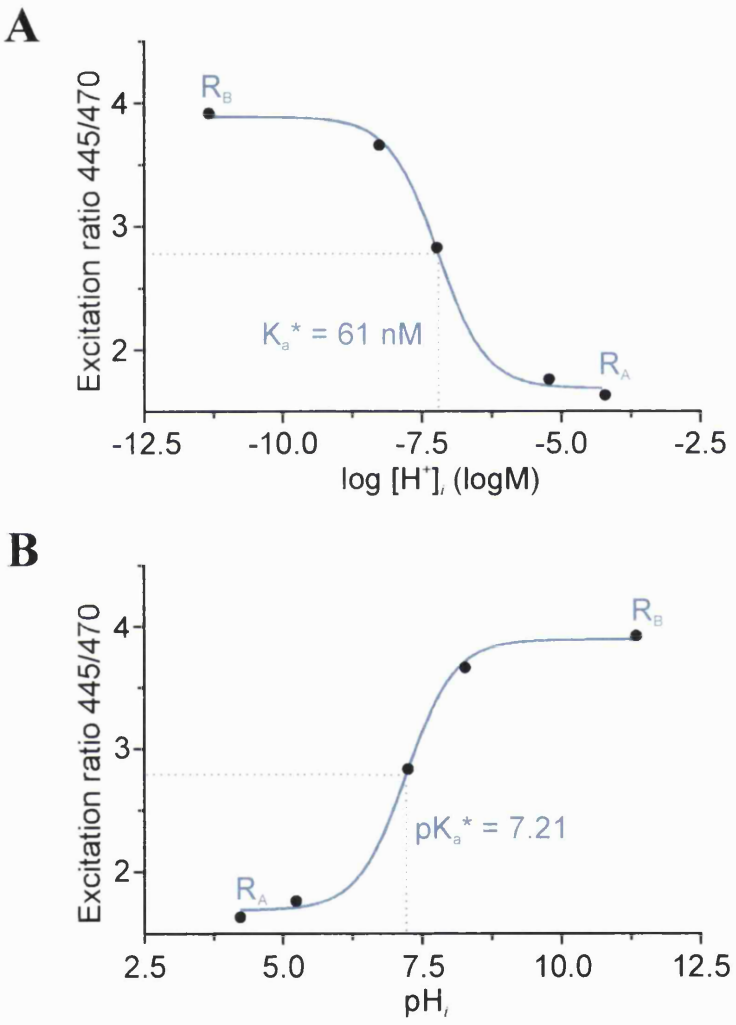

Figure 5: Calibration curve for the determination of the free intracellular H^+ concentration ($[H^+]_i$, A) and intracellular pH (pH_i, B) using the BCECF fluorescence ratio (data as mean S.E.M. included in the data points, see *Table 4*).

$$R = \left[\frac{R_A - R_B}{1 + \left(\frac{[H^+]_i}{K_a^*} \right)^n} \right] + R_B \quad \textit{Equation 9}$$

with R, R_A, R_B, $[H^+]$ and K_a^* as defined for *Equation 7* and the Hill slope (*n*) constrained to 1 (*i.e.* binding ratio 1:1). The fitted calibration curves are illustrated in *figure 5-A* and *5-B* (previous page) and the best fit is obtained with the following parameters:

$$R_A = 1.69 \pm 0.02 \text{ , } R_B = 3.89 \pm 0.02 \text{ and } K_a^* = 61 \pm 7 \text{ nM}$$

$$\text{with } pK_a^* = -\log K_a^* = 7.21 \pm 0.05$$

4.2.3. Cell loading with BCECF

The loading procedure used the AM-ester form of BCECF at a final concentration of 5 μM (see Methods section 3.3.4 for details).

4.2.4. Recording of the intracellular pH

At the start of the experiment, the chosen cell was alternatively excited at 445 and 470 nm and 12-bit grey-scale images of the fluorescence emitted at 535 nm were taken with the CCD camera for each excitation wavelength. The acquired images were optimised by adjustment of the camera exposure time, binning and digital gain at the excitation wavelength of 470 nm. Two regions of interest (ROI) were drawn on the acquisition frame, one in an area outside the cell (*i.e.* the background) and another on the cell's soma ('cell ROI') (445 and 470 nm *figure 6-A* and *6-B* respectively, see next page). The mean intensity of the pixels within the background ROI was then digitally subtracted from each pixel of the acquired frames. The resultant images was then

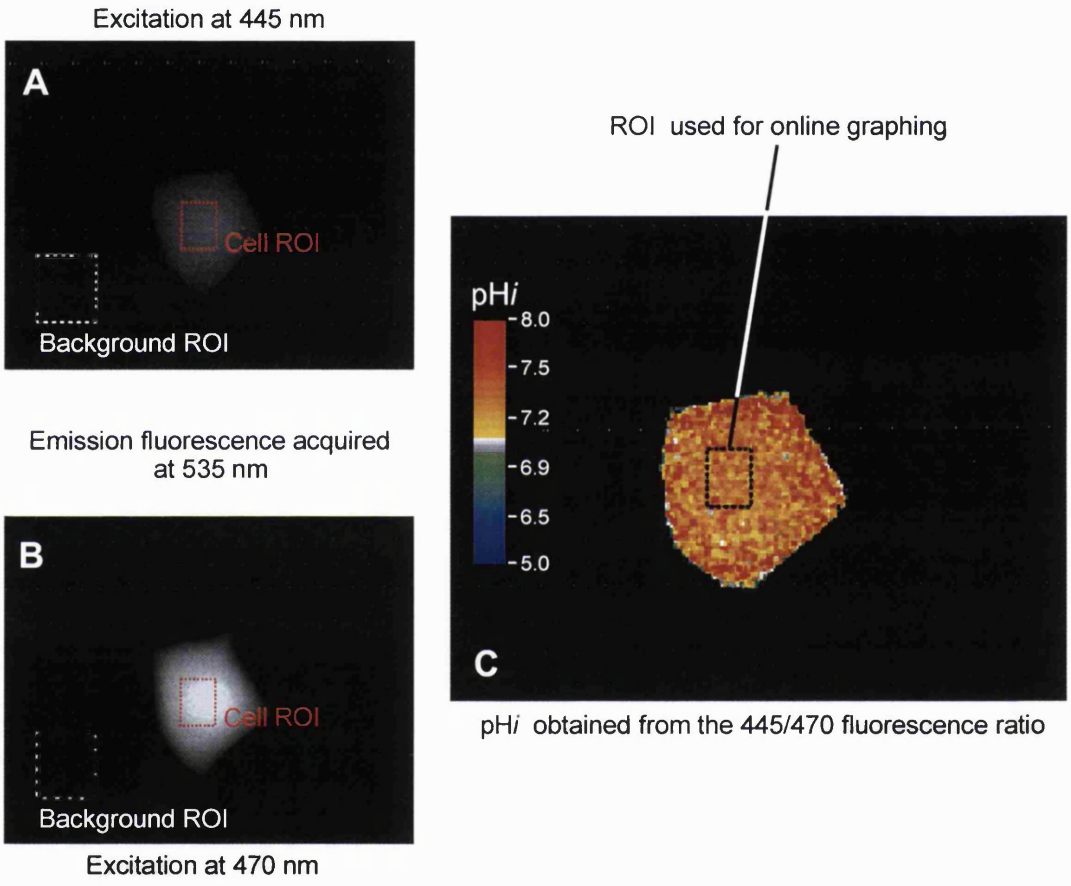

Figure 6: Intracellular pH recording
Images of the fluorescence emitted at 535 nm after excitation at 445 nm (A) and 470 nm (B) were acquired using a CCD camera. The background was removed by subtracting the mean intensity of the pixels in the 'background region of interest (ROI)' from each pixel in the acquired frames. The fluorescence ratio (C) was subsequently obtained by dividing pixel by pixel the frame (A) by the frame (B) and using the parameter of the BCECF calibration converted online in pH_i values. The region of interest drawn in the cell soma ('cell ROI') was subsequently used to plot online the time course of pH_i variations.

subjected to a 'ratioing' procedure, which divides the digital intensity values of the '445 image' by those found within the '470 image', on a pixel by pixel basis. An image of the 445/470 fluorescence ratio was then obtained and displayed in pseudo colour (*figure 6-C*). The ratio image was then subjected to a density calibration allowing an online estimate of pH_i values, using the parameters from the calibration curve (see Methods section 4.2.2). A graph of the pH_i variations *versus* time was then obtained from the mean of the 'cell ROI' ratio. Ratio images were normally acquired at 1Hz – 0.2 Hz.

5. Drugs and chemicals

All drugs and chemicals were purchased from *Sigma* except indo-1 acid, indo-1-AM, BCECF-AM, 5,6-succinylmidyl carboxyeosine (CE) (*Molecular Probes*) and cyclopiazonic acid (CPA) (*Calbiochem*). Indo-1-AM, BCECF-AM, CPA, thapsigargin, *m*-chlorophenylhydrazone (CCCP) and amphotericin B were dissolved in DMSO (final concentration <0.01%). For the experiments in immunocytochemistry (see Methods section 7) and molecular biology (see Methods section 8) the suppliers of solutions, enzymes and other compounds are mentioned in the text.

6. Data analysis

6.1. Calibration curves

The calibration curves for the fluorescent dyes were obtained within the Prism 3 software and fitted with equations mentioned in the Methods sections 3.3.2 and 4.2.2 for indo-1 and BCECF, respectively. The values of the fluorescence ratio at each $[Ca^{2+}]_i/pH_i$ were considered as replicates and their mean used for the fit. The goodness of the fit was assessed from χ^2 and the non-linear least square method (*i.e.* best fit obtained for χ^2 close to 0).

6.2. Decay time constants

The recovery phase of each Ca^{2+} transient was fitted using exponential decay functions of the first (monoexponential, *Equation 10*) or second order (biexponential, *Equation 11*):

$$y = y_o + A_1 \times e^{-(x-x_o)/\tau_1} \quad \textit{Equation 10}$$

$$y = y_o + A_1 \times e^{-(x-x_o)/\tau_1} + A_2 \times e^{-(x-x_o)/\tau_2} \quad \textit{Equation 11}$$

where x_o is the time at the peak and y_o resting $[Ca^{2+}]_i$. A_1 and A_2 represent the amplitudes of each exponential component and τ_1, τ_2 are the corresponding decay time constants. The fitting procedure was realised using the Origin 5 (*Microcal software*) and statistical weighting was applied. The goodness of the fit was assessed using the non-linear least squares methods (correlation coefficient close to 1 and χ^2 value close to 0) and visualised from the residue plot (see *figure 7-A*). From the fit (*figure 7-B*), the derivative function ($d[Ca^{2+}]/dt$, *figure 7-C*) was calculated. Finally, by plotting the negative of the derivative ($-d[Ca^{2+}]/dt$) against $[Ca^{2+}]_i$ obtained from the exponential fit, the clearance rate (see *figure 7-D*) could be determined for the recovery of each Ca^{2+} transient. The clearance rates were pooled from all the Ca^{2+} transients recorded in each condition (control *versus* inhibitor) and were then fitted with a linear regression (monoexponential decay) or a polynomial function of the second order (biexponential decay). The best fit in the presence of an inhibitor was subsequently subtracted from the best fit in control to generate the inhibitor-sensitive component. For more clarity, apart in the Results section 1.2 (see Results *figure 16-B*), only the best fit of the data is presented. When the fit of the decay phase was not possible, the time necessary to reach 50% ($t_{½}$) of the peak amplitude (A_{max}) was measured and the average values compared before and after the application of an inhibitor.

6.3. Statistics

All averaged data are expressed as mean ± S.E.M. and the statistical significance was determined by paired Student *t*-test ($P<0.05$) unless otherwise stated.

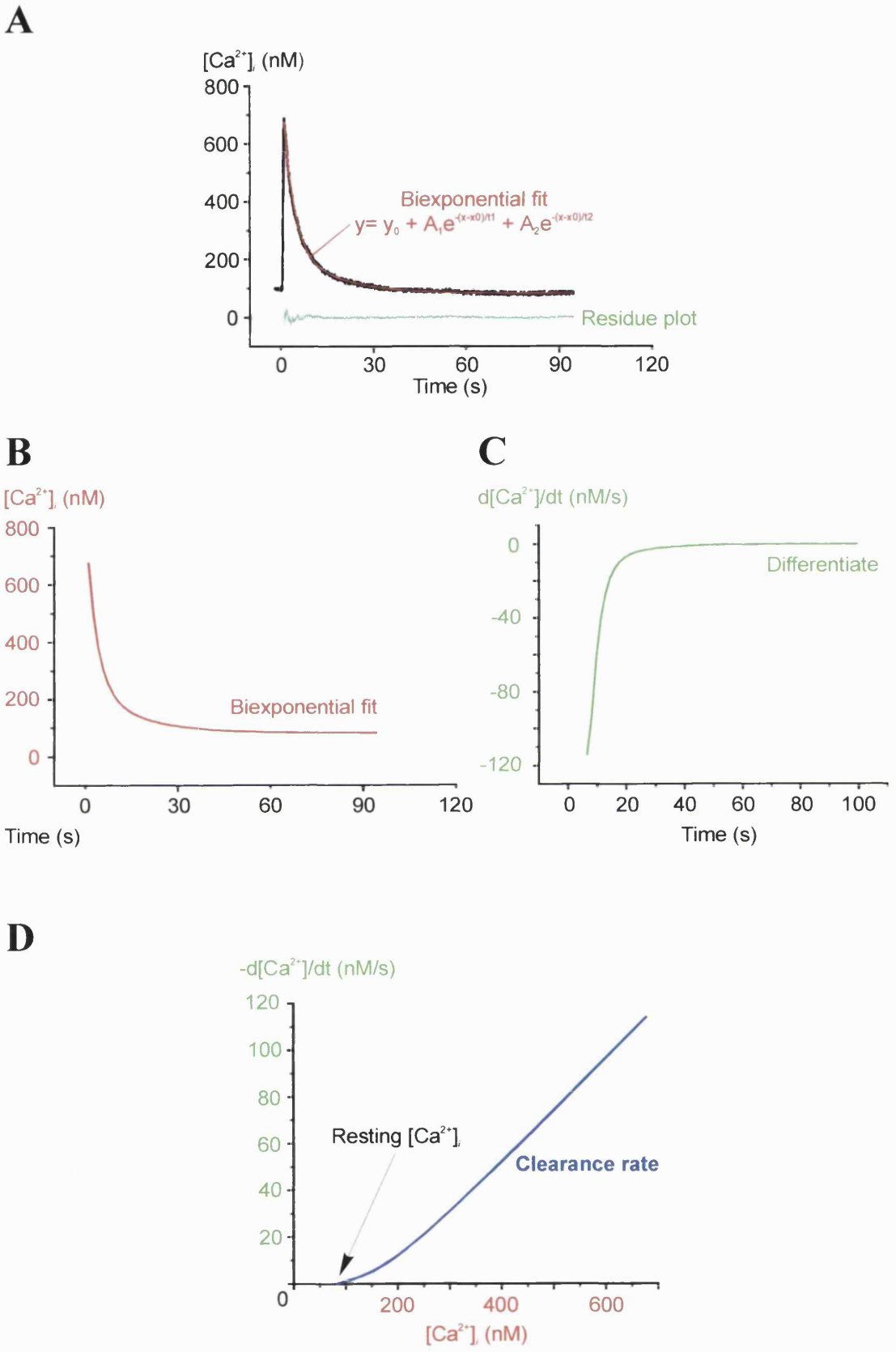

Figure 7: Fitting procedure and clearance rate determination for the Ca^{2+} transient's recovery (see text for details).

7. Immunocytochemistry

The nature and localisation of several proteins involved in Ca^{2+} homeostasis were determined with the immunocytochemical technique using the double labelling method. A primary antibody (see *Table 5*) directed against a specific antigenic epitope was subsequently labelled with a secondary antibody conjugated to a fluorescent marker (*Table 6*) visualised on to an inverted fluorescent microscope. The study was carried out to determine which SERCA and PMCA isoform(s) are expressed and if NCX is present in SCG neurones.

Table 5: List of the primary antibodies used in the immunocytochemical experiments

	Primary Antibody	Concentration and Animal Host	Antigenic peptide	Source
PMCA	Clone 5F10 [a] isoform non specific	1/50 Mouse monoclonal	NO	Gift from Dr. Filoteo
PMCA-1	PMCA-1 [b]	1/50 Rabbit polyclonal	NO	SWant® Swiss Antibodies
PMCA-2	PMCA-2 [b]	1/50 Rabbit polyclonal	NO	SWant® Swiss Antibodies
PMCA-3	PMCA-3 [b]	1/50 Rabbit polyclonal	NO	SWant® Swiss Antibodies
PMCA-4	PMCA-4 [b]	1/50 Rabbit polyclonal	NO	SWant® Swiss Antibodies
NCX	RDI-NaCaExch cardiac NCX- 1 [c]	1/50 Rabbit polyclonal	NO	Research Diagnostics Inc.
SERCA-1	sc-8093 SERCA-1(N-19)[d]	1/50 Goat polyclonal	sc-8093-P	Santa Cruz Biotechnology *Inc.*
SERCA-2	sc-8095 SERCA-2(N-19)	1/50 Goat polyclonal	sc-8095-P	Santa Cruz Biotechnology *Inc.*
SERCA-3	sc-8097 SERCA-3(N-19)[d]	1/50 Goat polyclonal	sc-8097-P	Santa Cruz Biotechnology *Inc.*
Plasma Membrane	F-143	25 µM	Specific PM marker	Molecular Probes
Endoplasmic Reticulum	DP-I	1/200	specific ER marker	Gift from Prof. Moss

[a] From Borke *et al.* (1989). [b] From Stauffer *et al.* (1995). [c] From Philipson *et al.* (1988). [d] From Aubier & Viires (1998).

7.1. Procedure for immunocytochemistry

Cell cultured on glass coverslips for 1-3 days were fixed with 0.2% glutaraldehyde/2% paraformaldehyde (in phosphate buffer saline, PBS; *Sigma*) for 20 minutes at room temperature and subsequently permeabilised with 0.1% triton X100 (*Sigma*) in PBS for 15 minutes. After several washes in PBS, cells were incubated at room temperature for 1 hour in a blocking buffer (PBS with 10 mg ml^{-1} bovine serum albumin, BSA; *Sigma*) and then for 1 hour at room temperature or overnight at 4°C with the primary antibodies (see *Table 5* for details). Secondary antibodies conjugated either to tetramethylrhodamine B isothiocyanate (TRITC) or fluorescein isothiocyanate (FITC) (1/50, *DAKO*, see *Table 6* for details) were used for fluorescent immuno-labelling. After several 5 minutes washes in PBS, the coverslips were then mounted on to a slide using a mounting medium (*DAKO*) and then refrigerated until examination. To estimate the level of auto-fluorescence under the examination conditions, control experiments without antibodies were carried out. Specificity of primary antibody binding was determined by pre-incubating overnight the primary antibody with its corresponding antigenic peptide (see *Table 5*). When no antigenic peptide was available, the staining was compared against a staining with the secondary antibody alone.

Table 6: Characteristic of the secondary antibodies

Primary Antibody	Secondary Antibody	Conjugates			
		Nature	Emission Wavelength	Excitation Wavelength	Dichroic Mirror
Mouse	**Swine anti-mouse IgG**	FITC	495 nm	510 nm	XF34 Omega
Rabbit	**Swine anti-rabbit IgG**	TRITC	555 nm	580 nm	XF14 Omega
Goat	**Swine anti-goat IgG**				

7.2. Image acquisition and analysis

7.2.1. Image acquisition

The results of the immunocytochemical experiments were examined with the experimental apparatus illustrated in *figure 4* using either a x40 (Oil, NA. 1.3) or

x100 (Glycerine, NA. 1.3) objective. The excitation and emission wavelengths as well as the dichroic mirrors used to visualise either the FITC or TRITC fluorescence are listed in *Table 6.* Images were acquired with a 12-bit grey-scale CCD camera and hardware controlled using the Openlab 2.2.4 software. The images were optimised by adjusting the camera exposure, digital gain and camera binning. A FITC or TRITC pseudo colour palette was subsequently applied to the acquired pictures.

7.2.2. Image analysis

The limitations of conventional optical microscopy implies that the digital images acquired will be subjected to a degree of 'blurring', as light emitted below and above the plane of focus invades the point at which the objective is focused. This phenomenon adds to the picture an out-of-focus haze, reduces the resolution and therefore the accuracy of any measurements taken. The development of laser confocal microscopy allowed high-resolution images to be obtained by using a series of apertures to removes this out-of-focus haze, leaving only a thin and highly focused plane or optical slice.

Another way to improve the acquisition of images and their resolution uses deconvolution algorithms (Agard *et al.*, 1989; Casteleman, 1996). These processes consist of correcting and removing the noise and haze originating from images in other focal planes using mathematical algorithms. The simplest of these algorithms is the *Nearest neighbour algorithm* (Agard *et al.*, 1989; Casteleman 1996), which yields reasonably good results. This method assumes that all contributors to a particular image plane come from the plane in the object and its nearest neighbours and uses a minimum of three optical slices (*i.e.* the image just below the plane of focus, the plane of focus itself and the image above the plane of focus) for the correction. With the Openlab 2.2.4 software and using the experimental apparatus illustrated in *figure 4*, it is possible to undertake this type of analysis to examine the results of immunocytochemical experiments. An automation for the Openlab 2.2.4 software was designed in our laboratory, which enables the acquisition of optical slices through a stained specimen (see *figure 8-A*). Briefly, the microscope was automatically focused to the bottom of the cell and then several optical slices (generally $\approx$ 30) were acquired in 0.5 μm steps up

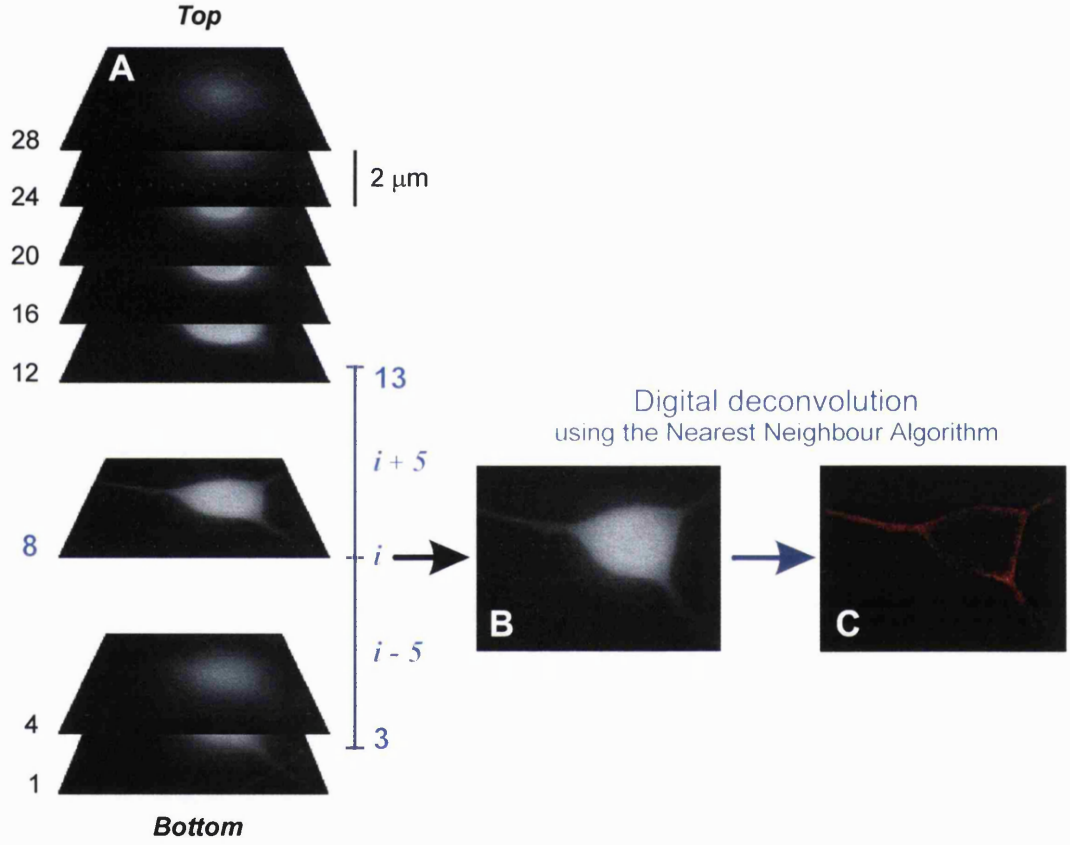

Figure 8: Principle of the digital deconvolution
From the bottom to the top of a cell, optical slices (A) were acquired using a CCD camera with 0.5 µm step. Then, the image (B) at a chosen plane of focus (*i*) was digitally deconvolved using the *Nearest neighbour algorithm.* Generally, 5 images above the plane of focus (*i* + *5*) and 5 under (*i* - *5*) were used to obtain the deconvolved image (C). This process enabled an improvement of the image resolution similar to the image obtained with a laser confocal microscope (see *figure 9-A*).

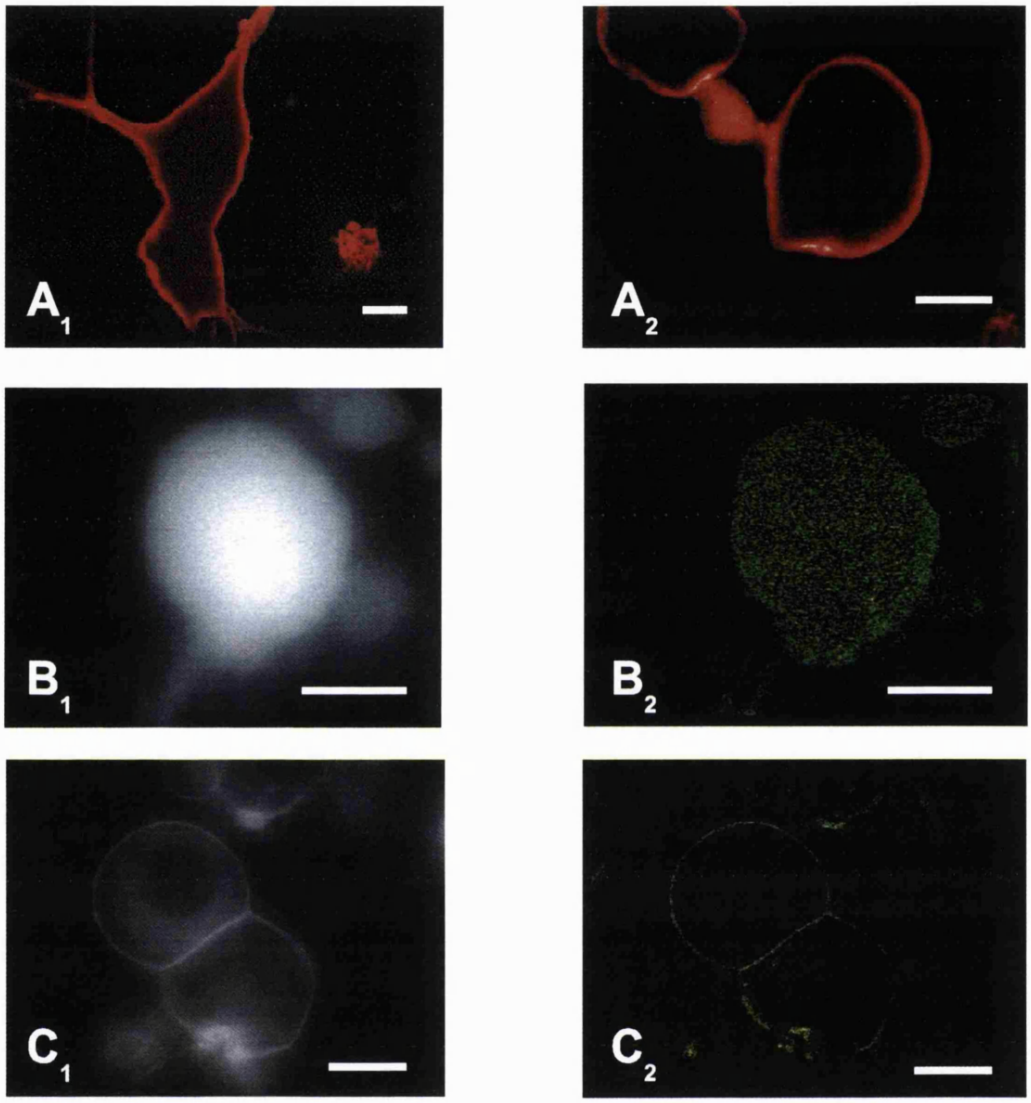

Figure 9: Determination of the validity of the digital deconvolution method to analyse the results of immunocytochemical experiments

(A) 5F10, an antibody that recognise the plasma membrane Ca^{2+}-ATPase (1/50, mouse monoclonal isoform non-specific antibody), was used to stain dissociated SCG neurones. The primary antibody was immunolabelled with a secondary antibody raised against mouse IgG and conjugated with TRITC (1/50). The same immunocytochemical experiment was then acquired using either a laser confocal microscope (A_1) or a CCD camera with digital deconvolution (A_2). (B) Cell transfected with *c*DNA for the green fluorescent protein (GFP) with a cytoplasmic distribution. Images were acquired with a CCD camera (B_1) before being analysed with the digital deconvolution (B_2). As expected from a cytoplasmic marker after deconvolution the fluorescence is homogeneously distributed in the cytosol. (C) Cells were superfused with a extracellular medium containing 25 μM of F-143. This compound is inserted into plasma membrane bilayer by endocytosis before acquiring fluorescent properties. Images were acquired with a CCD camera (C_1) before being analysed with the digital deconvolution (C_2). As expected from a plasma membrane marker after deconvolution the fluorescence is localised in the plasma membrane.

through the cell. Then, the image obtained from a particular focal plane (see *figure 8-B*) was deconvolved using the nearest 5 neighbours algorithm (*i.e.* 5 above and 5 below, *figure 8-A*). For the correct settings of this analysis it was necessary to estimate the point spread function (P.S.F.) of the microscope. This required that the objective, immersion solution, camera resolution and binning are all known. The deconvolution procedure generated an image with reduced blur and improved clarity (see *figure 8-C*). This technique was particularly useful in experiments where the presence of plasma membrane associated proteins were being investigated, as it enables the precise localisation of the staining. To make sure that the images generated with this technique were real and not artefacts of the deconvolution, two control image analysis experiments were carried out. The first consisted of using a laser confocal microscope to double-check the experimental result (*see figure 9-A*). The second involved the overexpression of a fluorescent protein with a cytoplasmic distribution (*e.g.* green fluorescent protein, *figure 9-B*) or a fluorescent marker localised in the plasma membrane (*e.g.* F-143, *figure 9-C*). The acquired data were then subjected to the same deconvolution parameters and algorithm (see *figure 9-2*) and compared to the results of the immunocytochemical experiments.

8. Molecular biology

The proteins involved in the Ca^{2+} extrusion processes (*i.e.* SERCA, PMCA and NCX, see General Introduction sections 4.2, 5.1 and 5.2) exist as different isoforms with numerous alternative splice variants. In order to determine the nature of the isoform(s) expressed in SCG neurones and also to confirm results obtained in immunocytochemistry, molecular biological experiments were carried out. These experiments consisted initially of messenger RNA[1] (*m*RNA) extraction from fresh tissue (see Methods section 8.1), subsequent reverse transcription into *c*DNA[2] (see Methods section 8.2) and finally a polymerase chain reaction (PCR) analysis (see Methods section 8.3).

[1] RNA: ribonucleic acid.
[2] *c*DNA: complementary DNA (deoxyribonucleic acid) synthesised *in vitro* as opposed to genomic DNA.

8.1. mRNA extraction

Although SCG tissues were mainly used in these experiments, comparisons were made with tissues isolated from cerebellar cortex, heart and skeletal muscles. All the tissues were freshly dissected from 15- to 17-day-old male Sprague-Dawley rats and stored on ice in RNAzol™ B (1 ml per 50-100 mg of tissue, *Biotecx Laboratories, Inc.*) in a closed 1.5 ml tube until the *m*RNA extraction procedure. The tissues were dissociated in RNAzol™ B by strong trituration using a needle (0.6 x 25 mm, *Sherwood*) attached to a 5 ml syringe until homogenisation and then stored on ice for 5 minutes. After adding 0.2 ml chloroform per ml of RNAzol™ B, the sample was vigorously shaken, allowed to stand for 5 minutes, then quickly 'vortexed' and finally centrifuged (12,000 g at 4°C for 15 minutes). The centrifugation separated the contents of the tube into three phases: a red organic phase containing proteins, an interphase containing DNA and a colourless upper aqueous phase containing the RNA. To isolate the RNA, the aqueous phase was transferred into a fresh tube and 0.5 ml isopropanol per ml of RNAzol™ B was added. Again the tube was vigorously shaken, allowed to stand for 5 minutes, quickly 'vortexed' and centrifuged (12,000 g at 4°C for 15 minutes) to precipitate the RNA at the bottom of the tube. The extracted RNA was then washed in 1 ml 75% ethanol and centrifuged at 12,000 g and 4°C for 15 minutes. The supernatant was then disposed off and the RNA left to air dry for ≈ 5 minutes before being resuspended in 10 µl of ultra-pure distilled water. One microliter of the suspension was then added to 500 µl of distilled water and the optical density (OD) measured at 260 nm and 280 nm using a spectrophotometer (*SmartSpec™ 3000, Biorad*). The OD obtained at 260 nm was then used to determine the RNA concentration of the sample (1 unit of OD per mg of RNA) and the 260/280 ratio used to determine the quality of the extraction (260/280 ratio ≈ 1.8 for a solution containing only RNA). At this stage, the isolated RNA was reverse transcribed into *c*DNA.

8.2. Reverse transcription

To remove traces of possible genomic DNA contamination, 10 µg of total RNA was incubated with 10 units (1 µl) of RNAse-free-DNAse I (*Boehringer Mannheim*) at 37°C for 30 minutes in 1x transcription buffer (*Boehringer Mannheim*).

The DNase-treated RNA was then extracted with phenol/chloroform and precipitated by centrifugation at 12,000 g for 2 minutes at room temperature. Finally, the RNA was resuspended in 5 µl of water and stored at -20°C until use. To further ensure the absence of any genomic DNA contamination, two parallel reverse transcriptions (RT) were carried out where in one of the reactions the reverse transcriptase was omitted and replaced by distilled water *i.e.* no *c*DNA would be synthesised. For the 'normal' RT, 2 µl (≈ 4 µg) of DNAse-treated RNA was added to 8 µl of ultra-pure distilled water containing 250 ng oligo $d(T)_{15}$ primer[3] (*Promega*), denatured at 65°C for 2 minutes and then immediately cooled on ice. First strand *c*DNA synthesis was carried out in 1x Superscript II buffer (*Life Technologies*) containing 10 mM DTT, 0.5 mM dGTP[4], 0.5 mM dCTP[4], 0.5 mM dATP[4] and 0.5 mM dTTP[4], 1 µl RNAse Inhibitor (*Boehringer Mannheim*) and 200 units (1 µl) M-MLV reverse transcriptase (*Promega*). The mix was then incubated for 1 hour at 37° C. Finally, 2 µl of *c*DNA template was subjected to a PCR analysis.

8.3. Polymerase chain reaction

The PCR reactions were performed in 20 µl of 1x Taq Extender buffer (*Stratagene*) containing 2 µl of *c*DNA template, 250 nM dGTP, 250 nM dCTP, 250 nM dTTP, and 250 nM dATP, 5 nM of each of the forward and reverse primers (see *Table 7*), 1.25 unit Taq polymerase™ (*Promega*) and 1.25 unit Taq Extender[5] PCR additive (*Stratagene*). The forward (sense, s) and revere (antisense, a) primers were designed (see details in *Table 7* and figures legend) to bind specific regions of the sequence of the studied gene so that only a fragment of this particular *c*DNA would be amplified. The selectivity of each primer was then controlled by sequence alignment against a DNA databank (*server of the National Center for Biotechnology Information at www.ncbi.nlm.nih.org, National Institute of Health, New York USA*). The designed primers were then obtained from *Sigma-Genosys.* The standard cycling conditions were

---

[3] oligo $d(T)_{15}$ primers: nucleotide sequence composed by 15 thymine deoxyribonucleoside 5'-triphosphate. Most *m*RNA are terminated by a tail composed by several adenosine nucleotides or poly-A tail, the oligo dT primers bind to the poly-A tail and help the initiation of the reverse transcription.

[4] dGTP, dCTP, dATP, and dTTP: guanine, cytosine, adenine and thymine deoxyribonucleoside 5'-triphosphate.

[5] Taq Extender: during the amplification of *c*DNA sequences some errors may occur (insertion of the wrong nucleotide, gap). The Taq Extender enzyme helps to correct these errors.

94°C for 2 minutes and 35 cycles of 94°C for 30 seconds, 60°C for 30 seconds and 70°C for 1 minute followed by a final step of 72°C for 10 minutes. The amplified products were electrophoresed through a 2% MetaPhor® agarose gel (*FMC BioProducts*) and their sized determined against a DNA molecular ladder (1 Kb plus, *Gibco BRL*).

Table 7: Forward and reverse primer sequences used in the PCR reactions

	Isoforms	Forward Primers 5'-3'	Reverse primers 5'-3'
PMCA	**PMCA-1 gi: J03753***	TBGGMGGBAAACCYTTCAGCTG[a] pmca1/3342s pmca2/3563s pmca3/3721s pmca4/3208s	CTTCTATCCTAAACTCGGGGTG[b] pmca1/3878a
	PMCA-2 gi: J03754		GTCAGGTTGATCCCGCTGTCG[b] pmca2/4076a
	PMCA-3 gi: J05087		GAGCTACGGAATGCTTTCAC[b] pmca3/4178a
	PMCA-4 gi: U15408		CAGCATCCGACAGGCGCTTGG[b] pmca4/3844a
NCX	**NCX-1 gi: U04933**	TAAAACCATTGAAGGCACAGC[c] ncx1/1713s	CACTTCCAGCTTGGTGTGTT[c] ncx1/2120a
	NCX-2 gi: U08141	GGAGCATCTTTGCCTATGTCTCT GGC[d] ncx2/611s	TCGATGCTCTTGGGCGGGTCT[e] ncx2/863a
	NCX-3 gi: U53420	GGAGCGTCTTTGCCTATATTTG[d] ncx3/620s	GCGAGATTCATCTACCTCCTTTC[e] ncx3/963a

* Accession number of the *c*DNA sequence submitted to GenBank. The forward or sense (s) and reverse or antisense (a) primers are termed after the gene isoform and the first and last nucleotides, respectively of the corresponding *m*RNA sequence. [a] Forward primer common to all 4 PMCA isoforms and designed to amplify a sequence coding for a region between transmembrane domains 9 and 10. [b] From Keeton *et al.* (1993). [c] Forward and reverse primers flanking the alternative splicing region on the NCX-1 gene, from Lee *et al.* (1994). [d] Forward primers selective to NCX-2 and NCX-3 designed to amplify a sequence coding for a region in transmembrane domain 4. [e] Reverse primers selective to NCX-2 and NCX-3 designed to amplify a sequence coding for a region in the large intracellular loop.

Chapter III

Results

1. Calcium currents and changes in intracellular calcium

In neurones, following depolarisation, changes in $[Ca^{2+}]_i$ can be induced. The main Ca^{2+} influx is through VACC (see General Introduction section 2.1) and the immediate role is to trigger neurotransmitter release at the synapses. However, rises in $[Ca^{2+}]_i$ can also regulate the neuronal activity (*e.g.* enzyme activation, second messenger production and gene expression) and the cellular excitability (activation of ionic channels). The size of the variation in $[Ca^{2+}]_i$, as a consequence of the induced Ca^{2+} influx, will depend on the properties of the Ca^{2+} channels, the duration and amplitude of the Ca^{2+} current, the site at which Ca^{2+} entry occurs and on the characteristics of the cell. Several VACC subtypes with different electrophysiological properties, molecular structure and tissue distribution have been identified (see Bean, 1989; Birnbaumer *et al.*, 1994 and Dunlap *et al.*, 1995 for review). Therefore, in this section, the nature of the somatic VACC present in SCG neurones and responsible for the rise in $[Ca^{2+}]_i$ was investigated. Furthermore, the properties of the depolarisation-induced Ca^{2+} transients were determined. In later sections, membrane voltage protocols were designed to investigate under which conditions a particular system might be activated for returning $[Ca^{2+}]_i$ back to its resting level.

1.1. Activation of voltage-dependent calcium channels

Neurones were voltage-clamped in the whole-cell configuration (see Methods section 2.2.2, *figure 1*) with a Cs^+-based intracellular solution, to block most of the potassium currents (see Methods section 2.4.3, *Table 2* - solution J), and with 500 nM extracellular TTX to block sodium currents. Currents were induced using depolarising steps from a holding potential of -60 mV to between -40 and +30 mV in 10 mV increments for 20 ms (*figure 10-A*). The calcium current (I_{Ca}) was defined as the current remaining after digital subtraction of the current recorded with the same voltage protocol in the presence of 100 µM Cd^{2+}, a selective blocker of VACC (Fox *et al.*, 1987). Typically, this voltage protocol elicited a Ca^{2+} current that began to activate around -30 mV, its amplitude peaked at 0 mV (700 ± 95 pA; n=5 - *figure 10-B*) and then progressively decreased at more depolarised potentials.

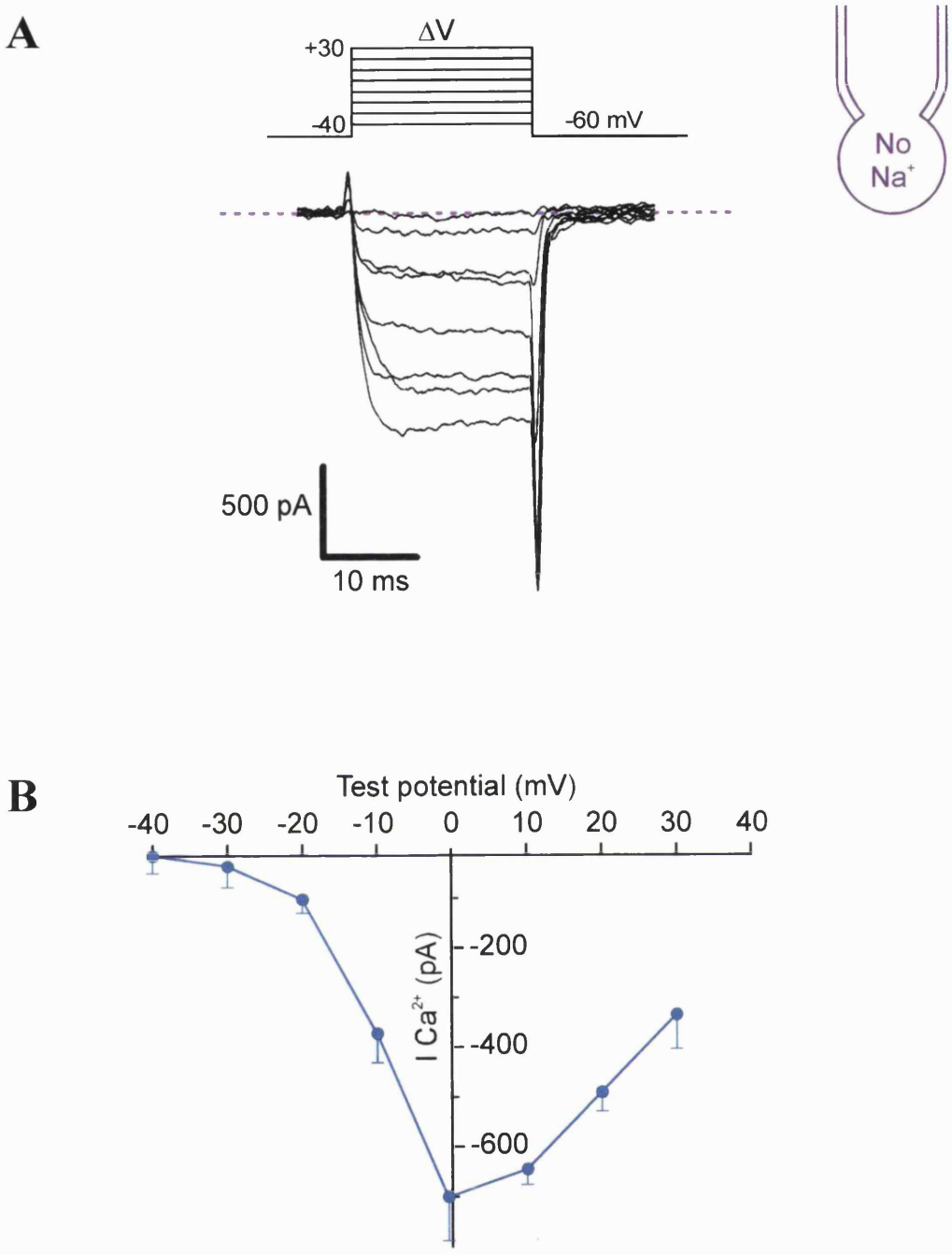

Figure 10: Somatic activation of high voltage-activated Ca^{2+} channels
(A) Representative Ca^{2+} currents recorded from the soma of a SCG neurone voltage-clamped in the whole-cell configuration (see inset) with a Cs^{+}-based intracellular solution and 500 nM extracellular TTX. Currents were elicited by 20 ms voltage steps (ΔV) from a holding potential of -60 mV to between -30 and +40 mV in 10 mV increments. The Ca^{2+} currents are defined as the currents remaining after digital subtraction of the currents elicited with the same protocol in the presence of 100 µM Cd^{2+}. (B) Corresponding current-voltage relationship from 5 different cells (data as mean ± S.E.M.).

In order to characterise further the nature of the Ca^{2+} current recorded from the soma of SCG neurones, selective Ca^{2+} channels inhibitors were used (*figure 11*). The Ca^{2+} current was elicited with a depolarising step from -60 mV to 0 mV (Ca^{2+} current peak as determined in *figure 10-B*) for 20 ms and the channel inhibitors were added cumulatively. Typically, a Ca^{2+} current was elicited in control (*figure 11-A*) and then ω-conotoxin GVIA (ω-CgTx GVIA, 500 nM) was added to the bath (*figure 11-A*). At the steady state inhibition, 10 μM nimodipine, a selective inhibitor of L-type Ca^{2+} channels, was then applied and finally the residual Ca^{2+} current was determined using 100 μM Cd^{2+} (*figure 11-A*). Most of the Ca^{2+} current was inhibited by ω-conotoxin GVIA, the remaining current was further inhibited by nimodipine and completely blocked with Cd^{2+} (84 ± 4% inhibition, 7 ± 3% and 9 ± 3% inhibition, respectively n = 7 - *figure 11-B*). As no selective inhibitors for the P/Q- and R-type Ca^{2+} channels were used, after ω-conotoxin GVIA and nimodipine inhibition, the remaining Ca^{2+} currents were regrouped under the denomination of residual current (P/Q/R- current in *figure 11-B*).

1.2. Changes in the free intracellular calcium concentration

Neurones were voltage-clamped in the perforated patch configuration (see Methods section 2.2.1, *figure 1* and Methods section 2.4.3, *Table 2* - solution I) and rise in $[Ca^{2+}]_i$ induced by depolarising steps from -60 mV to 0 mV. *Figure 12* illustrates a Ca^{2+} transient induced by a depolarising step for 60 ms and the top trace shows the actual changes in $[Ca^{2+}]_i$ calculated from the 407/480 nm emission ratio (blue trace and see Methods section 3.3.2 for details on the calibration procedure). The two traces in the bottom panels represent the corresponding changes in the indo-1 fluorescence emitted both at 407 (Ca^{2+}-bound form, green trace) and 480 nm (Ca^{2+}-free form, red trace). As expected, the rise in $[Ca^{2+}]_i$ induced a small increase in the fluorescence emitted at 407 nm and a larger decrease in the fluorescence emitted at 480 nm (*figure 12*, bottom panels).

Cells were depolarised from -60 mV to 0 mV for increasing length of time (from 15 to 210 ms in 15 ms increments for the first 4 traces and then in 30 ms increments) and the elicited Ca^{2+} transients analysed to determine the relationship between the depolarisation's duration and the characteristics of Ca^{2+} transients (*figure 13*). To make

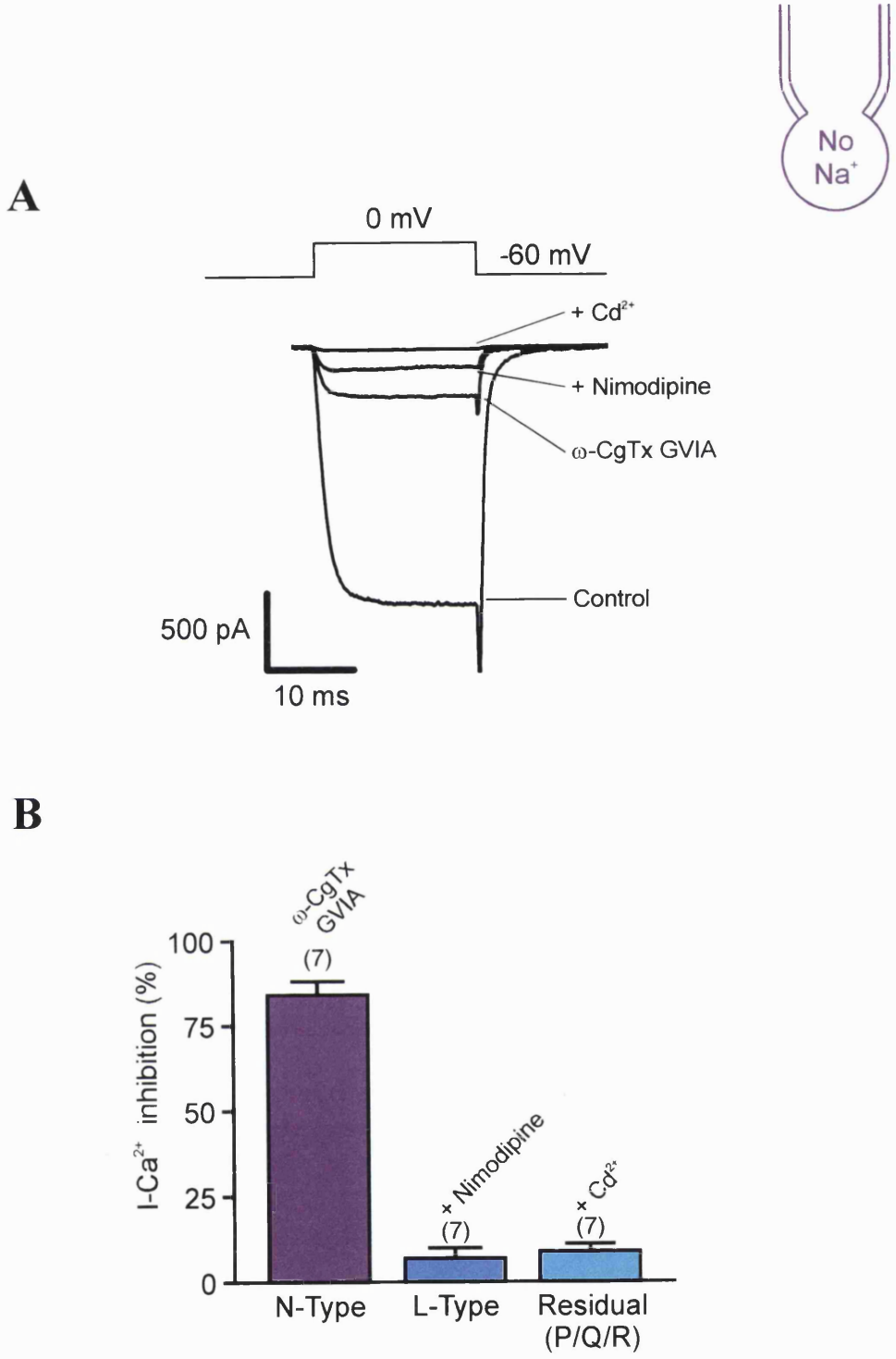

Figure 11: The N-type Ca^{2+} current is predominant in the soma of SCG neurones
(A) Representative macroscopic Ca^{2+} current in control and after application of ω-conotoxin GVIA (ω-CgTx GVIA, 500 nM), nimodipine (10 μM) and Cd^{2+} (100 μM) in an additive manner. Currents were generated by a single voltage step to 0 mV from a holding potential of -60 mV for 20 ms (see above recording). (B) Percentage inhibition of the different components of the somatic Ca^{2+} current as determined in (A) (n=7; data as mean ± S.E.M.).

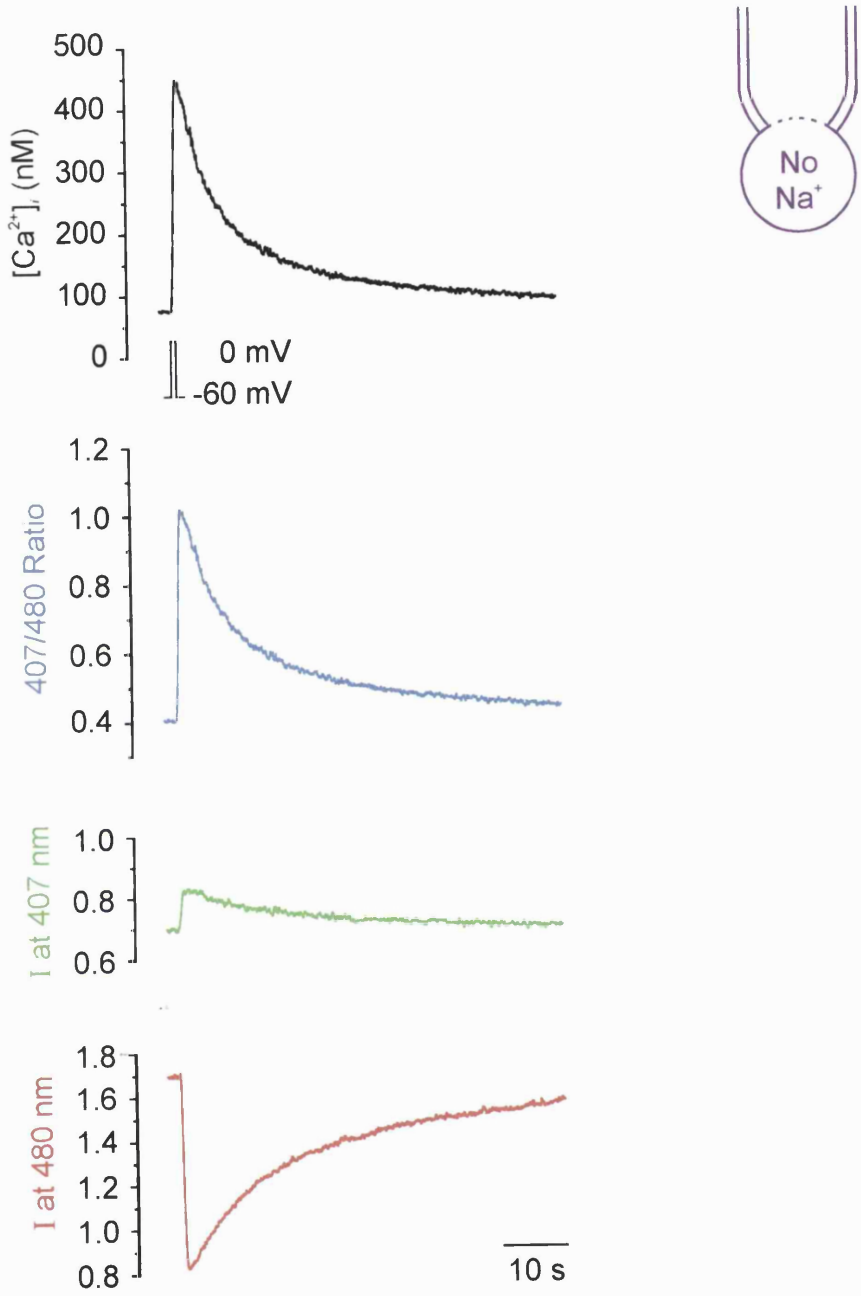

Figure 12: Variations in $[Ca^{2+}]_i$ recorded from the changes in the fluorescence properties of indo-1
Changes in $[Ca^{2+}]_i$ were induced by a 60 ms depolarising pulse (top panel). In this and subsequent figures, unless otherwise stated, neurones were voltage-clamped at a holding potential of -60 mV in the perforated patch configuration and the plasma membrane depolarised to 0 mV. When relevant, an inset in the top right corner of each figure illustrates the recording configuration. The middle panel represents the recording of the corresponding 407/480 fluorescence ratio (blue trace) and the two panels at the bottom show the changes in the intensity of the indo-1 fluorescence emitted at 407 nm (green trace) and 480 nm (red trace) following the binding of Ca^{2+} to indo-1.

the analysis of the recovery kinetics easier, intracellular Na^+ was omitted (see inset in *figure 13* and Results section 3.2 for further details on this particular aspect). Typically, the amplitude of the elicited Ca^{2+} transient increased linearly with the duration of the depolarisation until a plateau where any further increase in the depolarisation's duration only induced small additional rises in $[Ca^{2+}]_i$ but prolonged the recovery phase of the Ca^{2+} transients (*figure 13*). Moreover, it appears that the time course of the Ca^{2+} transients was dependent on the amplitude of the rise in $[Ca^{2+}]_i$ with a secondary phase developing for rises in $[Ca^{2+}]_i$ above 500 nM (see *figure 13 and 15-A*). In *figure 14*, three Ca^{2+} transients of increasing amplitude with the corresponding fit of their recovery phase and the analysis are represented. The Ca^{2+} transient on the left was elicited by a 60 ms depolarisation step and the amplitude of its peak was around 350 nM ($\approx$ 250 nM net increase, $\Delta[Ca^{2+}]_i$). The recovery of the Ca^{2+} transient was best fitted (see red line on top trace in *figure 14*, left) with a monoexponential function as can be seen from the residual plot (flat red line bottom trace in *figure 14*, left) and from the value of χ^2 close to zero (see inset in *figure 14*, left). The Ca^{2+} transient in the centre was elicited by the same voltage protocol but for 120 ms and its peak amplitude was above 500 nM. In this condition, the decay was no longer best fitted with a monoexponential function (large residual plot and $\chi^2 = 0.54$ - red lines in *figure 14*, centre). A better fit was obtained with a biexponential function (flat residual plot and $\chi^2 = 0.08$ - green lines in *figure 14*, centre). The trace on the right represents a rise in $[Ca^{2+}]_i$ elicited by a 500 ms depolarisation (*figure 14*, right). The recovery of such a large Ca^{2+} transient (> > 500 nM) was also best fitted with a biexponential decay function (flat residual plot and $\chi^2 = 0.08$ - green lines in *figure 14*, right). Therefore, it appears that the amplitude of the Ca^{2+} transients increased with the duration of the depolarisation and more importantly that the characteristics of the Ca^{2+} transient's recovery depended on the peak amplitude (A) associated with the exponential component (see Methods section 6.2 for more details). As shown in *figure 15-A*, for $[Ca^{2+}]_i$ below 500 nM (dashed line), the decay of Ca^{2+} transients was monophasic with a single decay time constant of 3.9 ± 0.2 s (τ, blue circles; n = 121) and an amplitude (A) that represented $\Delta[Ca^{2+}]_i$, (*i.e.* the peak amplitude minus resting $[Ca^{2+}]_i$). For $\Delta[Ca^{2+}]_i$ above 500 nM, the recovery phase of Ca^{2+} transients was biphasic and characterised by two decay time constants (τ_1 and τ_2) representing a

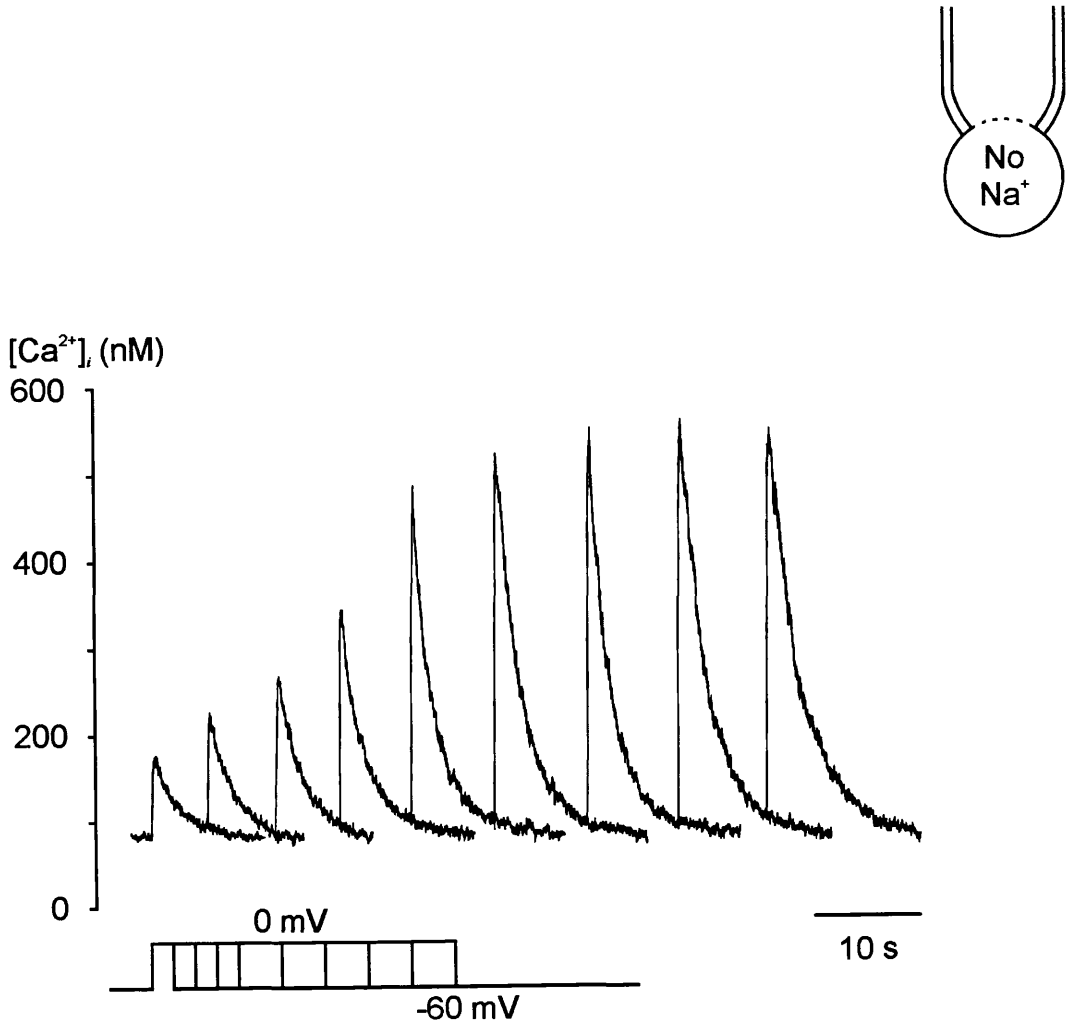

Figure 13: The kinetics of Ca^{2+} transients' recovery depends on the amplitude of the rise in $[Ca^{2+}]_i$
Representative recording of the changes in $[Ca^{2+}]_i$ induced by depolarising steps from -60 mV to 0 mV for increasing duration ranging from 15 to 210 ms (first 4 traces, 15 ms increments and next 5 traces, 30 ms increments - as shown under the recording).

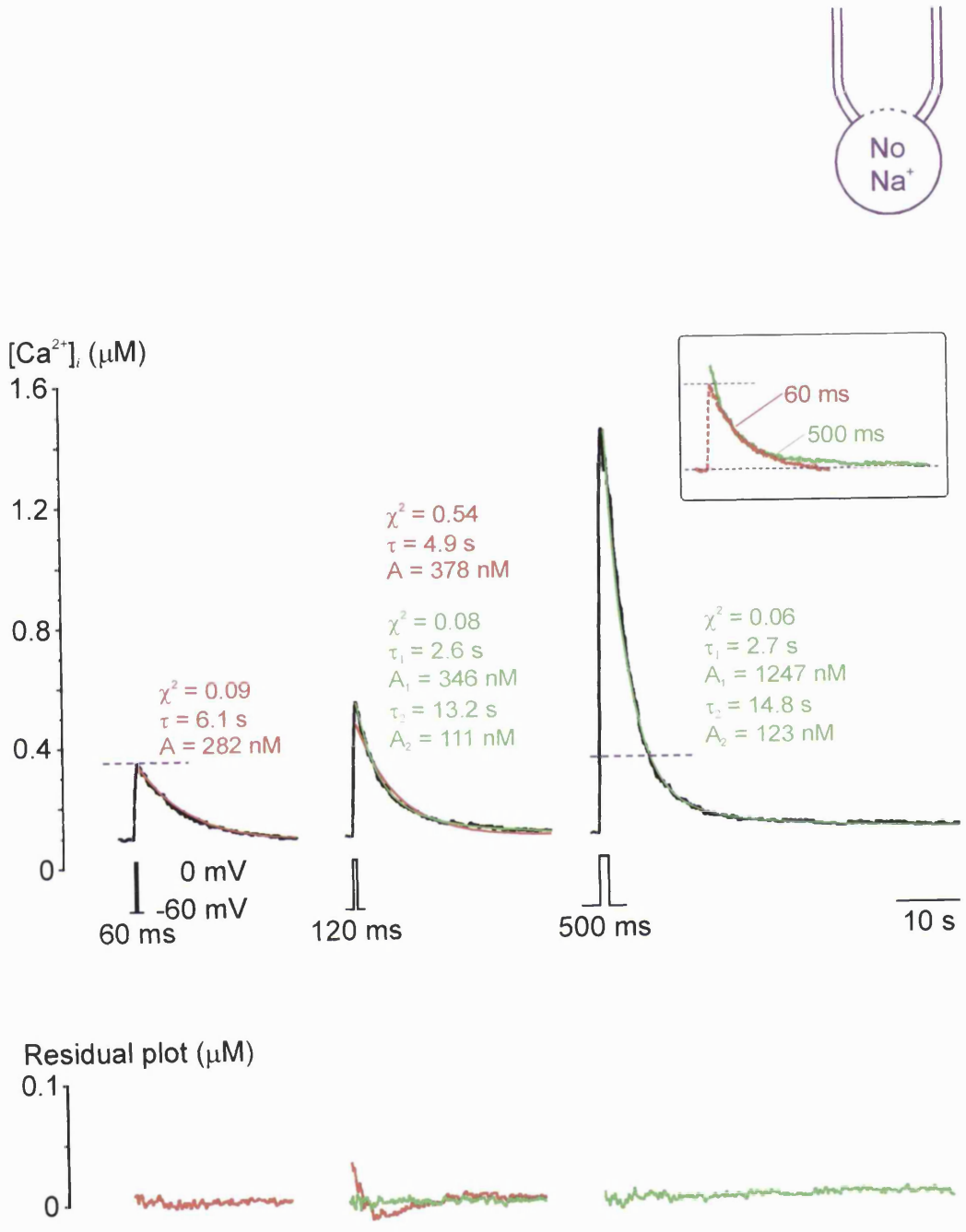

Figure 14: Changes in the kinetics of the Ca^{2+} transients' recovery phase with the increase in $[Ca^{2+}]_i$
Representative Ca^{2+} transients induced by depolarising steps of 60, 120 and 500 ms (top panel from left to right, respectively). The recovery phase of each Ca^{2+} transient has been fitted with an exponential decay function of the first and/or second order and the fits are superimposed on the traces (coloured line). For each fit, the value of the decay time constant(s) (τ, τ_1 and τ_2) and the amplitude(s) of the exponential component(s) (A, A_1 and A_2) are mentioned above the traces. The goodness of the fit was assessed from the value of χ^2 (close to 0 for the best fit) and from the residual plot (μM, lower panel) calculated as the difference between the fit and the experimental points (flat residual plot for the best fit).

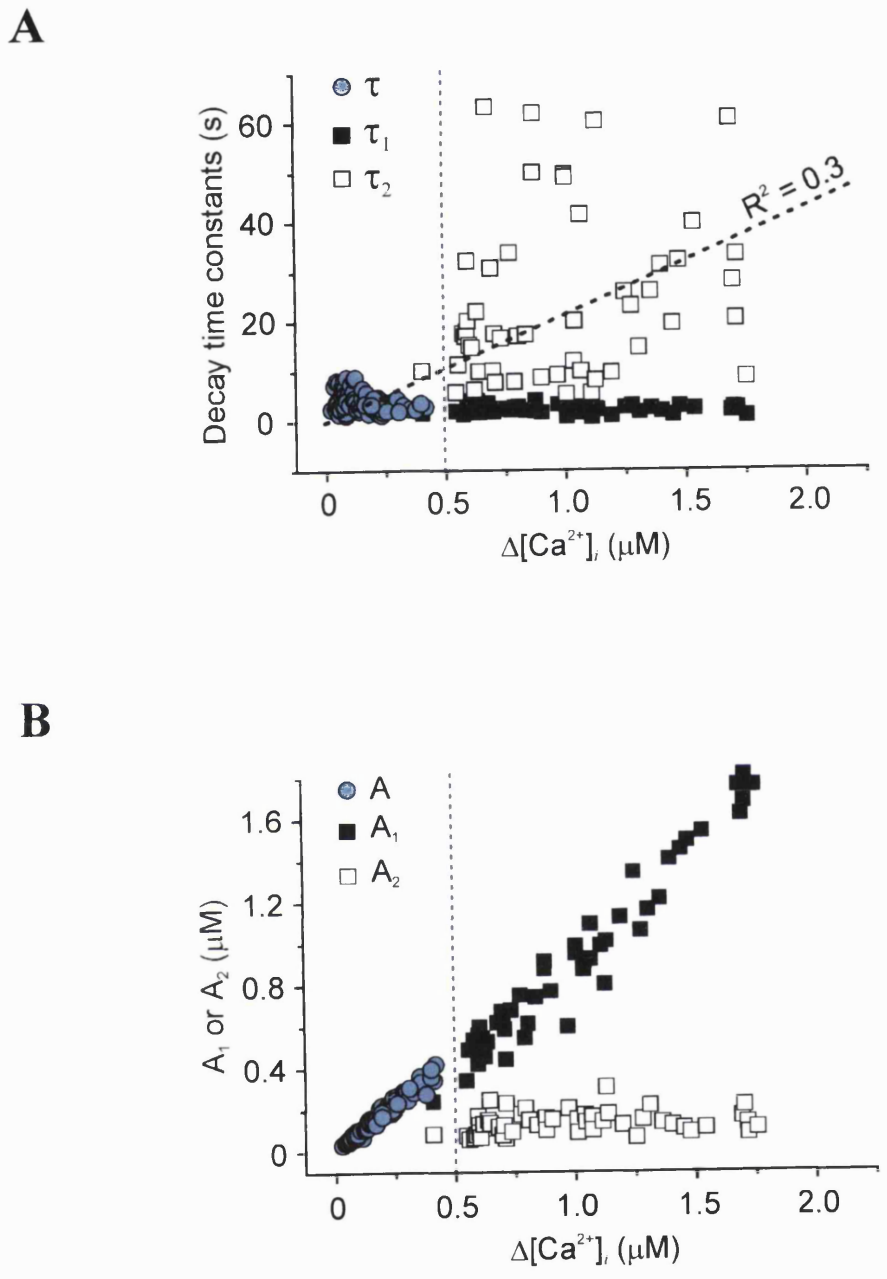

Figure 15: Plot of the decay time constant and amplitude for each component of the exponential recovery versus the net rise in $[Ca^{2+}]_i$

(A) For each Ca^{2+} transient the time constant(s) of the recovery phase has(have) been plotted against the net increase in $[Ca^{2+}]_i$ ($\Delta[Ca^{2+}]_i$) *i.e.* the difference between the peak amplitude and resting $[Ca^{2+}]_i$ (τ, blue circles for monoexponential recoveries; n=121 - τ_1, solid squares and τ_2, open squares for the fast and slow component of biexponential recoveries, respectively; n = 52). (B) Equivalent plot to (A) but with the amplitude(s) of each component(s) of the exponential recoveries (A, blue circles amplitude for monoexponential recoveries; n=121 - A_1, solid squares and A_2, open squares for the amplitude of the fast and slow component of biexponential recoveries, respectively; n = 52). The vertical dashed line at 0.5 μM represents the critical threshold concentration above which the recovery becomes biexponential.

fast and slow component of the recovery (τ_1 = 2.3 ± 0.1 s and τ_2 = 23.2 ± 2.2 s, solid and open squares, respectively; n = 52). The plot of the decay time constants against $\Delta[Ca^{2+}]_i$ indicated little dependence of the fast time constants on the peak $[Ca^{2+}]_i$ while there was no correlation between the slow time constant and the rise in $[Ca^{2+}]_i$ (R^2 = 0.3, *figure 15-A*).

The amplitude (A, A_1 and A_2) associated with each of the exponential decay component represents their respective contribution to the whole recovery process. When the amplitude of each exponential component of the fit was plotted against $\Delta[Ca^{2+}]_i$ (*figure 15-B*), the amplitudes of the monoexponential decays and of the fast component of the biexponential decays increased linearly with the rise in $\Delta[Ca^{2+}]_i$ (*figure 15-B*, blue circle and solid squares; n=121 and n=52, respectively). In contrast, the amplitude of the slow component of the biexponential decays appeared constant (122 ± 7 nM; n = 52) suggesting a contribution to the overall recovery process independent of variations in $\Delta[Ca^{2+}]_i$. (*figure 15*). This result suggested that different systems might be involved in the Ca^{2+} clearance process. The contribution of the fast component to the overall recovery can be estimated by calculating the ratio ($A_1/[A_1+A_2]$) of the fast component's amplitude over the sum of the amplitudes, as illustrated in *figure 16-A*. The data presented show that the contribution of the fast component for $\Delta[Ca^{2+}]_i \approx$ 500 nM represented ≈ 75% of the whole recovery process and increased with the rise in $\Delta[Ca^{2+}]_i$ (≈ 90% at 1 μM).

Finally, for each recovery phase, the clearance rate ($-d[Ca^{2+}]/dt$) can be calculated by differentiating the exponential fit (see Methods section 6.2 for more details) and plotted against the $[Ca^{2+}]_i$. For monoexponential decays, the clearance rate is linear ($y = A + Bx$). The slope of the line represents the rate of recovery (s^{-1}) and the intercept with the x-axis (*i.e.* for an apparent rate equal to 0) represents resting $[Ca^{2+}]_i$. Biexponential recovery have a clearance rate defined by a polynomial function of the second order ($y = A + Bx + Cx^2$) with two slopes representing the rate of at least two processes involved in the recovery. *Figure 16-B* illustrates the clearance rate for the recovery of Ca^{2+} transients for rises in $[Ca^{2+}]_i$ > 500 nM obtained for 60 Ca^{2+} transients. For more clarity, in the following sections (see Results sections 3 to 6) only the fit of the clearance rate obtained from the pooled data will be represented.

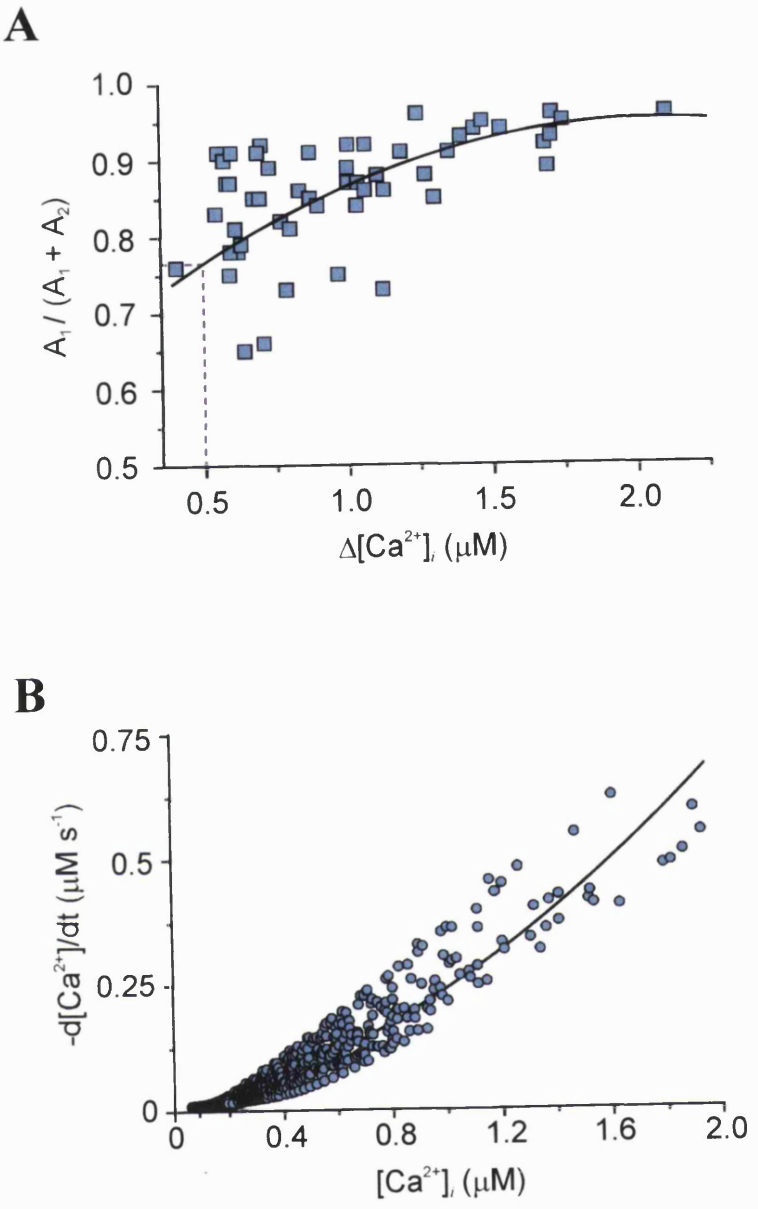

Figure 16: Plot of the fast component contribution to the overall recovery phase and clearance rate for biexponential decays

(A) For each biexponential recovery, the relative contribution of the fast component of the recovery phase has been determined and plotted against the net rise in $[Ca^{2+}]_i$ (n=52). This contribution has been calculated as the ratio $(A_1/[A_1+A_2])$ between the amplitude of the fast component (A_1) divided by the sum of the amplitude of the two components (A_1+A_2). (B) Clearance rate for Ca^{2+} transients above 500 nM obtained from 60 Ca^{2+} transients. For each Ca^{2+} transient, the clearance rate was obtained from the differentiate of the recovery fit and plotted against $[Ca^{2+}]_i$. The experimental data were then fitted with a polynomial function of the second order and the line represents the best fit.

Taken together, these results suggests that the changes in $[Ca^{2+}]_i$ were mainly due to the activation of somatic N-type Ca^{2+} channels and that the amplitude of the rise in $[Ca^{2+}]_i$ was proportional to the duration of the Ca^{2+} influx. Furthermore, the Ca^{2+} transient's recovery was exponential and switched from a monoexponential to a biexponential decay above a $[Ca^{2+}]_i$ of 500 nM. The biexponential recoveries were characterised by a fast component, whose amplitude became more predominant with the rise in $[Ca^{2+}]_i$ and a slow component independent of $[Ca^{2+}]_i$. Finally, the results suggested that there might be different mechanisms and/or different activation states of the Ca^{2+} clearance systems for rises in $[Ca^{2+}]_i$ below and above 500 nM.

1.3. Discussion

Rat sympathetic neurones have been shown to express N-type Ca^{2+} channels both on their soma and dendrites where they represent the predominant Ca^{2+} influx pathway (Hirning *et al.*, 1988; Plummer *et al.*, 1989; Regan *et al.*, 1991; Lin & Bennett, 1998 and Delmas *et al.*, 2000). Calcium influx through somatic N-type Ca^{2+} channels has been demonstrated to contribute to spike-frequency adaptation *via* activation of a Ca^{2+}-dependent potassium currents (Brown, 1990 and Davies *et al.*, 1996) whereas at the nerve terminals they are thought to induce neurotransmitter release. These Ca^{2+} channels are modulated by G protein-coupled receptors activated by hormones and neurotransmitters, particularly acetylcholine and noradrenaline (Marrion *et al.*, 1987; Plummer *et al.*, 1989; Ikeda & Schofield, 1989 and Delmas, 1998a, b, 2000). A comparison of somatic and dendritic N-type Ca^{2+} channels suggested that these channels exhibit different properties, are modulated differently and therefore the elicited Ca^{2+} signal would be site-specific (Delmas *et al.*, 2000).

The present study focuses on changes in $[Ca^{2+}]_i$ induced by activation of somatic N-type channels and the analysis of the depolarisation-induced Ca^{2+} transients showed that variations in $[Ca^{2+}]_i$ were proportional to the Ca^{2+} influx. In fact, there was a direct correlation between the amplitude of the rise in $[Ca^{2+}]_i$ and the duration and/or the amplitude of the Ca^{2+} current (see *figure 13* in this study and Trouslard *et al.*, 1993) and similar results were obtained in several other cell types (rat clonal pituitary cells, GH_3 - Benham, 1989; pancreatic β cells - Rorsman *et al.*, 1992; sensory DRG neurones - Benham *et al.*, 1992; nerve ending - Stuenkel, 1994 and spinal cord motoneurones -

Palecek *et al.*, 1999). However, it is difficult to compare quantitatively the characteristics of the Ca^{2+} transients' recovery between different studies because of the different properties of the cells, the type of the Ca^{2+} dye and the recording conditions used. The recovery of Ca^{2+} transients is defined by an exponential decay function, whose characteristics, in most neuronal cell types, depend on the amplitude of the rise in $[Ca^{2+}]_i$. Thus for low $[Ca^{2+}]_i$ (< 500 nM) the recovery is generally monoexponential (this study and see Benham *et al.*, 1992; Park *et al.*, 1996; Fierro *et al.*, 1998; Lin & Bennett, 1998 and Maeda *et al.*, 1999) whereas for higher $[Ca^{2+}]_i$ the recovery becomes biexponential (Park *et al.*, 1996; Fierro *et al.*, 1998 and Maeda *et al.*, 1999).

In most neurones during biexponential recoveries, there is a slow component at low $[Ca^{2+}]_i$ whose decay time constant is about 10-times slower than that of the fast component of the recovery (0.5 s *versus* 4 s in synaptic boutons of SCG neurones - Lin & Bennett, 1998; 2.5 s *versus* 35 s in mouse Purkinje neurones - Maeda *et al.*, 1999 and 0.6 s *versus* 3 s in rat Purkinje neurones - Fierro *et al.*, 1998). The data obtained from SCG neurones followed the same general pattern (2.5 s for the fast component *versus* 25 s for the slow component - this study) as that observed in other cell types (*e.g.* Park *et al.*, 1996; Fierro *et al.*, 1998 and Maeda *et al.*, 1999) and it appears that a $[Ca^{2+}]_i \approx 500$ nM represents a critical value where the recovery switched from a monoexponential to a biexponential recovery. These results also suggest that the time constant of monoexponential recoveries accelerated with the increase in $[Ca^{2+}]_i$ and tended to the value of the fast decay time constant of biexponential recoveries (see *figure 14 and 15-A*). Moreover, the amplitude associated with the fast component (monoexponential and biexponential recoveries) of the recovery increased linearly with the rise in $\Delta[Ca^{2+}]_i$ (see *figure 15-B*). Such behaviour would suggest that the Ca^{2+} extrusion process might result from a progressive Ca^{2+}-dependent acceleration of the clearance mechanisms and the activation of clearance processes with low Ca^{2+} affinity when $[Ca^{2+}]_i$ rises above 500 nM.

Calcium transients (in the absence of intracellular Ca^{2+}) with peak amplitudes above 500 nM exhibited a secondary slow component that appears to be mediated by an independent mechanism. Thus, this slow component was only observed following increase in $[Ca^{2+}]_i$ above 500 nM. Secondly, in contrast to the monoexponential and to the fast component of biexponential recoveries, the amplitude associated to this slow

component was constant and independent from the rise in $\Delta[Ca^{2+}]_i$ ($\approx$ 120 nM - see *figure 15-B*). Similarly, the decay time constant of this slow component appeared independent from the amplitude of the Ca^{2+} transient since no correlation was observed. Although the amplitude of this slow component was in a similar $[Ca^{2+}]_i$ range than that of monoexponential recoveries (see *figures 15-A* and *-B*) its decay time was $\approx$ 10-times slower (3.9 $\pm$ 0.2 s for monoexponential recoveries *versus* 23.2 $\pm$ 0.1 s for the slow component of biexponential recoveries). One could therefore consider that large rises in $[Ca^{2+}]_i$ might induce a secondary recovery phase that would compete with and delay the extrusion process. On the other hand, one could consider that the recovery from small rises in $[Ca^{2+}]_i$ would also be biexponential with the secondary slow phase not detectable with the analysis procedure.

Some authors (Neher & Augustine, 1992 and Neher, 1995) have suggested that the slow component of biexponential recoveries might correspond to the slow dissociation of Ca^{2+} from endogenous buffers acting as the limiting step in Ca^{2+} extrusion (Helmchen *et al.*, 1996; Airaksinen *et al.*, 1997; Lee *et al.*, 2000). However, such a biexponential recovery induced by the Ca^{2+} buffering system was observed for rises in $[Ca^{2+}]_i$ close to rest ($<<$ 500 nM in chromaffin cells, Neher & Augustine, 1992; in cerebellar Purkinje neurones, Airaksinen *et al.*, 1997; CA1 hippocampal neurones, Lee *et al.*, 2000) whereas, in the present study at low $[Ca^{2+}]_i$ the recovery appeared monoexponential. Therefore, the slow component of biexponential recovery is unlikely to be solely due to a slow Ca^{2+} dissociation from CaBPs but could also be attributed to Ca^{2+} release from intracellular organelles. Thus, the rise in $[Ca^{2+}]_i$ would activate Ca^{2+} uptake mechanisms and subsequently Ca^{2+} would be slowly released when $[Ca^{2+}]_i$ decreased to $\approx$ 120 nM resulting in a delay of the recovery time course (see also Park *et al.*, 1996). Nevertheless, it is important to consider that this situation does not reflect physiological condition since intracellular Na^+ was omitted in the intracellular solution and therefore Ca^{2+} release from the mitochondria is mostly inhibited (see Results section 3).

The results presented in this section demonstrated a clear difference in the properties of the Ca^{2+} transients' recovery depending on their peak amplitude with a threshold $[Ca^{2+}]_i \approx$ 500 nM (see *figures 14 and 15*). Therefore, voltage protocols were designed to elicit Ca^{2+} transients with peak amplitude below or above this threshold.

Figure 17 illustrates recording of Ca^{2+} transients elicited by either 60 or 500 ms depolarising steps to 0 mV that exhibited monoexponential (*figure 17-A*) and biexponential recovery (*figure 17-B*), respectively. The induced rise in $[Ca^{2+}]_i$ continued beyond the end of the Ca^{2+} current pulse (see *figures 17* and *18*). The recordings corresponded to spatially averaged Ca^{2+} transients and therefore the delay observed between the peak of the Ca^{2+} current and the peak of the Ca^{2+} transient might reflect the Ca^{2+} diffusion and equilibration within the soma. Thus, in mouse Purkinje neurones, equilibration of the Ca^{2+} gradient was observed in 0.2-0.3 second and 1 second after depolarisation steps for 50 ms and 500 ms, respectively (Maeda *et al.*, 1999). An alternative explanation could be an amplification process through Ca^{2+} release from intracellular stores. However in SCG neurones no evidence to support such a mechanism was observed (see Results section 4). Finally, it is important to emphasise that indo-1 is a high affinity Ca^{2+} indicator that can act as a Ca^{2+} buffer (Grynkiewicz, 1985; Neher & Augustine, 1992; Neher, 1995 and see also Results section 2.2) and that the kinetics of the variations in $[Ca^{2+}]_i$ would be limited by the kinetics of Ca^{2+} binding to indo-1. High concentrations of indo-1 would affect the characteristics of the Ca^{2+} transients by attenuating their amplitude and slowing their recovery phase (Neher & Augustine, 1992). However, Benham (1989), using 100 μM indo-1 in GH_3 cells, suggested that at this concentration the Ca^{2+} indicator did not significantly affect neither the Ca^{2+} buffering capacity nor the properties of the Ca^{2+} transients. A similar observation was made in rat Purkinje cerebellar neurones by Fierro *et al.* (1998), who showed that increasing the fura-2 concentration from 25 to 250 μM did not significantly perturb the recovery phase of depolarisation-induced Ca^{2+} transients. Under the recording conditions used in the present study and after 35 minutes loading period, the indo-1 concentration was estimated around 50 μM by comparison with the fluorescence intensity observed in whole-cell recordings where 50 μM was added to the intracellular solution. With shorter loading duration and up to 45 minutes, no significant variations in the properties of the Ca^{2+} transient were observed suggesting that indo-1 had minimal effect on the Ca^{2+} signal. However, since the Ca^{2+} response recorded corresponded to the somatic averaged Ca^{2+} transient and because of the indo-1 binding kinetics, the amplitude of the Ca^{2+} transient and the recovery time stated may be underestimated and

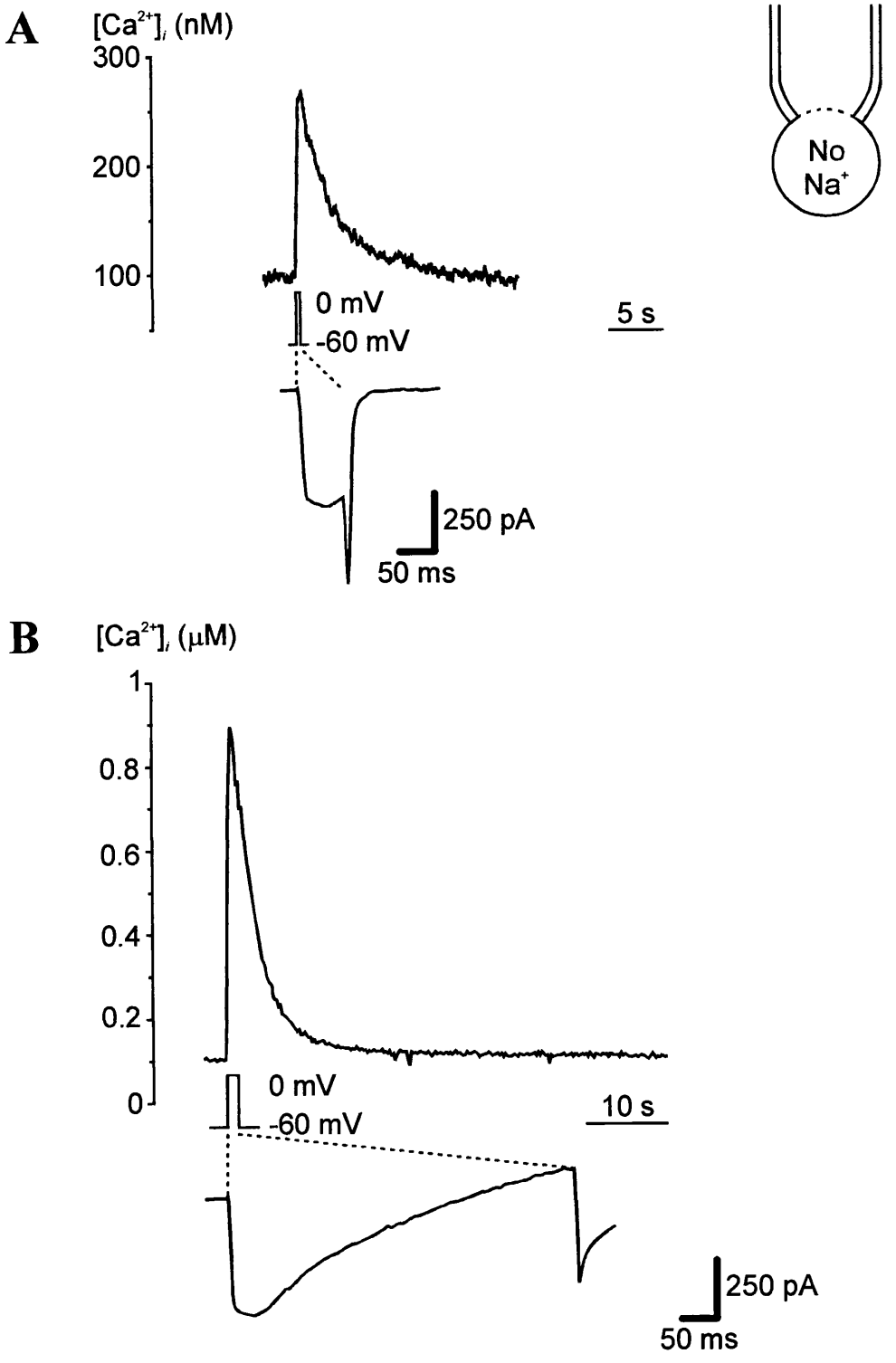

Figure 17: Small and Large Ca^{2+} transients and the corresponding Ca^{2+} current
Recording of Ca^{2+} transients induced by a 60 ms (A) and a 500 ms (B) depolarising pulse with the corresponding recording of the elicited Ca^{2+} currents. The recordings were carried out in the absence of intracellular Na^{+} (see inset and Results section 3.2 for further details on this aspect). From now on and for more simplicity, the Ca^{2+} transients induced by depolarisation for 60 and 500 ms will be denominated small and large Ca^{2+} transients respectively.

may not be representative of what occurs close to the plasma membrane. The use of a low affinity Ca^{2+} dye (Ca^{2+} green; oregon green or benzothiazide coumarin) and the study of Ca^{2+} signal close to the plasma membrane might give more accurate amplitude and recovery kinetics for depolarisation-induced Ca^{2+} transients. On the other hand, they would give less accurate measurements of resting $[Ca^{2+}]_i$. In the present study, the main attention was focused on the mechanisms involved in the regulation of $[Ca^{2+}]_i$ close to rest and of the Ca^{2+} transient's recovery. The involvement of a particular regulatory system was assessed by comparison of the control situation with a situation in the presence of a specific inhibitor and therefore the study could be carried out using indo-1 as Ca^{2+} indicator.

In conclusion, the data as shown represent the somatic average of $[Ca^{2+}]_i$ variations that appeared to be directly proportional to the duration of the depolarisation-induced Ca^{2+} influx. The rate of recovery from these Ca^{2+} transients was dependent on the amplitude of the rise in $[Ca^{2+}]_i$ and suggest a Ca^{2+}-dependent acceleration and a progressive activation of Ca^{2+} clearance systems. Following large rise in $[Ca^{2+}]_i$ (in the absence of intracellular Na^+), the recovery phase presented a secondary slow component that had an amplitude and a decay time constant that appeared independent from the rise in $[Ca^{2+}]_i$. Such a slow secondary phase might represent either a Ca^{2+} release from intracellular stores or the slow Ca^{2+} dissociation from CaBPs.

2. Endogenous calcium buffering capacity

In order to determine the Ca^{2+} buffering properties in SCG neurones, Ca^{2+} entry was generated with depolarisation of increasing duration and the corresponding changes in $[Ca^{2+}]_i$ measured with indo-1. From these recordings, the total concentration of Ca^{2+} entering the cell ($[Ca^{2+}]_{total}$) and the amount bound to the buffer ($[Ca^{2+}]_{bound}$) were calculated. The endogenous buffering capacity was then estimated from the Ca^{2+} binding ratio (κ_{endo}). Finally, to characterise further the properties of the endogenous buffering capacity, the Ca^{2+} binding ratio for EGTA (κ_{EGTA}) was determined theoretically and compared with the endogenous Ca^{2+} binding ratio.

2.1. Free calcium concentration versus calcium charge transfer

Neurones were voltage-clamped at -60 mV in the whole-cell configuration with 100 μM indo-1 added to the intracellular solution (Cs^+-based intracellular solution see Methods section 2.2.2, *figure 1* and Methods section 2.4.3, *Table 2* - solution J). Calcium currents were elicited with depolarising steps from -60 to 0 mV for between 10 to 300 ms and the induced rise in $[Ca^{2+}]_i$ measured with indo-1. *Figure 18* illustrates a typical recording where changes in $[Ca^{2+}]_i$ (*figure 18-A*) are represented with the corresponding Ca^{2+} currents (I_{Ca}, *figure 18-B*) elicited by depolarising steps for 10, 20, 40, 80 and 160 ms. The Ca^{2+} currents were obtained after digital subtraction of the outward current recorded with the same voltage protocol in presence of 100 μM Cd^{2+}. Therefore, the currents mainly represented Ca^{2+} influx through the plasma membrane during the depolarising step *i.e.* the total amount of Ca^{2+} ions that have entered the cytosol ($[Ca^{2+}]_{total}$, see Results section 2.2).

From the integral of I_{Ca}, it was then possible to calculate, the total Ca^{2+} charge transfer (Q_{Ca}):

$$Q_{Ca} = -\int I_{Ca}\,dt \quad \textit{Equation 12}$$

Q_{Ca} corresponds to the area under the current trace and is expressed in amperes second (A.s) or coulombs (C) (*figure 19-A*). *Figure 19-B* illustrates the mean of the Ca^{2+} charge

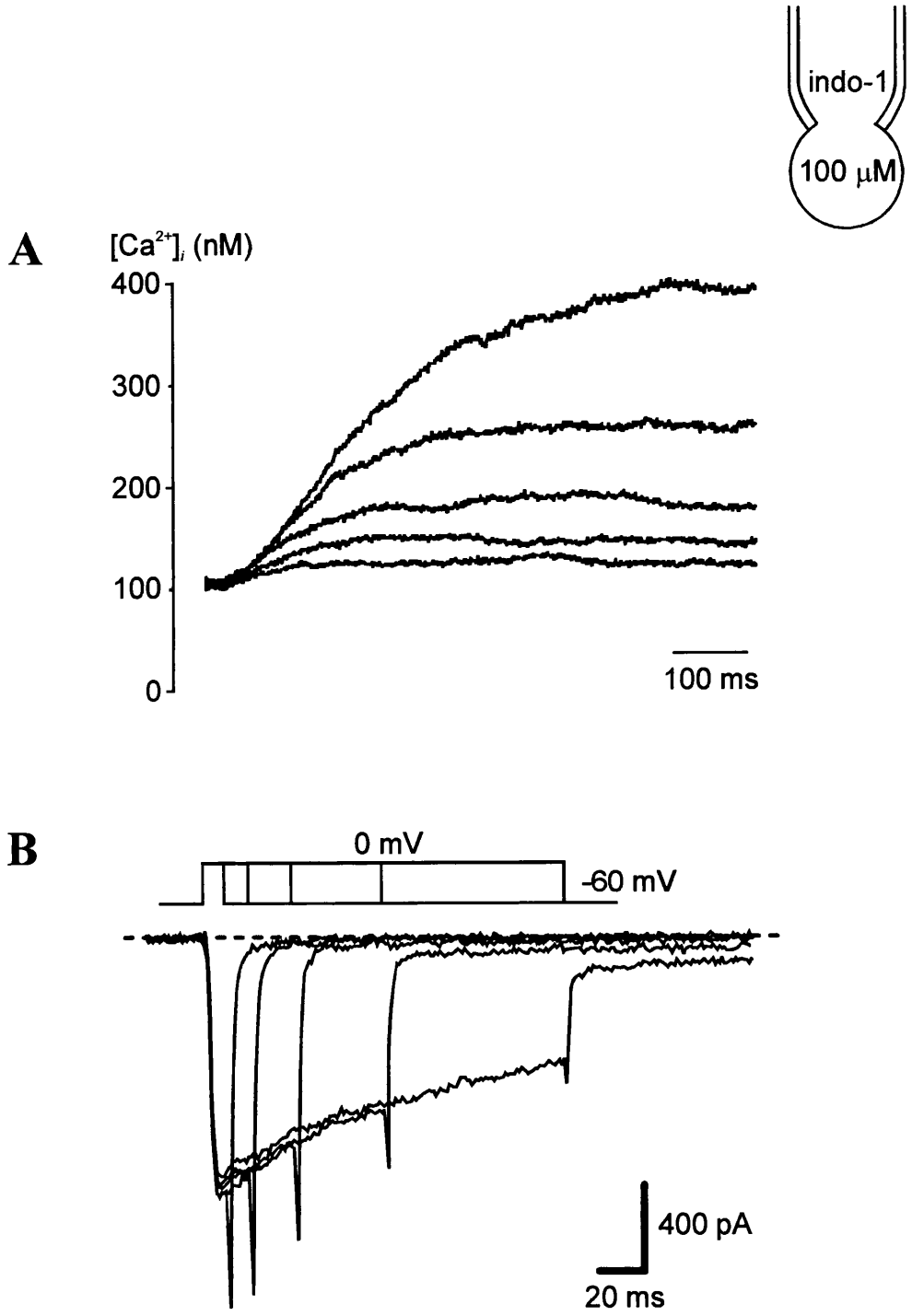

Figure 18: Rise in the $[Ca^{2+}]_i$ and the corresponding I_{Ca} induced by depolarising steps of increasing duration

(A) Transient rises in $[Ca^{2+}]_i$ induced by activation of VACC with depolarising steps of 10, 20, 40, 80 and 160 ms. (B) Corresponding currents traces elicited in the whole-cell patch clamp configuration (see inset - 100 μM indo-1) from a holding potential of -60 mV to 0 mV. The currents represent Ca^{2+} currents after digital subtraction of the outward current remaining in the presence of 100 μM cadmium.

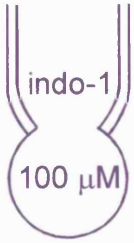

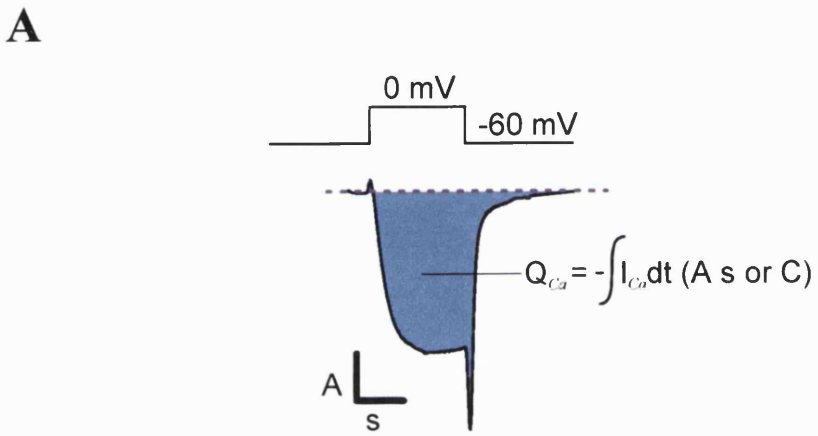

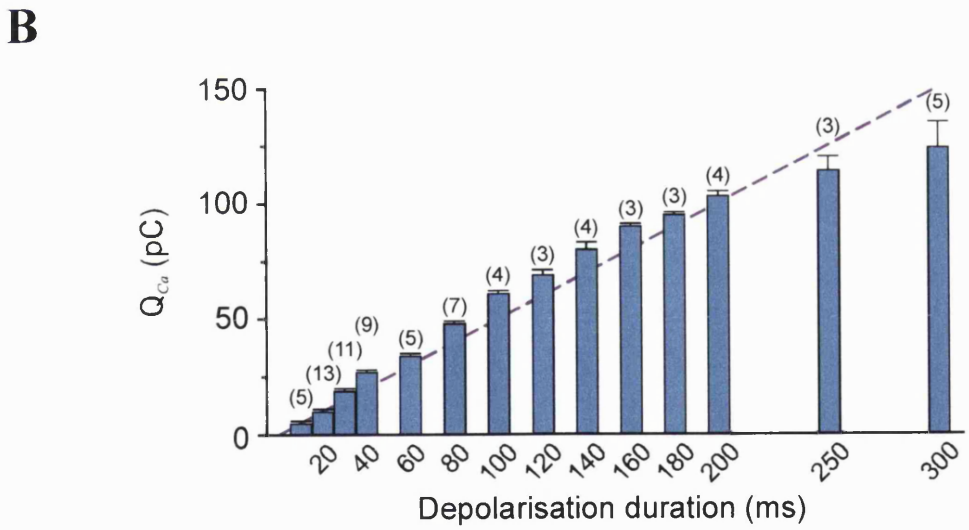

Figure 19: Net variation in the Ca^{2+} charge transfer as a function of the depolarisation duration
(A) Diagram of a Ca^{2+} current (I_{Ca}) and the corresponding integral representing the Ca^{2+} charge transfer (Q_{Ca}, blue area under the curve). (B) Plot of the Ca^{2+} charge transfer (regrouped in 10 pC increments) as a function of the duration of the depolarisation (as shown under the graph in ms, n number mentioned in bracket above each bar - data as mean ± S.E.M.). The dashed line represents the fit of the expected Ca^{2+} charge transfer based on the 10 ms depolarisation and assuming the absence of current inactivation.

transfer plotted against the depolarisation duration (bottom axis in *figure 19-B*; n=14 cells). The Ca^{2+} charge transfer increased with the duration of the depolarisation (from 5 ± 1 pC for 10 ms depolarisation; n=5 to 124 ± 11 pC for 300 ms depolarisation; n=5). However, the charge transfer did not appear linearly proportional to the depolarisation duration as a charge transfer of 5 pC for 10 ms depolarising step did not equate to 150 pC at 300 ms (see dashed line in *figure 19-B*, which represents the linear fit of the expected charge transfer). This result suggested a time and/or Ca^{2+}-dependent current inactivation as shown by the decrease in the amplitude of I_{Ca} observed for longer depolarisation durations (*figure 18-B*).

The changes in $[Ca^{2+}]_i$ induced by I_{Ca} were simultaneously recorded, as illustrated in *figure 18-A*, and the net change in $[Ca^{2+}]_i$ ($\Delta[Ca^{2+}]_i$) calculated as the difference between the peak amplitude ($[Ca^{2+}]_{peak}$) of the induced Ca^{2+} transient and the $[Ca^{2+}]_i$ at rest ($[Ca^{2+}]_{rest}$). The $\Delta[Ca^{2+}]_i$ is represented against the corresponding calculated Ca^{2+} charge transfer and increased linearly with Q_{Ca} (data pooled from 14 cells were fitted with a linear regression, *figure 20-A*). This result suggested that the changes in $[Ca^{2+}]_i$ were directly dependent on and proportional to the amount of Ca^{2+} ions that entered the cell through the Ca^{2+} channels (see also below Results section 2.2).

2.2. Calculation of the total calcium entering the cytosol

To improve the efficiency of the voltage-clamp and the quality of the current recordings, experiments were conducted on neurones with small neurites and a measured cell diameter ≈ 20 μm. It was then possible to select neurones of similar size using the field aperture of the microscope set to its minimum (≈ 20 μm, see Methods section 3.2).

If one assumes that a neurone is a perfect sphere, its volume can then be estimated from the following equation:

$$V = \frac{4}{3} \times \pi \times R^3 \quad \textit{Equation 13}$$

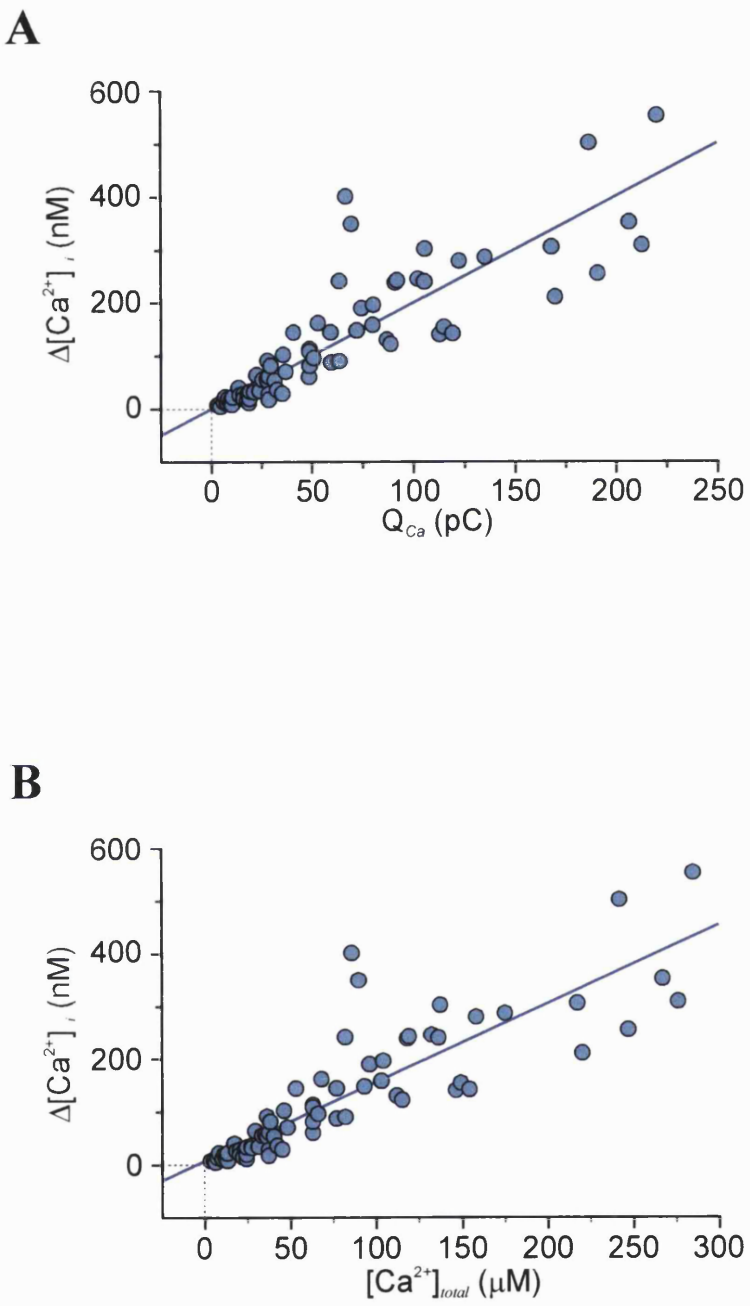

Figure 20: Net variation in $[Ca^{2+}]_i$ as a function of the Ca^{2+} charge transfer and the estimated $[Ca^{2+}]_{total}$
(A) Pooled data of the net increase in $[Ca^{2+}]_i$ ($\Delta[Ca^{2+}]_i$, nM) against the Ca^{2+} charge transfer (Q_{Ca}, pC) recorded from 14 different cells. (B) Pooled data of $\Delta[Ca^{2+}]_i$ as a function of the $[Ca^{2+}]_{total}$ calculated from Q_{Ca} and the estimated cell volume ($[Ca^{2+}]_{total} = Q_{Ca}/2FV$ - see text for detail) recorded from 14 different cells. The solid lines in (A) and (B) represent the best fit obtained from a linear regression.

where R was the measured radius of the soma (≈ 10 μm) and π ≈ 3.14. Therefore, an estimate of the cell volume was given by:

$$V = 4.2 \times 10^{-15} \mu m^3 = 4.2 \text{ pl}$$

Knowing Q_{Ca}, the total Ca^{2+} entry ($[Ca^{2+}]_{total}$) during a voltage step can be calculated as follow:

$$[Ca^{2+}]_{total} = \frac{Q_{Ca}}{zFV} \quad \textit{Equation 14}$$

where F is the *Faraday* constant (96485 $C.mol^{-1}$), z the valence of the Ca^{2+} ion (z = 2) and V the accessible cell volume (*Equation 13*). In the absence of any buffer and with an instantaneous Ca^{2+} influx, all the Ca^{2+} that enters the cytosol would be in its free ionic form and would represent the total Ca^{2+} concentration ($[Ca^{2+}]_{total}$). *Figure 20-B* illustrates the relationship between the measured $\Delta[Ca^{2+}]_i$ (as defined in Results section 2.1) and $[Ca^{2+}]_{total}$ (calculated from I_{Ca}, *Equation* 14). This result confirmed the observation from *figure 20-A* by showing that the rise in $\Delta[Ca^{2+}]_i$ was directly proportional to the increase of $[Ca^{2+}]_{total}$. However, it can be noticed that the calculated $[Ca^{2+}]_{total}$ entering the cytosol was in the micromolar range whereas the measured $\Delta[Ca^{2+}]_i$ was in the nanomolar range *i.e.* $\Delta[Ca^{2+}]_i$ was at least 1000-times smaller than expected.

Knowing $\Delta[Ca^{2+}]_i$ and $[Ca^{2+}]_{total}$, the variation in the concentration of the Ca^{2+} bound to the buffers ($[Ca^{2+}]_{bound}$) can be deduced from the mass action equation:

$$[Ca^{2+}]_{total} = [Ca^{2+}]_i + [Ca^{2+}]_{bound} \quad \textit{Equation 15}$$

$$\text{and } [Ca^{2+}]_{bound} = [Ca^{2+}]_{total} - [Ca^{2+}]_i \quad \textit{Equation 16}$$

2.3. The endogenous calcium binding ratio in SCG neurones

The Ca^{2+} binding ratio (κ) is defined at a particular $[Ca^{2+}]_i$ (Neher & Augustine, 1992) by:

$$\kappa = \frac{\Delta[Ca^{2+}]_{bound}}{\Delta[Ca^{2+}]_i} \quad \textit{Equation 17}$$

where $\Delta[Ca^{2+}]_i$, is obtained as described above in Results section 2.1 and $[Ca^{2+}]_{bound}$ is calculated from *Equation 16*.

In fact, in *Equation 17*, κ represents the total Ca^{2+} binding ratio (κ_{total}) because indo-1, which was added to the cytosol, also acts as a Ca^{2+} buffer and competes with the endogenous Ca^{2+} buffer for the free Ca^{2+}. Therefore, κ_{total} is defined as:

$$\kappa_{total} = \kappa_{endo} + \kappa_{indo-1} \quad \textit{Equation 18}$$

where κ_{endo} and κ_{indo-1} represent the endogenous Ca^{2+} binding ratio and the Ca^{2+} buffering component added by indo-1, respectively. The Ca^{2+} binding ratio for indo-1 was determined as described by Palecek *et al.* (1999) using the following equation:

$$\kappa_{indo-1} = \frac{[\text{indo} - 1] \times K_{d(indo-1)}}{\left([Ca^{2+}]_{rest} + K_{d(indo-1)}\right)\left([Ca^{2+}]_{peak} + K_{d(indo-1)}\right)} \quad \textit{Equation 19}$$

where [indo-1] is the total indo-1 concentration (100 μM) at the diffusion's equilibrium (≈ 10 minutes) and $K_{d(indo-1)}$ (93.3 nM) is the dissociation constant for Ca^{2+} binding to indo-1 and was obtained from the calibration procedures (see Methods section 3.3.2). *Figure 21-A* represents the total Ca^{2+} binding ratio (κ_{total}) plotted against the measured $\Delta[Ca^{2+}]_i$ (pooled data; n=14 cells). The data points for the Ca^{2+} binding ratio were then regrouped according to the Ca^{2+} charge transfer (≈ 10 pC increments, see *figure 19-B*). The plot represents as a function of $\Delta[Ca^{2+}]_i$ the mean of the determined κ_{total} (solid squares, see *Equation 17*), of the calculated κ_{indo-1} (orange diamonds, see *Equation 19*) and of κ_{endo} (blue squares, see *Equation 18*) for each class (*figure 21-B*). *Table 8* summarises the Ca^{2+} binding ratio values at three representative $\Delta[Ca^{2+}]_i$ *i.e.* $[Ca^{2+}]_{total}$. At low $\Delta[Ca^{2+}]_i$, κ_{endo} was around 1000, which suggested that out of 1000 Ca^{2+} ions that entered the cytosol only 1 remained in the free ionic form. With the increase in $\Delta[Ca^{2+}]_i$ (up to ≈ 180 nM and an equivalent Ca^{2+} increase to ≈ 90 μM - see first row *Table*

A

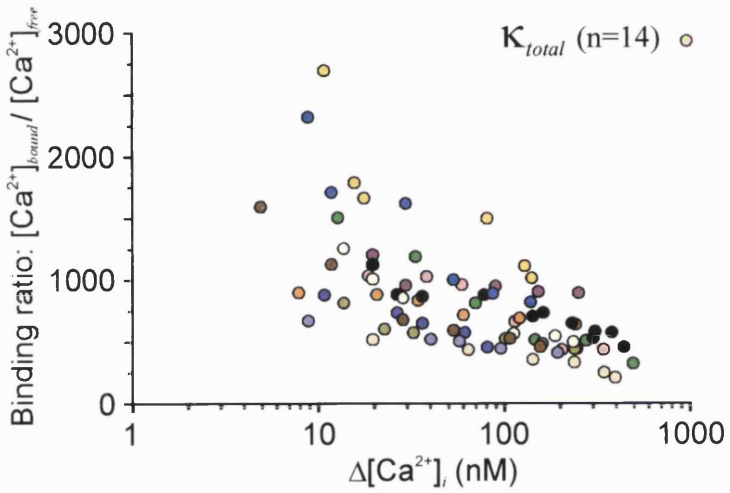

B

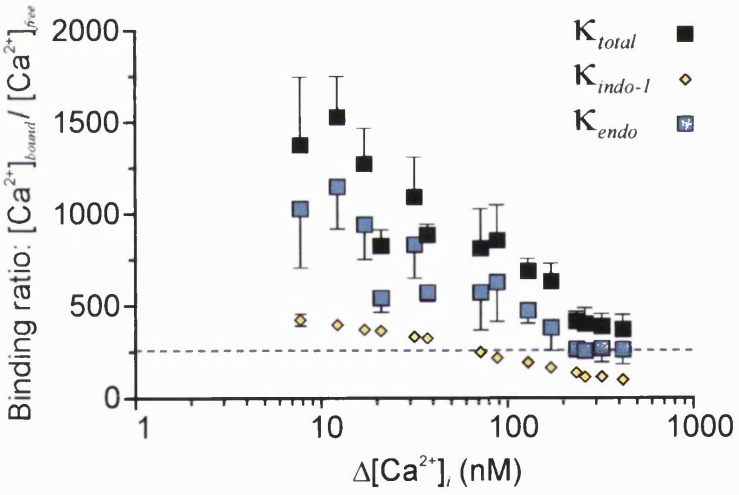

Figure 21: Endogenous calcium buffering capacity

(A) Plot of the pooled total Ca^{2+} binding ratio (κ_{total}) determined as the ratio of the $[Ca^{2+}]$ bound to the buffer ($[Ca^{2+}]_{bound}$) divided by $\Delta[Ca^{2+}]_i$ and plotted against $\Delta[Ca^{2+}]_i$ (n=14). (B) The pooled data in (A), have been binned according to the increase in the Ca^{2+} charge transfer (≈ 10 pC increments - data as mean ± S.E.M., n number in each class from *figure 19-B*) and represented as a function of $\Delta[Ca^{2+}]_i$. The total binding ratio (κ_{total}, solid squares) is determined as mentioned in (A) (see text for more details). The binding ratio for indo-1, the exogenous buffer (κ_{indo-1}, orange diamonds), was determined as described by Palecek *et al.* (1999) with 100 µM indo-1 in the recording pipette and the $K_{d(indo-1)}$ (93.3 nM) determined within the whole-cell calibration procedure (more details in Methods section 3.3.2). The endogenous buffer (κ_{endo}, blue squares) was then calculated, for each value of $\Delta[Ca^{2+}]_i$, as $\kappa_{endo} = \kappa_{total} - \kappa_{indo-1}$.

8), κ_{endo} decreased to around 250 and stayed constant for any further rise in $[Ca^{2+}]_i$ (see *Table 8* and *figure 21-B*). Therefore, at $\Delta[Ca^{2+}]_i$ in the micromolar range, only ≈ 0.4% of the total Ca^{2+} entry was in the free ionic form (*i.e.* 4 out of 1000 Ca^{2+} ions are in the free ionic form).

Table 8: Ca^{2+} binding ratio at representative $\Delta[Ca^{2+}]_i$ and the corresponding $[Ca^{2+}]_{total}$

$[Ca^{2+}]_{total}$	**6 ± 1 μM**	**97 ± 3 μM**	**160 ± 15 μM**
$\Delta[Ca^{2+}]_i$	**8 ± 0.1 nM**	**180± 5 nM**	**417 ± 30 nM**
κ_{total}	1376 ± 372	687 ± 68	329 ± 77
$\kappa_{indo\text{-}1}$	424 ± 33	192 ± 8	100 ± 6
κ_{endo}	1028 ± 322	381 ± 126	261 ± 80
n	n = 5	n = 4	n = 5

Taken together, the results indicated that there was a linear correlation between Ca^{2+} entry and $[Ca^{2+}]_i$ suggesting that the rise in $[Ca^{2+}]_i$ was directly proportional to the Ca^{2+} influx and that there was no amplification mechanism of the Ca^{2+} response (such as Ca^{2+} induced Ca^{2+} release process; see also Results section 4). On the other hand, the data indicated that SCG neurones exhibit a high Ca^{2+} buffering capacity since most of the Ca^{2+} entering the cytosol during a depolarisation step was strongly buffered by endogenous CaBPs. Finally, the results also suggested that the Ca^{2+} buffer system was a least partially saturable as the Ca^{2+} binding ratio decreased with the rise in $[Ca^{2+}]_i$.

2.4. Discussion

The determination of the Ca^{2+} binding ratio in SCG neurones gives an estimated value of 250 for $\Delta[Ca^{2+}]_i \approx 500$ nM and suggests that SCG neurones have a higher buffering capacity than chromaffin cells ($\kappa \approx 40$, Zhou & Neher, 1993), gonadotrophs ($\kappa \approx$ 100-130, Tse *et al.*, 1994), neurohypophysal nerve endings ($\kappa \approx 174$, Stuenkel, 1994) and hippocampal CA1 pyramidal cells ($\kappa \approx$ 168-207, Helmchen *et al.*, 1996). On the other hand, SCG neurones present a similar Ca^{2+} binding ratio than that found in mouse occulomotor neurones ($\kappa \approx 265$, Vanselow & Keller, 2000) but a far smaller binding ratio than rat and mouse Purkinje neurones ($\kappa \approx 2000$, Fierro & Llano,

1996 and Maeda *et al.*, 1999, respectively). However, in most of the studies the determination of the Ca^{2+} binding ratio was carried out with the 'added buffer' method and extrapolated to a situation in the absence of exogenous buffer (see Neher & Augustine, 1992). This method only gives an estimate of the Ca^{2+} binding ratio for resting $[Ca^{2+}]_i$ (≈ 100 nM) but not as a function of changes in $[Ca^{2+}]_i$. In fact, the buffering capacity corresponds to a dynamic process that would vary with the changes in the $[Ca^{2+}]_i$ (*i.e.* the buffering capacity would decrease with the rise in $[Ca^{2+}]_i$) and therefore would only be relevant at a particular $[Ca^{2+}]_i$. Thus, in mouse Purkinje neurones, Maeda and colleagues (1999) used another approach in that they directly determined the Ca^{2+} binding ratio and expressed it as a function of $[Ca^{2+}]_i$. At rest ($[Ca^{2+}]_i \approx 100$ nM) they obtained a Ca^{2+} binding ratio of ≈ 2000 but for a rise in $[Ca^{2+}]_i$ to ≈ 500 nM, κ_{endo} decreased by ≈ 90% to ≈ 250. These values of κ_{endo} are similar to those obtained in SCG neurones as κ_{endo} is ≈ 1000 at rest and decreases to 250 for $[Ca^{2+}]_i \approx 500$ nM (see *figure 21-B*) and therefore SCG neurones appeared to have a Ca^{2+} buffering capacity equivalent to mouse Purkinje neurones. One can therefore conclude that SCG neurones have a high buffering capacity at rest and that up to ≈ 1 μM only a minute proportion of the Ca^{2+} that enters the soma would remain in the free ionic form (≈ 0.1-0.4%). However, the rises in Ca^{2+} elicited under the recording conditions were not large enough to induce saturation of the Ca^{2+} buffering system. Therefore, it is not possible to determine precisely either the Ca^{2+} affinity or the concentration of the endogenous buffering system present in SCG neurones. To characterise further the properties of the endogenous buffer and in order to have a point of comparison, the Ca^{2+} binding ratio for EGTA has been calculated.

EGTA is an extensively well used Ca^{2+} chelator with one Ca^{2+} binding site and a high affinity for calcium ($K_{d(EGTA)} = 5.54.10^{-8}$ M at 33°C, pH 7.4 and 300 mosm.l^{-1}). Using a $[Ca^{2+}]_{total}$ ranging from 1 nM to 1 mM, the free Ca^{2+} concentration ($[Ca^{2+}]_{free}$) was determined for various EGTA concentrations (10 to 250 μM) and the $[Ca^{2+}]_{bound}$ then calculated using the mass action equation (*Equation 16*). *Figures 22-A* and *-B* illustrate, as a function of $[Ca^{2+}]_{total}$ and for various concentrations of EGTA, the variation in $[Ca^{2+}]_{bound}$ and in $[Ca^{2+}]_{free}$, respectively. Upon the rise in $[Ca^{2+}]_{total}$, $[Ca^{2+}]_{bound}$ to EGTA increased (*i.e.* $[Ca^{2+}]_{free}$ is close to zero) until the $[Ca^{2+}]_{total}$ and the

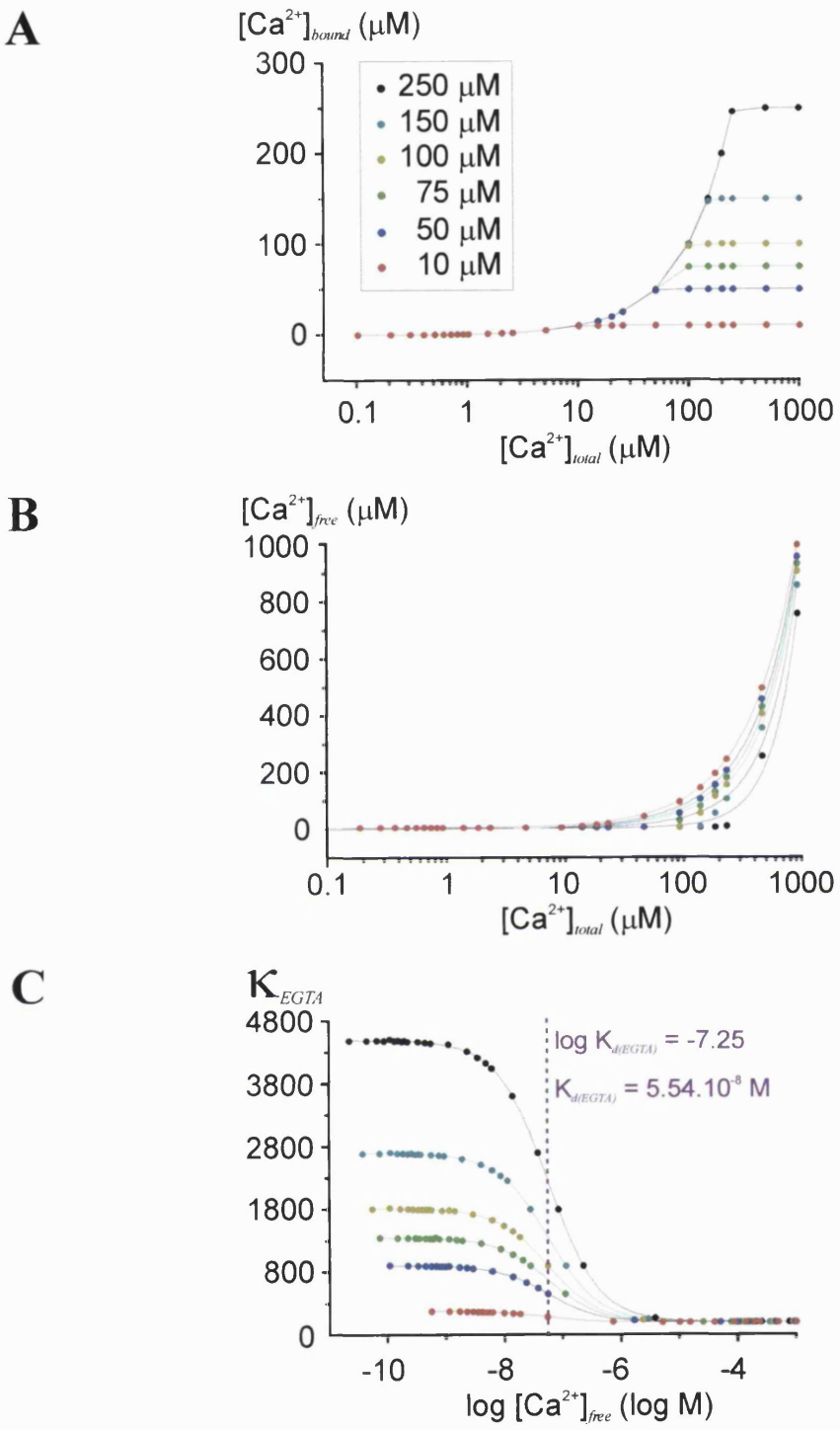

Figure 22: Properties of the calcium binding to EGTA

(A) Plot of $[Ca^{2+}]_{bound}$ to increasing concentration of EGTA ([EGTA] = 10 to 250 µM - see inset) against a $[Ca^{2+}]_{Total}$ ranging from 1 nM to 1 mM. (B) Plot of $[Ca^{2+}]_{free}$ in the presence of increasing [EGTA] (see inset in A) against a $[Ca^{2+}]_{total}$ ranging from 1 nM to 1 mM. (C) Plot of the Ca^{2+} binding ratio for EGTA (κ_{EGTA} - calculated as in *figure 21-A*) against $[Ca^{2+}]_{free}$ for increasing [EGTA] (see inset in A). The $K_{d(EGTA)}$ (log $(5.54.10^{-8})$ = -7.256) value is shown by the dashed line.

$[EGTA]_{total}$ are equal. At this point, the maximum $[Ca^{2+}]$ that EGTA can bind has been reached (*i.e.* the buffer is saturated) and therefore $[Ca^{2+}]_{bound}$ becomes constant (*i.e.* $[Ca^{2+}]_{free}$ starts to increase - right part of the curves, *figures 22-A* and *B*). The higher the concentration of buffer is, the more Ca^{2+} can be added before the buffer starts to saturate. From the determined values of $[Ca^{2+}]_{free}$ and of $[Ca^{2+}]_{bound}$ to EGTA, the Ca^{2+} binding ratio for EGTA (κ_{EGTA}, *figure 22-C*) was determined for each concentration of the buffer.

To compare κ_{endo} to κ_{EGTA}, the data obtained experimentally from *figure 21-B* were superimposed to the calculated κ_{EGTA} (*figure 22-C*). It appears that the experimental data points (κ_{endo}) fit between the κ_{EGTA} curves generated for 50 and 75 µM EGTA. However, above a $\Delta[Ca^{2+}]_i \approx 180$ nM (with log(180nM) ≈ -6.75), κ_{endo} deviated from the curves generated for κ_{EGTA} and remained constant around 250 for any further increase in $\Delta[Ca^{2+}]_i$ (dashed line in *figure 23-A*).
In fact, for buffer with a low affinity for Ca^{2+}, the Ca^{2+} binding ratio is assumed constant (see *figure 22-C*, left part of the curve) and equivalent to:

$$\kappa_{buffer} = \frac{[\text{Buffer}]}{K_{d(buffer)}} \quad \textit{Equation 20}$$

This analysis therefore suggested that there might be at least two buffering systems in SCG neurones: a high affinity buffering system equivalent to a $[EGTA]_{total}$ between 50 and 75 µM and a buffering system with a lower affinity for Ca^{2+} with a constant Ca^{2+} binding ratio (≈ 250) in the range of the measured $\Delta[Ca^{2+}]_i$. Therefore, κ_{endo} can be described as the sum of the Ca^{2+} binding ratios for a high (*HB*) and a low (*LB*) affinity Ca^{2+} buffer:

$$\kappa_{endo} = \kappa_{HB} + \kappa_{LB} \quad \textit{Equation 21}$$

$$\text{with } \kappa_{HB} = \frac{d[Ca^{2+}]_{bound}}{d[Ca^{2+}]_i} = \frac{[\text{HB}]}{\left(\kappa_{d(HB)} + [Ca^{2+}]_i\right)^2} \quad \textit{Equation 22}$$

$$\text{and } \kappa_{LB} = \frac{[\text{LB}]}{K_{d(LB)}} \quad \textit{Equation 23}$$

A

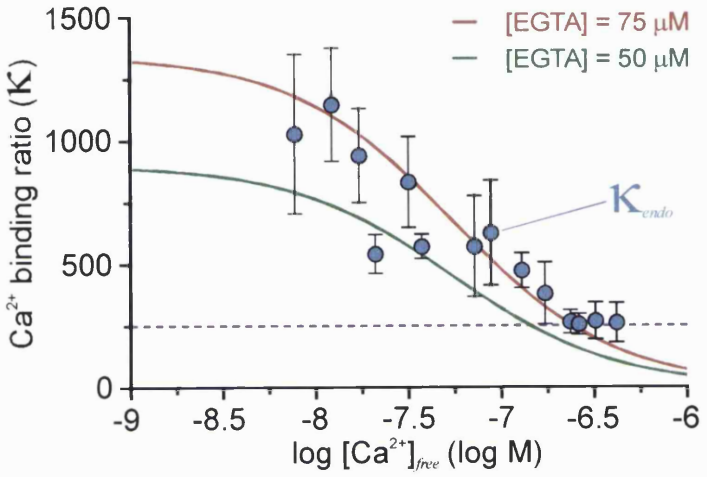

B

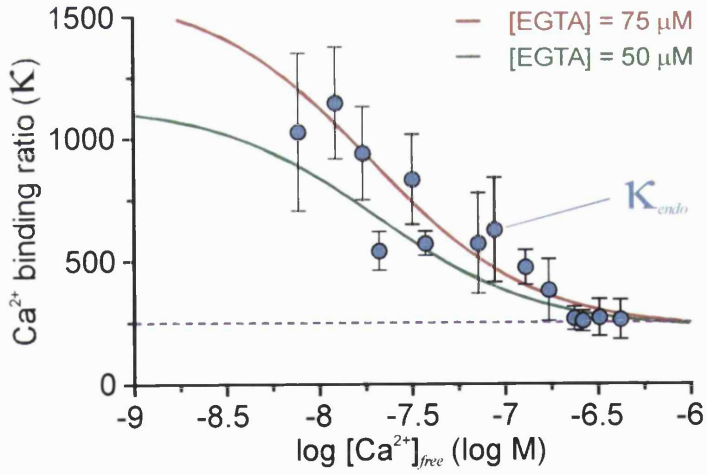

Figure 23: Comparison of the Ca^{2+} binding ratios calculated for EGTA and determined in situ
(A) Ca^{2+} binding ratio calculated for 50 and 75 µM EGTA (green and red lines, respectively) along with the endogenous Ca^{2+} binding ratio (κ_{endo}, blue circles - data from *figure 21-B*). (B) Recalculated Ca^{2+} buffering ratio for 50 and 75 µM EGTA (green and red lines, respectively) taking into account a low affinity buffering system with a Ca^{2+} binding ratio constant and equal to ≈ 250. The data for κ_{endo} are also represented (blue circles).

where the subscripts *HB* and *LB* represent the high and low affinity buffers, respectively. When the Ca^{2+} binding ratios for 50 and 75 μM EGTA were determined using *Equation 21* with κ_{LB} equal to ≈ 250, the curves illustrated in *figure 23-B* were generated. This analysis confirmed the presence of two buffering systems in SCG neurones and suggested that the high affinity buffering component was equivalent to ≈ 75 μM EGTA.

Little is known about the nature of the CaBPs expressed in SCG neurones and it is therefore difficult to correlate the Ca^{2+} buffering capacity to the expression of particular CaBPs. However from immunocytochemical experiments, it appears that these neurones express high levels of parvalbumin along with calbindin D_{28k} (Marsh & Wanaverbecq unpublished observations). Although the expression of parvalbumin was proposed to induce fast spiking in neurones (Kawaguchi *et al.*, 1987), the exact role of CaBPs remains unclear. However, rat sympathetic neurones posses both large (BK - Smart, 1987) and small (SK - Selyanko, 1996) conductance potassium channels that are selectively activated by Ca^{2+} influx through L-type and N-type Ca^{2+} channels, respectively. It is therefore tempting to propose that Ca^{2+} binding to a specific set of CaBPs might relay the selective channel activation by a particular Ca^{2+} influx. Such a system would serve two main functions by limiting the rise in $[Ca^{2+}]_i$ to region close to the plasma membrane and more importantly inducing site specific cellular responses. Sanchez-Vives and colleagues (1993, 1994a and b) demonstrated that in mature SCG neurones axotomy induced an upregulation of the calbindin D_{28k} expression. These authors observed that the axotomy induced both a slowing in the onset and the recovery of action potential-induced Ca^{2+} transients and therefore suggested that calbindin D_{28k} upregulation could explain this phenomenon. Therefore, it appears that the expression of particular CaBPs would depend on the state of the neurone and that the buffering capacity might vary during development, following injury or with ageing.

Finally, in rat dorsal root ganglion neurones, it was found that the relation between peak $[Ca^{2+}]_i$ and depolarisation-induced Ca^{2+} influx saturated around 500 nM and that the relationship became more linear after mitochondria inhibition (Thayer & Miller, 1990 and similar observations were made in chromaffin cells see Park *et al.*, 1996). Moreover, it was suggested that mitochondrial Ca^{2+} uptake could be fast enough to occur during the few hundred milliseconds of the depolarisation step and therefore to

be capable of a substantial role in Ca^{2+} buffering (Thayer & Miller, 1990; Park *et al.*, 1996 and Herrington *et al.*, 1996). The mitochondrial Ca^{2+} uptake in SCG neurones appeared important (see Results section 3) and therefore might suggest that mitochondria could partly represent the low and not saturable endogenous buffering system. It would therefore be interesting to measure the Ca^{2+} buffering capacity of cells where the mitochondrial uptake has been inhibited and to determine how this would influence the ability of a cell to buffer Ca^{2+}. The data presented in this section indicated that Ca^{2+} ions entering the cytosol bind to endogenous CaBPs and this binding most certainly serves to activate Ca^{2+}-dependent processes such as ionic channels modulation, enzyme activation or stimulation of gene transcription.

3. Mitochondrial regulation of the intracellular calcium

In this section, small and large Ca^{2+} transients were induced following somatic depolarisation and the mitochondrial activity inhibited using CCCP to determine the role of mitochondria in the regulation of resting $[Ca^{2+}]_i$ and on the recovery phase of Ca^{2+} transients. The Ca^{2+} release mechanism was further investigated to determine its sodium dependency by comparing the recovery phase of Ca^{2+} transients in the presence and absence of intracellular sodium.

3.1. Mitochondrial calcium sequestration and release mechanisms

Neurones were voltage-clamped in the perforated patch configuration with 10 mM sodium in the intracellular solution (see Methods section 2.4.3, *Table 2* - solution H and inset in *figure 24*). Typically, small Ca^{2+} transients (maximum amplitude < 500 nM), induced by 60 ms depolarising steps, presented a monoexponential decay whereas large Ca^{2+} transients (≥1 μM) had a multiphasic recovery phase with (*i*) an initial rapid decrease to a $[Ca^{2+}]_i \approx 300$ nM, (*ii*) a plateau phase (maximum amplitude of 217 ± 18 nM; n=11) lasting for tens of seconds and finally (*iii*) the $[Ca^{2+}]_i$ slowly returned to its resting value (*figure 24-A*).

Upon bath application of 2 μM CCCP (*figure 24-B*), resting $[Ca^{2+}]_i$ transiently increased (peak amplitude of 183 ± 8 nM; n=11) and then returned to its initial value after ≈ 1 minute. However, CCCP did not have a long lasting effect on resting $[Ca^{2+}]_i$ as there was no significant differences in resting $[Ca^{2+}]_i$ in the presence of CCCP compared to the control level (102 ± 5 nM and 110 ± 8 nM, respectively - n=11; P= 0.4). In the absence of extracellular Ca^{2+}, CCCP still induced a transient rise in $[Ca^{2+}]_i$ indicating that the increase in resting $[Ca^{2+}]_i$ was not a consequence of a CCCP-induced Ca^{2+} influx. Concomitant with the rise in $[Ca^{2+}]_i$, there was the development of an inward current that persisted for the whole duration of the CCCP application (*figure 24-B*, bottom panel). This current was mostly unaffected in a Ca^{2+}-free extracellular solution but completely inhibited upon extracellular alkalisation (pH 9 - data not shown) suggesting that it mainly corresponded to a 'flux' of protons through the plasma membrane.

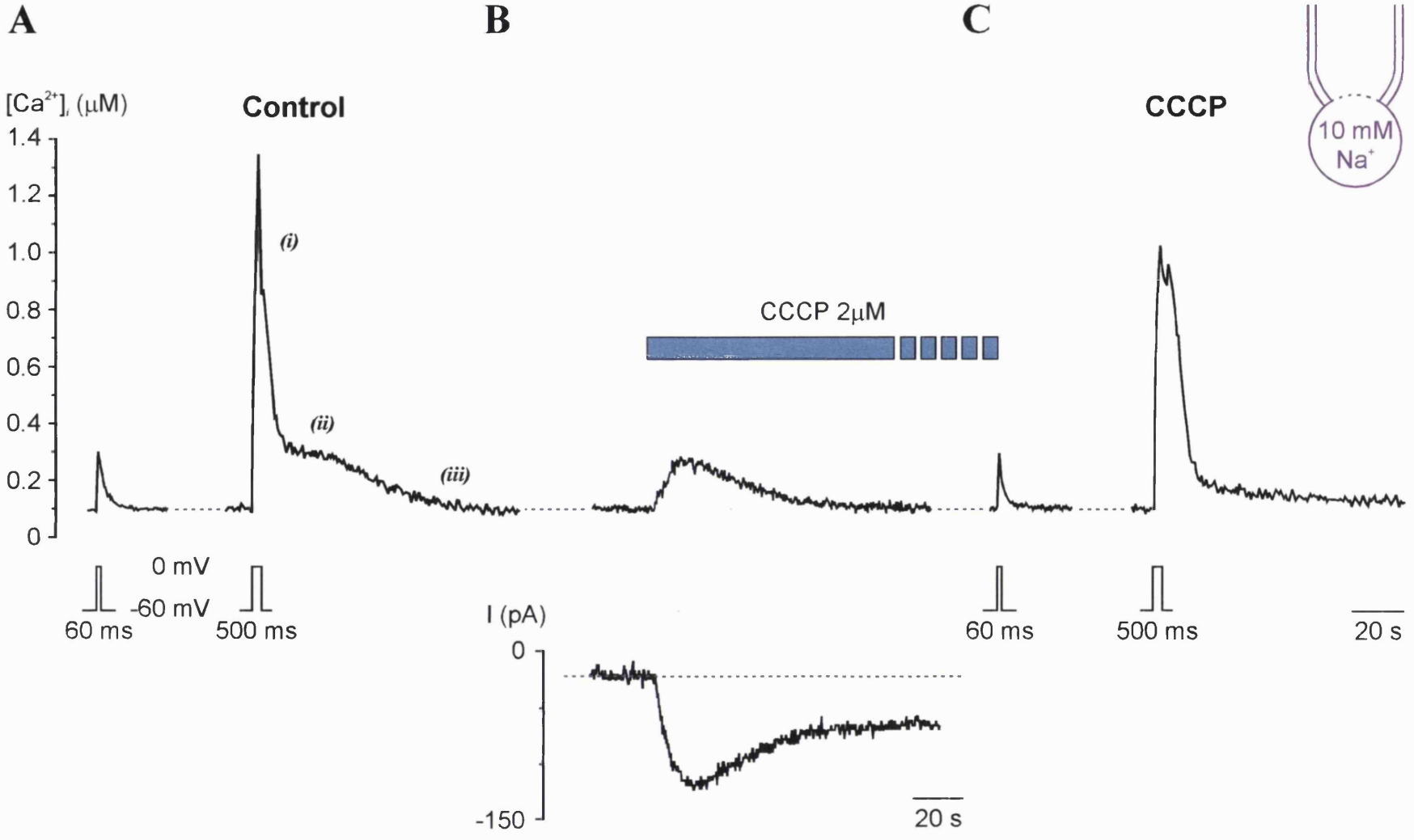

Figure 24 (see next page for legend)

Although CCCP was without effect on the net amplitude ($\Delta[Ca^{2+}]_i$) of Ca^{2+} transients, it dramatically affected the properties of their recovery phase, especially during large Ca^{2+} loads (*Tables 9* and *10* and *figure 24-C*). Thus, CCCP abolished the plateau phase observed in control and delayed the recovery phase of large Ca^{2+} transients (compare *figures 24-A* and 24-*C* and see also *figure 25-A*). It was not possible to fit an exponential function to the recovery phase of Ca^{2+} transients recorded in control because of their multiphasic decay. Therefore, $t_{1/2}$, the time necessary for the recovery to reach 50% of the maximal amplitude (A_{max}), was measured in control and in the presence of CCCP (*figure 25-A* and *Table 9*). Upon application of CCCP, $t_{1/2}$ was increased by ≈ 1.5 fold compared to control suggesting that $[Ca^{2+}]_i$ stayed elevated for a longer period of time when the mitochondria were inhibited. However, $[Ca^{2+}]_i$ was brought back to resting level through a mechanism that appears CCCP-insensitive since its kinetics was mostly unaffected (compare recovery phase of the Ca^{2+} transients in *figure 25-A* and see below *Table 10* and *figure 27* in Results section 3.2).

Table 9: Effect of CCCP on the properties of Ca^{2+} transients

		Control	+ CCCP	n	*t*-test
$[Ca^{2+}]_i$ < 500 nM	$\Delta[Ca^{2+}]_i$	157 ± 17 nM	165 ± 11 nM	8	paired, P=0.9
	τ	3.6 ± 0.5 s	2.0 ± 0.2 s		paired, P< 0.001
$[Ca^{2+}]_i$ > 500 nM	$\Delta[Ca^{2+}]_i$	909 ± 106 nM	908 ± 105 nM	11	paired, P=0.7
	$t_{1/2}$	2.5 ± 0.1 s	3.5 ± 0.3 s		paired, P< 0.05
	Recovery	Multiphasic	Biexponential		(-)

(Previous page)

Figure 24: Mitochondrial inhibition with CCCP affects the regulation of $[Ca^{2+}]_i$
(A) Calcium transients induced by depolarisation to 0 mV for 60 and 500 ms in a neurone voltage-clamped (10 mM intracellular sodium, see inset). (B) Bath application of 2 µM *m*-chlorophenylhydrazone (CCCP) induces a transient rise in $[Ca^{2+}]_i$ and the development of a persistent inward current. (C) In the presence of CCCP, the recovery of both small and large Ca^{2+} transients is modified.

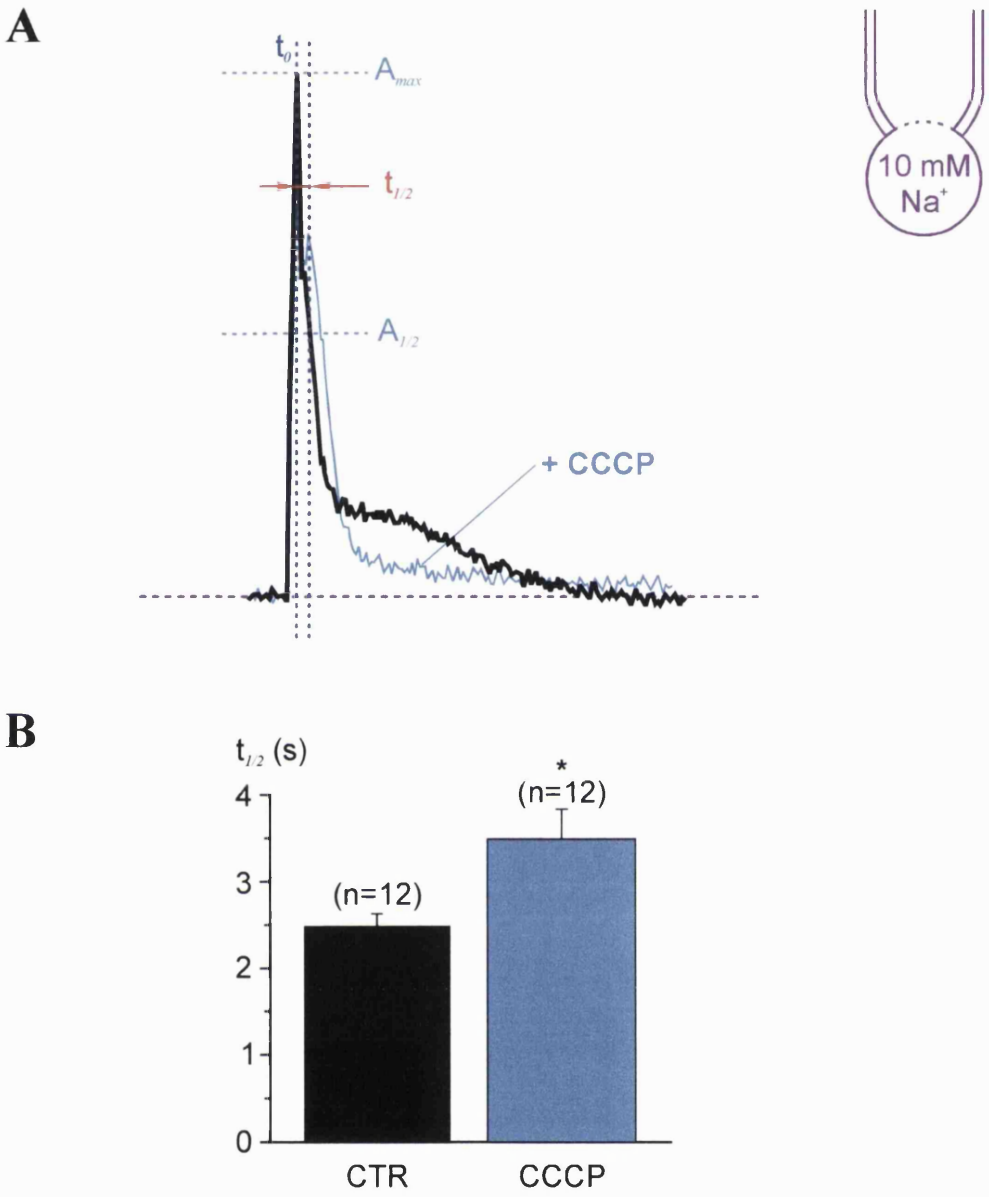

Figure 25: CCCP delays the initial phase of the recovery form large Ca^{2+} transients but also abolishes the plateau phase

(A) Large Ca^{2+} transients recorded in the presence of intracellular sodium (see inset) in control (CTR, thick line) and after bath application of 2 μM CCCP (+CCCP, blue line). The traces are superimposed to compare the time ($t_{1/2}$) necessary for the Ca^{2+} transient's decay to reach 50% ($A_{1/2}$) of the maximum amplitude (A_{max}). The initial time (t_0) of the decay was set at the peak of the Ca^{2+} transient. (B) CCCP effect on $t_{1/2}$ (CTR, solid bar and CCCP, blue bar; n=11, data as mean ± S.E.M. * $P< 0.05$).

In contrast, the recovery phase of small Ca^{2+} transients, was accelerated in the presence of CCCP as can be seen from the superimposed traces in *figure 26-A*, from the plot of the clearance rate ($-d[Ca^{2+}]/dt$ against $[Ca^{2+}]_i$ see Methods section 6.2 for more details - *figure 26-B*) and from the measurement of the decay time constant (inset in *figure 26-B* and *Table 9*). In the presence of CCCP, the clearance rate was accelerated from 0.15 s^{-1} to 0.2 s^{-1} (obtained from the slope of the best fit in *figure 26-B*) and the CCCP-sensitive component was negative suggesting a Ca^{2+} efflux from the mitochondria at this low $[Ca^{2+}]_i$.

CCCP is a proton shuttle and upon its application, the intracellular pH will equilibrate with the extracellular pH. However, intracellular pH measurements with BCECF (see Methods section 4 for more details) showed that this flux of protons induced little changes in the cytosolic pH (data not shown). Moreover, an equivalent intracellular acidification, induced with 20 mM sodium acetate, did not significantly affect the recovery time of small Ca^{2+} transients (decay time of 3.5 ± 0.1 s; n=5). On the other hand, intracellular alkalisation, with 15 mM ammonium chloride, elicited large and rapid Ca^{2+} rises (see Willoughby *et al.*, 2001 and Marsh & Wanaverbecq unpublished observations), which were not observed upon CCCP application (data not shown). Therefore the acceleration of the recovery from small Ca^{2+} transients did not appear to be due to changes in pH_i.

3.2. Sodium dependence of the mitochondrial calcium release

Following CCCP application and with 10 mM intracellular Na^+, the recovery phase of large Ca^{2+}transients became biexponential with a predominant fast component and a secondary component lasting for over 30 s (*Table 10, figures 24-C, 25-A* and *27*). Removing the intracellular sodium was without effect on the Ca^{2+} transients' amplitude, but did modify the properties of the large Ca^{2+} transients' recovery (*Table 10* and *figure 27-C*). Thus, in the absence of intracellular sodium and similarly to the situation in the presence of CCCP (*figures 24-C* and *27*), the recovery had lost the plateau phase and became biexponential with a similar fast component (compare panels in *figure 27-A* and see *Table 10*). However, the amplitude and the time constant of the slow component were respectively larger and faster in the absence of

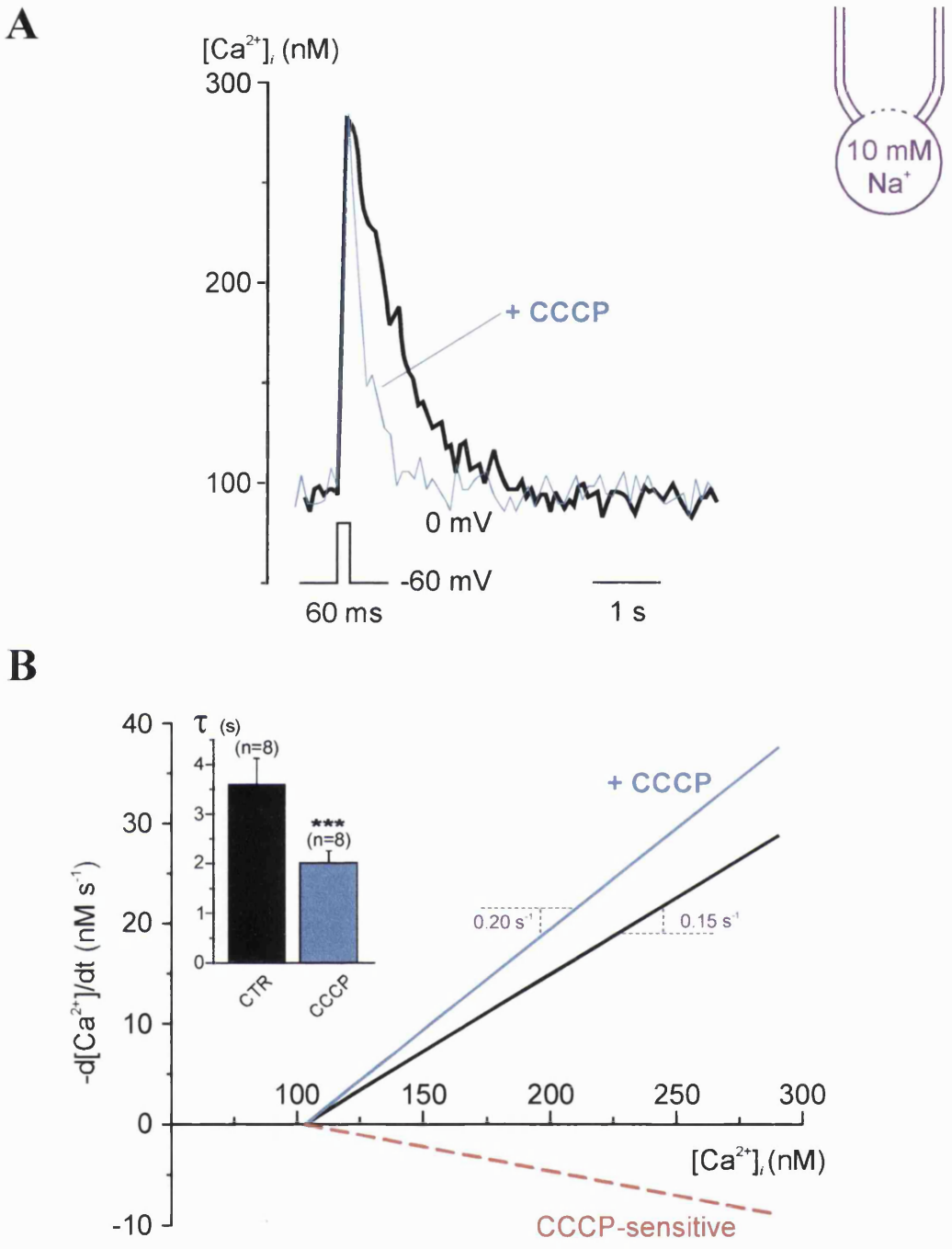

Figure 26: In the presence of CCCP the recovery phase of small calcium transient is accelerated
(A) Superimposed traces of small Ca^{2+} transients recorded in the presence of 10 mM intracellular sodium (see inset) before (thick line) and after bath application of 2 µM CCCP (+CCCP, blue line). (B) Plot of the clearance rate (-d[Ca^{2+}]/dt in nM s^{-1} *versus* [Ca^{2+}]$_i$) in control and in the presence of CCCP. Data from 32 Ca^{2+} transients (16 in control and 16 in CCCP) were pooled from 8 cells and fitted with a linear regression. The best fit in CCCP (blue line) was then subtracted to the best fit in control (solid line) to determine the CCCP-sensitive component (red dashed line). The inset represents the decay time constant of the Ca^{2+} transient's recovery in control and in CCCP (black bar, CTR and blue bar, CCCP; n=8, data as mean ± S.E.M. *** P< 0.001).

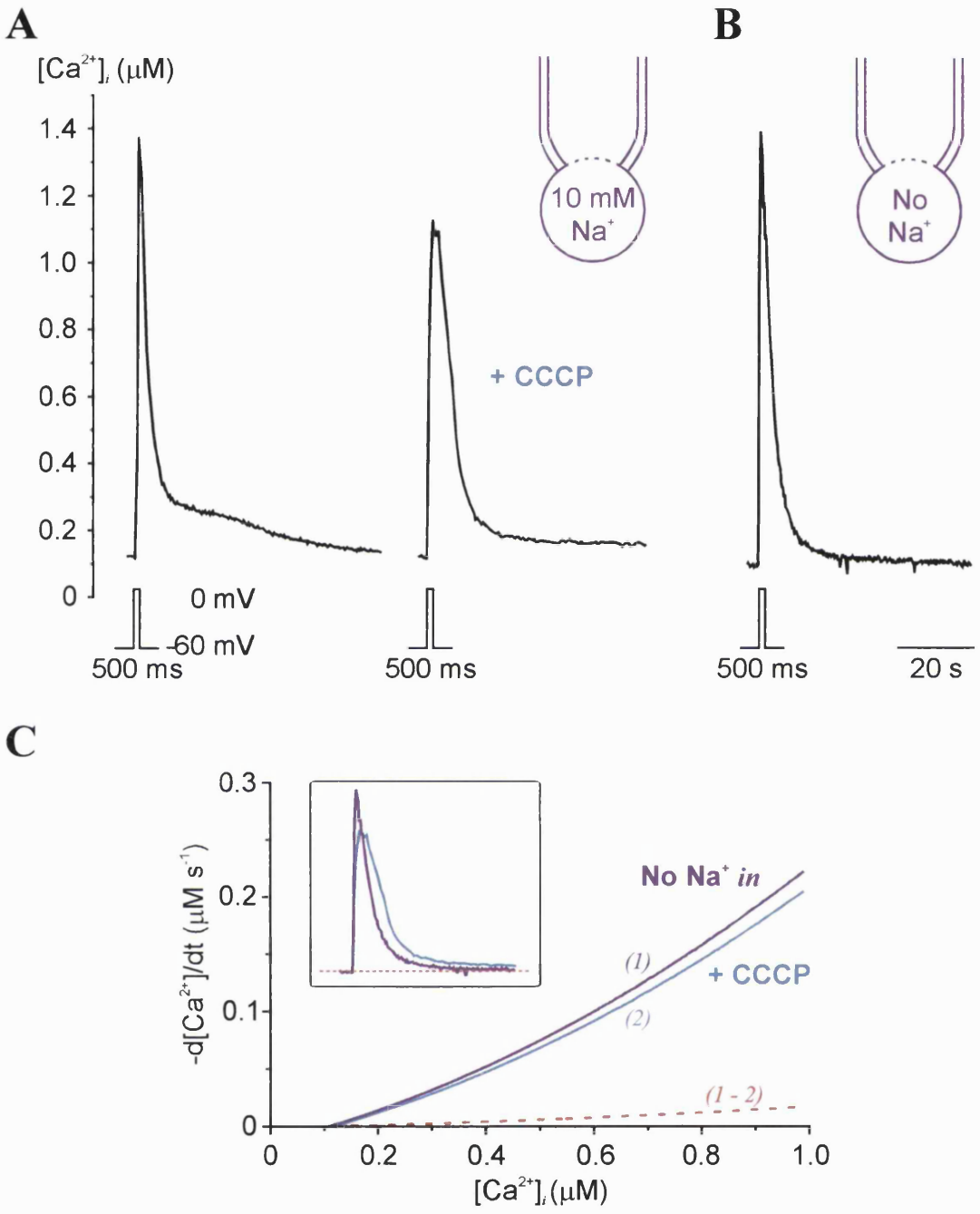

Figure 27: Sodium dependence of the mitochondrial Ca^{2+} release during large Ca^{2+} transients
(A) Typical recording of a large Ca^{2+} transient in the presence of 10 mM intracellular sodium (see inset) before (left) and after bath application of 2 μM CCCP (right). (B) Typical Ca^{2+} transient recorded in the same conditions as in (A) but in the absence of intracellular sodium (see inset). (C) Plot of the clearance rate as a function of $[Ca^{2+}]_i$ in the presence of intracellular Na^+ and CCCP (+ CCCP, blue line; n=11) and in the absence of intracellular sodium (No Na^+ *in*, purple line; n=34). Data obtained from different cells were pooled together in each condition and fitted with a polynome of the second order. The dashed line represents the difference between the clearance rate in the absence of intracellular Na^+ and after CCCP application. The inset illustrates superimposed traces in the presence of CCCP (blue trace) and in the absence of intracellular sodium (purple trace) on a slower time scale to compare the recovery phase in each condition.

intracellular sodium than after CCCP application (see inset in *figure* 27-*C* and *Table 10*). Finally, in the absence of intracellular sodium or in the presence of CCCP, there were little differences in the clearance rate of large Ca^{2+} transients (≈ 0.2 μM s^{-1} at 1 μM, *figure 27-C*).

Table 10: Effect of intracellular sodium removal on the properties of Ca^{2+} transients

		No Na^+ *in*	n	Na^+ *in* + CCCP	n	*t*-test
$[Ca^{2+}]_i$ < 500 nM	$\Delta[Ca^{2+}]_i$	159 ± 12 nM	57	165 ± 11 nM	8	indep*, P=0.6
	τ	3.5 ± 0.1 s		2.0 ± 0.2 s		indep, P< 0.001
$[Ca^{2+}]_i$ > 500 nM	$\Delta[Ca^{2+}]_i$	1064 ± 72	34	908 ± 105 nM	11	indep, P=0.27
	A_1	875 ± 63 nM		705 ± 101		indep, P=0.32
	τ_1	2.3 ± 0.1 s		2.6 ± 0.2 s		indep, P=0.25
	A_2	122 ± 7 nM		45 ± 5 nM		indep, P< 0.001
	τ_2	23.2 ± 2.2 s		44 ± 17 s		indep, P< 0.001

*indep: independent

In contrast, the removal of intracellular Na^+ did not affect the properties of small Ca^{2+} transients (*figure 28-A*). In fact, the decay time constant in the presence of CCCP was 2-times faster irrespective of the presence or absence of intracellular sodium (*figure 28-B* and *Table 10*). Moreover, the clearance rates in the presence or absence of intracellular sodium were equivalent (≈ 0.15 s^{-1}) and about 1.5-times slower than after CCCP application (*figure 28-C* and compare decay in *figure 28-A* and see *Tables 9* and *10*).

In conclusion, in SCG neurones mitochondrial regulation of $[Ca^{2+}]_i$ appeared to represent an important component of Ca^{2+} homeostasis. Thus, following large rise in $[Ca^{2+}]_i$, mitochondria would rapidly sequester Ca^{2+} and subsequently release it in a Na^+-dependent manner when $[Ca^{2+}]_i$ had decreased to a concentration of ≈ 200 nM. Mitochondria appeared to act as a Ca^{2+} store at rest and to be capable to transport Ca^{2+} at concentrations as low as 200-300 nM. Finally, there are evidence for a mitochondrial Ca^{2+} release system at low $[Ca^{2+}]_i$ that appeared to be mainly Na^+-independent.

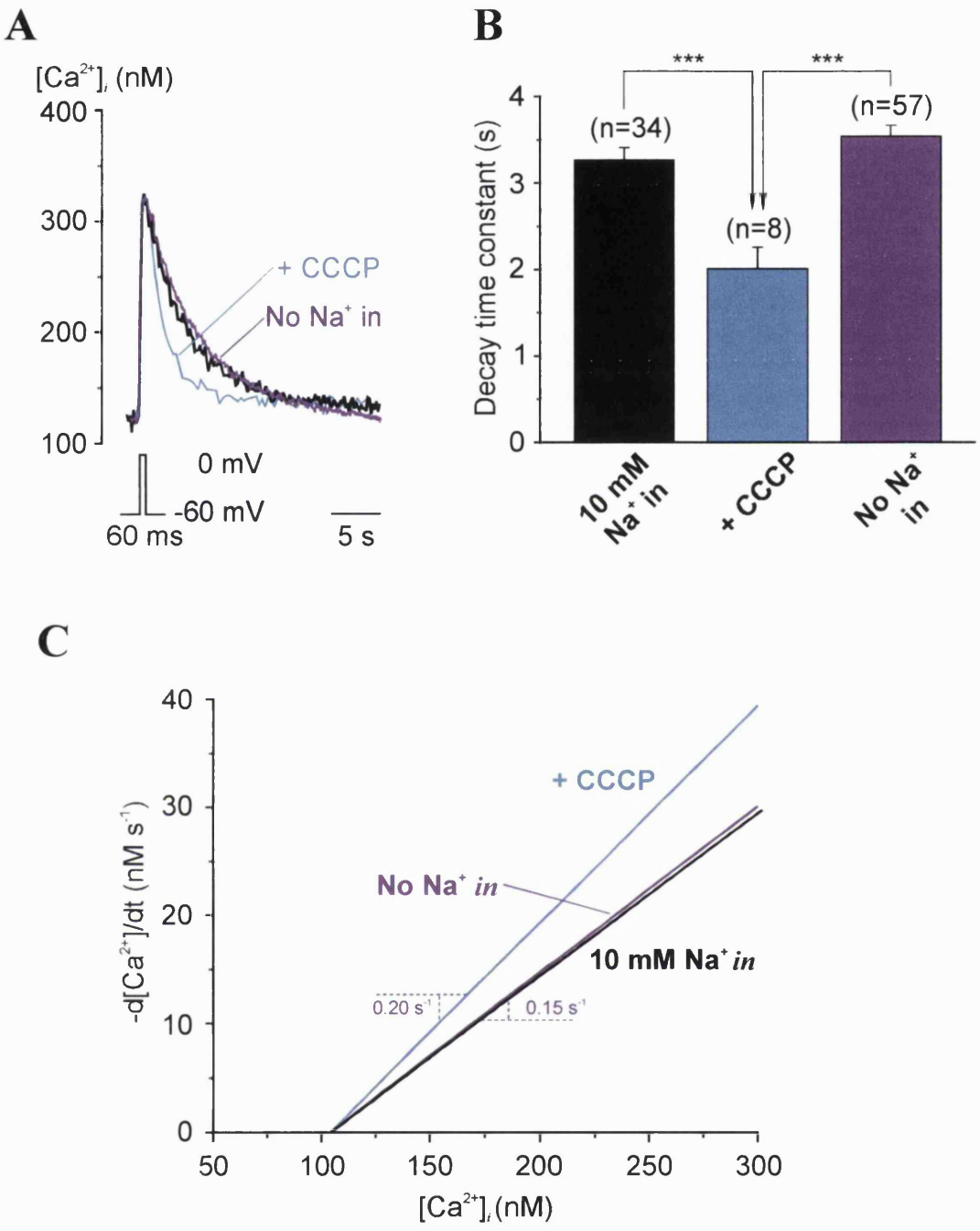

Figure 28: The recovery of small Ca^{2+} transients is not affected by the removal of intracellular sodium
(A) Superimposed traces of small Ca^{2+} transients recorded in the presence of intracellular sodium before (black line) and after CCCP application (blue line) and in the absence of intracellular sodium (purple line). (B) Decay time constant of the recovery phase (same colour code as in (A) with n=34; n=11 and n=57 respectively; data as mean ± S.E.M. *** P< 0.001, independent *t*-test). (C) Comparison of the clearance a rate as a function of $[Ca^{2+}]_i$ in the presence of intracellular sodium (10 mM Na^+ in, black line; n=11), after CCCP application (+CCCP, blue line; n=11) and in the absence of intracellular sodium (No Na^+ *in*, purple line; n=57). The data for '10 mM Na^+ in' and '+CCCP' are obtained from *figure 26* and the data for 'No Na^+ *in*' were pooled from 57 different transients and fitted with a linear regression.

3.3. Discussion

The application of CCCP induces at rest (see *figure 24-B*) a transient rise in $[Ca^{2+}]_i$ that mainly corresponded to Ca^{2+} release from the mitochondria since it was still observed in the absence of extracellular Ca^{2+} or after depletion of the intracellular stores with SERCA inhibitors (data not shown). This result is further supported by direct measurements of the mitochondrial Ca^{2+} content that indicate a resting mitochondrial $[Ca^{2+}] \approx$ 80-200 nM (Rizzuto *et al.*, 1993 and Babcock *et al.*, 1997). Although mitochondria would have the capacity to act as a Ca^{2+} store they did not appear to be involved in the regulation of basal $[Ca^{2+}]_i$ since mitochondrial inhibition was without effect on resting $[Ca^{2+}]_i$.

In the presence of 10 mM intracellular Na^+, which corresponds to the physiological intracellular Na^+ concentration, the recovery from large depolarisation-induced Ca^{2+} transients was multiphasic with an initial rapid decay followed by a secondary slow decrease towards resting $[Ca^{2+}]_i$. In agreement with numerous previous studies, mitochondrial uncoupling with protonophores, such as CCCP, induced in SCG neurones both a delay in the initial fast decay phase and the abolition of the slow secondary plateau phase (Thayer & Miller, 1990; Friel & Tsien; 1994; Herrington *et al.*, 1996; Park *et al.*, 1996; Babcock *et al.*, 1997; Pivovarova *et al.*1999; Montero *et al.*, 2000 and Colegrove *et al.*, 2000). A notable exception to this was found in cerebellar Purkinje neurones where the recovery from large Ca^{2+} transients is biexponential and unaffected by mitochondrial inhibition (Fierro *et al.*, 1998). However, the experimental conditions and particularly the low intracellular Na^+ concentration (see below) might explain this discrepancy. Similarly to CCCP application, a delay in the initial rapid recovery was observed upon intracellular application of ruthenium red, an inhibitor of the Ca^{2+}-uniporter (*e.g.* see Babcock *et al.*, 1997) indicating that mitochondria accelerate the clearance of large increase in $[Ca^{2+}]_i$ by sequestering Ca^{2+} *via* the *m*CU.

In the present study, in the absence of intracellular Na^+ or after CCCP application, the plateau phase was no longer observed and instead the recovery became biexponential suggesting that Ca^{2+} release from the mitochondria is Na^+-dependent (see also Colegrove *et al.*, 2000). This Na^+-dependent Ca^{2+} efflux appears to be mediated through the mitochondrial NCX (*m*NCX). Thus, CGP, a selective inhibitor of this exchanger, also abolishes the plateau phase of the recovery in the presence of 10 mM

intracellular Na^+ but is ineffective when intracellular Na^+ is omitted (Baron & Thayer, 1997 and Colegrove *et al.*, 2000). However, both CGP application or intracellular Na^+ removal do not prevent mitochondrial Ca^{2+} uptake since under these conditions, a transient rise in resting $[Ca^{2+}]_i$ (smaller in amplitude) and a prolongation of the Ca^{2+} transient's recovery were still observed following CCCP or FCCP application (data not shown and see also Colegrove *et al.*, 2000).

Colegrove and colleagues (2000) observed that following CCCP application the Ca^{2+} transient's amplitude is increased and the recovery markedly prolonged. These authors, in agreement with previous studies (*e.g.* Thayer & Miller, 1990; Friel & Tsien, 1994 and Pivovarova *et al.*, 1999) therefore concluded that mitochondria represent a major Ca^{2+} clearance system during the initial phase of large increase in $[Ca^{2+}]_i$. However, several observations appear in contradiction with this conclusion. Firstly, the increase in the amplitude of Ca^{2+} transients was generally observed in experiments where cellular depolarisation was induced by KCl application but not under voltage-clamped conditions (compare with Park *et al.*, 1996; Herrington *et al.*, 1996; Babcock *et al.*, 1997). Secondly, it has been reported that protonophores also affect the plasma membrane and intracellular Ca^{2+} store suggesting that the observed increase in the Ca^{2+} transient amplitude is not due to mitochondrial inhibition but rather to CCCP secondary effects (discussion in Friel & Tsien, 1994 and Park *et al.*, 1996). This observation is further supported by the development of the inward current during CCCP application (see *figure 24-B*) that would induce a depolarisation of the plasma membrane and an activation of VACC. Finally, although CCCP delays the Ca^{2+} transient's recovery, the CCCP-resistant recovery phase had kinetics similar to that of the initial fast decay in control or to the Ca^{2+} transient's recovery in the absence of intracellular Na^+ (see *figure 25-A* and *27*). Moreover, after CCCP application, inhibition of the plasma membrane NCX by extracellular Na^+ removal or of the Ca^{2+} uptake into intracellular store with SERCA inhibitors markedly affected the recovery of these large Ca^{2+} transients (data not shown and see Herrington *et al.*, 1996). Therefore, it appears that the rapid recovery phase is mediated by extrusion or storage systems rather than by mitochondria. One could suggest that mitochondria accelerate the Ca^{2+} recovery through both a rapid Ca^{2+} uptake and a temporary storage system. Thus, at high $[Ca^{2+}]_i$ mitochondria would promote Ca^{2+} extrusion through the plasma membrane NCX or storage into intracellular

stores whereas mitochondria release the accumulated Ca^{2+} at lower $[Ca^{2+}]_i$ where PMCA is most efficient for Ca^{2+} extrusion.

The mitochondrial Ca^{2+} uptake, because of its high transport rate and steep dependence on $[Ca^{2+}]_i$, is thought to be predominant at high $[Ca^{2+}]_i$ (> 500 nM) while at lower $[Ca^{2+}]_i$ the direction of the net Ca^{2+} flux would be determined by the respective contribution of the Ca^{2+} uptake and release systems (see also General Introduction section 4.1.3.1). The $[Ca^{2+}]_i$ where Ca^{2+} uptake and release systems balance each other corresponds to the 'set-point', which can be visualised as the plateau phase during the recovery. The value of this set-point appears to vary between cell types. Thus, in the present study, the set-point was measured at 217 ± 18 nM (n=11) which is similar to that measured in chromaffin cells (180 ± 25 nM, Park *et al.*, 1996), in pituitary gonadotrophs (≈ 200 nM, Tse *et al.*, 1994) and bullfrog sympathetic neurones (≈ 200 nM, Friel & Tsien, 1990 and Colegrove *et al.*, 2000) but far lower than in rat dorsal root ganglion neurones (≈ 500 nM, Thayer & Miller, 1990). This variation in the set point value suggests that the relative contribution of mitochondrial Ca^{2+} uptake and release varies amongst different cell types possibly as a result of different Ca^{2+} affinity of the transport systems or different level of expression. Nevertheless, in a particular cell type, the amplitude of the plateau phase is constant and independent from both the Ca^{2+} transient amplitude and the duration of the depolarisation (Thayer & Miller, 1990 and Friel & Tsien, 1994). However, the recovery time from the plateau phase increases with the duration of the depolarisation (Thayer & Miller, 1990 and Friel & Tsien, 1994). This suggests that with the increase in the depolarisation's duration (*i.e.* the increase in the duration of elevated $[Ca^{2+}]_i$), more Ca^{2+} will be accumulated into mitochondria however when $[Ca^{2+}]_i$ decreases below the set-point, Ca^{2+} is released at a constant rate.

A surprising result was the fact that mitochondrial uncoupling with CCCP accelerated the recovery of Ca^{2+} transients with a peak amplitude below 300 nM. The mitochondrial contribution to the regulation of $[Ca^{2+}]_i$ close to rest (100-300 nM) has already been reported in bullfrog sympathetic neurones (Colegrove *et al.*, 2000) and rat heart cells (Zhou *et al.*, 1998). Moreover, if one considers that at this low $[Ca^{2+}]_i$ the cytosolic Ca^{2+} binding ratio is ≈ 500 (see Results section 2.3), the free Ca^{2+} close to the plasma membrane would be in the micromolar range (≈ 100 μM for 200 nM free Ca^{2+}) and a substantial mitochondrial Ca^{2+} transport could therefore occur. Furthermore,

electron microscopic study showed that SCG neurones contain numerous mitochondria largely distributed close to the plasma membrane (Marsh, unpublished observations). Therefore mitochondria appear to be localised close to the source of Ca^{2+} influx where $[Ca^{2+}]_i$ is thought to be in the submicromolar range. This localisation of the mitochondria under the plasma membrane is an additional argument for a mitochondrial role in Ca^{2+} transport following 'small' rise in $[Ca^{2+}]_i$ and in Ca^{2+} buffering (see Results section 2.4) and also reconcile the apparent contradiction of the low affinity of *m*CU (K_d ≈ 1-5 μM) with a physiological role of mitochondria in the regulation of $[Ca^{2+}]_i$.

At high $[Ca^{2+}]_i$, mitochondrial Ca^{2+} sequestration would predominate whereas with at low $[Ca^{2+}]_i$ mitochondria would primarily release Ca^{2+}. The Ca^{2+} release observed at low $[Ca^{2+}]_i$ would be in agreement with the set-point value (≈ 200 nM), which would predict a predominant net mitochondrial Ca^{2+} efflux through *m*NCX and therefore CCCP application would accelerate the recovery (see *figure 28*). However, by contrast with the situation observed for the recovery of large Ca^{2+} transients, the Ca^{2+} release observed at low $[Ca^{2+}]_i$ appeared to be Na^+-independent (see *figure 28*). Thus, in the presence or absence of intracellular Na^+ there was no difference in the recovery of small Ca^{2+} transients while CCCP application accelerated in both situations the recovery phase. Furthermore, the recovery from large rises in $[Ca^{2+}]_i$ was essentially monoexponential after CCCP application since the second component of the decay was both minute and slow (≈ 50 nM and ≈ 40 s). In contrast, in the absence of intracellular Na^+, the Ca^{2+} transient's recovery was clearly biexponential (see *figure 27*) suggesting the presence of a secondary slow phase that might correspond, at least in part, to a mitochondrial Ca^{2+} release via a Na^+-independent mechanism. It has been reported that the mitochondrial permeability transition pore, (MPTP), which is stimulated by a rise in mitochondrial $[Ca^{2+}]_i$, could transiently open under physiological condition and therefore change the mitochondrial membrane potential (MPTP) leading to Ca^{2+} efflux (Petronilli *et al.*, 1999; Murchison & Griffith, 2000 and Montero *et al.*, 2000). Since the CCCP effect observed during the recovery of small Ca^{2+} transient is unlikely to be an artefact (see above section 3.1), the possibility of a Ca^{2+} release through MPTP and/or through the *m*CU operating in the reverse mode would represent a possible mechanism for a Na^+-independent Ca^{2+} release. However, there is no evidence that MPTP activation

occurs in SCG neurones and further experiments would be necessary to investigate this possibility.

In agreement with previous studies in excitable and non-excitable cells, it appears that mitochondrial Ca^{2+} transport plays an important role in the Ca^{2+} homeostasis of SCG neurones. Firstly, through the rapid Ca^{2+} uptake, mitochondria would have a protective role against long cytosolic exposure to high $[Ca^{2+}]_i$. Secondly, mitochondrial Ca^{2+} transport might operate to redistribute Ca^{2+} so that it could be extruded by the most efficient system. Thus, Ca^{2+} uptake at high $[Ca^{2+}]_i$ would help Ca^{2+} extrusion through low affinity transport system whereas the Ca^{2+} would be released at low $[Ca^{2+}]_i$ where the high affinity system are the most efficient. The Ca^{2+} cycling into the mitochondria would also enable these organelles to sense the cellular activity and enable the necessary ATP production to respond to the metabolic need. Finally, there is increasing evidence for a mitochondrial role in the shaping and propagation of Ca^{2+} responses through interaction with intracellular stores and such mechanism might also occur in SCG neurones.

4. Intracellular calcium regulation and endoplasmic reticulum

Using caffeine and SERCA inhibitors, the characteristics of the Ca^{2+} release from and uptake into the intracellular stores were determined. Secondly, the involvement of the ER in the recovery phase of depolarisation-induced Ca^{2+} transients was investigated following either SERCA inhibition or activation of Ca^{2+} release with caffeine. Finally, the nature of the SERCA expressed in SCG neurones was investigated using experiments in immunocytochemistry.

4.1. Intracellular stores release and sequester calcium

Neurones were voltage-clamped at a holding potential of -60 mV (perforated patch configuration and no intracellular sodium; see Methods section 2.2.1, *figure 1* and Methods section 2.4.3, *Table 2* - solution H) and Ca^{2+} release from the intracellular stores was induced with 10 mM caffeine (Caff, *figure 29-A*). Caffeine was dissolved in the standard perfusion solution in the presence or absence of Ca^{2+} (see Methods section 2.4.1, *Table 1* - solution A and D) and pressure-applied (10 p.s.i.) for 5 s using a 'puffer-electrode' (tip diameter ≈ 1 μm) positioned at ≈ 20 μm from the cell soma. Consecutive caffeine applications (every ≈ 60 s) induced rapid $[Ca^{2+}]_i$ rises of similar amplitude (rise time ≈ 5 s and $\Delta[Ca^{2+}]_i$ = 397 ± 62 nM; n=14). The recovery of the caffeine-induced Ca^{2+} transients, which was faster than that of a depolarisation-induced Ca^{2+} transient (see Results section 1.2 and below sections 4.2 and 4.3), had a monoexponential recovery phase with a mean decay time constant of 2.5 ± 0.1 s and a Ca^{2+} clearance rate ≈ 0.26 s^{-1} (see *figures 29-A* and *-B*). At the end of the recovery phase, $[Ca^{2+}]_i$ often decreased below the resting concentration (undershoot) before returning to the basal $[Ca^{2+}]_i$ in tens of seconds (92 ± 3 nM at the end of the recovery *versus* 102 ± 3 nM in control; n=14; $P < 0.05$ - see *figures 29-A* and 33-*A*). The caffeine-

(Next page)

Figure 29: Calcium release from and sequestration into the endoplasmic reticulum
(A) Typical rises in $[Ca^{2+}]_i$ induced in a voltage-clamped neurone following pressure-application of 10 mM caffeine (Caff, arrows for 5 s). (B) Clearance rate *versus* $[Ca^{2+}]_i$ of caffeine-induced Ca^{2+} transients (data pooled from 14 cells and fitted with a linear regression). (C) Caffeine application (10 mM for 5 s, arrow) before and after SERCA inhibition with cyclopiazonic acid (CPA, 50 μM) in a Ca^{2+}-free extracellular solution and (D) SERCA inhibition with CPA in the presence of extracellular Ca^{2+}.

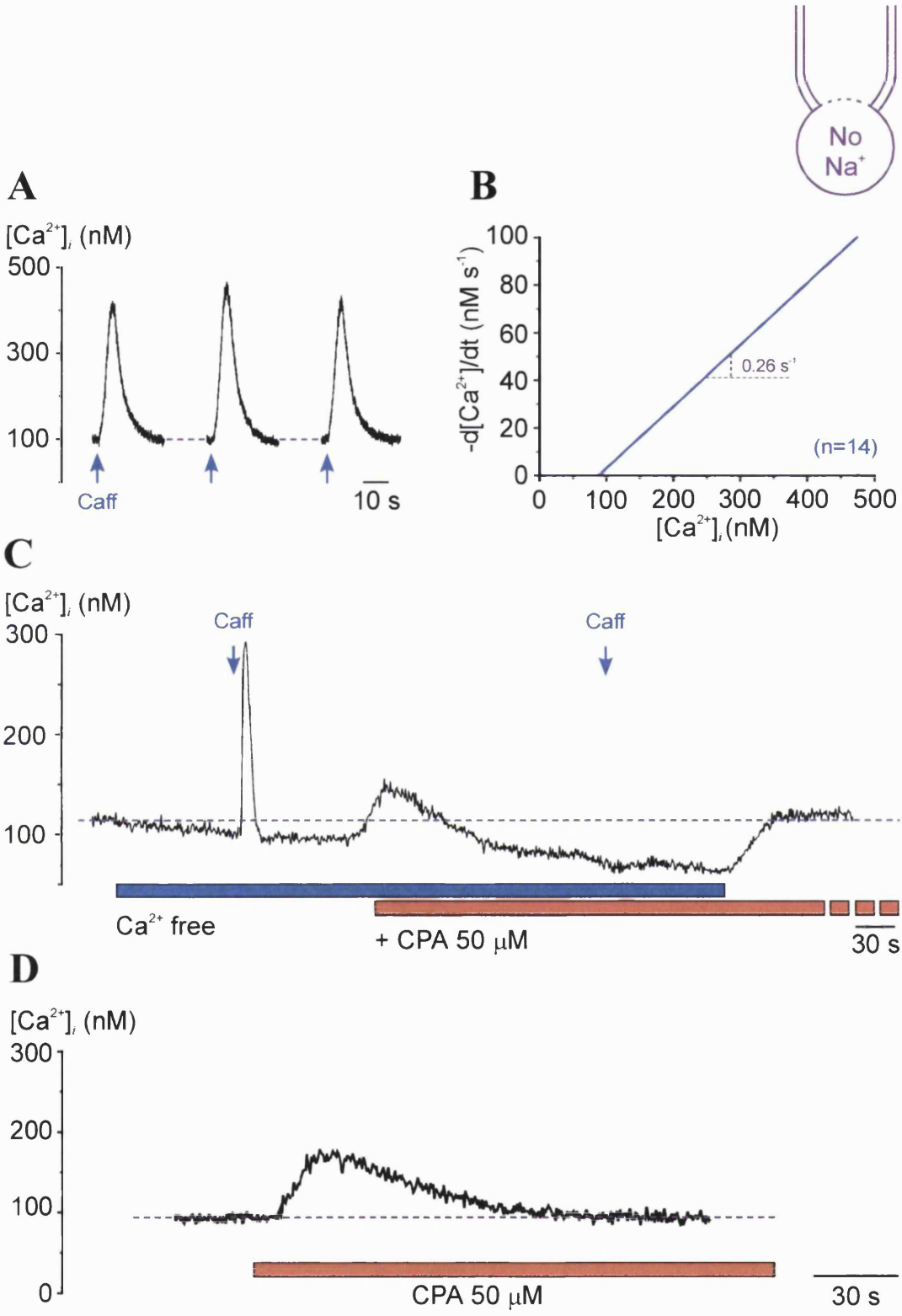

Figure 29 **(see previous page for legend)**

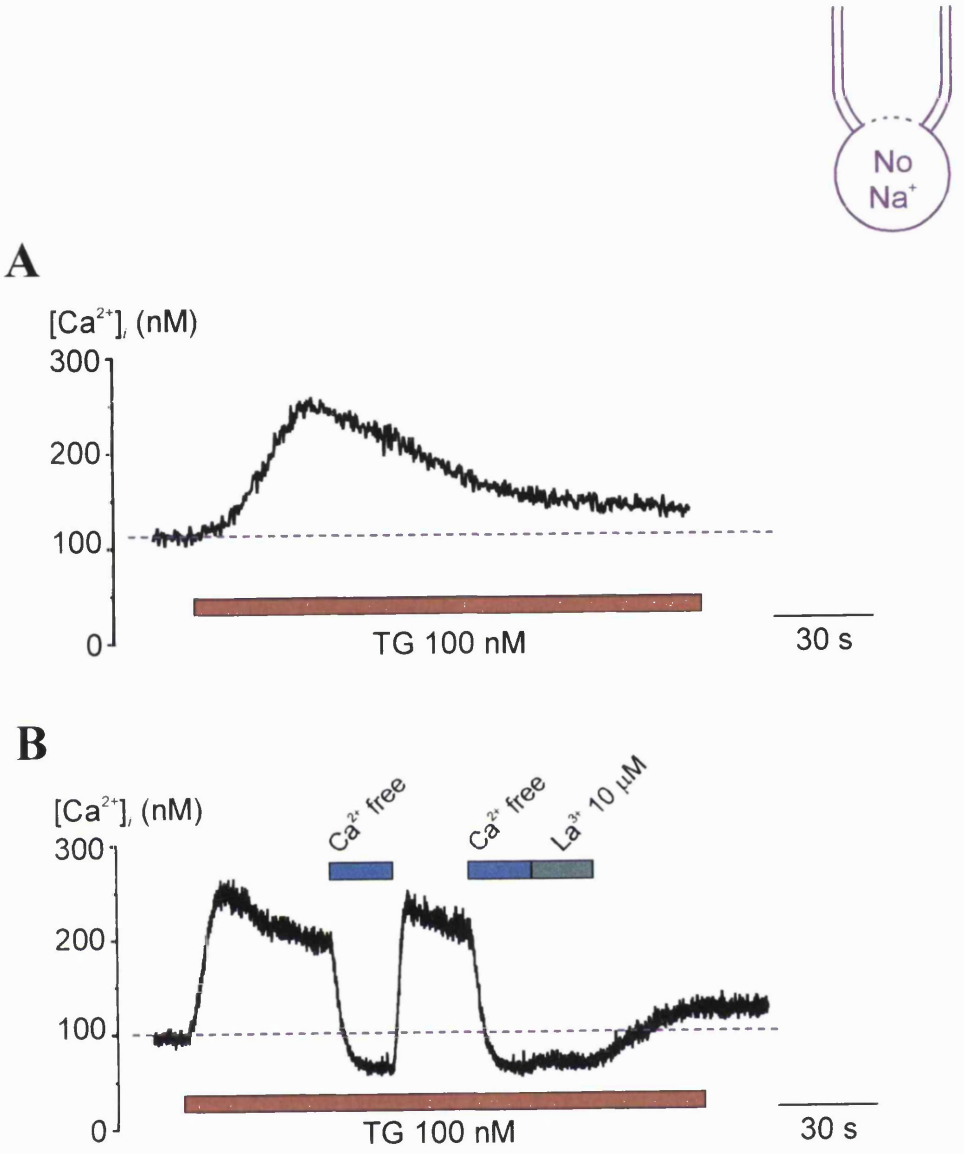

Figure 30: Thapsigargin inhibits Ca^{2+} sequestration into the endoplasmic reticulum and activates a Ca^{2+} influx through the plasma membrane

(A) SERCA inhibition with bath application of thapsigargin (TG, 100 nM) in the presence of extracellular Ca^{2+}. (B) Thapsigargin induces a persistent rise in resting $[Ca^{2+}]_i$ that is abolished in a Ca^{2+}-free extracellular solution or in the presence of 10 µM lanthanum (La^{3+}).

induced Ca^{2+} transients were maintained in a Ca^{2+}-free extracellular solution (less than 2 minutes - *figure 29-C*) and abolished in a use-dependent manner in the presence of 10 μM ryanodine (data not shown).

Bath application of 50 μM cyclopiazonic acid (CPA) or 100 nM thapsigargin (TG) both induced, at rest, a transient rise in the $[Ca^{2+}]_i$ and inhibited the caffeine-induced Ca^{2+} transients (*figures 29-C* and *29-D* for CPA and *figure 30-A* for TG). However, there were differences in the effects of these two compounds since upon CPA application the rise in $[Ca^{2+}]_i$ was transient (109 ± 5 nM in CTR *versus* 101 ± 3 nM in CPA; n=15, P=0.11, *figure 29-D*) whereas after TG application, $[Ca^{2+}]_i$ remained higher than in control (105 ± 10 nM in control *versus* 143 ± 7 nM in TG; n=12, P< 0.01 - *figure 30-A*). This TG-induced persistent rise in $[Ca^{2+}]_i$ was abolished upon removal of extracellular Ca^{2+} as well as in the presence of 10 μM lanthanum (La^{3+}, *figure 30-B*), a blocker of SOCC, suggesting the activation of a Ca^{2+} influx trough the plasma membrane.

4.2. Role of the intracellular stores in the clearance of calcium transients

Neurones were voltage-clamped at -60 mV in the perforated patch configuration and in the absence of intracellular Na^+ to abolish Ca^{2+} release from the mitochondria (see Results section 3.2). Calcium transients were elicited through depolarising steps to 0 mV for 60 and 500 ms prior to the application of 50 μM CPA or 100 nM TG. Depletion of intracellular stores and inhibition of the Ca^{2+} uptake was assessed using caffeine application (10 mM for 5 s) before and after SERCA inhibition (protocol illustrated in Results section 4.1, *figure 29-C*).

4.2.1. SERCA inhibition with cyclopiazonic acid

Inhibition of SERCA with 50 μM CPA was without effect on the properties of small Ca^{2+} transient (< 500 nM) as neither $\Delta[Ca^{2+}]_i$ nor the time constant of the decay were changed compared with control (*Table 11*, *figure 31-A* and inset in *figure 31-B*). Furthermore, the determination of the clearance rate showed no difference after CPA application (rate of 0.15 s^{-1} in CTR and CPA, *figure 31-B*).

For larger Ca^{2+} transients (> 500 nM) the time course of the recovery was unaffected by CPA but $\Delta[Ca^{2+}]_i$ was attenuated by ≈ 50% (*Table 11*). The analysis of

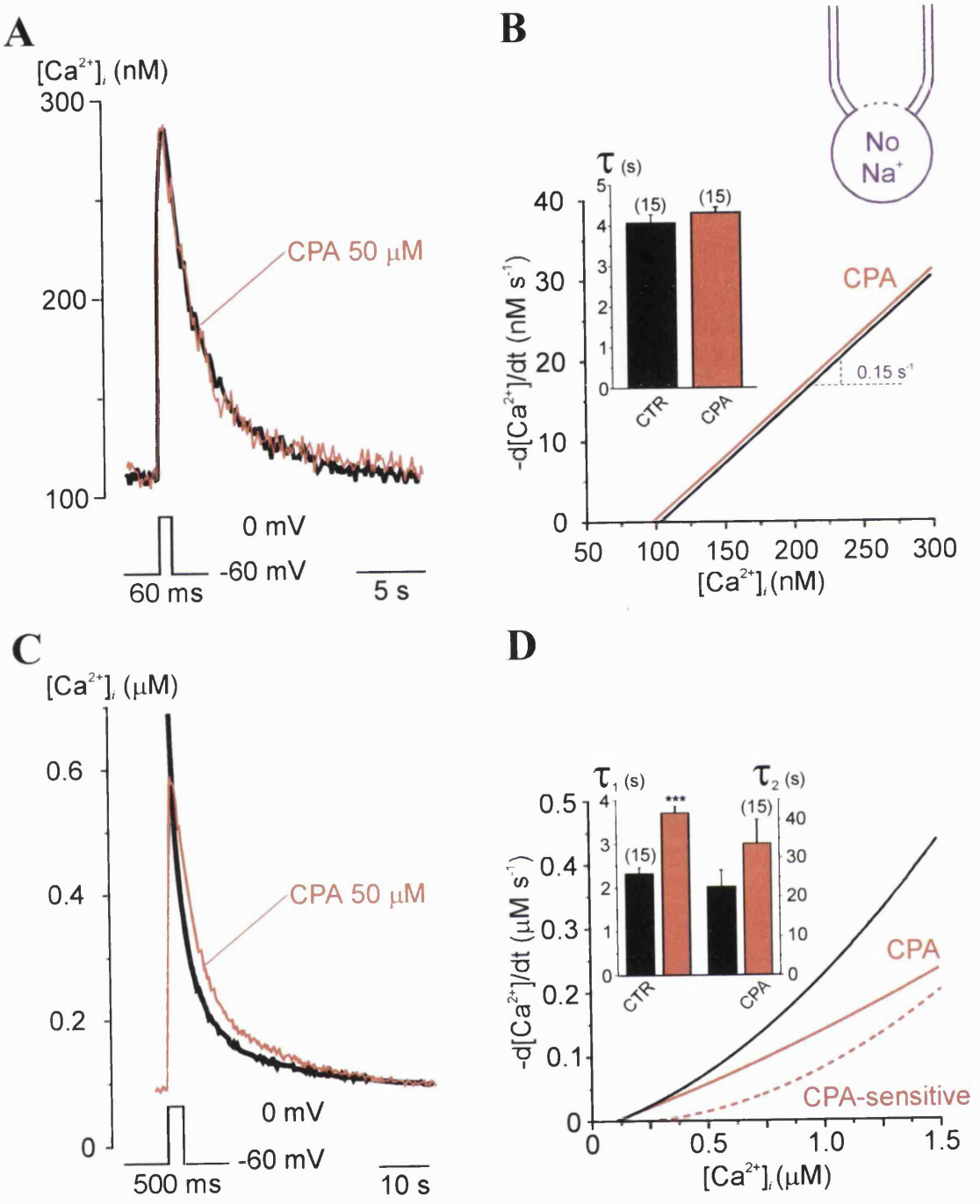

Figure 31: CPA is without effect on the recovery of small Ca^{2+} transients but prolongs the decay of large Ca^{2+} transients

(A) Small Ca^{2+} transients induced by depolarising steps for 60 ms (no intracellular sodium, see inset) before and after bath application of 50 µM CPA. (B) Plot of the clearance rate in control and in CPA for small Ca^{2+} transients (data from 15 cells) were pooled in each condition and fitted with a linear regression. The inset represents the decay time constant of the Ca^{2+} transient's recovery in control and in CPA (black bar, CTR and orange bar, CPA; n=15, data as mean ± S.E.M.). (C) Large Ca^{2+} transients induced by depolarising steps for 500 ms in control and in CPA. In control only the recovery phase of the Ca^{2+} transient is represented because of the reduction of the Ca^{2+} transient's amplitude in the presence of CPA (see text for more details). (D) Plot of the clearance rate in control and in the presence of CPA for large Ca^{2+} transients and determination of the CPA-sensitive component (dashed line - data from 15 cells pooled and fitted with a polynomial function). The inset represents the decay time constants of the Ca^{2+} transient's recovery in control and in CPA (black bar, CTR and orange bar, CPA; n=15, data as mean ± S.E.M. *** P< 0.001).

the voltage-clamp recordings showed that CPA inhibited the peak Ca^{2+} current by about 30% (n=5) and this inhibition of the Ca^{2+} current may underlie the reduction in $\Delta[Ca^{2+}]_i$. However, in the presence of CPA both the fast (τ_1) and slow (τ_2) decay time constants were slowed compared with the control recovery as can be seen from the superimposed Ca^{2+} transient in *figure 31-C* (*Table 11* and inset in *figure 31-D*).

Table 11: Effect of CPA on the properties of Ca^{2+} transients

		Control	CPA	n	*t*-test
$[Ca^{2+}]_i$ < 500 nM	$\Delta[Ca^{2+}]_i$	169 ± 15 nM	177 ± 14 nM	15	paired, P=0.55
	τ	4.1 ± 0.3 s	4.3 ± 0.2 s		paired, P=0.44
$[Ca^{2+}]_i$ > 500 nM	$\Delta[Ca^{2+}]_i$	998 ± 100 nM	436 ± 21	15	paired, P< 0.001
	A_1	878 ± 115 nM	278 ± 14 nM		paired, P< 0.001
	τ_1	2.3 ± 0.1 s	3.7 ± 0.1 s		paired, P< 0.001
	A_2	147 ± 15 nM	106 ± 11 nM		paired, P< 0.01
	τ_2	22.8 ± 4 s	33.9 ± 6 s		paired, P=0.06

As the amplitude of the Ca^{2+} transient was attenuated upon CPA application, only the recovery part of the control Ca^{2+} transient is represented. The plot of the clearance rate, obtained from the fit of the experimental data, was extrapolated to 1.5 µM in the presence of CPA to enable a better comparison and the determination of the CPA-sensitive component (*figure 31-D*). As expected from the time constant measurements, the rate of clearance was slower in CPA than in control (0.2 µM s^{-1} in CTR and 0.15 µM s^{-1} in CPA at $[Ca^{2+}]_i \approx 1$ µM - *figure 31-D*). Finally no saturation of the CPA-sensitive component was observed up to a $[Ca^{2+}]_i \approx 1.5$ µM. Therefore, despite the CPA effect on the amplitude of the Ca^{2+} transients, the results presented above suggest that SERCA inhibition affected the kinetics of the recovery of large Ca^{2+} transients (> 500 nM).

4.2.2. SERCA inhibition with thapsigargin

For small Ca^{2+} transients, the results obtained in the presence of 100 nM TG were in agreement with those obtained after CPA application (*figures 32-A* and *-B*). Although TG induced a persistent rise in resting $[Ca^{2+}]_i$ there were no difference

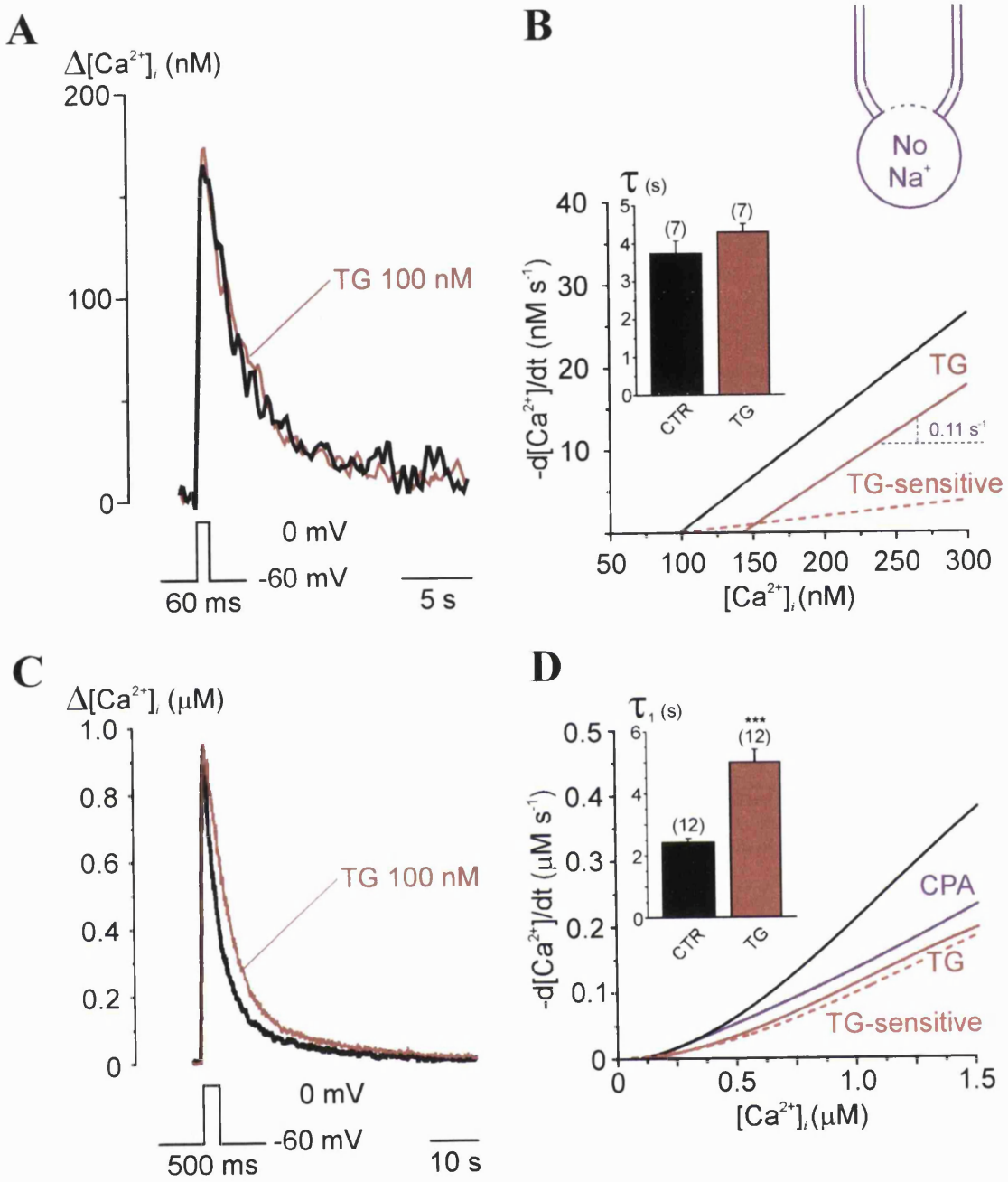

Figure 32: Thapsigargin is without effect on the recovery of small Ca^{2+} transients but prolongs the decay of large Ca^{2+} transients

(A) Small Ca^{2+} transients induced by depolarising steps for 60 ms before and after bath application of 100 nM TG. (B) Plot of the clearance rate in control and in TG for small Ca^{2+} transients with the TG-sensitive component (dashed line, data from 7 cells). The inset represents the decay time constant of the Ca^{2+} transient's recovery in control and in TG (black bar, CTR and orange bar, TG; n=7, data as mean ± S.E.M.). (C) Large Ca^{2+} transients induced by depolarising steps for 500 ms in control and in TG. (D) Plot of the clearance rate in control and in the presence of TG for large Ca^{2+} transients and determination of the TG-sensitive component (dashed line - data from 12 cells). The CPA-sensitive component (violet line) of the recovery is also represented for comparison. The inset represents the decay time constants of the Ca^{2+} transient's recovery in control and in TG (black bar, CTR and orange bar, TG; n=12, data as mean ± S.E.M. *** P< 0.001). Note that in (A) and (C), because of the TG-induced rise in resting $[Ca^{2+}]_i$, the Ca^{2+} transients are represented as $\Delta[Ca^{2+}]_i$ to enable a better comparison of the recovery phase.

neither in $\Delta[Ca^{2+}]_i$ nor in the decay time constant compared with the control situation (*Table 12*). The plot of the clearance rate show little difference in the rate of the recovery (0.13 s^{-1} in CTR *versus* 0.11 s^{-1} in TG, *figure 32-B*) but a shift in resting $[Ca^{2+}]_i$ was observed, which could be explained by a Ca^{2+} influx at ≈ 5 nM s^{-1} (*figure 32-B*).

Table 12: Effect of thapsigargin on the properties of Ca^{2+}transients

		Control	TG	n	*t*-test
$[Ca^{2+}]_i$ < 500 nM	$\Delta[Ca^{2+}]_i$	240 ± 17 nM	241 ± 10 nM	7	paired, P=0.4
	τ	3.7 ± 0.3 s	4.3 ± 0.2 s		paired, P=0.25
$[Ca^{2+}]_i$ > 500 nM	$\Delta[Ca^{2+}]_i$	763 ± 101 nM	677 ± 51 nM	12	paired, P=0.4
	A_1	614 ± 104 nM	536 ± 54 nM		paired, P=0.3
	τ_1	2.4 ± 0.1 s	5.0 ± 2 s		paired, P< 0.001
	A_2	140 ± 10 nM	136 ± 12 nM		paired, P=0.1
	τ_2	21.9 ± 2 s	23.5 ± 2 s		paired, P=0.8

Unlike with CPA, in the presence of TG, $\Delta[Ca^{2+}]_i$ of large Ca^{2+} transients was unaffected as illustrated from the superimposed traces in *figure 32-C* (see *Table 12*). However, the fast decay time constant was slowed by nearly 2-times whilst the slow one remained unchanged (*Table 12* and inset in *figure 32-D*). The clearance rate plot for larger rises in $[Ca^{2+}]_i$ shows that SERCA inhibition slowed the recovery compared to control (≈ 0.2 μM s^{-1} in CTR and ≈ 0.1 μM s^{-1} in TG at $[Ca^{2+}]_i$ ≈ 1 μM - *figure 32-D*) and that the TG-sensitive component, obtained from the difference of the clearance rates in control and in TG did not show any saturation up to $[Ca^{2+}]_i$ ≈ 1.5 μM. Finally, up to ≈ 1 μM, TG appeared to have a stronger inhibitory effect than CPA on the recovery of Ca^{2+} transients as can be seen from the comparison of the clearance rate following CPA and TG application (*figure 32-D*, clearance rate in CPA as determined in *figure 31-D*).

4.3. Calcium clearance following SERCA activation

Calcium transients were elicited by depolarisation steps only or by depolarisation steps followed by caffeine application at the end of the depolarising step (at 60 ms, triggered through the digital output with the pClampex8 software). The caffeine application was meant to induce Ca^{2+} release from the ER and as a consequence to stimulate the uptake mechanism into the ER. This protocol was

designed to determine how Ca^{2+} release from the intracellular stores and SERCA activation could affect the characteristics of Ca^{2+} transients induced by depolarisation.

Calcium transients elicited by 60 ms depolarising steps (depolarisation-induced Ca^{2+} transients) had a rise time of hundreds of milliseconds, a monoexponential recovery phase and a mean decay time constant of 4.0 ± 0.1 s (n=11 - *figure 33-A*, centre). On the other hand, the caffeine-induced Ca^{2+} transients presented a slower rise time (≈ 5 s) but a faster monoexponential recovery phase (τ = 2.5 ± 0.1; n=14 - *figure 33-A*, left and see Results section 4.1, *figure 29-A*). When caffeine was applied at the end of the depolarising pulse, the amplitude of the depolarisation-induced Ca^{2+} transients was increased and equal to the sum of the amplitude of equivalent depolarisation-induced and caffeine-induced Ca^{2+} transients (574 ± 192 nM *versus* 463 ± 70; n=6, P=0.67). Furthermore, in this condition, the rise time of the Ca^{2+} transient induced by both depolarising step and caffeine application was similar to the depolarisation-induced Ca^{2+} transient but its recovery was accelerated and equivalent to the recovery of a caffeine-induced Ca^{2+} transient (τ = 2.4 ± 0.1 s; n=6, P< 0.001 *versus* depolarisation-induced Ca^{2+} transient; n=11, independent Student *t*-test - see superimposed traces in *figure 33-A*, right). Moreover, similarly to caffeine-induced Ca^{2+} transients (see Results section 4.1) and following the recovery phase, resting $[Ca^{2+}]_i$ transiently decreased below the control level (87 ± 2; n=6 and 107 ± 10; n=14, respectively and see *figure 33-A right*).

The determination of the clearance rate showed that caffeine-induced or both caffeine- and depolarisation-induced Ca^{2+} transients had a similar rate of recovery, which was faster than the clearance rate of a Ca^{2+} transient induced by depolarisation alone (≈ 0.26 s^{-1} and ≈ 0.15 s^{-1}, respectively *figure 33-B*). By subtracting the clearance rate of the depolarisation-induced Ca^{2+} transient to the clearance rate of the depolarisation- and caffeine-induced Ca^{2+} transient, the rate of the 'SERCA uptake' could be estimated ≈ 0.11 s^{-1} (*figure 33-B*).

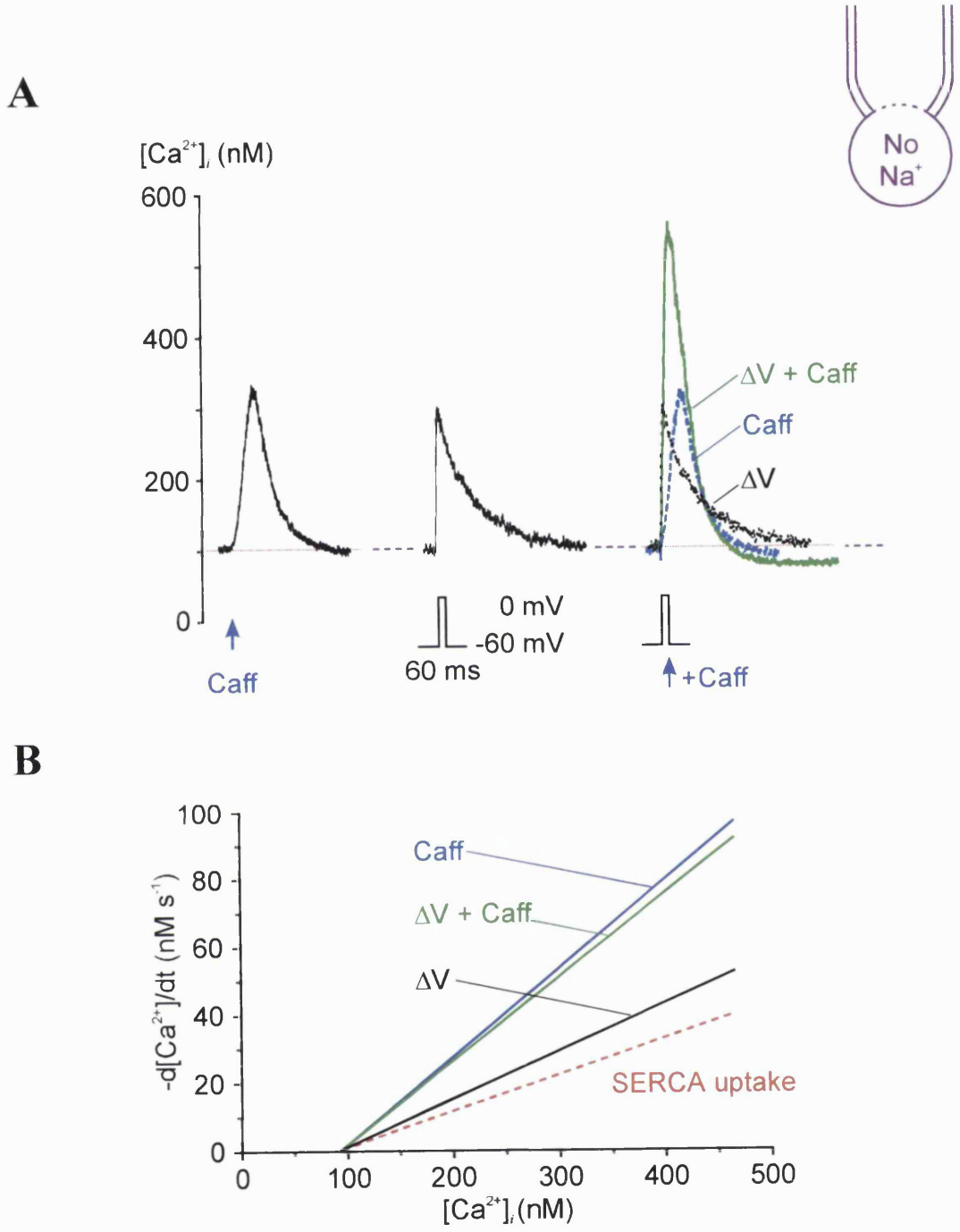

Figure 33: Caffeine effects on calcium uptake into the reticulum endoplasmic and on the recovery of depolarisation-induced calcium transients

(A) Calcium transients induced by caffeine (Caff, 10 mM for 5 s, left) and elicited by 60 ms depolarising steps without (ΔV, centre) and with an additional application of caffeine (ΔV+Caff, right) in a neurone voltage-clamped in the perforated patch configuration. The different traces have been superimposed to enable the comparison of the recovery phase. (B) Comparison of the clearance rate of Ca^{2+} transients induced by caffeine alone (Caff, blue line; n=14), by depolarisation alone (ΔV, black line; n=11) and by depolarisation and caffeine (ΔV + Caff, green line; n=6). The component corresponding to the 'SERCA uptake' (difference between ΔV + Caff and ΔV) is represented (dashed line).

4.4. SCG neurones mainly express the SERCA-3 isoform

So far three main SERCA isoforms have been characterised in living cells (see General Introduction section 4.2.2.2), therefore experiments in immunocytochemistry were carried out to determine which isoform was expressed in SCG neurones. After two days in culture, neurones were fixed using 0.2% glutaraldehyde/2% paraformaldehyde before incubation with a selective goat polyclonal antibody directed against the N-terminal region of each SERCA isoform (1/50, SERCA-1 to -3, respectively, see Methods section 7.1 and *Table 5* for more details). The primary antibodies were subsequently labelled using swine anti-goat IgG conjugate to TRITC (1/50 - see Methods section 7.1 and *Table 6*). The selectivity of the labelling was assessed by the absence of significant labelling using solution of antibodies pre-incubated with the corresponding antigenic peptides. The results of the immunolabelling were examined on a fluorescent microscope, images acquired with a CCD camera and analysed using the deconvolution methods with the *Nearest neighbours algorithm* (*figure 34* and see Methods section 7.2 and *figure 8*). For the three antibodies, images were acquired and analysed using the same parameters to enable a comparison of the staining's results. Images taken at a particular plane of focus are illustrated in *figures 34-A_1*, *-B_1* and *-C_1* for each of the three antibodies with the corresponding deconvolved image (SERCA-1, -2 and -3 in *figures 34-A_2*, *-B_2* and *-C_2*, respectively). It appears that SERCA-3 was the SERCA isoform the most largely expressed in SCG neurones. The deconvolution analysis suggested that SERCAs are localised close to the somatic plasma membrane with the exception of SERCA-3, which appeared to be also present in neurites (*figure 34-C_2*). This localisation of SERCA close to the plasma membrane was in agreement with the distribution of the ER, which appeared mainly localised around the nucleus and in the first 2 μm under the plasma membrane (*figure 34-D_2*). The localisation of the ER was determined using an antibody directed against the disulphydryl protein isomerase (DPI, 1/50), a protein of the ER, and immunolabelled with a TRITC conjugate (1/200).

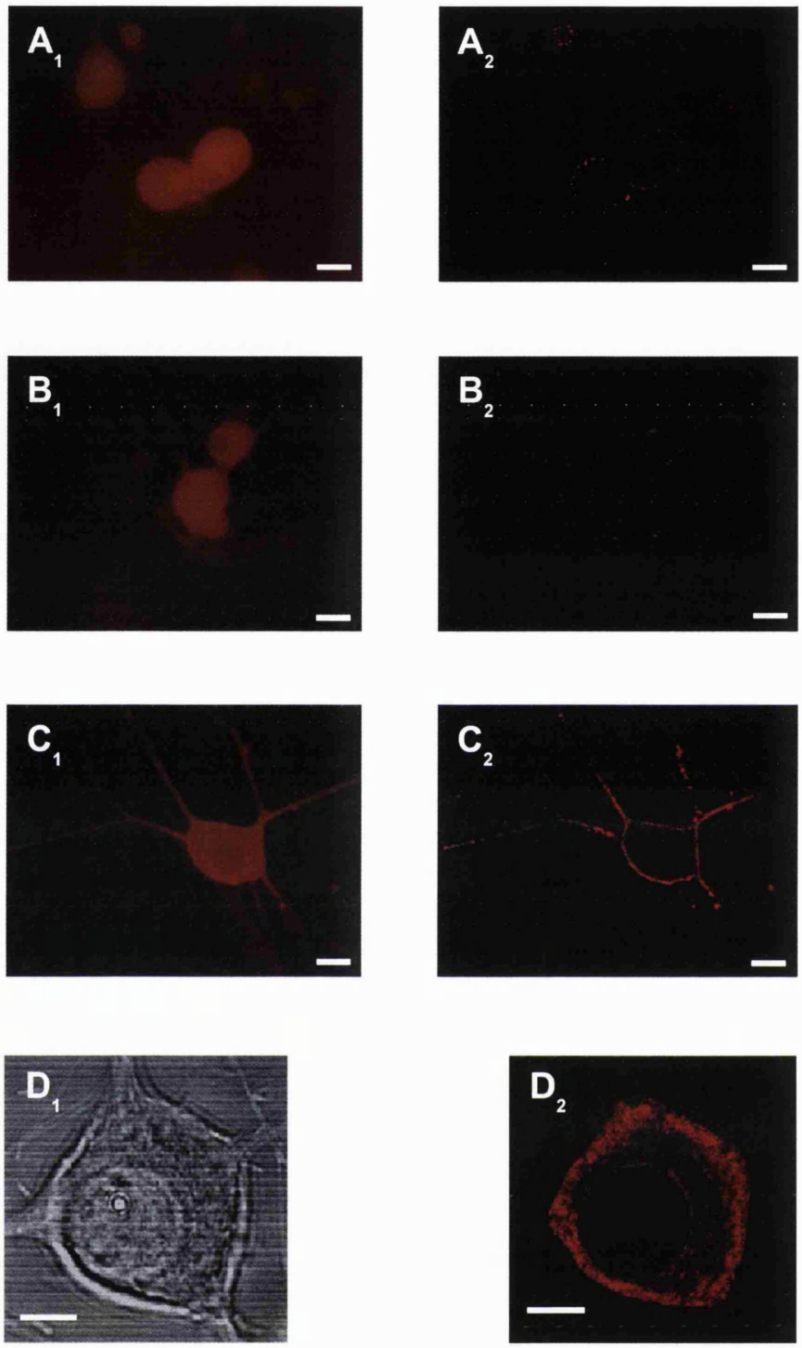

Figure 34: SERCA-3 is the predominant isoform expressed in SCG neurones and is primarily localised close to the somatic plasma membrane

Goat polyclonal antibodies (1/50) raised against each of the three SERCA isoforms were used to determined which isoform is expressed in SCG neurones (SERCA-1, -2 and -3 in panel A_1, B_1 and C_1, respectively). The primary antibodies were labelled with swine anti-goat polyclonal antibodies conjugated to TRITC (1/50) and images acquired using a CCD camera attached to a fluorescent microscope. The images in A_1, B_1 and C_1 were subsequently analysed with the digital deconvolution technique using the *Nearest neighbours algorithm* to generate the images in panels A_2, B_2 and C_2 (scale bar 10 μm, x40 oil immersion fluorescent objective). (D_1) Bright field image of a SCG neurone labelled with a rabbit polyclonal antibody raised against DPI (1/200) and immunolabelled with a secondary antibody conjugated with TRITC (D_2). Images acquired using a confocal microscope (scale bar 5 μm, x63 oil immersion fluorescent objective).

Taken together, the results suggested that the ER presented functional Ca^{2+} release pathways, mainly through RyRs, and a fast Ca^{2+} uptake system *via* SERCA. The SERCA-3 isoform appeared to be the predominant isoform in these neurones and to be primarily distributed close to the somatic plasma membrane, where the ER it thought to be localised. The results suggested further that intracellular stores did not participate either as an amplification system or as a sequestration mechanism during small rise in $[Ca^{2+}]_i$ Nevertheless, when the SERCA were activated, following stores depletion, the recovery of depolarisation-induced Ca^{2+} transients, even at low $[Ca^{2+}]_i$, was accelerated. In contrast, the recovery from larger Ca^{2+} loads, that might have invaded the cytosol, appeared to be accelerated through Ca^{2+} sequestration into the ER suggesting that Ca^{2+} store was capable of sequestering Ca^{2+} following Ca^{2+} influx through the plasma membrane.

4.5. Discussion

The data presented in this section suggested that the Ca^{2+} store is filled, at least partially, at rest. Thus, prior to store 'loading' through the activation of VACC, large amount of Ca^{2+} could be released by an application of caffeine (this study and see also Hernandez-Cruz *et al.*, 1995; Garaschuk *et al.*, 1997 and Seymour-Laurent & Barish, 1995). This observation is in agreement with earlier results suggesting that Ca^{2+} store would be filled at ≈ 80% in peripheral neurones at rest but contrast with the situation observed in most central neurones where intracellular stores are thought to be empty (Shmigol *et al.*, 1994a). Finally, direct measurements of the free luminal $[Ca^{2+}]_i$ ($[Ca^{2+}]_L$) in the intracellular stores indicated that there is ≈ 5-10 mM Ca^{2+} of which between 0.1 and 0.3 mM are thought to be in the free ionic form (see Meldolesi & Pozzan, 1998 for review).

Since caffeine-induced Ca^{2+} transients are observed in a Ca^{2+}-free extracellular solution and are inhibited in the presence of both SERCA inhibitors or high concentrations of ryanodine (10 μM), it can be assumed that Ca^{2+} is released from caffeine- and ryanodine-sensitive intracellular stores (this study and see also Sadoshima & Akaike, 1991; Friel & Tsien, 1992; Hua *et al.*, 1993; Hernandez-Cruz *et al.*, 1995 and Garaschuk *et al.*, 1997). In SCG neurones, this result is further supported by data

showing that membrane preparations from rat sympathetic ganglia posses a high number of ryanodine binding sites (Hernandez-Cruz *et al.*, 1995) about 3-fold larger than any other neuronal preparation and comparable to cardiac tissue (Meissner & Henderson, 1987).

The recovery from caffeine-induced Ca^{2+} transients was faster than that of a depolarisation-induced Ca^{2+} transient suggesting that these two Ca^{2+} responses might be regulated by different mechanisms. The Ca^{2+} released by caffeine would be transported by systems close to the release sites and could therefore be re-sequestered through the activation of SERCA back into the same Ca^{2+} store. It has been shown that high $[Ca^{2+}]_L$ would inhibit the SERCA activity and facilitate Ca^{2+} release whereas lower $[Ca^{2+}]_L$ is thought to have the opposite effect (Inesi & de Meis, 1989; Gilchrist *et al.*, 1992; Favre *et al.*, 1996 and Mogami *et al.*, 1998). The activity of SERCA has been shown to be upregulated in a Ca^{2+}-dependent manner by both direct CaM-dependent phosphorylation processes and by the phosphorylation of phospholamban (see Carafoli, 1987 and Pozzan *et al.*, 1994 for review). In contrast, the $[Ca^{2+}]_i$ threshold for RyR activation has been shown to be lower when the Ca^{2+} content of the ER is high, therefore Ca^{2+} release would be promoted (Gilchrist *et al.*, 1992; Lukyanenko *et al.*, 1996 and Marie & Silva, 1998). Therefore, after activation of RyRs and depletion of the Ca^{2+} store, Ca^{2+} replenishment would be ensured by stimulating Ca^{2+} uptake and inhibiting Ca^{2+} release (RyR inactivation). Such a system would optimise the activity of the intracellular store and enable regenerative Ca^{2+} response by promoting Ca^{2+} release when the luminal $[Ca^{2+}]$ is high and stores refilling after store depletion (Friel & Tsien, 1992 and Hernandez-Cruz *et al.*, 1995 and Garaschuk *et al.*, 1997).

Several observations suggested that the released Ca^{2+} would only partially be re-sequester into Ca^{2+} store. Firstly, although the recovery from caffeine-induced Ca^{2+} transients was rapid ($\approx$ 2-3 s) a minimum delay ($\approx$ 60 seconds in SCG neurones) was necessary to induce two consecutive equivalent caffeine responses (see *figure 29-A* and see also Friel & Tsien, 1992; Hernandez-Cruz, 1995 and Usachev & Thayer, 1999b). In addition, the refilling of the Ca^{2+} store was shown to be accelerated by an intercalated depolarisation-induced Ca^{2+} transient (Sorimachi, 1993; Hernandez-Cruz, 1995 and Garaschuk *et al.*, 1997). Secondly, in the absence of extracellular Ca^{2+}, caffeine-induced responses would progressively run down and completely disappear after long exposure

to a Ca^{2+}-free perfusion solution (Sorimachi, 1993; Garaschuk *et al.*, 1997 and Usachev & Thayer, 1999b). Therefore, although Ca^{2+} appears to cycle in and out of the ER, ryanodine-sensitive Ca^{2+} store would depend on extracellular Ca^{2+} to maintain their 'resting' $[Ca^{2+}]_L$. In fact, in CA1 pyramidal neurones and sensory neurones the refilling of the ryanodine-sensitive Ca^{2+} store is prevented in the presence of Ca^{2+} channels antagonists (D600 and nickel - Garaschuk *et al.*, 1997 and Usachev & Thayer, 1999b) or in a Ca^{2+}-free extracellular medium suggesting the involvement of a plasma membrane Ca^{2+} influx (Garaschuk *et al.*, 1997 and Usachev & Thayer, 1999b). Similar results were observed in rat sympathetic neurones where following depletion of the intracellular stores the rise in resting $[Ca^{2+}]_i$ was abolished in a Ca^{2+}-free extracellular solution or in the presence of La^{3+}, an inhibitor of the capacitative channels (this study see *figure 30-B*). Therefore there must be at rest a Ca^{2+} influx through the plasma membrane to enable the spontaneous refilling of Ca^{2+} store. This mechanism would be analogous to the capacitative or store-operated Ca^{2+} influx activated by IP_3-sensitive Ca^{2+} store (Tsien & Tsien, 1990; Berridge, 1995; Boulay *et al.*, 1999 and Kiselyov *et al.*, 1999, 2000). This result also suggest that intracellular stores might play a role in the regulation of resting $[Ca^{2+}]_i$ (see Results section 7.2).

The necessity of a Ca^{2+} influx to maintain the $[Ca^{2+}]_L$ is further supported by the observation that Ca^{2+} store appeared to be 'leaky'. Firstly, in a Ca^{2+}-free extracellular solution the caffeine response ran down (see above) and secondly the inhibition of SERCA induced a slow dissipation of Ca^{2+} that was visualised as a transient rise in $[Ca^{2+}]_i$ (see *figures 29-D* and *30-A*). The exact nature of this leak mechanism is still unclear. However Ca^{2+} leak might be mediated through RyR open at a low probability or channel flickering (Hernandez-Cruz *et al.*, 1995 and Armisen *et al.*, 1996). Since cyclic ADP ribose (cADPr) was proposed to correspond to the endogenous RyR ligand and was shown to stimulate Ca^{2+} release through RyR (Galione, 1993, 1994; Empson & Galione, 1997), an alternative mechanism to explain the Ca^{2+} leak from the intracellular stores could be a basal production of cADPr that would maintain RyR in low open probability state.

The ryanodine-sensitive Ca^{2+} signal is known to be the basis of the process of Ca^{2+}-induced Ca^{2+} release (CICR - see Kuba, 1994 and Usachev & Thayer, 1999a for review). Surprisingly, although SCG neurones present strong caffeine- and ryanodine-

sensitive Ca^{2+} transient and have been shown to posses high level of ryanodine binding sites (Hernandez-Cruz *et al.*, 1995), there was no evidence for a CICR process (this studies and see also Hernandez-Cruz, 1995). This results is paradoxical and contrasts with the situation observed in bullfrog sympathetic neurones (Hua *et al.*, 1993; Narita *et al.*, 1998; Hongpaisan *et al.*, 2001 and Albrecht *et al.*, 2001), in rat sensory neurones (Usachev *et al.*, 1993, 1997 and Shmigol *et al.*, 1995) or rat cerebellar Purkinje neurones (Kano *et al.*, 1995; Llano *et al.*, 1994 and Womack *et al.*, 2000). All these cell types present robust caffeine-induced Ca^{2+} responses and Ca^{2+} influx through the plasma membrane elicits an amplification of the Ca^{2+} signal that is sensitive to both ryanodine and SERCA inhibitors. In SCG neurones, there was a linear correlation between transmembrane Ca^{2+} influx and rise in $[Ca^{2+}]_i$ (see Results section 2 and *figure 19*), the rising phase of depolarisation-induced Ca^{2+} transient was monophasic and application of ryanodine or SERCA inhibitors did not modify the amplitude of the Ca^{2+} transient. However, the inhibition of the Ca^{2+} uptake with thapsigargin significantly prolonged the recovery of submicromolar rises in $[Ca^{2+}]_i$ suggesting that SERCA activation might accelerate the recovery from large changes in $[Ca^{2+}]_i$. Interestingly, the stimulation of Ca^{2+} release from the intracellular stores during a depolarisation-induced Ca^{2+} transient, even following small rises in $[Ca^{2+}]_i$, significantly accelerated the recovery phase. Moreover, in this condition the recovery was similar to that of a caffeine-induced Ca^{2+} transient suggesting that after stimulation of Ca^{2+} release from the ER, Ca^{2+} would preferentially be transported back into the Ca^{2+} store. Thus, SCG neurones posses all the systems required for the induction of the CICR process and their intracellular stores appear to exhibit the ability to regulate rises in $[Ca^{2+}]_i$ induced by Ca^{2+} influx through the plasma membrane providing the proper pathway is activated. The absence of amplification of the Ca^{2+} response cannot be explained by Ca^{2+} store in an empty state, as there was clearly a releasable Ca^{2+} pool even at rest. The amplitude of the Ca^{2+} influx and of the rise in $[Ca^{2+}]_i$ can neither be responsible for the lack of CICR because in other cell types similar rises in $[Ca^{2+}]_i$ are sufficient to trigger this process (Hua *et al.*, 1993; Usachev *et al.*, 1993; Llano *et al.*, 1994; Shmigol *et al.*, 1995; Kano *et al.*, 1995; Usachev & Thayer, 1997; Narita *et al.*, 1998, 2000; Womack *et al.*, 2000; Hongpaisan *et al.*, 2001 and Albrecht *et al.*, 2001). On the other hand, because SCG neurones exhibit high endogenous Ca^{2+} buffering capacity, one could suggest that larger

increase in $[Ca^{2+}]_i$ would be necessary to overcome the Ca^{2+} buffering system and to be still large enough to trigger CICR. The net Ca^{2+} flux in the ER would depend on the respective contribution of Ca^{2+} uptake *via* SERCA and Ca^{2+} release through RyR.
The rise in $[Ca^{2+}]_i$ might not be large enough nor fast enough to trigger Ca^{2+} release and would instead stimulate Ca^{2+} uptake since SERCA activity is upregulated by a rise in $[Ca^{2+}]_i$ (Albrecht *et al.*, 2001). Another possible answer to this paradoxical result may be the experimental conditions since it has been reported that neurones in culture behave differently than *in vivo* or even in slice (see Womack *et al.*, 2000). One could therefore suggest that under culture conditions the absence of tonic activation through synaptic inputs might induce the down regulation in the expression of activatory pathways necessary for a functional CICR. However there are several studies in dissociated neurones that successfully demonstrated CICR (Hua *et al.*, 1993; Usachev *et al.*, 1993; Usachev & Thayer, 1997 and Narita *et al.*, 1998). Another explanation might lie in the recording's conditions with the CICR process being lost by the measurement of somatic averaged Ca^{2+} transients. However, if such a phenomenon occurred one could expect the application of selective inhibitors to unmask it. Finally, since neurones were loaded with indo-1-AM, the indo-1 trapped in the ER might increase the Ca^{2+} buffering capacity of Ca^{2+} store and perturb the Ca^{2+} release process. This issue could be further addressed by carrying out new experiments with either membrane localised or low affinity Ca^{2+} indicators and by comparing the Ca^{2+} response in dissociated neurones with those in slices. Finally, at low concentrations caffeine does not induce Ca^{2+} release through RyR but sensitises the receptor to lower $[Ca^{2+}]_i$ and the involvement of CICR could therefore be tested using this protocol.

In conclusion, SCG neurones express high level of ryanodine receptor (Hernandez-Cruz *et al.*, 1995) and of SERCA (this study), which is the basis for the robust ryanodine-sensitive Ca^{2+} release system associated to an efficient Ca^{2+} sequestration system. In bullfrog sympathetic neurones, the involvement of Ca^{2+} store was demonstrated to play an important role in the regulation of the cellular excitability through the modulation of Ca^{2+}-dependent potassium conductance (Akita & Kuba, 2000 and Lu & Kuba, 2001). Rat sympathetic neurones also exhibit such Ca^{2+}-dependent potassium conductance (Smart, 1987 and Selyanko, 1996) and there is evidence for a

modulation of Ca^{2+}-dependent potassium channel by ryanodine-sensitive Ca^{2+} store (Davies *et al*, 1996). Furthermore, these Ca^{2+} store might be involved in the generation of Ca^{2+} waves necessary to relay throughout the cytosol signals from the cell environment. The fact that SERCA are distributed close to the plasma membrane and throughout neurites would support the idea of both a modulation of ionic channels of the plasma membrane and a relay of Ca^{2+} signal.

5. Plasma membrane calcium ATPase and intracellular calcium

In this section, the role of PMCA in the control of resting $[Ca^{2+}]_i$ and the extrusion of small (< 500 nM) but also larger (≈ 1 μM) rises in $[Ca^{2+}]_i$ following depolarisation was determined using extracellular alkalisation (pH 9) and intracellular addition of 5,6-succinylmidyl carboxyeosin (CE) to inhibit the Ca^{2+} pump. Secondly, the variations in the intracellular pH following rises in $[Ca^{2+}]_i$ and the subsequent Ca^{2+} clearance was measured using BCECF a fluorescent pH indicator. Finally, to determine which PMCA isoforms are expressed in SCG neurones, PCR analysis along with experiments in immunocytochemistry were carried out.

5.1. Calcium extrusion through PMCA

Neurones were voltage-clamped in the perforated patch configuration and rises in $[Ca^{2+}]_i$ were induce by depolarising step from -60 mV to 0 mV for 60 ms and 500 ms before, during and after extracellular alkalisation (pH 9). Following extracellular alkalisation, resting $[Ca^{2+}]_i$ increased from 102 ± 5 nM in control to 254 ± 27 nM at pH 9 (n=9, P< 0.001 *figure 35-A*, see also Results section 7.1) whereas the Ca^{2+} transients $\Delta[Ca^{2+}]_i$ remained unaffected (*Table 13*).

Upon extracellular alkalisation, the time course of the small Ca^{2+} transients' recovery was strongly affected and the decay time constant was nearly 3-times slower than in control (*Table 13*, *figure 35-A* and inset in *figure 35-C*). To enable a better comparison of the recovery phase and because of the difference in the basal $[Ca^{2+}]_i$, only the net rise in $[Ca^{2+}]_i$ ($\Delta[Ca^{2+}]_i$) is illustrated in *figure 35-B* (see dashed line in *figure 35-A*). As soon as the extracellular pH was brought back to 7.4, resting $[Ca^{2+}]_i$ returned to its control value and the recovery of Ca^{2+} transients induced after wash out was identical to the one prior to pH 9 application (in *figure 35-A* compare left and right panels). The determination of the clearance rate showed that up to ≈ 250 nM all the Ca^{2+} clearance was mediated through a pH-sensitive process and above this $[Ca^{2+}]_i$ the clearance rate was slow (0.06 s^{-1} at pH 9 compare to 0.17 s^{-1} in CTR, *figure 35-C*).

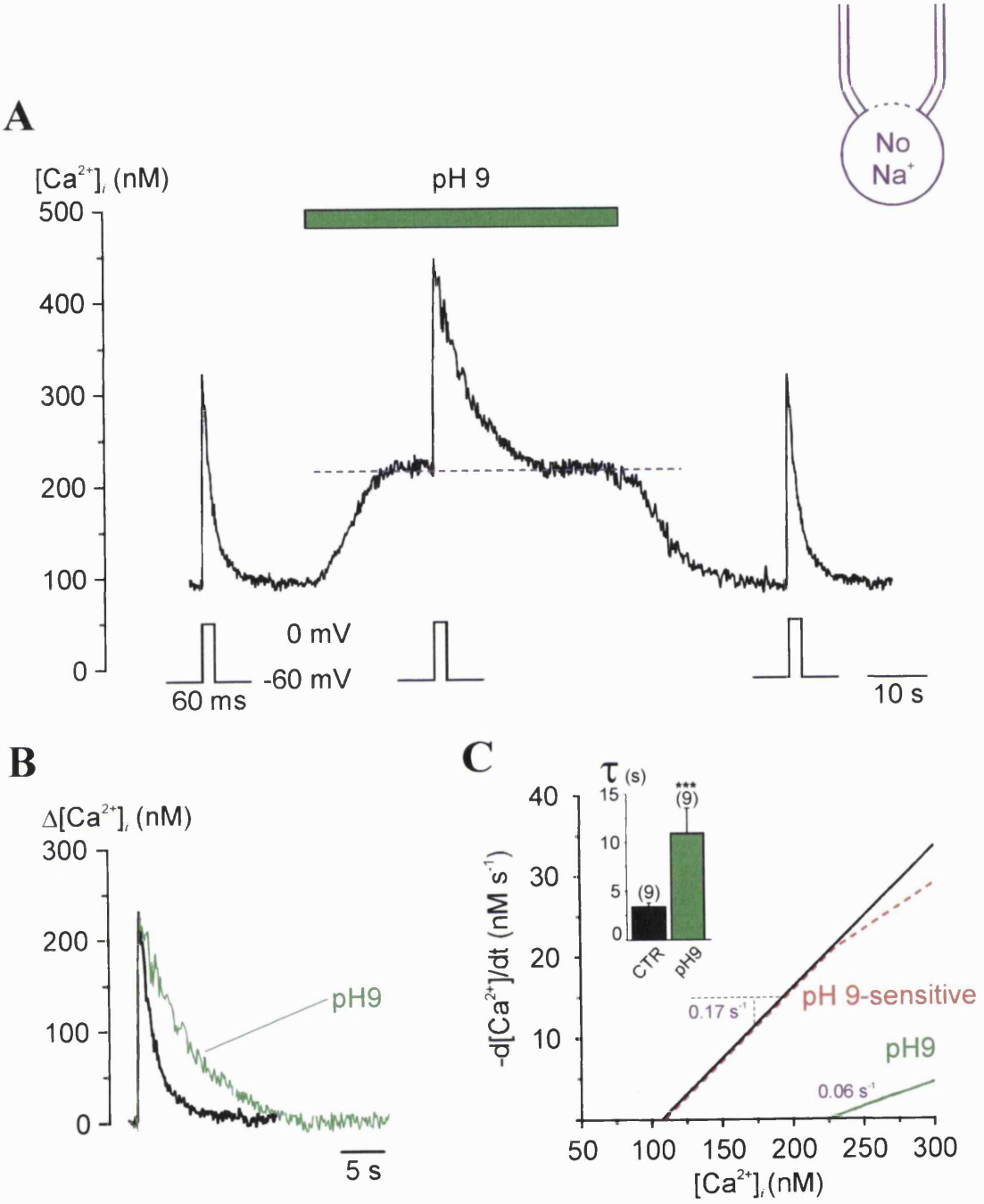

Figure 35: Effects of extracellular alkalisation on resting $[Ca^{2+}]_i$ and on the clearance of small depolarisation-induced Ca^{2+} transients

(A) Small Ca^{2+} transients induced by depolarising steps for 60 ms before, during and after extracellular alkalisation (pH 9) to inhibit the PMCA. (B) Superimposed traces from (A) on a slower time scale and represented as $\Delta[Ca^{2+}]_i$ to compare the recovery phase. (C) Plot of the clearance rate in control and at pH 9 for small Ca^{2+}transients with the pH-dependent component (dashed line, data from 9 cells). The inset represents the decay time constant of the Ca^{2+} transient's recovery in control and at pH 9 (black bar, CTR and green bar, pH 9; n=9, data as mean ± S.E.M. *** P< 0.001).

Table 13: Effect of extracellular alkalisation on the properties of Ca^{2+} transients

		Control	pH 9	n	*t*-test
$[Ca^{2+}]_i$ < 500 nM	$\Delta[Ca^{2+}]_i$	176 ± 10 nM	188 ± 21 nM	9	paired, P=0.29
	τ	4.2 ± 0.7 s	11 ± 3 s		paired, P< 0.001
$[Ca^{2+}]_i$ > 500 nM	$\Delta[Ca^{2+}]_i$	1079 ± 166 nM	1034 ± 160 nM	7	paired, P=0.66
	A_1	785 ± 144 nM	758 ± 164 nM		paired, P=0.3
	τ_1	3.3 ± 0.6 s	5.1 ± 0.7 s		paired, P< 0.01
	A_2	286 ± 43 nM	254 ± 17 nM		paired, P=0.33
	τ_2	17.7 ± 2 s	30.7 ± 2 s		paired, P< 0.001

The recovery from larger rise in $[Ca^{2+}]_i$ (> 500nM) was also markedly affected at pH 9 (*figure 36-A*) and both decay time constants were ≈ 2-times slower than in control (*figures 36* and *Table 13*). This prolongation of the recovery phase at pH 9 is even more evident in *figure 36-B* where $\Delta[Ca^{2+}]_i$ in control and at pH 9 are superimposed, because of the difference in the basal $[Ca^{2+}]_i$ (see dashed line in *figure 36-A*). In agreement with the results obtained for small Ca^{2+} transients (see above *figure 35*), extracellular alkalisation induced a rise in resting $[Ca^{2+}]_i$ to ≈ 250 nM. However at pH 9 and at the end of the recovery of large Ca^{2+} transients the $[Ca^{2+}]_i$ only returned to 366 ± 35 nM (*figure 36-A*; n=7 and compare with *figure 35-A*). The plot of the clearance rate shows that, in agreement with the situation observed for smaller Ca^{2+} transients, the Ca^{2+} clearance is mostly pH-sensitive up to a $[Ca^{2+}]_i$ of 250-300 nM (pH-sensitive component in *figure 36-C*). Over this concentration, the contribution of the pH-sensitive component appeared to reach saturation with a maximal rate of 0.1 μM s^{-1} at 1 μM (*figure 36-C*).

(Next page)

Figure 36: Effects of extracellular alkalisation on the clearance of large depolarisation-induced Ca^{2+} transients

(A) Large Ca^{2+} transients induced by depolarising steps for 500 ms before, during and after extracellular alkalisation (pH 9) to inhibit the PMCA. (B) Superimposed traces from (A) on a slower time scale and represented as $\Delta[Ca^{2+}]_i$ to compare the recovery phase. (C) Plot of the clearance rate in control and at pH 9 for large Ca^{2+} transients with the pH-dependent component (dashed line, data from 7 cells). Decay time constants for the fast (D) and slow (E) component of the Ca^{2+} transient's recovery in control and at pH 9 (black bar, CTR and green bar, pH 9; n=7, data as mean ± S.E.M. ** P< 0.01 and *** P< 0.001).

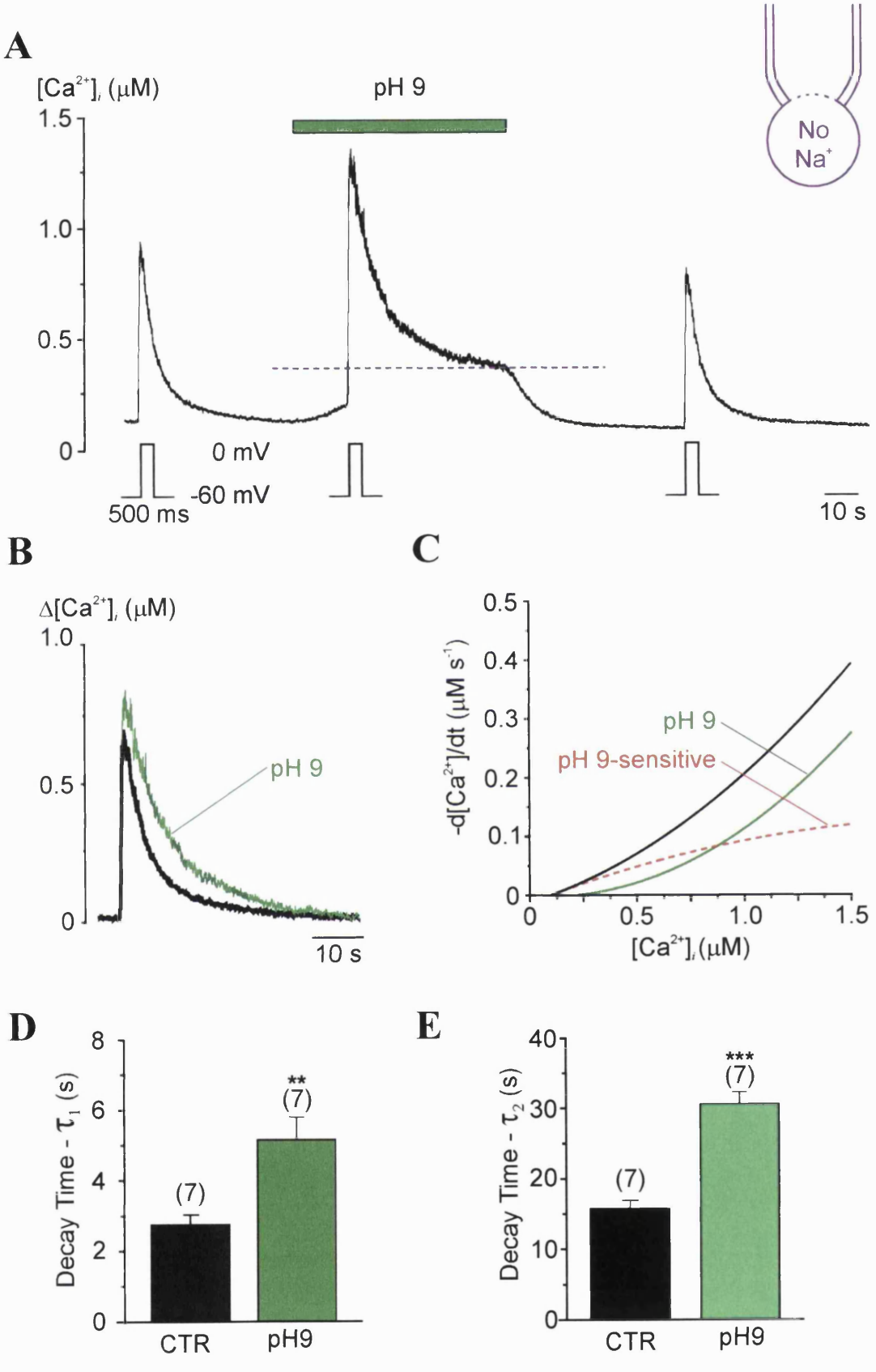

Figure 36 **(see previous page for legend)**

5.2. PMCA inhibition with carboxyeosin

Neurones were voltage-clamped in the whole-cell configuration (see inset in *figure 37-A* and Methods section 2.2.2, *figure 1* and Methods section 2.4.3, *Table 2* - solution J) and Ca^{2+} transients were induced by depolarising steps from -60 mV to 0 mV for 60 and 500 ms. To allow for complete dialysis of both the intracellular solution and indo-1 (100 μM added to the intracellular solution), the recordings were started 10 minutes after achieving the whole-cell configuration and Ca^{2+} transients were subsequently induced every ≈ 2 minutes. In the perforated patch configuration, recordings of the $[Ca^{2+}]_i$ were stable for over 60 minutes whereas, in the whole-cell mode, resting $[Ca^{2+}]_i$ increased from ≈ 100 nM to ≥ 200 nM and the recovery phase of Ca^{2+} transients was markedly prolonged 20-25 minutes after rupture of the membrane patch (*figure 37-A*). However, since within the first 15 minutes, recordings acquired in the whole-cell mode were similar to those in the perforated patch configuration, only Ca^{2+} transients obtained within this 'time window' were considered for analysis (compare *Tables 13 and 14* in control). In the whole-cell mode, 5,6-succinylmidyl carboxyeosin (CE), a potent non- membrane-permeant inhibitor of PMCA was added to the intracellular solution (Methods section 2.4.3, *Table 2* - solution J together with 100 μM indo-1 and 50 μM CE). It is important to note that the addition of CE to the intracellular solution did not affect the spectral properties of indo-1. The effects of intracellular CE on resting $[Ca^{2+}]_i$ and on the properties of Ca^{2+} transients, were determined from the comparison of recordings obtained in control cells and in cells containing 50 μM CE after the same time of dialysis (15 minutes, open arrow in *figures 37-A* and *-B*).

Although in the whole-cell mode, $[Ca^{2+}]_i$ increases with time, the addition of 50 μM CE induced a larger rise in resting $[Ca^{2+}]_i$ than in control (291 ± 24 nM in CE; n=4 and 115 ± 2 nM in CTR; n=26, $P< 0.001$ independent *t*-test). While no difference in $\Delta[Ca^{2+}]_i$ of Ca^{2+} transients was observed (*Table 14*), the presence of CE markedly affected the recovery phase of Ca^{2+} transients (*figures 37-A* and *–B* and *38*).

In the presence of CE, the decay time constant of small Ca^{2+} transients was slowed by 30% whilst both decay time constants of larger Ca^{2+} transients were

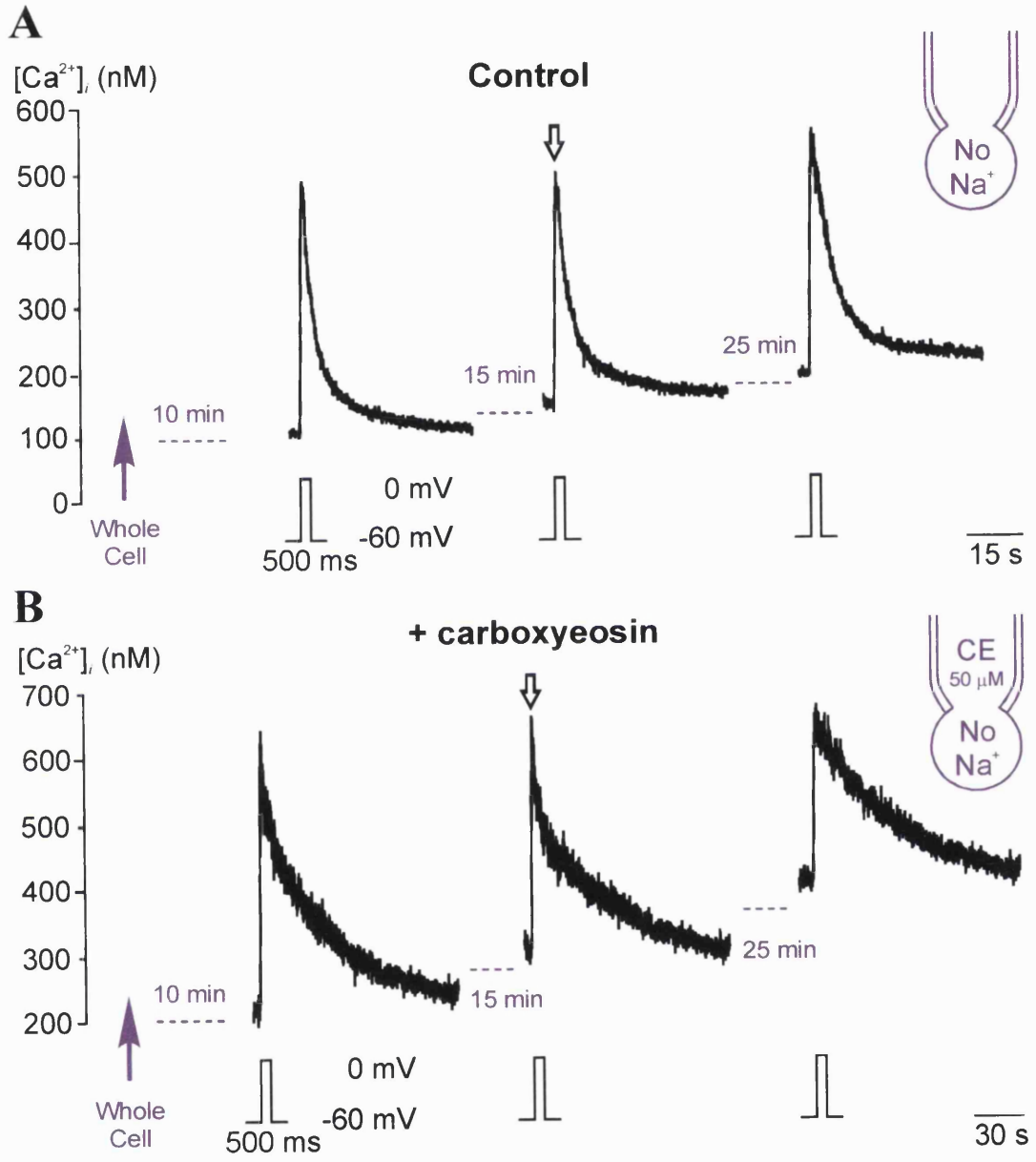

Figure 37: Effects of intracellular carboxyeosin on resting $[Ca^{2+}]_i$ and on the clearance of large depolarisation-induced Ca^{2+} transients

Ca^{2+} transients induced by depolarising steps for 500 ms in neurones voltage-clamped in the whole-cell configuration (see inset) with 100 µM indo-1 in a control cell (A) and in a cell where 50 µM carboxyeosin was added to the intracellular solution (B) to inhibit the PMCA. Recordings were started 10 minutes after rupture of the membrane patch (violet arrow, left) and Ca^{2+} transients were elicited every 2 minutes. Only Ca^{2+} transients obtained within the first 15 minutes were analysed (open arrow, centre and see text for details).

Table 14: Effect of intracellular carboxyeosin on the properties of Ca^{2+} transients

		Control	n	CE	n	*t*-test
$[Ca^{2+}]_i$ < 500 nM	$\Delta[Ca^{2+}]_i$	144 ± 20 nM	12	103 ± 19 nM	8	indep*, P=0.13
	τ	6.5 ± 0.4 s		9.5 ± 1 s		indep, P< 0.05
$[Ca^{2+}]_i$ > 500 nM	$\Delta[Ca^{2+}]_i$	452± 29 nM	14	421 ± 42nM	6	indep, P=0.6
	A_1	286 ± 38 nM		225 ± 42 nM		indep, P=0.67
	τ_1	2.9 ± 0.3 s		7.3 ± 2 s		indep, P< 0.001
	A_2	132 ± 15 nM		143 ± 10 nM		indep, P=0.75
	τ_2	17.3 ± 1.1 s		44.9 ± 5.6 s		indep, P< 0.001

*indep: independent

prolonged by 50% compared with control cells (*figures 38-A* and *-C*, respectively and see *Table 14*).The plot of the clearance rate against $[Ca^{2+}]_i$ confirmed the slowing of the Ca^{2+} transients' recovery (*figures 38-B* and *38-D*). Thus up to ≈ 200 nM, most of the Ca^{2+} clearance was mediated through a CE-sensitive mechanism and, above ≈ 200 nM, the rate of recovery was strongly reduced in the presence of CE (0.04 s^{-1} in CE and 0.16 s-1 in CTR, *figure 38-B*). For larger $[Ca^{2+}]_i$ (> 500 nM), the CE-sensitive component appeared to saturate ≈ 0.5-1 μM as the rate of clearance remained constant and ≈ 0.15 μM s^{-1} (*figure 38-D*). The results obtained with intracellular CE are in agreement with those observed with extracellular alkalisation (see Results section 5.1) and show that at low $[Ca^{2+}]_i$ most of the Ca^{2+} extrusion is mediated through PMCA. However CE appeared to have a stronger inhibitory effect (*figures 38-B* and *-D* and compare with *figure 37*).

5.3. Intracellular acidification following PMCA activation

After loading with BCECF, a fluorescent pH indicator (see Methods section 4.2.4), neurones were superfused with the standard extracellular solution (see Methods section 2.4.1, *Table 1* - solution A). To activate the VACC and induce rises in $[Ca^{2+}]_i$, an extracellular solution of 50 mM KCl was bath applied for 15 seconds (see Methods section 2.4.1 - solution G). Under these conditions, the plasma membrane would be depolarised from a resting potential of ≈ -60 mV to ≈ -20 mV and induce a rise in $[Ca^{2+}]_i$ ≥500 nM.

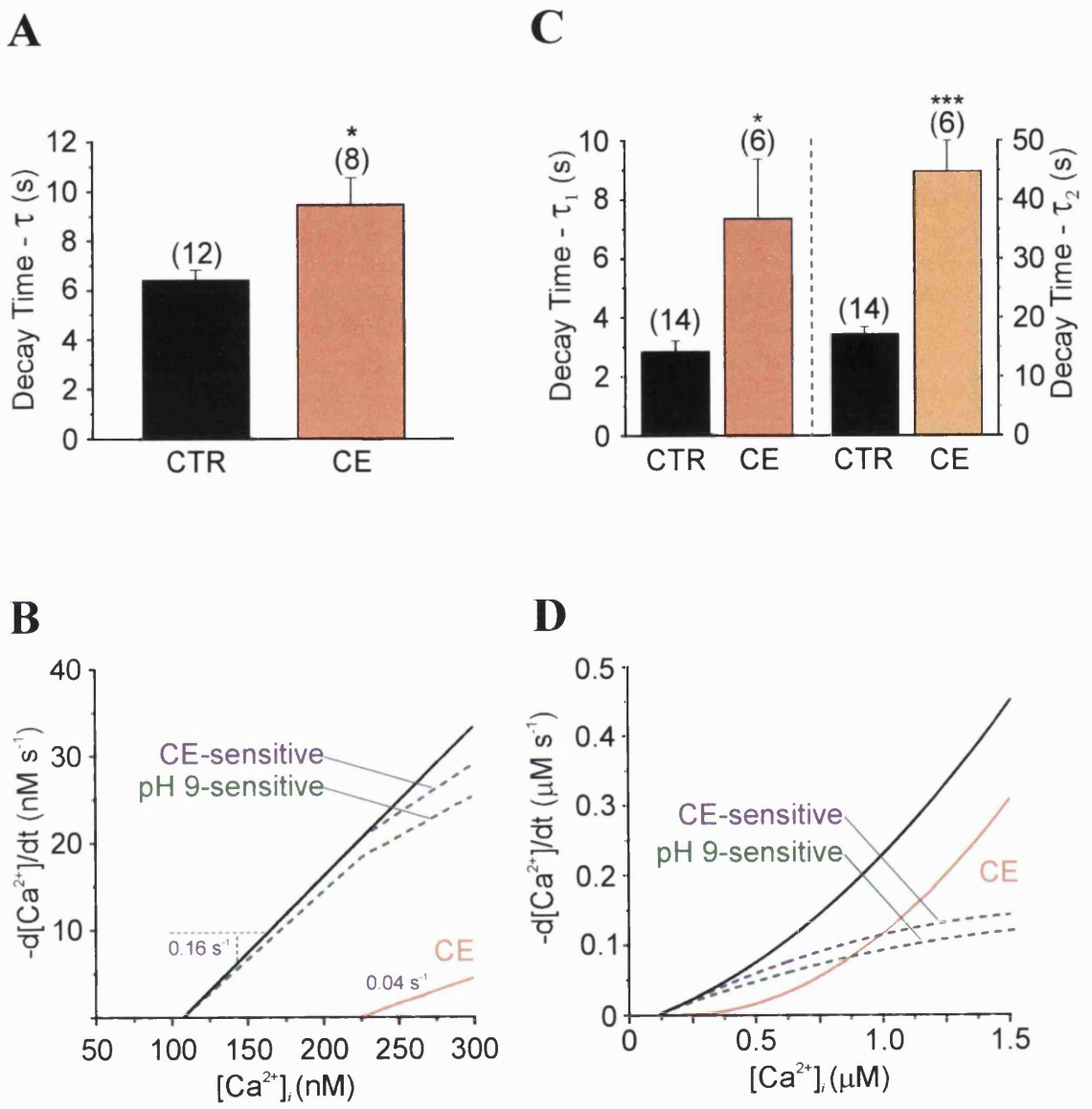

Figure 38: Intracellular carboxyeosin prolongs the Ca^{2+} transients' recovery
Decay time constant of the recovery for small (A) and large (C) rises in $[Ca^{2+}]_i$ in control (black bar; n=12 in A and n=14 in C) and with 50 μM intracellular CE (orange bar; n=8 in A and n=12 in C) (data represent mean ± S.E.M., * P< 0.05 *** P< 0.001, independent *t*-test). Plot of the clearance rate in control (black line) and with intracellular CE (orange line) for small (B) and large (D) Ca^{2+} transients and determination of the CE-sensitive component (dashed line). The pH-sensitive component (green line) of the recovery is also represented for comparison.

At rest the intracellular pH (pH_i) measured with BCECF was at 7.29 ± 0.03 and a cytoplasmic acidification to pH 7.14 ± 0.02 was observed following depolarisation with 50 mM KCl (*figures 39-A* and *-B*; n=24, P< 0.001). Upon removal of the extracellular Ca^{2+} (*figure 39-C*), the pH_i decreased from 7.28 ± 0.06 in control to 7.11 ± 0.08 (n=7, P< 0.01 - *figure 39-D*). However, in a Ca^{2+}-free extracellular solution (Methods section 2.1, *Table 1* - solution E), no further changes were observed following a KCl-induced depolarisation (pH_i = 7.10 ± 0.08; n=7, P=0.75 - *figures 39-C* and *-D*). These results suggest that the cytoplasmic acidification observed after membrane depolarisation was Ca^{2+}-dependent. To determine if the Ca^{2+}-dependent acidification of the cytoplasm was due to Ca^{2+} extrusion, PMCA was inhibited by extracellular alkalisation (see Results section 5.1). Although extracellular alkalisation induced an increase in pH_i from 7.27 ± 0.03 in control to 7.38 ± 0.04 at pH 9 (n=6, P< 0.001 - *figure 39-F*) following KCl application at pH 9 no cytoplasmic acidification was observed (pH_i = 7.32 ± 0.04 at pH 9 + KCl; n=6, P=0.1 - *figure 39-E*). Therefore these results suggest that the Ca^{2+} extrusion through PMCA induced a cytoplasmic acidification that could be explained by a counter-transport of protons.

5.4. PMCA expression in SCG neurones

5.4.1. In SCG mRNA transcripts for all PMCA isoforms are found

To determine which PMCA isoforms are expressed in SCG neurones, a PCR analysis was carried out. A common forward (s for sense) and four isoform-specific reverse (a for antisense) primers were designed using rat gene sequences for PMCA obtained from 'GenBank': *pmca1/3342s* and *pmca1/3878a*, *pmca2/3563s and pmca2/4076a*, *pmca3/3721s* and *pmca3/4178a*, *pmca4/3208s* and *pmca4/3844a*. The selectivity of the primers was assessed using sequences alignment against the gene databank (see Methods section 8.3 and *Table 7* for more details). The PCR reaction was carried out against *c*DNA (10 µg) extracted from <u>whole</u> SCG tissue and cerebellar cortex (CB). The sequence coding for the ubiquitously expressed hypoxanthine-guanine phosphoribosyltransferase (hprt) was successfully amplified in all *c*DNA templates (data not shown) suggesting that the *c*DNA templates were intact and the amplification

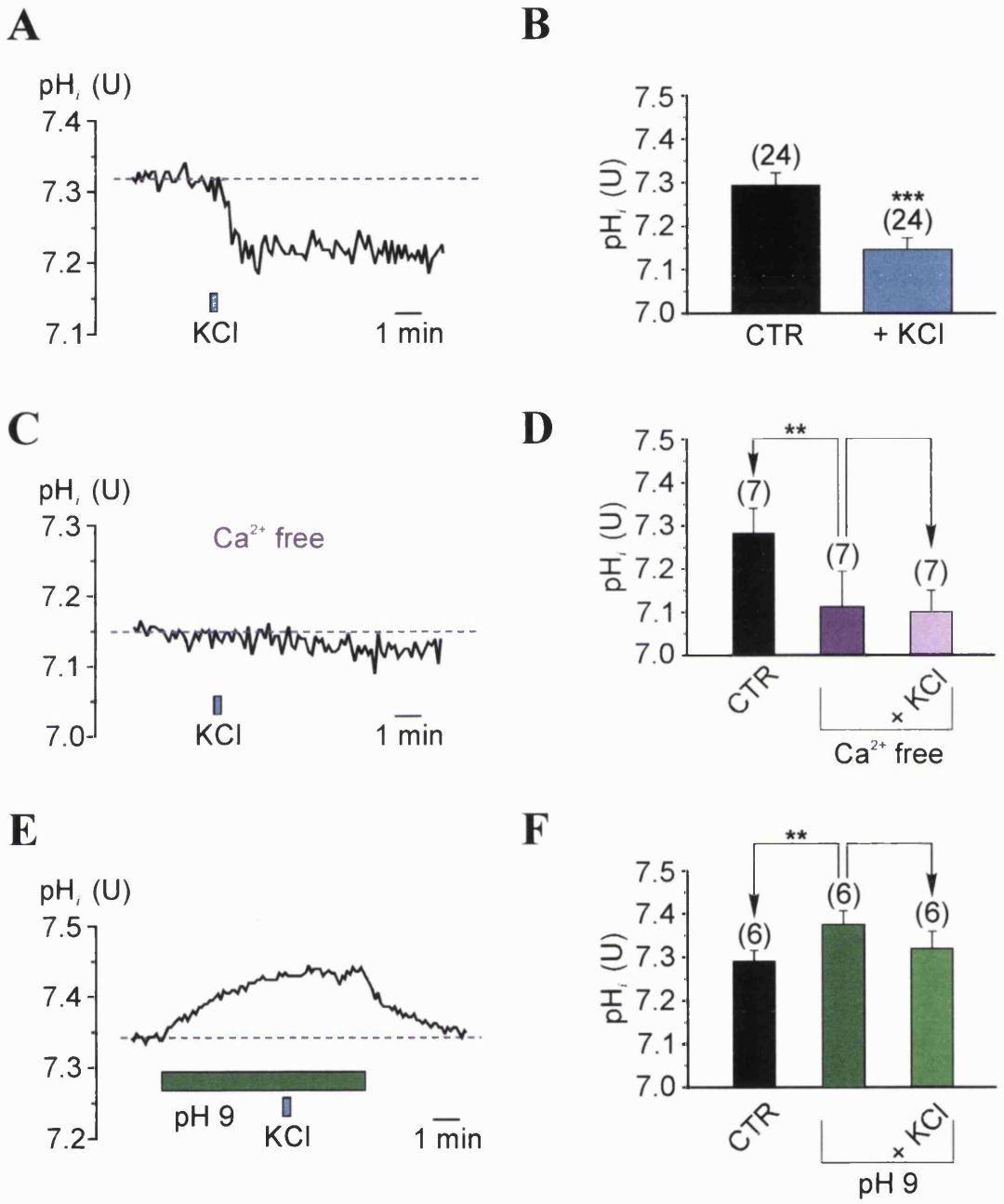

Figure 39: Intracellular acidification following Ca^{2+} extrusion through the PMCA
Neurones were loaded with BCECF, a fluorescent pH indicator to measure variations in intracellular pH (pH_i). Plasma membrane depolarisation was induced by 15 seconds application of high potassium extracellular solution (KCl, blue bar) in a standard extracellular solution (A and B), in the absence of extracellular Ca^{2+} (C and D) and after extracellular alkalisation (E and F). In B, D and F, intracellular pH_i values expressed as mean ± S.E.M. with ** P< 0.01, *** P< 0.001.

reaction successful. In contrast, no signal was present in the absence of templates (-ve, lanes 3, 6, 9 and 12 in *figure 40-A*) or with mock templates', in which the reverse transcriptase was omitted during the reverse transcription (data not shown).

For all four PMCA isoforms, a PCR product of the expected size was observed in SCG tissue and for cerebellar cortex, except for PMCA3, which was not found in cerebellar cortex (lane 8 in *figure 40-A*): 536 base pairs (bp) for pmca1 (lanes 1 and 2), 513 bp for pmca2 (lanes 4 and 5), 457 bp for pmca3 (lane 7) and 636 for pmca4 (lanes 10 and 11) (*figure 40-A*). However, for each isoform and each tissue, numerous bands were also observed either of larger or smaller size but generally amplified at a lower level (*figure 40-A*).

5.4.2. All four PMCA isoforms are present in SCG neurones

Immunocytochemical experiments were carried out to confirm PMCA expression at the level of the plasma membrane in SCG neurones. After fixation, neurones were incubated with an isoform non-specific mouse monoclonal antibody raised against PMCA (5F10, 1/50; *gift from Dr. Filoteo* - see Methods section 7.1 and *Table 5*), which was subsequently immunolabelled with a swine anti-mouse IgG conjugate to TRITC (1/50 - see Methods section 7.1 and *Table 6*). The selectivity of the labelling was assessed by the absence of significant difference in the labelling compared with the background when the secondary antibody was used alone. The results of the immunolabelling were examined on a confocal microscope and suggested a distribution at the level of the somatic and neuritic plasma membrane (0.5 μm optical slice, *figure 40-B_2*). To determine which isoform is expressed, specific antibodies were used (PMCA-1 to -4 rabbit polyclonal antibodies 1/50 labelled with swine anti-rabbit IgG conjugated to FITC, 1/50 - see Methods *Tables 5 and 6*). The results of the immunolabelling were examined on a fluorescent microscope, images acquired with a CCD camera and analysed using the deconvolution methods with the *Nearest 5 neighbours algorithm* (see Methods section 7.2, *figure 8*). For the four staining runs, images were acquired and analysed using the same parameters to enable a comparison of the results. Images taken at a particular plane of focus are illustrated in *figure 41* for each of the four antibodies with the corresponding deconvolved images (PMCA-1, -2,

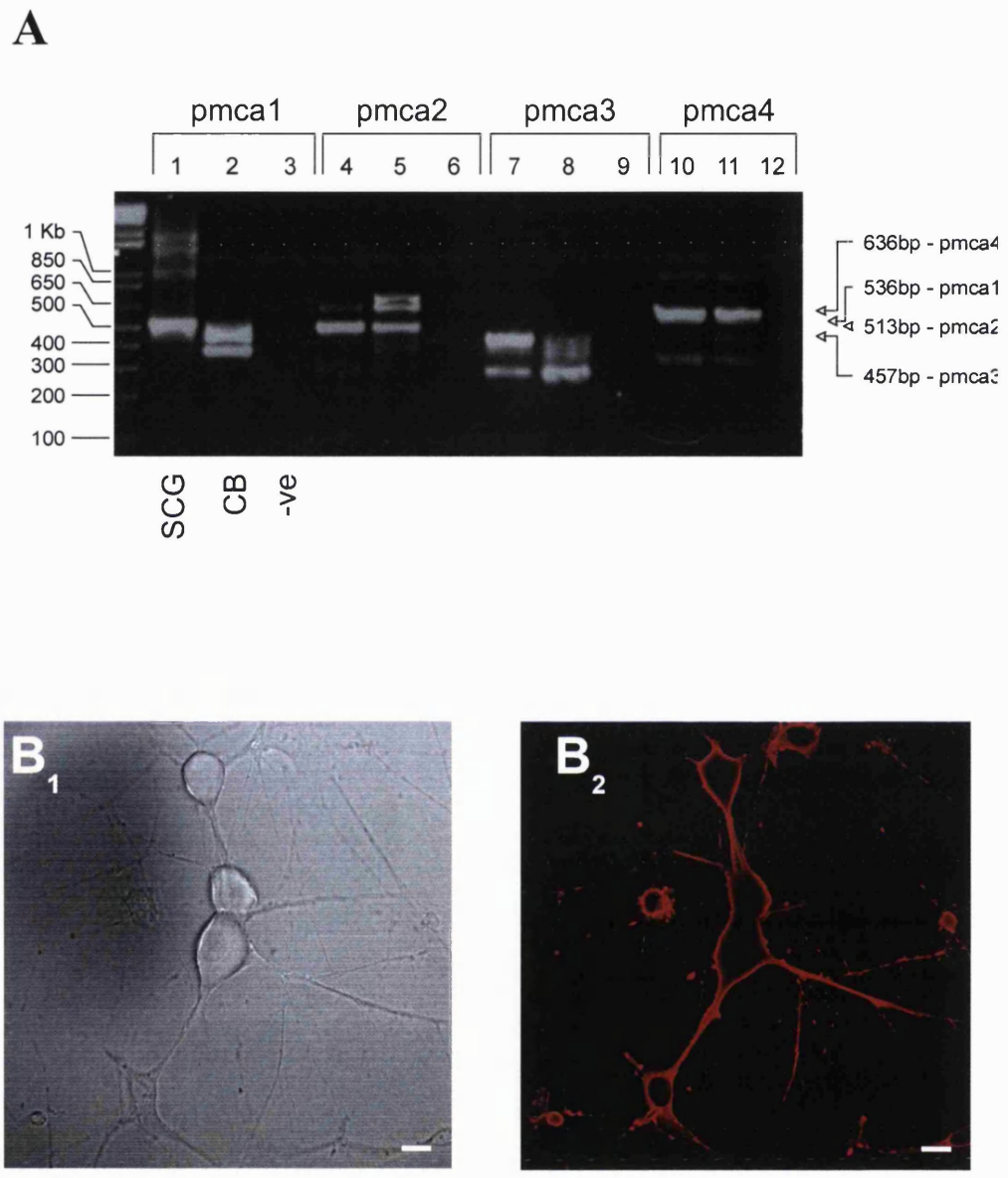

Figure 40: Superior cervical ganglia express mRNA for all PMCA isoforms and the PMCA protein is present in the plasma membrane

(A) PCR analysis of the PMCA expression in SCG and cerebellar cortex (CB). For the determination of PMCA expression, selective set of primers were used as follow: lanes 1 to 3, PCR amplification of pmca1 (pmca1/3342s and pmca1/3878a); lanes 4 to 6, of pmca2 (pmca2/3563s and pmca2/4076a); lanes 7 to 9, of pmca3 (pmca3/3721s and pmca3/4178a); lane 10 to 11, of pmca4 (pmca4/3208s and pmca4/3844a). For each PCR reaction a negative control was used (-ve, lanes 3, 6, 9 and 12). (B) PMCA immunolabelling with an isoform non-specific mouse monoclonal antibody (5F10, 1/50) counter-stained with swine anti-mouse polyclonal antibodies conjugated to TRITC (1/50). Images were acquired using a confocal microscope for B_1 (bright field) and for B_2 (TRITC) (optical slice of 0.5 μm, scale bar 10 μm, x63 oil immersion fluorescent objective).

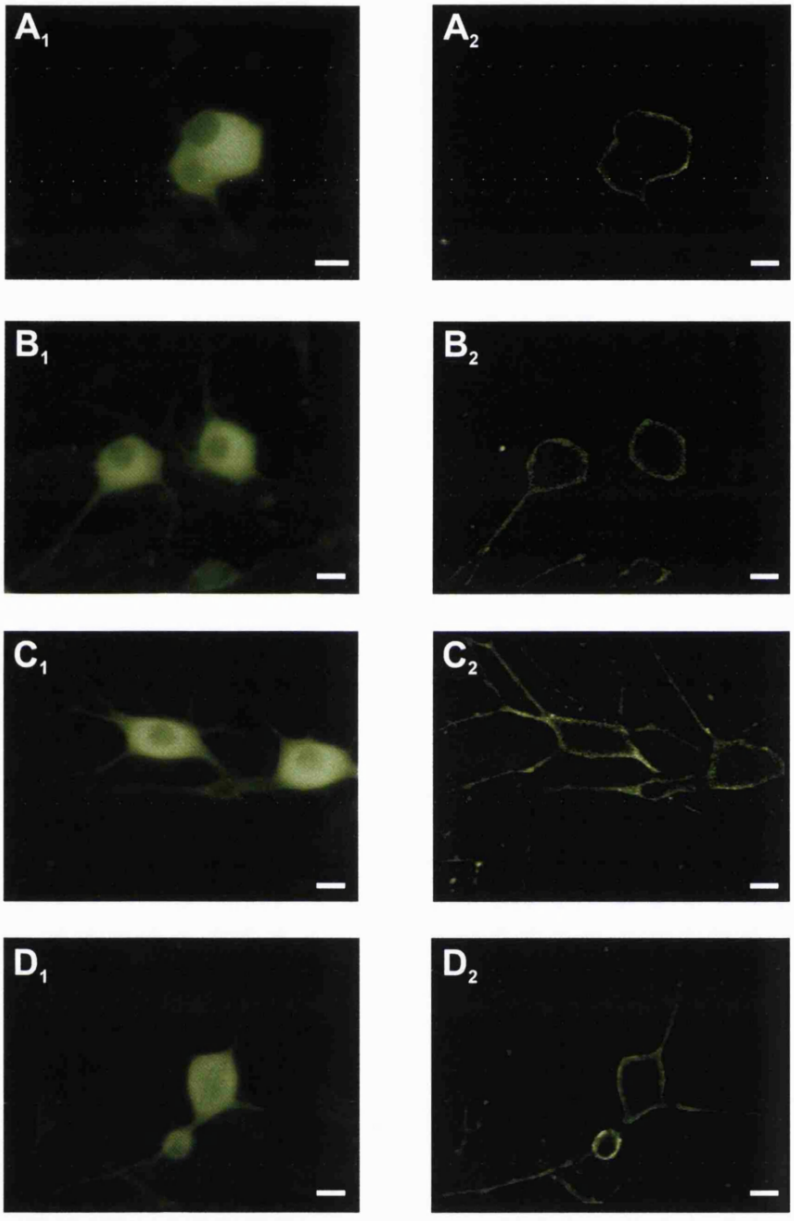

Figure 41: Neurones in SCG express all four PMCA isoforms at the level of the plasma membrane
PMCA immunolabelling with isoform specific rabbit polyclonal antibodies (PMCA-1, -2, -3 and -4, 1/50 in figures A, B, C and D, respectively) counter-stained with swine anti-rabbit polyclonal antibodies conjugated to FITC (1/50). Images were acquired using a CCD camera attached to a fluorescent microscope and analysed with the digital deconvolution technique using the *Nearest neighbours algorithm* to generate the images in panels A_2, B_2, C_2 and D_2 for PMCA-1, -2, -3 and -4 respectively (scale bar 10 μm, x40 oil immersion fluorescent objective).

-3and -4 in *figures 41-A_2, -B_2, -C_2* and *-D_2*, respectively). A staining was observed for all four isoforms, in agreement with the PCR analysis and suggested that SCG neurones express all four PMCA isoforms (see Results section 5.4.1). However, it appears that the level of staining is higher for PMCA-3 and PMCA-4. Finally, all PMCA isoforms appeared localised on the somatic plasma membrane whereas PMCA-3 and PMCA-4 were also expressed in neurites.

The results presented in this section suggest that PMCA is the major regulatory system for resting $[Ca^{2+}]_i$ (see also Results section 7) and for the extrusion of small increases in $[Ca^{2+}]_i$. However they also show that PMCA is active up to 500 nM and able to extrude larger rise in $[Ca^{2+}]_i$ while above this concentration the Ca^{2+}-ATPase appears to be saturated. Finally, the measurements of the intracellular pH suggest that following Ca^{2+} extrusion through PMCA an acidification of the cytoplasm occurs, presumably underlying a proton counter-transport during PMCA activity. The PCR and immunocytochemical analyses suggested further that SCG neurones express all PMCA isoforms, whose distribution appears to be isoform-specific.

5.5. Discussion

The determination of PMCA expression using PCR analysis showed that products for all four isoforms as well as several bands for a particular isoform are present in SCG (see *figure 40-A*). There are two splicing sites on the sequence of the PMCA isogenes and following alternative splicing more than 30 different transcripts can be generated (see Carafoli, 1994 for review). Therefore, the multiple bands observed for a particular PMCA isoform suggest that different splice variants are expressed, or at least that their transcripts are present, in SCG tissue. It is also necessary to point out that the PCR analyses were carried out on the whole ganglion and therefore some PCR products observed could have amplified *m*RNA sequences from glial origin. Although several types of transcript appear to be expressed for each PMCA isoform, the exact nature of the different splice variants was not further investigated as the main concern was to determine which of the four principal PMCA isoforms are expressed in these tissues.

The results obtained from the immunocytochemical study are in agreement with the PCR analysis and indicate further that the distribution of the Ca^{2+}-ATPases appears isoform-specific (see *figure 41*). Thus, while isoforms 1 and 2 are mainly somatic, isoforms 3 and 4 are present throughout the cell (see *figure 41*). Interestingly, no labelling was observed in regions of contact between neurones suggesting the presence of regulatory factors for protein expression and insertion into the plasma membrane in order to optimise its function (see *figures 40-B* and *41-A*). One might wonder why a cell population would express four isoforms of the same protein involved in Ca^{2+} extrusion. However, although the different PMCA isoforms have the same function, it has been shown that the Ca^{2+} affinity, the rate of Ca^{2+} transport and the regulatory pathways are isoform-specific (see Carafoli, 1994 for review). Moreover, the fact that the four proteins are expressed in the SCG neuronal population does not imply that one particular neurone would express all four isoforms but would suggest that some neurones could express different set of proteins. From studies on the PMCA tissue distribution, it appears that PMCA-1 and -4 are the ubiquitous isoforms since they are found in all tissues while PMCA-2 and -3 are more tissue-specific (see Brandt & Neve, 1992; Stauffer *et al.*, 1995; Carafoli, 1994 for review). Therefore, it could be suggested that SCG neurones would express PMCA-1 and/or -4 along with either PMCA-2 and/or -3. However, this is just speculative since no evidence for such a distribution is available in SCG neurones. Further experiments would be necessary to address this issue and the single cell PCR technique would be of great use for such a study. This analysis would also allow the determination of developmental and/or activity-dependent upregulation of a particular PMCA isoform.

The extracellular alkalisation induced both an increase of resting $[Ca^{2+}]_i$ and the prolongation of the recovery from small rise in $[Ca^{2+}]_i$ (< 500 nM). Similar results have been obtained in giant squid axon (DiPolo & Beaugé, 1982), in dorsal root ganglion neurones (Benham *et al.*, 1992), rat cerebellar granules cells (Khodorov *et al.*, 1995) and in CA1 pyramidal neurones (Trapp *et al.*, 1996). These pH-sensitive effects on $[Ca^{2+}]_i$ almost certainly resulted from the impairment of the $[Ca^{2+}]_i$ regulation after PMCA inhibition. Firstly, since PMCA activity has been shown to depend on the counter-transport of protons, one would expect to inhibit the Ca^{2+}-ATPase by reducing the availability of extracellular protons (DiPolo & Beaugé, 1982; Carafoli *et al.*, 1988;

Benham *et* al., 1992). In turns, during Ca^{2+} extrusion a Ca^{2+}-dependent and pH-sensitive cytosolic acidification was observed following plasma membrane depolarisation (Schwiening *et al.*, 1993; Khodorov *et al.*, 1995; Park *et al.*, 1996; Trapp *et al.*, 1996 and Xu *et al.*, 2000). Thus, in SCG neurones, there was a decrease in the intracellular pH by ≈ 0.15 unit, a value that is consistent with those reported in other cell types either using fluorescent pH indicator (Daugirdas *et al.*, 1995 - vascular smooth muscle; Trapp *et al.*, 1996 - CA1 pyramidal neurones) or proton-sensitive microelectrodes (Schwiening *et al.*, 1996 - snail neurones). Furthermore, extracellular alkalisation produced similar effects to those observed using either inhibitor of ATPase activity (vanadate, Benham *et al.*, 1992; Bassani *et al.*, 1995; Trapp *et al.*, 1996 or lanthanum Usachev *et al.*, 1993 and Park *et al.*, 1996) or eosin and carboxyeosin, the most potent inhibitors of the PMCA (this study see *figures* 37 and 38 and see also Gatto & Milanick, 1993, 1996; Bassani *et al.*, 1995; Park *et al.*, 1996 and Yamoah *et al.*, 1998). However, the prolongation of the recovery and the slowing of the clearance rate from depolarisation-induced Ca^{2+} transients appeared to be more pronounced in the presence of carboxyeosin (this study, see *figures 38-B* and *-D*) or vanadate (compare figure 4 and 5 in Benham *et al.* 1992) than following extracellular alkalisation. The main reason for such a result might be the fact that vanadate inhibits all ATP-dependent Ca^{2+} transport systems and that carboxyeosin have been shown to affect both PMCA and SERCA activity (Bassani *et al.*, 1995) suggesting that both these compounds would not only affect the PMCA activity. Finally, Xu and colleagues (2000) suggested that half-maximal inhibition of the Ca^{2+} pump would be observed at $[H^+] \approx 2$ nM *i.e.* a pH ≈ 8.7 suggesting that PMCA would not be completely inhibited at pH 9. The activity of PMCA is strongly dependent on CaM therefore the rise in resting $[Ca^{2+}]_i$ and the prolongation of the recovery of Ca^{2+} transient observed in the presence of calmidazolium, a CaM inhibitor, support further the involvement of PMCA in the regulation of $[Ca^{2+}]_i$ (Benhan, 1992 and Marsh & Wanaverbecq unpublished observations).

In agreement with previous studies, PMCA appears to be the major system controlling $[Ca^{2+}]_i$ close to rest (DiPolo & Beaugé, 1982; Baker & DiPolo, 1984; Carafoli *et al.*, 1988; Benham *et* al., 1992; Schwiening *et al.*, 1993; Usachev *et al.*, 1993; Khodorov *et al.*, 1995; Park *et al.*, 1996; Trapp *et al.*, 1996; Yamoah *et al.*, 1998

and Xu *et al.*, 2000). In fact, in almost all cell types, PMCA inhibition markedly affects $[Ca^{2+}]_i$ by either inducing a rise in $[Ca^{2+}]_i$ at rest (this study and see Benham, 1992 and Yamoah *et al.*, 1998) or a sustained elevation in $[Ca^{2+}]_i$ following the initial recovery phase from a micromolar rise in $[Ca^{2+}]_i$ (Usachev *et al.*, 1993). One of the noteworthy exceptions came from the study of Llano and colleagues (1998) in cerebellar Purkinje neurones where these authors did not observe any variation in resting $[Ca^{2+}]_i$ and only a minor prolongation of the recovery from small rises in $[Ca^{2+}]_i$ (< 500 nM). They therefore suggested that $[Ca^{2+}]_i$ is regulated by three mechanisms (PMCA, SERCA and NCX) that equally contribute to the Ca^{2+} clearance at low $[Ca^{2+}]_i$. However, these authors were working with cerebellar slices and used the ester form of carboxyeosin to inhibit PMCA. One might therefore suggest that under their experimental conditions the intracellular concentration of carboxyeosin was not sufficient (short loading period, low hydrolysis of the ester form) to greatly inhibit the Ca^{2+} extrusion through PMCA.

The results presented in this section indicated further that PMCA appears to be the major system for the control of resting $[Ca^{2+}]_i$ since the inhibition of any other regulatory systems was without effect on resting $[Ca^{2+}]_i$ with the exception of the intracellular stores (see Result sections 4 and 7 for more details on this aspect). The PMCA inhibition induced a rise in $[Ca^{2+}]_i$, which was dependent on the extracellular $[Ca^{2+}]$ and appeared to be due to a Ca^{2+} influx through the plasma membrane (see Results section 7). Following, PMCA inhibition by extracellular alkalisation, $[Ca^{2+}]_i$ increased ≈ 250-300 nM than reached a plateau suggesting the involvement of another regulatory system that would counter-balance the Ca^{2+} influx (see Results section 6). The determination of the clearance rate of the pH-sensitive component indicated that PMCA activity increased up to $[Ca^{2+}]_i$ ≈ 500 nM and was saturated at higher $[Ca^{2+}]_i$ (see *figures 35-C*, *36-C*, *38-B* and *D*). Following PMCA inhibition, both decay time constants are prolonged suggesting that PMCA was involved in both components of the recovery phase. However, because of the Ca^{2+} affinity of PMCA one would suggest that at high $[Ca^{2+}]_i$, PMCA would have a less important role in Ca^{2+} extrusion as can be observed from the clearance rate (see Results section 4 and 6). In contrast, at lower $[Ca^{2+}]_i$, PMCA appears to play a major role in the regulation of the slow phase of biexponential recoveries and a predominant role in the monoexponential recoveries. One could therefore propose that the acceleration observed with the increase in $[Ca^{2+}]_i$

for the recovery time constant of the monoexponential component could reflect a Ca^{2+}-dependent increase in PMCA activity until it reaches its maximum at which point other systems like the plasma membrane NCX, mitochondria or Ca^{2+} store might become active or predominant. The PMCA-1 and -4 are thought to correspond to the ubiquitous PMCA isoforms, it is tempting to consider these isoforms as the house-keeping Ca^{2+}-ATPAse (see Carafoli, 1994) involved in the control of resting $[Ca^{2+}]_i$. In contrast, PMCA-2 and -3 could be involved in the extrusion of Ca^{2+} following depolarisation-induced Ca^{2+} transients. One could suggest a site-specific expression of PMCA with the isoforms involved in returning $[Ca^{2+}]_i$ to rest after the activation of VACC localised close to these channels while PMCA isoforms controlling resting $[Ca^{2+}]_i$ would be expressed throughout the cell (*e.g.* see Juhaszova *et al.*, 2000).

In conclusion, PMCA appears to play a major role in Ca^{2+} homeostasis and a predominant role in both the regulation of resting $[Ca^{2+}]_i$ and in the extrusion of small rise in $[Ca^{2+}]_i$. The activity of PMCA would depend on the isoforms expressed and on the stage of development of a cell type. Thus, following the differentiation of human neuroblastoma cells and in parallel with the development of functional VACC, the expression of PMCA isoforms changes and the control of $[Ca^{2+}]_i$ becomes more efficient and more rapid (Usachev *et al.*, 2001). Similar results were observed in cerebellar granule cells where during the development a down regulation of the PMCA-4 isoform was accompanied by an upregulation of isoforms -1, -2 and -3 (Guerini *et al.*, 1999). Finally, when PMCAs were overexpressed in chinese hamster ovary (CHO) cells, they significantly accelerated the recovery of agonist-induced Ca^{2+} transient but also reduced the filling state of Ca^{2+} store presumably due to an accelerated extrusion of Ca^{2+} (Brini *et al.*, 2000). Therefore, although PMCA represents an important element of Ca^{2+} regulation its activity would be modulated by other factor (see Results section 6 and 7).

6. Sodium/calcium exchanger and intracellular calcium

In this section, the role of NCX in the control of resting $[Ca^{2+}]_i$ and in the extrusion of Ca^{2+} following neuronal excitation was determined in SCG neurones by removing extracellular Na^+ but also by reversing the direction of the Ca^{2+} transport using high intracellular Na^+ concentration. Finally, the nature of the isoform(s) expressed in SCG neurones was investigated using both PCR analysis and experiments in immunocytochemistry.

6.1. Calcium extrusion through the sodium/calcium exchanger

Small and large Ca^{2+} transients were induced in neurones voltage-clamped in the perforated patch configuration following depolarising steps for 60 ms and 500 ms, respectively. Recordings were carried out in the standard extracellular solution and after substitution of extracellular Na^+ with N-methyl D-glucamine to inhibit NCX (NMDG, see Methods section 2.4.2, *Table 1* - solution B). Following removal of extracellular Na^+, neither changes in resting $[Ca^{2+}]_i$ (99 ± 2 nM in control *versus* 97 ± 9 nM in Na^+-free; n=14, P=0.48) nor in $\Delta[Ca^{2+}]_i$ of Ca^{2+} transients were observed (see *Table 15*).

Table 15: Effect of extracellular Na^+ removal on the properties of Ca^{2+} transients

		Control	0[Na^+]$_{Out}$	n	*t*-test
$[Ca^{2+}]_i$ < 500 nM	$\Delta[Ca^{2+}]_i$	186 ± 10 nM	187 ± 9 nM	14	paired, P=0.9
	τ	3.8 ± 0.2 s	4.2 ± 0.3 s		paired, P=0.12
$[Ca^{2+}]_i$ > 500 nM	$\Delta[Ca^{2+}]_i$	1228 ± 105 nM	1073 ± 116 nM	14	paired, P=0.8
	A_1	1159 ± 127 nM	1021 ± 90 nM		paired, P=0.3
	τ_1	2.2 ± 0.1 s	4.3 ± 0.3 s		paired, P< 0.001
	A_2	130 ± 25 nM	148 ± 8 nM		paired, P=0.1
	τ_2	21.0 ± 4 s	26.0 ± 17		paired, P=0.3

The extracellular Na^+ substitution with NMDG did not affect the recovery phase of small Ca^{2+} transient as can be seen from the superimposed traces in *figure 42-A* and from the plot of the clearance rate (0.17 s^{-1} in CTR and 0.16 s^{-1} in Na^+-free, *figure 42-B* and see inset for the decay time constants).

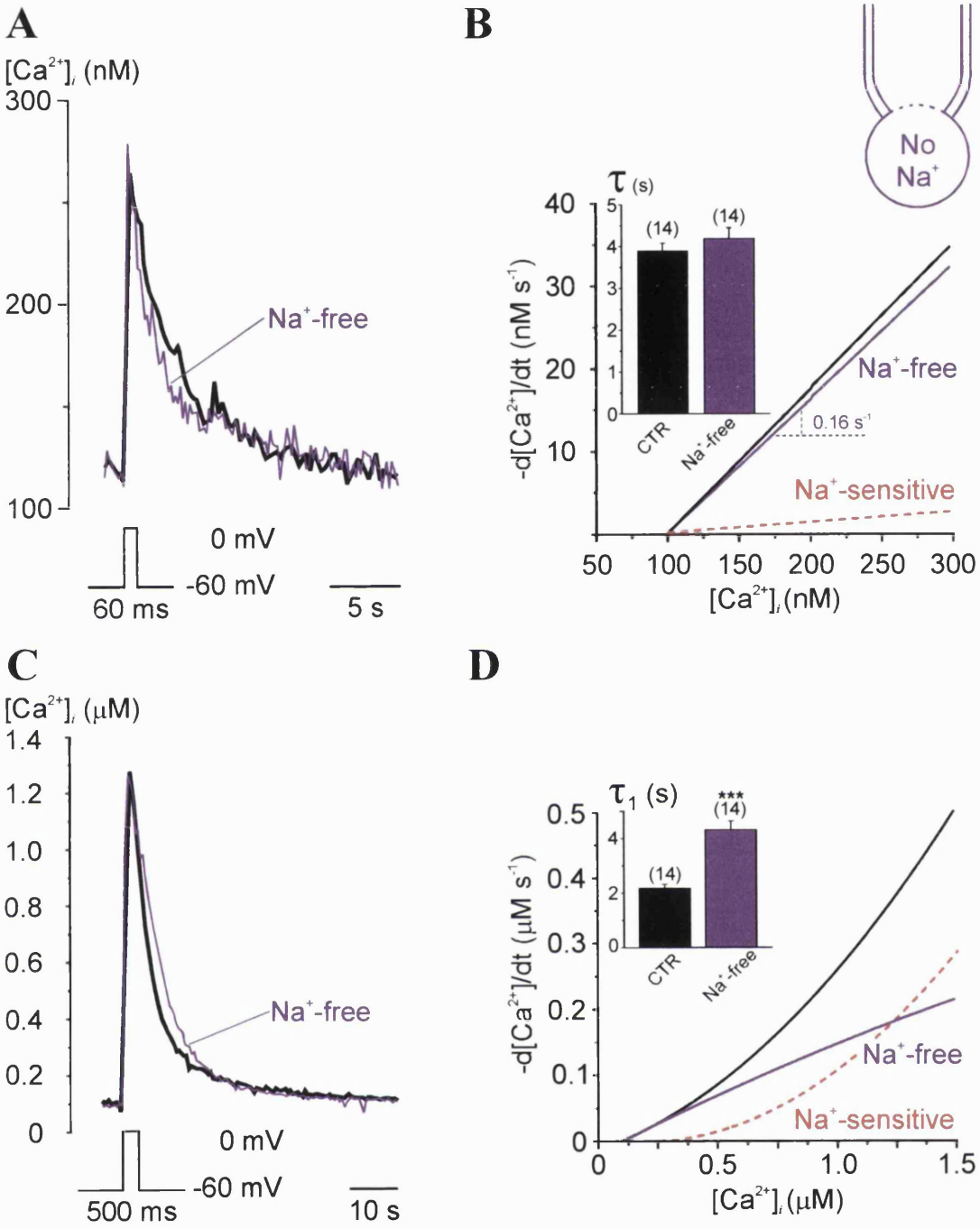

Figure 42: Sodium-dependent extrusion of large but not small rises in $[Ca^{2+}]_i$
(A) Depolarisation-induced small Ca^{2+} transients in control and after extracellular Na^+ substitution with N-methyl D-glucamine (Na^+-free). (B) Plot of the clearance rate in control and in Na^+-free solution for small Ca^{2+} transients with the Na^+-dependent component (dashed line, data from 14 cells). The inset represents the decay time constant of the Ca^{2+} transient's recovery in control and in Na^+-free (black bar, CTR and violet bar, Na^+-free; n=14 ,data as mean ± S.E.M.). (C) Large Ca^{2+} transients induced by depolarising steps for 500 ms in control and in Na^+-free. (D) Plot of the clearance rate in control and in Na^+-free for large Ca^{2+} transients and determination of the Na^+-dependent component (dashed line - data from 14 cells). The inset represents the decay time constants of the Ca^{2+} transient's recovery in control and in Na^+-free (black bar, CTR and orange bar, Na^+-free; n=14, data as mean ± S.E.M. *** P< 0.001).

Although the time course of the recovery for larger Ca^{2+} transients was unaffected in the absence of extracellular Na^+, the fast decay time constant, but not the slow one, was prolonged compared to control (see *Table 15*, *figure 42-C* and inset in *figure 42-D*). The determination of the clearance rate showed that for $[Ca^{2+}]_i$ above 500 nM, the removal of extracellular Na^+ slowed the Ca^{2+} extrusion (rate $\approx$ 0.25 $\mu M\ s^{-1}$ in CTR and $\approx$ 0.15 $\mu M\ s^{-1}$ in Na^+-free - *figure 42-D*). The contribution of Na^+-sensitive component, obtained from the difference of the clearance rate in control and in Na^+-free, became more predominant with the increase in $[Ca^{2+}]_i$. Therefore, these results suggested that the regulation of low $[Ca^{2+}]_i$ was mostly Na^+-independent whereas at larger $[Ca^{2+}]_i$ a Na^+-dependent process was involved and its contribution increased with $[Ca^{2+}]_i$.

6.2. Reverse mode of the sodium/calcium exchanger

Alkalisation of the extracellular medium (pH 9) has been shown to inhibit PMCA and to induce a rise in resting $[Ca^{2+}]_i$ (see Results sections 5 and 7 for more details). The results in this section suggested that NCX was without effect on resting $[Ca^{2+}]_i$ since the removal of extracellular Na^+ did not induce changes in $[Ca^{2+}]_i$ at rest (see Results section 6.1). However, after PMCA inhibition, $[Ca^{2+}]_i$ increased initially linearly but then reached a plateau with a maximal concentration of 333 ± 114 nM (n=3, $P< 0.05$ - *figure 43-A* and see also Results section 5 and 7). When extracellular Na^+ was removed at pH 9, an additional rise in the $[Ca^{2+}]_i$ to 594 ± 139 nM was observed (n=3, $P< 0.05$ - *figure 43-A* and inset). As soon as extracellular Na^+ was re-introduced, $[Ca^{2+}]_i$ decreased back to the concentration observed after PMCA inhibition (*figure 43-A*). These results suggested that a Na^+-dependent mechanism was active at $[Ca^{2+}]_i < 500$ nM in parallel with PMCA or at least able to compensate for the PMCA inhibition (see Results section 5.5 and 6.4).

The direction of the Ca^{2+} transport through NCX depends on the driving force (ΔV), which is defined as the difference between the membrane potential (E_m) and the reversal potential of the exchanger (E_{NCX}) (Blaustein, 1988a, b and Wier, 1990):

$$\Delta V = E_m - E_{NCX} \quad \textit{Equation 24}$$

$$\text{with } E_{NCX} = 3 \times E_{Na} - 2 \times E_{Ca} \quad \textit{Equation 25}$$

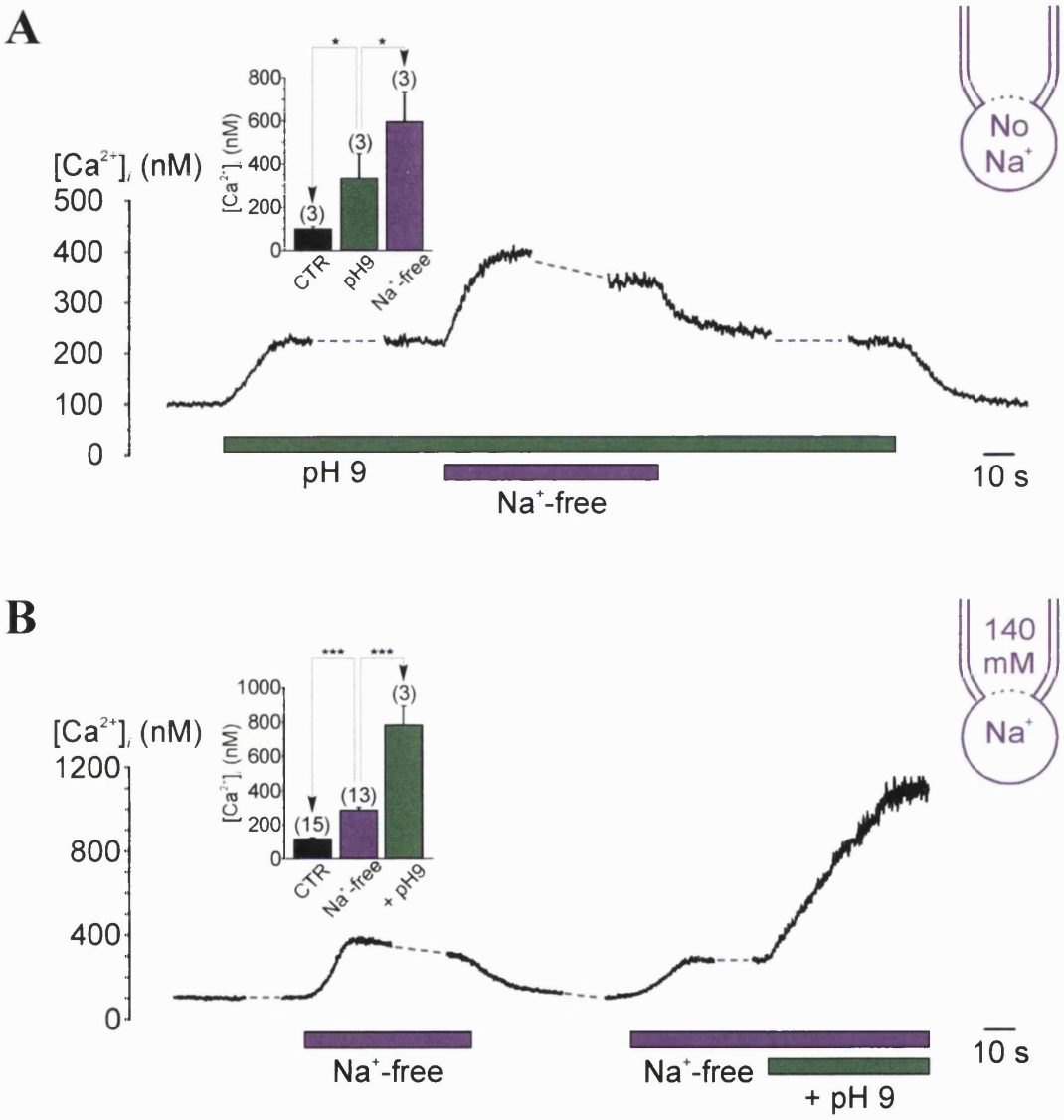

Figure 43: NCX regulates low $[Ca^{2+}]_i$ when PMCA is inhibited and induces Ca^{2+} influx in the reverse transport mode

(A) Rise in resting $[Ca^{2+}]_i$ induced by extracellular alkalisation in a neurone voltage-clamped at -60 mV in the presence or absence of extracellular Na^+ (Na^+-free). Inset represents $[Ca^{2+}]_i$ in control (black bar; n=3), at pH 9 (green bar; n=3) and at pH 9 in the absence of extracellular Na^+ (violet bar; n=3) (data represent mean ± S.E.M., * P< 0.05). (B) Rise in resting $[Ca^{2+}]_i$ induced by removal of extracellular Na^+ in a neurone voltage-clamped at -60 mV in the perforated patch with 140 mM intracellular Na^+ (see inset) at pH 7.4 and pH 9. Inset represents $[Ca^{2+}]_i$ in control (n=15), in the absence of extracellular Na^+ (violet bar; n=13) and at pH 9 in the absence of extracellular Na^+ (green bar; n=3) (data represent mean ± S.E.M., * P< 0.05).

E_{Na} and E_{Ca} are the reversal potential for Na^+ and Ca^{2+}, respectively and are obtained from the Nernst equation:

$$E_{Na} = \frac{RT}{zF} \times \ln \frac{[Na^+]_{out}}{[Na^+]_{in}} \quad \textit{Equation 26}$$

$$E_{Ca} = \frac{RT}{zF} \times \ln \frac{[Ca^{2+}]_{out}}{[Ca^{2+}]_{in}} \quad \textit{Equation 27}$$

with z the ion valence (1 for Na^+ and 2 for Ca^{2+}), n_{Na} and n_{Ca} the number of Na^+ and Ca^{2+} ions respectively transported (3 Na^+ and 1 Ca^{2+}).

For a Δv negative (-ve), the exchanger works in forward mode and Ca^{2+} is extruded from the cytosol. In contrast, when Δv is positive (+ve), the Ca^{2+} is transported into the cytosol. In the recording conditions used in the Results section 6.1, the membrane potential was -60 mV, the extracellular concentration of Na^+ and Ca^{2+} were 140 mM and 2.5 mM, respectively and the $[Ca^{2+}]_i$, in the absence[6] of intracellular Na^+, was ≈ 100 nM. Therefore, NCX was in the forward mode, *i.e.* Ca^{2+} would be extruded from the cytosol, with:

at -60 mV and $\mathbf{[Na^+]_{out} = 140\ mM}$

E_{NCX} = +1205 mV and ΔV = -1265 mV

Thus, in theory, when the extracellular Na^+ is removed, the direction of the Ca^{2+} transport should be inverted and $[Ca^{2+}]_i$ should increase since:

at -60 mV and $\mathbf{[Na^+]_{out} = 0\ mM}$

E_{NCX} = -265 mV and ΔV = +205 mV

However, in the absence of extracellular Na^+, resting $[Ca^{2+}]_i$ remained unchanged (see Results section 6.1).

In contrast, when the intracellular Na^+ is increased to 140 mM, the Na^+ gradient is inverted and therefore a Ca^{2+} influx should be observed. Under these conditions:

---

[6] To enable the calculation of the reversal potential, the intracellular Na^+ concentration was set to 1 nM

at -60 mV and $[Na^+]_{out}$ = **140 mM**

E_{NCX} = -265 mV and ΔV = +205 mV

and

at -60 mV and $[Na^+]_{out}$ = **0 mM**

E_{NCX} = -1735 mV and ΔV = +1675 mV

Neurones were therefore voltage-clamped at -60 mV with an intracellular solution containing 140 mM Na^+ (see Methods section 2.4.3, *Table 2*- solution K). In the control situation, with 140 mM extracellular Na^+, resting $[Ca^{2+}]_i$ was not significantly increased (99 ± 11 nM with $[Na^+]_i \approx 0$ and 118 ± 6 nM with $[Na^+]_i$ = 140 mM). In contrast, when the extracellular Na^+ was removed, a rise in $[Ca^{2+}]_i$ was observed (from 118 ± 6 nM in control to 284 ± 17 in the absence of extracellular Na^+; n= 15 and n=13, respectively; P< 0.001- *figure 43-B*). Upon re-introduction of the extracellular Na^+, the $[Ca^{2+}]_i$ returned to the control level (*figure 43-B*). When, in the absence of extracellular Na^+, PMCA was inhibited (pH 9) an additional rise in $[Ca^{2+}]_i$ to 784 ± 111 nM was observed (*figure 43-B*; n=3, P< 0.001 and compare with *figure 43-A*). Thus, a Na^+-dependent system is functional in these neurones and able to reverse its transport mode to induce a Ca^{2+} influx.

6.3. NCX expression in SCG neurones

6.3.1. The three NCX isoforms are expressed in whole SCG

To determine which NCX isoform is expressed in SCG neurones, a PCR analysis was carried out. Selective forward and reverse primers for each NCX isoform were designed using rat gene sequences for NCX obtained from 'GenBank' and their selectivity controlled using sequence alignment against a gene databank (see Methods section 8.3 and *Table 7* for more details). Each set of primers was tested against *c*DNA (10 µg) extracted from <u>whole</u> SCG tissue and against tissues previously shown to express particular isoform: *ncx1/1713s* and *ncx1/2120a* against heart *c*DNA (Ht), *ncx2/611s* and *ncx2/863a* against cerebellar *c*DNA (CB) and *ncx3/620s* and *ncx3/963a* against skeletal muscle *c*DNA (SkM). In the presence of *c*DNA templates, PCR products were observed for each tissue with the hprt primers, suggesting that the *c*DNA templates were intact and the amplification reaction had been successful (*figure 44-A*,

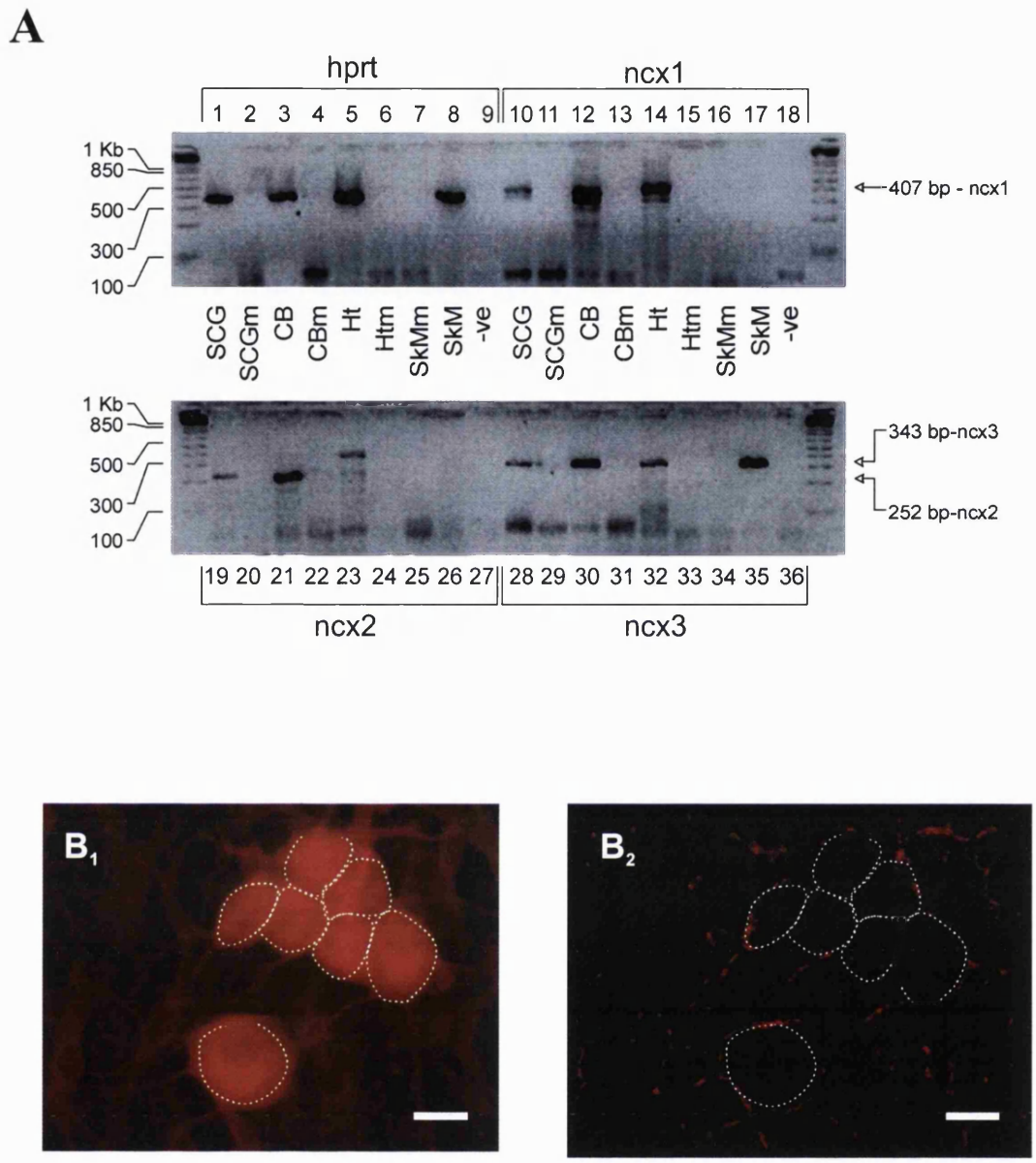

Figure 44: NCX is expressed at a low level on the soma of SCG neurones

(A) PCR analysis of NCX expression in whole SCG, Heart (Ht), cerebellar cortex (CB) and skeletal muscle (SkM). Lanes 1 to 9, control of the PCR amplification with hprt. For the determination of NCX expression, selective set of primers were used as follow: lanes 10 to 18, PCR amplification of ncx1 (ncx1/1713s and ncx1/2120a), lanes 19 to 27, of ncx2 (ncx2/611s and ncx2/863a) and lanes 28 to 36, of ncx3 (ncx3/620s and ncx3/963a). For each PCR reaction a negative control (-ve, lanes 9,18,27 and 36) and for each tissue a 'mock *c*DNA template' (labelled with the letter m for mock) were used. (B) Rabbit polyclonal antibody (1/50) raised against the cardiac isoforms (NCX-1) was used to determine the expression of NCX in SCG neurones. The primary antibody was labelled with a swine anti-rabbit polyclonal antibody conjugated to TRITC (1/50) and images acquired using a CCD camera attached to a fluorescent microscope. The image in B_1 was subsequently analysed with the digital deconvolution technique using the *Nearest neighbours algorithm* to generate the images in panels B_2. In B_1 and B_2, the contours of the neurones have been marked to enable a better visualisation of the labelling (scale bar 10 μm, x40 oil immersion fluorescent objective).

top panel left, lane 1,3,5 and 8). In contrast, no signal was present in the absence of any template (-ve, lanes 9, 18, 27 and 36 in *figure 44-A*) or when 'mock templates', in which the reverse transcriptase was omitted during the reverse transcription were used (m for 'mock' in *figure 44-A* - see Methods section 8.2 for more details).

The PCR reactions for the different NCX isoforms produced a PCR product of the expected size with each control template (ncx-1: 407 bp in lane 14, ncx-2: 252 bp in lane 21 and ncx-3: 343 bp in lane 35 - *figure 44-A*). In addition a band of the correct size was observed for SCG and cerebellar tissues with ncx-1 primers (lane 10 and 12 in *figure 44-A*). For ncx-2, a product of the correct size was present for SCG and cerebellar tissue (lane 19 and 21 in *figure 44-A*). However there was also a signal for heart tissue but of a larger size (lane 23, 400 bp instead of 252 bp). Finally all *c*DNA templates amplified a signal of the expected size for ncx-3 (lane 28, 30, 32 and 35 in *figure 44-A*). Therefore these results suggest that in superior cervical ganglia transcripts for all three NCX isoforms are present but at a level that appears to be low if compared with the control tissues (see lanes for each isoform and also hprt).

6.3.2. NCX is expressed at a low level in SCG neurones

Immunocytochemical experiments were carried out to corroborate the expression of NCX at the level of the plasma membrane in SCG neurones. Unfortunately, there are, so far, no isoform-specific antibodies available but only an antibody raised against the cardiac isoform (NCX-1, recommended concentration of 1/1000 for immunocytochemistry). However, this antibody is thought to cross react with NCX-2 and NCX-3 at higher concentrations. Neurones after two days in culture were fixed and incubated with a rabbit polyclonal antibody raised against NCX-1 (1/50- see Methods section 7.1 and *Table 5*), which was subsequently revealed with a swine anti-rabbit IgG conjugate to TRITC (1/50 - see Methods section 7.1 and *Table 6*). The selectivity of the labelling was assessed by the absence of significant difference in the labelling compared with the background when the secondary antibody was used alone. The results of the immunolabelling were examined on a fluorescent microscope, images acquired with a CCD camera (*figure 44-B_1*) and analysed using the deconvolution method with the *Nearest neighbours algorithm* (*figure 44-B_2* and see Methods section 7.2). These results confirmed those obtained in the PCR analysis and would indicate

that NCX was expressed at a low level in the somatic plasma membrane. However, from the immunocytochemical experiment, it is unfortunately not possible to determine which isoform is expressed in SCG neurones.

Taken together, the results presented in this section indicate that SCG neurones express a functional Ca^{2+} extrusion system mainly active for high $[Ca^{2+}]_i$ that depends on the Na^+ gradient and might therefore correspond to NCX since both *m*RNA transcripts and immunolabelling for this exchanger were detected. The results show also that NCX is able to reverse its transport mode and induce Ca^{2+} influx depending on the intracellular Na^+ concentration.

6.4. Discussion

The relative importance of the plasma membrane NCX in the control of neuronal $[Ca^{2+}]_i$ has only be addressed in few studies. However, it appears that a clear difference exist between peripheral and central neurones. Thus, in neurones from the central nervous system, the inhibition of NCX was shown to induce both an increase in resting $[Ca^{2+}]_i$ and a prolongation of depolarisation-induced Ca^{2+} transients (Taglialatela *et al.*, 1990a, b in rat brain synaptosomes; Segal & Manor, 1992 and Koch & Barish, 1994 in cultured hippocampal neurones; Kiedrowski *et al.*, 1994 in cultured cerebellar granule cells; Fierro *et al.*, 1998 in Purkinje neurones recorded from slices of the cerebellar cortex). In peripheral neurones, removal of extracellular Na^+, did not significantly affect resting $[Ca^{2+}]_i$ or the recovery from transient rises in $[Ca^{2+}]_i$ (Thayer & Miller, 1990; Duchen *et al.*, 1990; Benham *et al.*, 1992 and Shmigol *et al.*, 1995b). The results obtained in rat sympathetic neurones were in agreement and suggest that NCX is neither involved in the control of resting $[Ca^{2+}]_i$ nor in the recovery of small Ca^{2+} transients (< 500 nM). With a rise in $[Ca^{2+}]_i$ above 500 nM, NCX would appear to be activated especially during the recovery of the fast component and the NCX contribution became more predominant with the increase in $[Ca^{2+}]_i$ (see *figure 42-B*). These observations are consistent with the characteristics of NCX and because of its lower affinity for Ca^{2+} ($K_d \approx 750$ nM see Blaustein & Lederer, 1999 for review). However, although NCX is involved in the recovery from large rises in $[Ca^{2+}]_i$, it appears to have only a moderate role in the recovery of Ca^{2+} transients and to work in co-operation with other Ca^{2+} homeostatic systems. This result might be explained by the

low NCX expression level as observed from both PCR and immunocytochemical analysis (see *figure 43*). An alternative explanation for the small contribution of NCX might be an expression primarily in dendrites and nerves terminal and therefore a predominant role in non somatic regulation of $[Ca^{2+}]_i$ (Blaustein 1988b; Luther *et al.*, 1992; Reuter & Porzig, 1995 and Juhaszova *et al.*, 1996, 2000).

The stoichiometry of NCX has been shown to be 3 Na^+ for 1 Ca^{2+}, to be electrogenic and therefore the NCX activity is expected to be modulated by both the ionic gradients and the membrane potential (see Blaustein & Lederer, 1999 for review). Blaustein (1988b) suggested that during a depolarisation (*i.e.* an action potential) of the plasma membrane, NCX would promote Ca^{2+} influx by reversing and transporting Ca^{2+} into the cytosol. Thus, theoretically at 0 mV (or +20 mV, the peak of an action potential), the driving force (ΔV) for the Ca^{2+} transport is strongly positive and NCX should induce a Ca^{2+} influx. Although such a Ca^{2+} influx through the 'reversed' NCX was observed in the giant squid axon (Allen & Baker, 1985 and DiPolo & Beaugé, 1988) and synaptosomes (Turner & Goldin, 1985 and Taglialatela *et al.*, 1990a, b), there is no strong evidence that it may occur under physiological conditions. Under the experimental conditions of the study presented in *figure 43-A* ($[Ca^{2+}]_{out}$ = 2.5 mM, $[Ca^{2+}]_{in}$ = 100 nM, $[Na^+]_{out}$ = 140 mM and $[Na^+]_{in}$ = 0 mM) the depolarisation of the plasma membrane to 0 mV would not induce the reversal of the exchanger at rest (ΔV = -1205 mV for $[Ca^{2+}]_i \approx$ 100 nM) even if one considers a rise in $[Ca^{2+}]_i$ from 100 nM to 1 μM (ΔV = -1265 mV for $[Ca^{2+}]_i \approx$ 1 μM). These theoretical values for ΔV are in agreement with the experimental data, since no difference in the amplitude of the depolarisation-induced Ca^{2+} transient in the presence or absence of extracellular Na^+ were observed. On the other hand, the removal of extracellular Na^+ at rest (-60 mV, ΔV = +205 mV) or at 0 mV (Δv = +265 mV) is expected to induce a Ca^{2+} influx. However neither resting $[Ca^{2+}]_i$ nor the amplitude of the depolarisation-induced Ca^{2+} transients were increased under these conditions. One of the reasons for the absence of Ca^{2+} influx could be the dissipation of the Na^+ gradient with both intracellular and extracellular $[Na^+]$ equal to zero, however experiments were carried out in the presence of 10 mM intracellular Na^+ and no change in $[Ca^{2+}]_i$ were observed (data not shown). The other reason could be the fact that the $[Ca^{2+}]_i$ was too low to bind to the Ca^{2+} regulatory site and to induce Ca^{2+} transport since it was suggested that $[Ca^{2+}]_i$ should rise to

micromolar concentration to activate NCX (see Blaustein & Lederer, 1999 and Philipson & Nicoll, 2000 for review). However, the affinity of the Ca^{2+} regulatory site is an unresolved issue as some authors proposed a value between 0.1-0.3 μM and other between 20-50 nM (Miura & Kimura, 1989 and Fang *et al.*, 1998 and see Philipson & Nicoll, 2000 for review). Furthermore, the data presented in *figure 43-B* would suggest that both the Na^+ gradient and the $[Ca^{2+}]_i$ would determine the transport of Ca^{2+} ions since in the presence of high intracellular $[Na^+]$ and the absence of extracellular Na^+ a significant Ca^{2+} influx was observed. Finally, one could argue that the role of NCX in Ca^{2+} extrusion was underestimated under the experimental conditions since firstly the recordings consisted of averaged somatic Ca^{2+} transients and secondly the rise in $[Ca^{2+}]_i$ were not large enough to maximally activate NCX. Again, recordings close to the plasma membrane or in specialised structures of the neurone (synapses or synaptic boutons) might generate different results.

Interesting results were obtained following PMCA inhibition and suggested that NCX was capable to transport Ca^{2+} at concentration as low as 300 nM. Thus, when PMCA was inhibited (see *figure 43-A* for example), $[Ca^{2+}]_i$ increased up to 200-300 nM and remained at this plateau as long as PMCA was inhibited. However, the removal of extracellular Na^+ induced an additional rise suggesting that $[Ca^{2+}]_i$ was maintained at 200-300 nM by a Na^+-dependent process presumably NCX (see *figure 43-A*). In contrast, the rise in $[Ca^{2+}]_i$ induced in the reverse mode of NCX (high $[Na^+]_i$) was limited to around 300-400 nM by a pH-sensitive mechanism, most certainly PMCA. Under these conditions, where NCX transport is reversed and PMCA inhibited, $[Ca^{2+}]_i$ increases to micromolar concentration.

In conclusion, the results presented in this section indicate that SCG neurones express at a low level functional NCX. NCX appear to be involved, along with other regulatory mechanisms, in the Ca^{2+} clearance when $[Ca^{2+}]_i$ rises to micromolar ranges. However, this study also provides evidence for two important and novel features on the Ca^{2+} transport through NCX. Firstly, NCX appears capable of extruding Ca^{2+} at concentration as low as 200-300 nM. Secondly, at $[Ca^{2+}]_i \approx 500$ nM, PMCA and NCX, and presumably other Ca^{2+} homeostatic factors, operate in parallel to control and limit the rise in $[Ca^{2+}]_i$.

7. Control of resting calcium concentration

Most eukaryotic cells maintain resting $[Ca^{2+}]_i \approx 100$ nM and therefore a large inwardly directed gradient is created across the plasma membrane. It is thought that resting $[Ca^{2+}]_i$ results from a constant Ca^{2+} 'leak' counter-balanced by regulatory mechanisms present in the plasma membrane or in the cytosol. Authors agree that PMCA, because of its high affinity for Ca^{2+}, would represent the main mechanism of control for resting $[Ca^{2+}]_i$. However, since most cells posses Ca^{2+} buffering and sequestration systems, other mechanisms might be involved in the regulation of resting $[Ca^{2+}]_i$.

In order to determine how resting $[Ca^{2+}]_i$ is controlled in rat SCG neurones, experiments in which either the extracellular calcium was removed or PMCA and SERCA inhibited were undertaken. This study focused on both the determination of the nature of the Ca^{2+} influx and of the regulatory systems.

7.1. Passive calcium influx and active extrusion

Under voltage-clamp conditions, in the perforated patch configuration and a holding potential of -60 mV, resting $[Ca^{2+}]_i$ was 99 ± 4 nM (CTR; n = 31) and decreased to 80 ± 4 nM upon removal of extracellular Ca^{2+} (Ca^{2+}-free; n = 13, $P< 0.01$, independent *t*-test - *figures 45-A and 46*). Intracellular Ca^{2+} concentration then returned to control values when Ca^{2+} was reintroduced and sometimes a small and transient overshoot was observed (*figure 45-A*). Cells were hold at various hyperpolarised holding potential (between -90 mV and -60 mV) and no change either in resting $[Ca^{2+}]_i$ or in the amplitude of the decrease in $[Ca^{2+}]_i$ after extracellular Ca^{2+} was observed (data not shown), suggesting the involvement of a voltage-independent mechanism.

The data presented in Results section 5, suggested that SCG neurones express PMCAs as primary extrusion system at low $[Ca^{2+}]_i$ (see Results section 5.1, *figures 35-A* and *-C*). Thus at pH 9, resting $[Ca^{2+}]_i$ increased to 249 ± 12 nM (n = 23; $P< 0.001$ independent *t*-test - *figure 45-B* and *figures* in Results section 5). This pH-induced response was reproducible upon several applications of pH 9 and fully reversible (see *figure 45-B*). In the absence of extracellular Ca^{2+}, pH 9 failed to elicit an elevation of

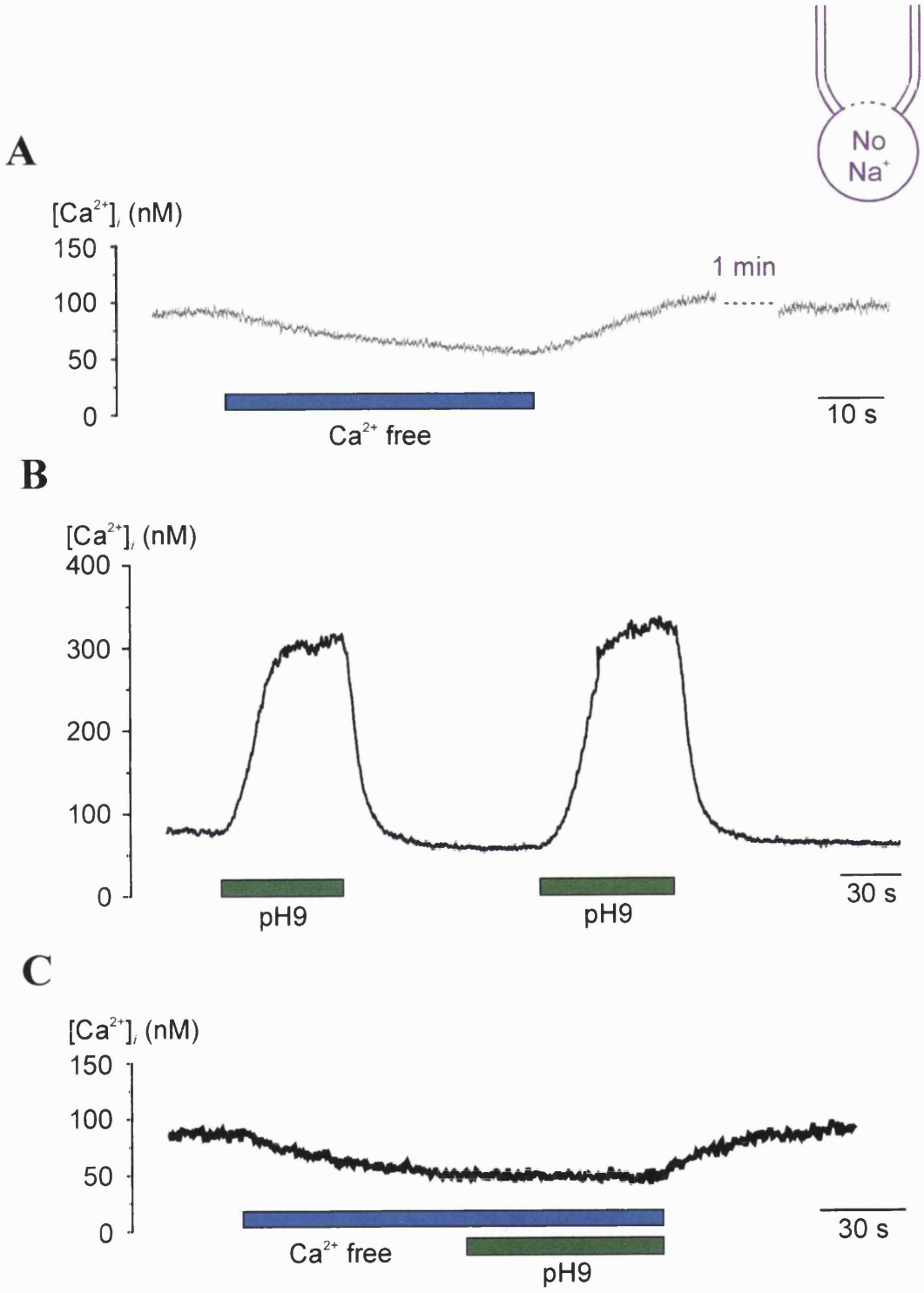

Figure 45: Resting $[Ca^{2+}]_i$ is maintained through a passive influx and an active extrusion of Ca^{2+}
Effect on resting $[Ca^{2+}]_i$ of extracellular Ca^{2+} removal (A, Ca^{2+} free) or PMCA inhibition by extracellular alkalisation (B, pH 9). (C) Changes in $[Ca^{2+}]_i$ in the absence of extracellular Ca^{2+} at pH 7.4 and pH 9. Neurones were voltage-clamped at -60 mV in the perforated patch configuration (no sodium in the patch pipette - see inset).

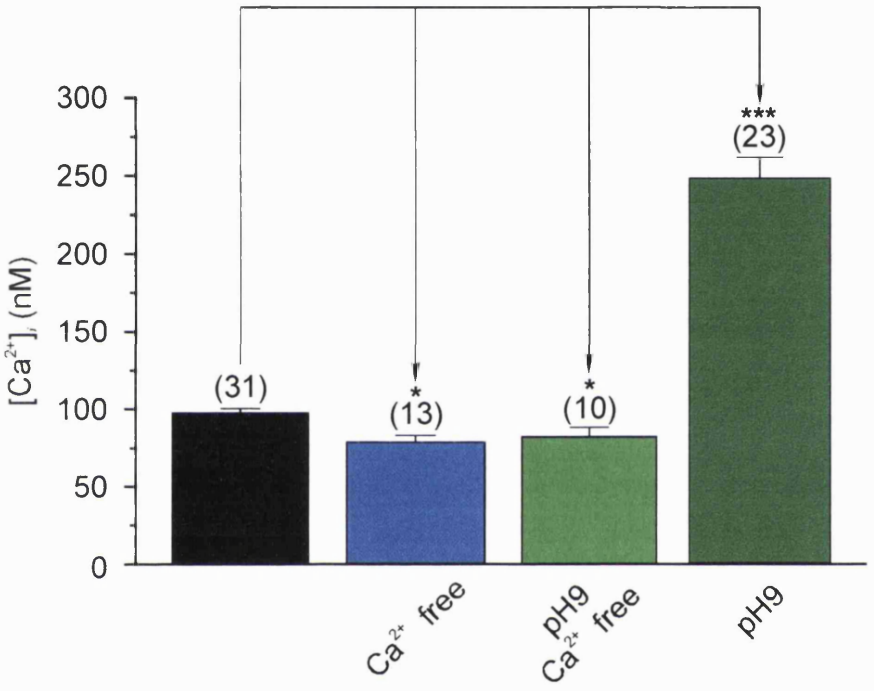

Figure 46: Effect of extracellular Ca^{2+} removal and/or extracellular alkalisation on resting $[Ca^{2+}]_i$
Resting $[Ca^{2+}]_i$ in control (black bar; n= 31), after removal of the extracellular Ca^{2+} at pH 7.4 (Ca^{2+} free; n=13) and at pH 9 (pH 9 Ca^{2+} free; n=10) and after extracellular alkalisation (pH 9; n=23). Data represent mean ± S.E.M. and statistical significance of the differences was compared against the control value with an independent *t*-test (* $P< 0.05$, *** $P< 0.001$).

$[Ca^{2+}]_i$ but $[Ca^{2+}]_i$ decreased to a level equivalent to that measured at pH 7.4 in a Ca^{2+}-free extracellular solution (to 83 ± 6 nM in pH 9 Ca^{2+}-free; n = 10 *versus* 80 ± 4 in Ca^{2+}-free; n=13, P= 0.6, independent *t*-test-*figures 45-C* and *46*).

7.2. Intracellular stores and maintenance of resting calcium

From the data presented in the Results section 4, it was suggested that SCG neurones possess functional intracellular Ca^{2+} store able to release and to sequester Ca^{2+}. The Ca^{2+} release from the ER appeared to be mainly mediated through a caffeine- and ryanodine-sensitive pathway and the sequestration occurred *via* the activation of SERCA, which were inhibited by CPA or TG (see *figures 29* and *30-A*). In neurones voltage-clamped at -60 mV in the perforated patch configuration, the decrease in $[Ca^{2+}]_i$, observed upon removal of extracellular Ca^{2+}, was more pronounced following SERCA inhibition (compare panels *A* and *B* in *figure 47* and 82 ± 1 nM in Ca^{2+}-free and 39 ± 2 nM in Ca^{2+}-free + CPA; n=13, P< 0.001 - *figure 47-C*). Moreover, when the Ca^{2+} store was depleted and its Ca^{2+} uptake system inhibited, the decrease in $[Ca^{2+}]_i$ following extracellular Ca^{2+} removal and the subsequent recovery appeared to have faster kinetics (*figure 47-B*).

7.3. Nature of the passive calcium influx

The results presented in section 7.1 suggest that, at rest, there is a passive Ca^{2+} influx. However, the nature of this Ca^{2+} entry pathway is unknown. From the results in section 4, there is evidence for a Ca^{2+} influx through store-operated Ca^{2+} channels (SOCC - Results section 4.1, see *figure 30-B*). Since one of the possible candidates for this Ca^{2+} influx might be related to SOCC, experiments were therefore carried out with La^{3+}, a potent SOCC inhibitor (Kwan *et al.*, 1990 and Rom-Glas *et al.*, 1992), testing its effect on both resting $[Ca^{2+}]_i$ and the pH-induced rise in $[Ca^{2+}]_i$. Lanthanum applied at a concentration of 10 μM induced no change in resting $[Ca^{2+}]_i$, whereas at 100 μM, La^{3+} reduced resting $[Ca^{2+}]_i$ from 99 ± 4 nM to 77 ± 5 nM, the same level as that reached upon removal of extracellular Ca^{2+} (80 ± 4 nM - *figures 48* and *49-A*). The reduction in $[Ca^{2+}]_i$ induced by 100 μM La^{3+} was reversible but the recovery was slow and only complete after ≈ 5 minutes (see *figure 48-D*).

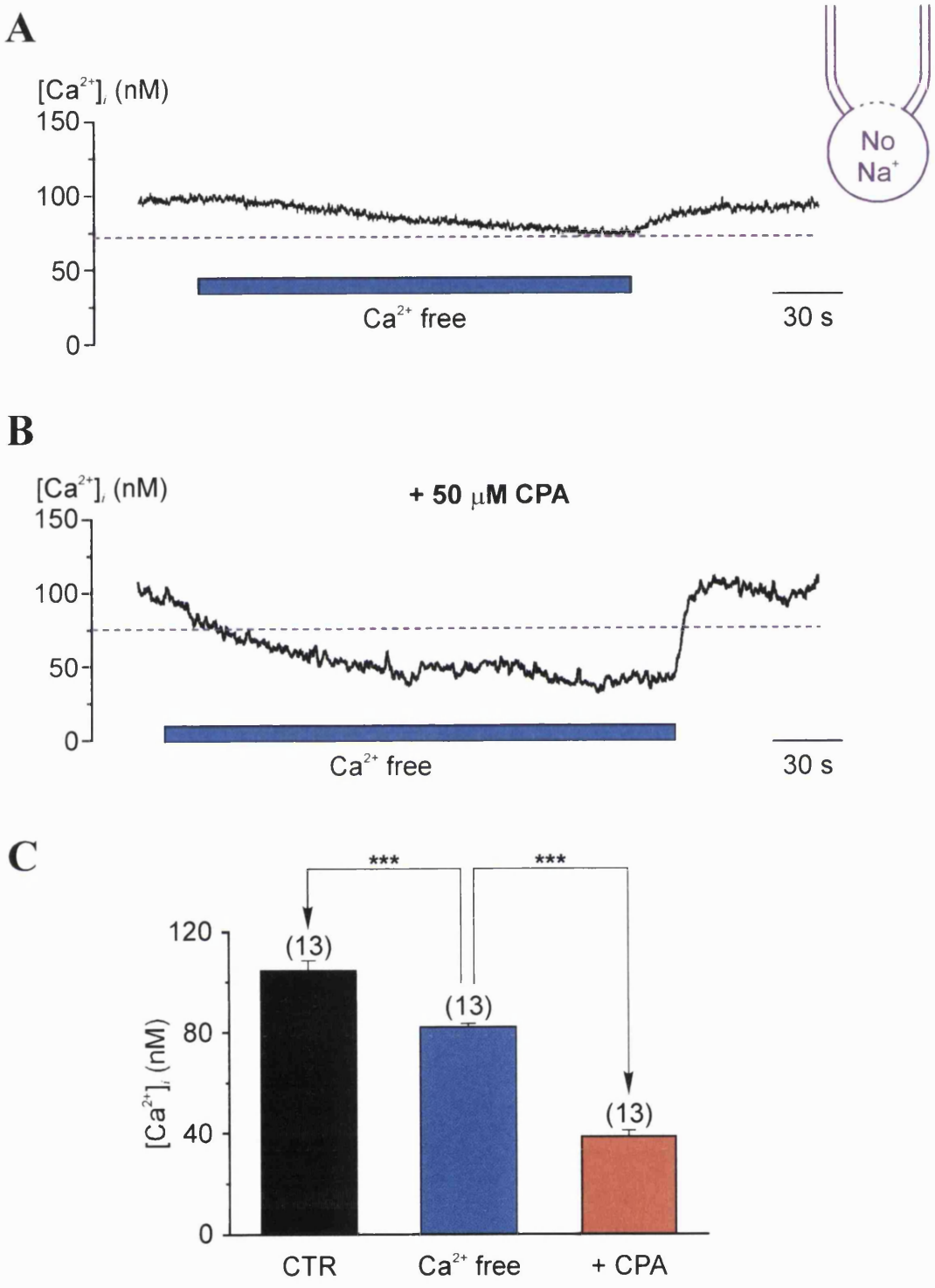

Figure 47: SERCA inhibition induces larger and faster decrease in $[Ca^{2+}]_i$ when the extracellular Ca^{2+} is removed

Extracellular Ca^{2+} removal in a neurone voltage-clamped at -60 mV in the perforated patch configuration in control (A) and after SERCA inhibition with 50 μM CPA (B). (C) Decrease in resting $[Ca^{2+}]_i$ induced in a Ca^{2+}-free extracellular solution prior (blue bar) and after CPA application (orange bar) (data represent mean ± S.E.M.; n=13, *** P< 0.001).

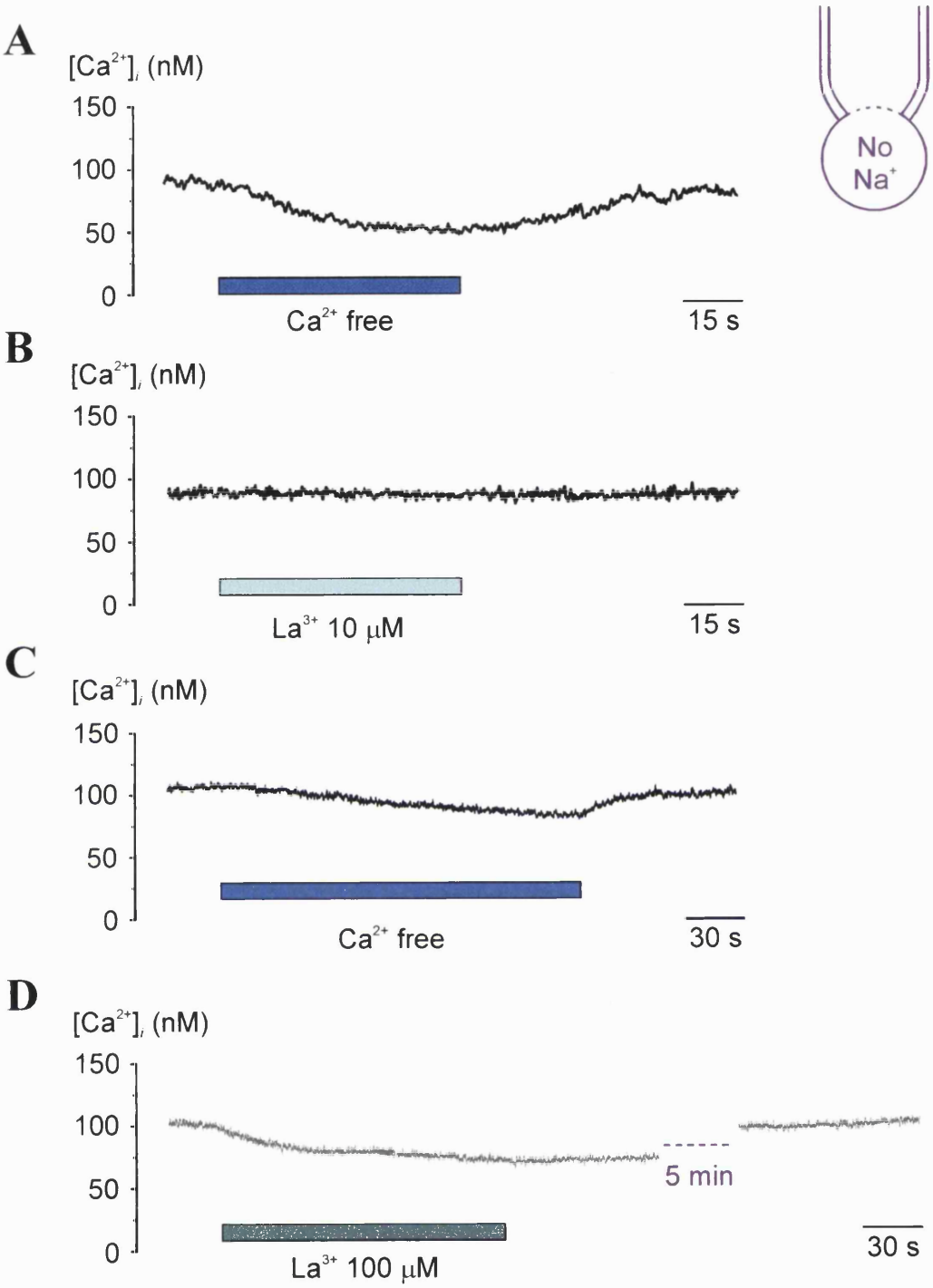

Figure 48: The passive Ca^{2+} influx is lanthanum-sensitive
Neurones were voltage-clamped at -60 mV in the perforated patch mode (no sodium in the patch pipette) and the effects of extracellular Ca^{2+} removal (Ca^{2+} free – A and C) and lanthanum (La^{3+} - 10 μM in B and 100 μM in D) application on resting $[Ca^{2+}]_i$ were compared (see also *figure 49-A*). The extracellular Ca^{2+} removal was used as a control for the presence of a passive Ca^{2+} influx prior to bath application of La^{3+}.

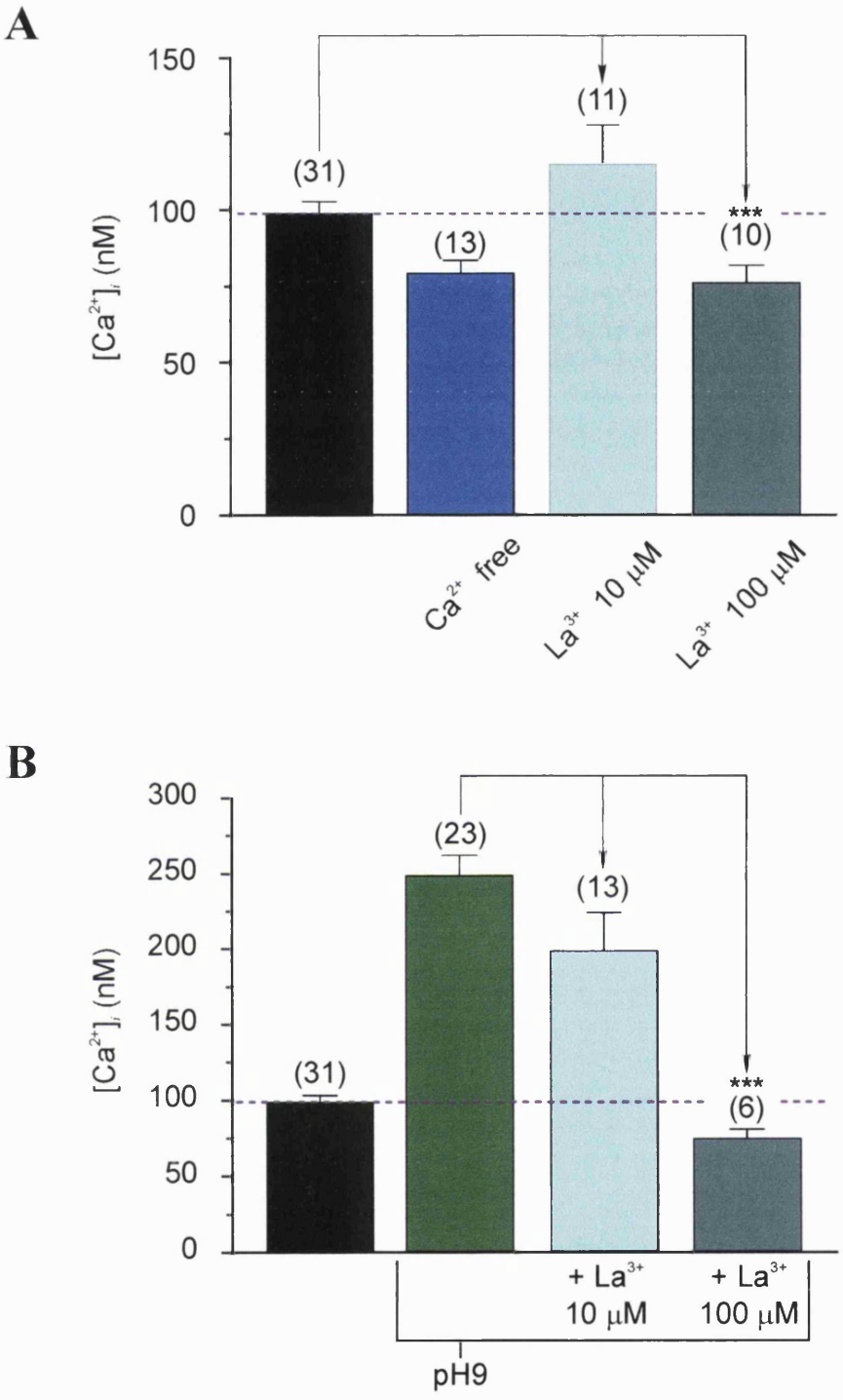

Figure 49: Effects of lanthanum on resting $[Ca^{2+}]_i$ and on the rise in $[Ca^{2+}]_i$ induced after PMCA inhibition

(A) Effect of La^{3+} 10 (n=11) and 100 µM (n=10) on resting $[Ca^{2+}]_i$ compared to control (black bar; n= 31) and in absence of extracellular Ca^{2+} (Ca^{2+} free; n=13) (data as mean ± S.E.M. *** P< 0.001, independent *t*-test – see also *figure 48*). (B) Effect of La^{3+} 10 (n=13) and 100 µM (n=6) on the $[Ca^{2+}]_i$ rise induced in pH 9 compared to control value (black bar; n=31) and after inhibition of the PMCA (pH 9; n=23) (data as mean ± S.E.M. *** P< 0.001, independent *t*-test – see also *figure 50*).

To confirm the involvement of a La^{3+}-sensitive passive Ca^{2+} influx, it was necessary to determine if La^{3+} was able to block the rise in $[Ca^{2+}]_i$ when PMCA is inhibited at pH 9. As expected from the result illustrated in *figure 48-B*, 10 μM La^{3+} was without significant effect on the pH-induced rise in $[Ca^{2+}]_i$ (*figure 49-B*). In contrast, application of 100 μM La^{3+} resulted in a complete inhibition of the pH-induced rise in $[Ca^{2+}]_i$ in 6 out of 8 cells (*figure 50* and 249 ± 12 nM at pH 9; n=23 and 75 ± 5 nM at pH 9 + 100 μM La^{3+}; n=6 - *figure 49-B*). Moreover, in the presence of 100 μM La^{3+} and at pH 9, the $[Ca^{2+}]_i$ felt to a level equivalent to that measured with 100 μM La^{3+} or in the absence of extracellular Ca^{2+} (see *figures 49-A* and *-B*). After ≈ 5 minutes wash out of the La^{3+}, extracellular alkalisation induced an increase in $[Ca^{2+}]_i$, which was similar to the one observed in control (compare panels *A* and *C* in *figure 50*).

The rise in $[Ca^{2+}]_i$ observed at pH 9 could be due to an influx through VACC because of a pH-dependent change in the gating properties of these channels. Lanthanum has been shown to block VACC (Hagiwara & Takahashi, 1967), it was therefore necessary to test that the La^{3+} blocking effect was not due to the inhibition of VACC opened by pH 9 treatment. Cadmium (Cd^{2+}), at a concentration of 100 μM, has been shown to block VACC (Fox *et al.*, 1987 and see *figure 11*). It was therefore used to demonstrate the 'selectivity' of the La^{3+} block of the passive Ca^{2+} influx. Cadmium, added to the extracellular solution prior to and during the extracellular alkalisation (*figure 51*), was without effect either on resting $[Ca^{2+}]_i$ or on the amplitude of the increase in $[Ca^{2+}]_i$ induced following PMCA inhibition (90 ± 7 and 317 ± 80, respectively; n = 3). In contrast, Cd^{2+} and La^{3+} both blocked the VACC.

Finally, as the properties of fluorescent dyes may be affected by other multivalent ions and by variations in the cell environment, experiments were undertaken to test that extracellular alkalisation or La^{3+} application did not change the spectral properties of indo-1. *Figure 52-A* shows that upon reduction of the $[Ca^{2+}]_i$, in a Ca^{2+}-free extracellular solution, the fluorescence (F) emitted by indo-1 at 480 nm (Ca^{2+}-unbound form) was increased whereas the fluorescence emitted at 407 nm (Ca^{2+}-bound form) was slightly reduced. In *figure 52-B*, the rise in $[Ca^{2+}]_i$ observed at pH 9 was consistent with a decrease in the fluorescence emitted at 480 nm and an increase in the fluorescence emitted at 407 nm (see also results section 1.1, *figure 12*, for comparison).

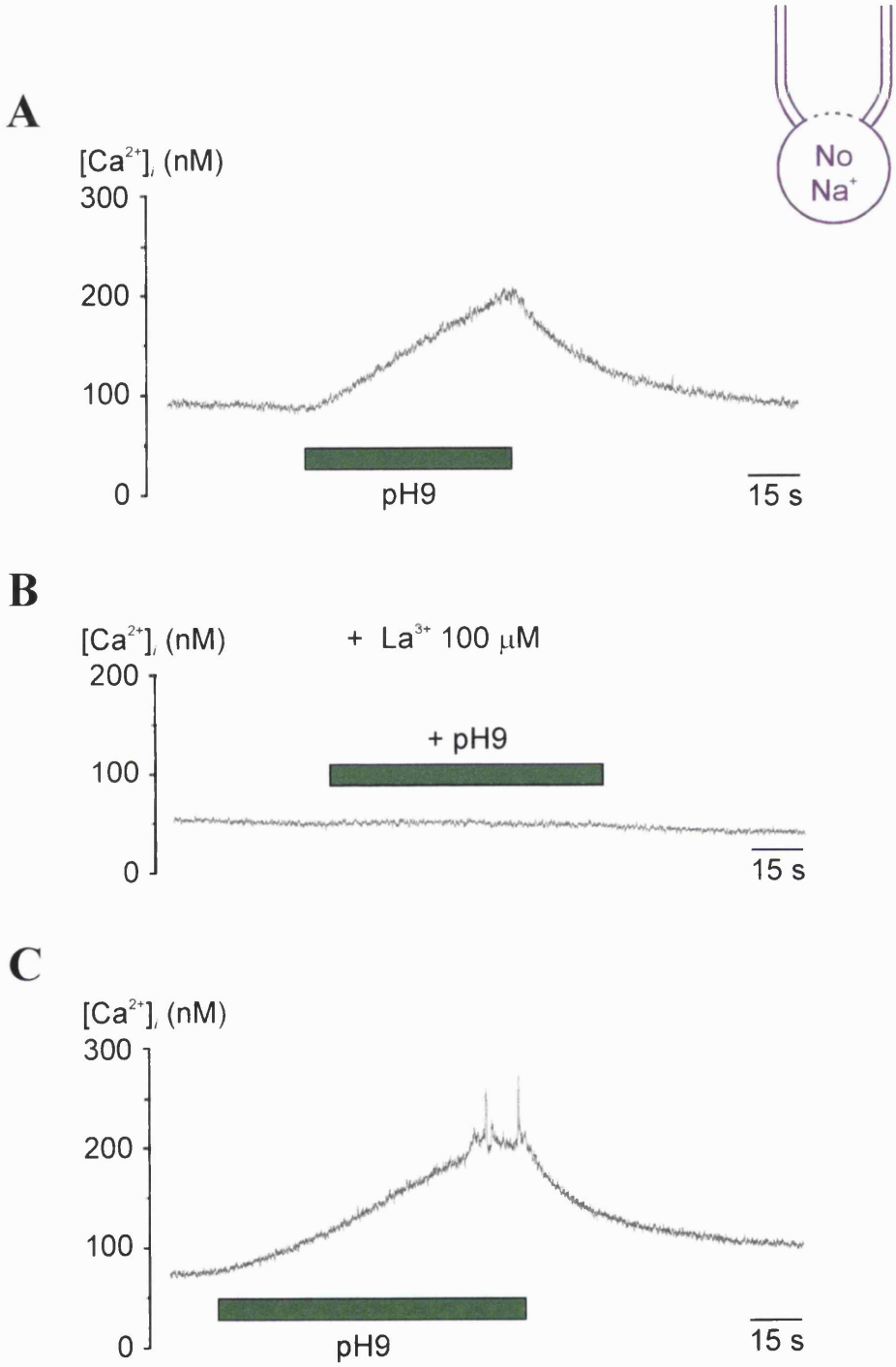

Figure 50: Lanthanum completely blocks the rise in $[Ca^{2+}]_i$ induced at pH 9
PMCA was inhibited at pH 9 and the rise in $[Ca^{2+}]_i$ recorded in a SCG neurone voltage-clamped at -60 mV in the perforated patch configuration (no sodium in the patch pipette – see inset). The $[Ca^{2+}]_i$ changes were recorded before (A), during (B) and after (C) bath application of 100 µM La^{3+} and at pH 9 (see also *figure 49-B*). Upon wash out of La^{3+} (≈ 5 min), the re-inhibition of the PMCA at pH 9 induces a new rise in $[Ca^{2+}]_i$.

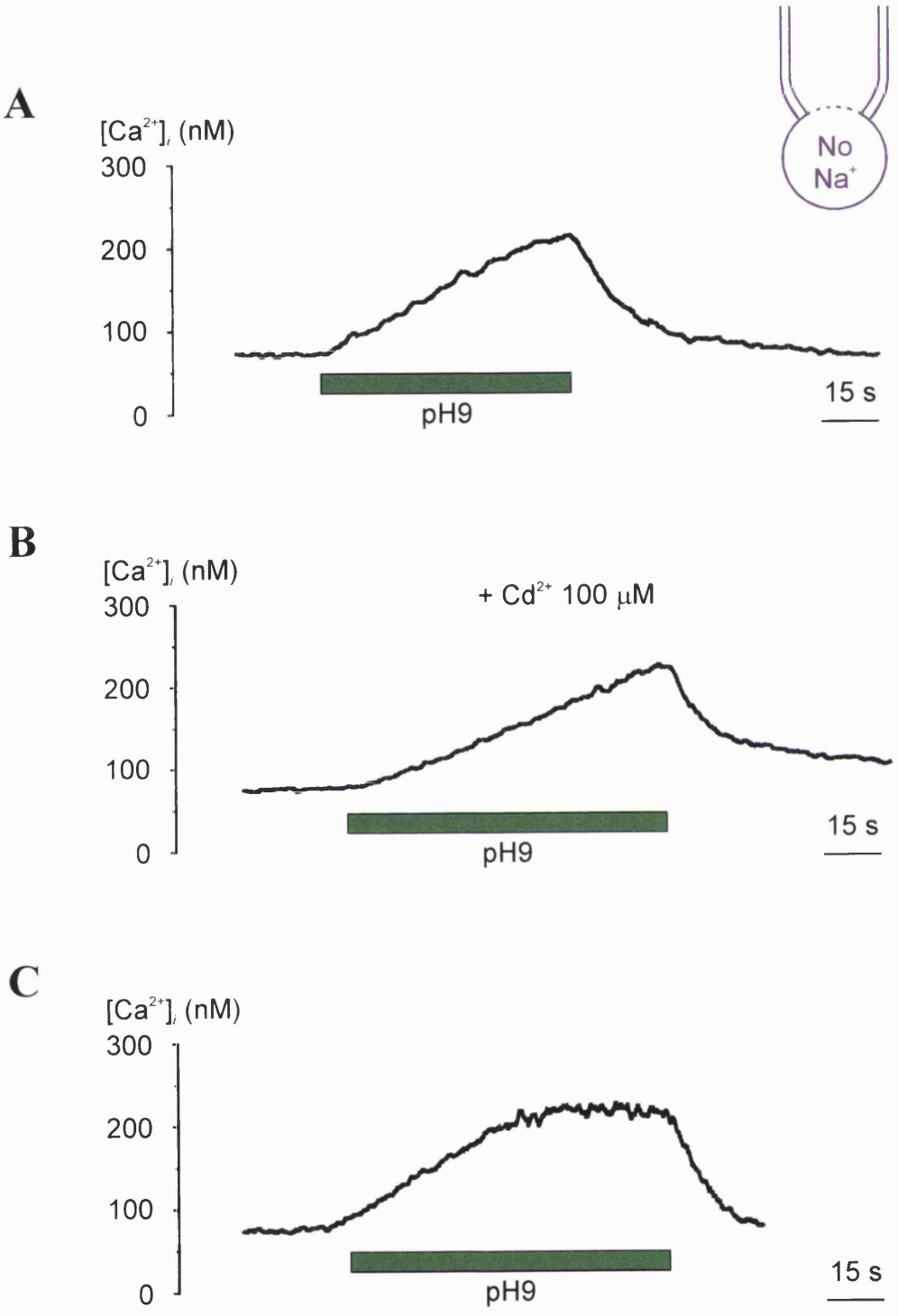

Figure 51: Cadmium is without effect on resting $[Ca^{2+}]_i$ and does not block the pH-induced rise in $[Ca^{2+}]_i$

PMCA was inhibited in pH 9 before (A), during (B) and after (C) bath application of 100 µM Cd^{2+} to test the possible involvement of VACC.

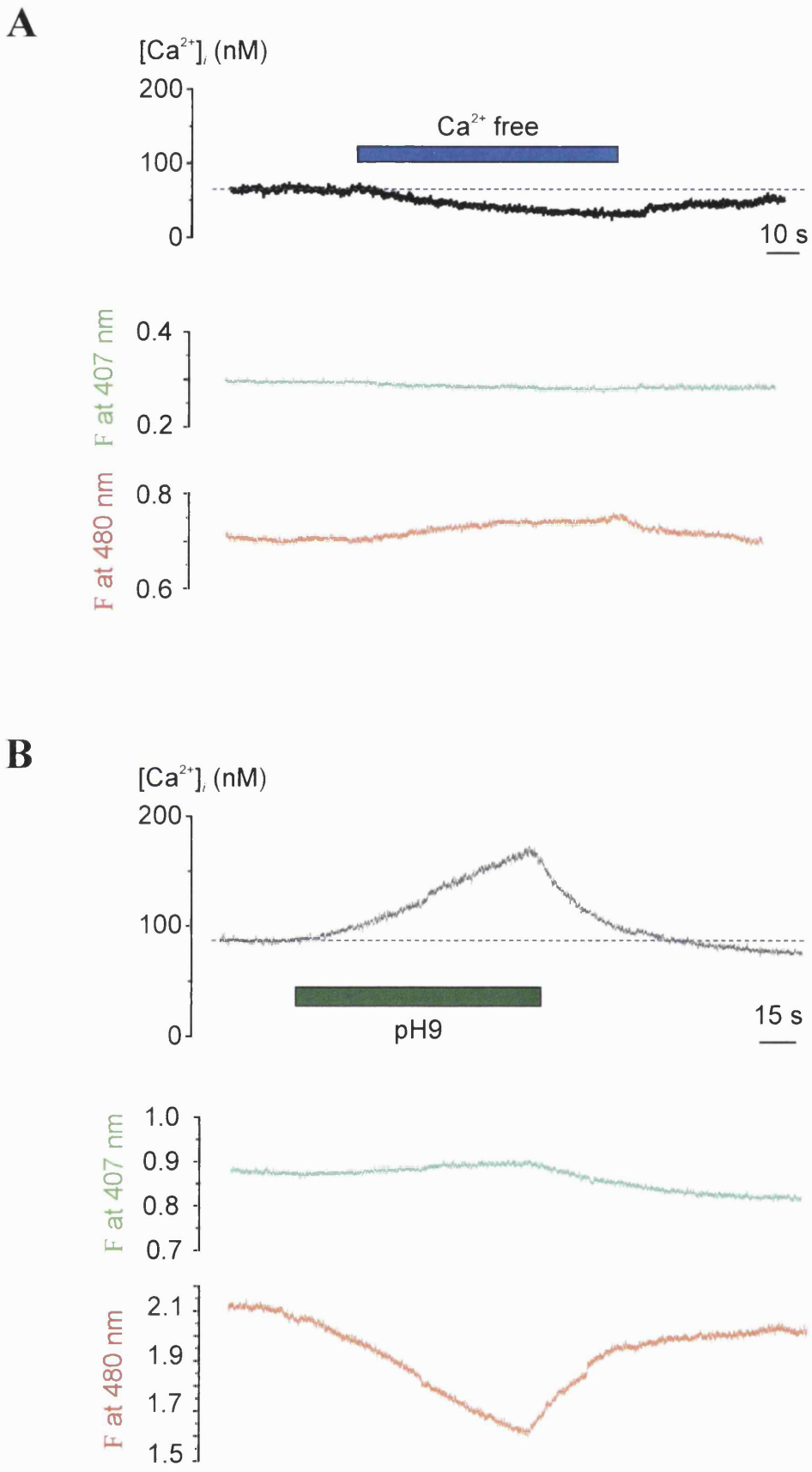

Figure 52-A and -B **(see next page for legend)**

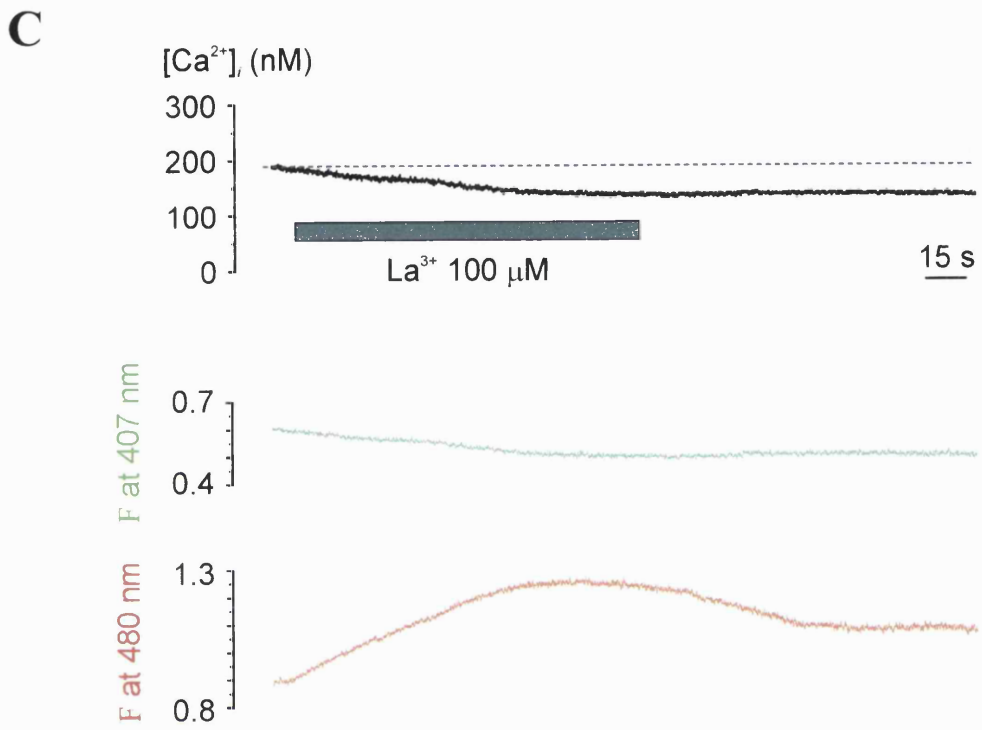

Figure 52: Extracellular alkalisation and lanthanum are without effect on the spectral properties of indo-1

To test eventual alteration of the indo-1 spectral properties due to extracellular alkalisation (pH 9) and La^{3+} application, recording of the fluorescence emitted at 407 nm (Ca^{2+}-bound form of indo-1) and 480 nm (Ca^{2+}-unbound form of indo-1) were realised along with Ca^{2+} measurement. (A) Removal of the extracellular Ca^{2+}, (B) pH 9 and (C) application of 100 µM La^{3+}

Finally, it has been reported that lanthanides may quench Ca^{2+} indicators (Kwan and Putney, 1990; Halaszovich *et al.*, 2000). However, upon La^{3+} application, the increase in the fluorescence emitted at 480 nm and decrease in the fluorescence emitted at 407 nm are in agreement with the decrease in $[Ca^{2+}]_i$ (*figure 52-C*). Moreover, in the absence of extracellular Ca^{2+}, no changes in the indo-1 fluorescence ratio were observed, upon La^{3+} application (data not shown). These observations suggested that La^{3+} did not appear to affect the spectral properties of indo-1 nor to bind directly to indo-1 and give a false reading of the $[Ca^{2+}]_i$. Therefore, the effects observed at pH 9 and/or in the presence of La^{3+} appeared to be the consequence of changes in $[Ca^{2+}]_i$ and not due to changes in the spectral properties of indo-1.

Taken together, the results presented in this section, suggest that resting $[Ca^{2+}]_i$ is maintained around 100 nM as a consequence of a passive La^{3+}-sensitive Ca^{2+} influx counter-balanced by the active Ca^{2+} extrusion through PMCA. Moreover, intracellular stores appear to play a regulatory role in the control of resting $[Ca^{2+}]_i$ by either sequestering or releasing Ca^{2+} depending on the $[Ca^{2+}]_i$.

7.4. Discussion

In most cell types resting $[Ca^{2+}]_i$ is maintained ≈ 50-100 nM and is tightly controlled through several homeostatic mechanisms. Since SCG neurones exhibit high Ca^{2+} buffering capacity especially at rest (Ca^{2+} binding ratio ≈ 1000 at $[Ca^{2+}]_i$ ≈ 100 nM), one can assume that part of the regulation of resting $[Ca^{2+}]_i$ is carried out through CaBPs (see Results section 2). However, the Ca^{2+} buffering is a dynamic equilibrium and is saturable, therefore other mechanisms have to be involved to insure the control of resting $[Ca^{2+}]_i$. Most authors agree that, because of its high affinity for Ca^{2+}, PMCA would represent a regulatory system of resting $[Ca^{2+}]_i$ however very few studies have tried to characterised the mechanisms responsible for the control of resting $[Ca^{2+}]_i$ (*e.g.* Usachev & Thayer, 1999b). Inhibition of PMCA by extracellular alkalisation induced a large rise in resting $[Ca^{2+}]_i$ that did not appear to be a secondary effect of extracellular alkalisation. Thus, similar effects are observed using other PMCA inhibitors (see Results section 5.2) and the increase in resting $[Ca^{2+}]_i$ was both abolished in the absence of extracellular Ca^{2+} and selectively blocked by lanthanum (see *figures 45* and *48*).

Furthermore, changes in resting $[Ca^{2+}]_i$ were not observed following inhibition of NCX (see Results section 6) or of mitochondria (see Results section 3). These results therefore suggested that Ca^{2+} extrusion *via* PMCA was the major control mechanism of resting $[Ca^{2+}]_i$ and, more importantly, they indicated that PMCA was constitutively active to counter-balance a passive Ca^{2+} influx at rest (see below). The presence of a Ca^{2+} influx across the plasma membrane is further supported by the fact that removal of extracellular Ca^{2+} induced a decrease in resting $[Ca^{2+}]_i$ (this study and see also Kennedy & Thomas, 1995; Usachev & Thayer, 1999b). Moreover, the decrease in $[Ca^{2+}]_i$ upon removal of extracellular Ca^{2+} was reproduced by bath application of La^{3+}, a blocker of store-operated Ca^{2+} channels (SOCC; Kwan *et al.*, 1990 and Rom-Glas *et al.*, 1992). The selective sensitivity to La^{3+} but not VACC blockers of the rise in $[Ca^{2+}]_i$ unmasked following PMCA inhibition further supported the presence of a specific Ca^{2+} influx at rest. It is interesting to note that La^{3+} application both at pH 7.4 and at pH 9 induced a decrease in resting $[Ca^{2+}]_i$ to concentrations similar to those observed upon extracellular Ca^{2+} removal. Therefore, one could propose that the rise in $[Ca^{2+}]_i$ observed following PMCA inhibition and the decrease in $[Ca^{2+}]_i$ observed after removal of extracellular Ca^{2+} is mediated through the same set of channels that is La^{3+} sensitive. The fact that the La^{3+} effects were not reproduced by specific VACC blockers further excluded the involvement of a VACC as suggested earlier by some authors (DiPolo *et al.*, 1982 and Tsien *et al.*, 1987) but rather suggests the presence of a selective channels types in SCG neurones. Since the experiments presented here were carried out in the presence of TTX the possibility of a Ca^{2+} leak through TTX-sensitive Na^+ channels can also be excluded (DiPolo *et al.*, 1982). Finally, it has been suggested that Ca^{2+} influx at rest could be explained by Ca^{2+} transport into the cytosol *via* NCX working in the reverse mode as it is sometimes observed in neurones from the central nervous system (Taglialatela *et al.*, 1990a, b; Segal & Manor, 1992 and Kiedrowski *et al.*, 1994). However, in SCG neurones and similarly to most peripheral neurones (Thayer & Miller, 1990; Duchen *et al.*, 1990; Benham *et al.*, 1992; Shmigol *et al.*, 1995 and Usachev & Thayer, 1999b), NCX inhibition was without effect on resting $[Ca^{2+}]_i$ suggesting that the Ca^{2+} influx at rest is not mediated by this exchanger (see also Results section 6). Therefore, the data presented in this section suggest the presence, at rest, of a novel La^{3+}-sensitive Ca^{2+} entry pathway that appears to be constitutively active since it is unmasked by PMCA

inhibition or abolished by removal of extracellular Ca^{2+} (see *figure 45* and see below). Usachev and Thayer (1999b) draw similar conclusions and also proposed the presence in DRG neurones of a specific set of channels responsible for this Ca^{2+} influx at rest.

In non-excitable cells, the predominant Ca^{2+} entry pathway is mediated through capacitative Ca^{2+} channels (also known as SOCC), which are activated either by intracellular second messenger or by Ca^{2+} store depletion (see Putney & McKay, 1999 for review). There is evidence for the presence of such a Ca^{2+} entry route in neurones (this study and see Usachev & Thayer, 1999b) and it is interesting to consider that the Ca^{2+} influx observed at rest shares similar features to Ca^{2+} influx through SOCC. Thus, depletion of the Ca^{2+} store activates a sustained rise in $[Ca^{2+}]_i$ that is abolished either by removal of extracellular Ca^{2+} or bath application of lanthanum (this study *figure 30-B*; Garaschuk *et al.*, 1997 and Usachev & Thayer, 1999). Secondly, cell exposure to a Ca^{2+}-free perfusion medium, generally induces an overshoot in resting $[Ca^{2+}]_i$ upon reintroduction of extracellular Ca^{2+}, presumably mediated through SOCC (this study and see Garaschuk *et al.*, 1997 and Usachev & Thayer, 1999b). Calcium store appears to replenish spontaneously *via* Ca^{2+} influx across the plasma membrane since a minimum delay is required between two caffeine-induced Ca^{2+} transients to generate responses of similar amplitude (see Results section 4.5 and Garaschuk *et al.*, 1997 and Usachev & Thayer, 1999b).

The channels involved in the store-operated Ca^{2+} influx in non-excitable cells are thought to be related to *trp* channels or their mammalian homologues (see General Introduction section 2.2.2; Putney & McKay, 1999 and Clapham *et al.*, 2001 for review). Since neurones appear to express high level of *trp* channels (see Clapham *et al.*, 2001 for review) it has been proposed that the Ca^{2+} influx observed after store depletion might be mediated through these channels. The fact that Ca^{2+} store appeared to take part in the regulation of resting $[Ca^{2+}]_i$ would suggest that channels related to SOCC or *trp* could mediate the Ca^{2+} influx observed at rest. Thus, following SERCA inhibition and Ca^{2+} store depletion, the decrease observed in resting $[Ca^{2+}]_i$ upon extracellular Ca^{2+} removal was more pronounced (see *figure 47*) suggesting that Ca^{2+} is released from intracellular stores to maintain resting $[Ca^{2+}]_i$. Considering that Ca^{2+} store has been suggested to be leaky (see Results section 4.5 and Garaschuk *et al.*, 1997), one could propose that there might be a basal activation of SOCC or related channels and

that Ca^{2+} might cycle from the extracellular medium to the Ca^{2+} store *via* the cytosol. This Ca^{2+} influx activated by Ca^{2+} store would serve both to maintain resting $[Ca^{2+}]_i$ and refill leaky Ca^{2+} store. However, regarding the Ca^{2+} influx observed at rest, two aspects remain paradoxical to conclude that it is mediated through SOCC. Firstly, SOCC are, per definition, supposed to be operated by intracellular stores and especially following their depletion. Secondly, Ca^{2+} influx through SOCC has been shown to be enhanced by hyperpolarisation whereas in SCG no change in the amplitude of the rise in $[Ca^{2+}]_i$ was observed with hyperpolarising step (but see Usachev & Thayer, 1999b and see Clapham *et al.*, 2001 for review). Further experiments would be necessary to characterise the channels involved in the passive Ca^{2+} influx at rest and to determine if they are related to SOCC and how they are regulated.

In conclusion, the data presented in this section indicate that resting $[Ca^{2+}]_i$ results from an equilibrium between a constant passive Ca^{2+} entry and leak from the intracellular stores counter-balanced by Ca^{2+} extrusion through PMCA and Ca^{2+} sequestration *via* SERCA. One could therefore suggest that resting $[Ca^{2+}]_i$ is set by a dynamic Ca^{2+} cycle from the extracellular environment into the Ca^{2+} store *via* the cytosol. The resting $[Ca^{2+}]_i$ would therefore depend on the activity of the different component of Ca^{2+} homeostasis and particularly the binding kinetics to CaBPs both from the cytosol and from the ER. These CaBPs by determining the amount of free Ca^{2+} would influence the PMCA and SERCA activity and also the extent of Ca^{2+} influx and Ca^{2+} leak (see General Discussion for more details on this aspect)

Chapter IV

General Discussion and Conclusion

1. Calcium homeostasis in rat sympathetic neurones

The work presented in this thesis represents, to our knowledge, the first study to characterise the various mechanisms involved in the regulation of somatic $[Ca^{2+}]_i$ in neurones from rat superior cervical ganglion. The data presented do not allow the precise determination of the kinetics of Ca^{2+} transients' recovery nor the study of localised Ca^{2+} responses because the recordings of $[Ca^{2+}]_i$ represent spatially averaged somatic Ca^{2+} signals and might therefore not be representative to what occurs close to the plasma membrane.

Although amongst a particular neuronal population there might be heterogeneity in the level of expression of the different component involved in Ca^{2+} homeostasis, the results obtained in this study appear consistent from cell to cell suggesting a homogeneity in the Ca^{2+} regulatory mechanisms. Furthermore, under the perforated patch configuration, the properties of the depolarisation-induced Ca^{2+} transients were stable over long recording periods with little alteration in their amplitude or their decay time constant(s) suggesting that the Ca^{2+} influx and the activity of the Ca^{2+} clearance systems remained constant during the experiments. The results collected therefore allow the characterisation of the mechanisms involved in Ca^{2+} homeostasis in rat SCG neurones.

The major features of Ca^{2+} homeostasis in rat SCG neurones are summarised below and in the following sections hypothetical models based on the experimental data are presented to try to explain how the different elements of Ca^{2+} homeostasis might interact to both maintain resting $[Ca^{2+}]_i$ and return $[Ca^{2+}]_i$ to basal level after a period of cellular activity.

1) In SCG neurones, the Ca^{2+} binding ratio was $\approx$ 1000 close to rest and decreased with the rise in $[Ca^{2+}]_i$ to reach a value of $\approx$ 250 when $[Ca^{2+}]_i \approx 1$ μM. This suggests the presence of, at least, two Ca^{2+} buffering systems: a high affinity Ca^{2+} buffer saturated close to rest ($\approx$ 150 nM) and a second buffer system with a lower Ca^{2+} affinity that appears non-saturable for rises in $[Ca^{2+}]_i$ within the physiological range and which might involve rapid mitochondrial Ca^{2+} uptake.

2) Resting $[Ca^{2+}]_i$ might be the result of a dynamic Ca^{2+} cycle from the extracellular medium to the Ca^{2+} store *via* the cytosol. Calcium is extruded through

PMCA that counter-balances a constant passive Ca^{2+} influx. Calcium store appears to both sequester and release Ca^{2+} and therefore to be also involved in the regulation of resting $[Ca^{2+}]_i$.

3) During cellular activity, rises in $[Ca^{2+}]_i$ appear directly proportional to the amplitude and duration of the Ca^{2+} current mainly mediated through N-type VACCs and there was no evidence for a CICR-like amplification of the Ca^{2+} influx.

4) PMCA was the major Ca^{2+} clearance system for small rises in $[Ca^{2+}]_i$ (<500 nM) and there is some evidence for a mitochondrial Ca^{2+} release presumably through a Na^+-independent mechanism that would delay the recovery of small Ca^{2+} transients.

5) For larger rises in $[Ca^{2+}]_i$ (>500 nM), mitochondria sequestered Ca^{2+} during the rising phase while Ca^{2+} was extruded through NCX and taken up into Ca^{2+} store *via* SERCA. With the decrease in $[Ca^{2+}]_i$, the recovery of Ca^{2+} transients was mainly mediated by PMCA and delayed by Ca^{2+} release from the mitochondria, mainly through *m*NCX.

2. Regulation of resting intracellular calcium

Under resting conditions (see *figures* in Results section 7), $[Ca^{2+}]_i$ would result from a dynamic equilibrium between active Ca^{2+} extrusion (PMCA) or sequestration (SERCA) and passive Ca^{2+} leak from the intracellular stores (ER) or Ca^{2+} influx across the plasma membrane (PM). In addition Ca^{2+} ions in the free ionic form would be in equilibrium with Ca^{2+} binding proteins from both the cytosol (CaBPs - see results section 2) and the ER (ER-CaBPs). One could therefore suggest a constant Ca^{2+} cycling from the extracellular environment to the intracellular stores *via* the cytosol and back to the extracellular space (*figure 53* - top panel). The results presented in this work (see *figures 48* to *50*) suggest that Ca^{2+} would enter the cytosol through La^{3+}-sensitive Ca^{2+}-permeable channels, presumably related to SOCC, and be in equilibrium with CaBPs. In the same time, the free Ca^{2+} would be transported into the ER by SERCA functioning at a basal rate (see *figures 29-C, 47* and *figure 53,* top panel right). However, under resting conditions, the ER appears to be filled up to ≈ 80% (Shmigol *et*

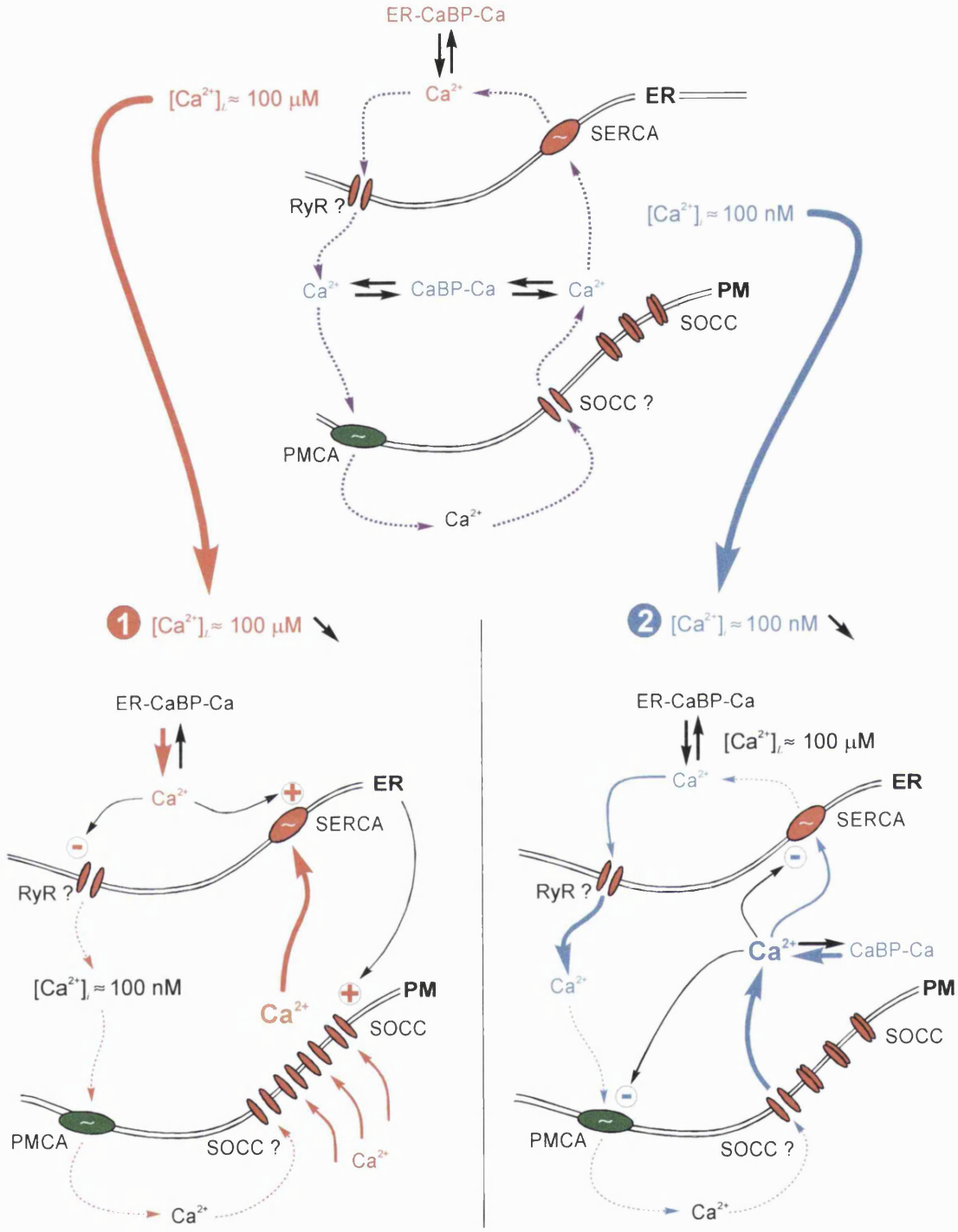

Figure 53: A model for the maintenance of resting intracellular calcium concentration

Calcium cycling from the extracellular medium into the intracellular stores via the cytosol might be responsible for the maintenance of resting $[Ca^{2+}]_i$ and restoration of resting free $[Ca^{2+}]$ in the endoplasmic reticulum (1) and in the cytosol (2) following a decrease in the $[Ca^{2+}]_i$.

Plasma membrane (PM); plasma membrane Ca^{2+}-ATPase (PMCA); store-operated Ca^{2+} channels (SOCC), cytosolic Ca^{2+} binding protein (CaBP); cytosolic free Ca^{2+} concentration ($[Ca^{2+}]_i$); endoplasmic reticulum (ER); sarco/endoplasmic Ca^{2+}-ATPase (SERCA); Ca^{2+} binding protein from the ER (ER-CaBP); free Ca^{2+} concentration in the ER ($[Ca^{2+}]_L$) and ryanodine receptor (RyR).

al., 1994b; Pozzan *et al.*, 1994 and Mogami *et al.*, 1998). The high Ca^{2+} content of the ER was proposed to limit Ca^{2+} uptake into the stores (Inesi & DeMeis, 1989; Favre *et al.*, 1996 and Mogami *et al.*, 1998) and to promote Ca^{2+} release into the cytosol by lowering the $[Ca^{2+}]_i$ threshold for RyR activation (Gilchrist *et al.*, 1992; Usachev & Thayer, 1997, 1999a; Lykyanenko *et al.*, 1996; Marie & Silva, 1998 and Sitsapesan & Williams, 1997, 2000). The resting luminal free $[Ca^{2+}]_i$ ($[Ca^{2+}]_L$) appears to be maintained ≈ 100 μM and Ca^{2+} store have been suggested to be leaky (Garaschuk, 1997; Mogami *et al.*, 1998 and Usachev & Thayer, 1999b) and therefore, one could propose that Ca^{2+} uptake during basal activity of SERCA might be compensated by this Ca^{2+} leak. The mechanism or the channel type mediating the Ca^{2+} leak from the ER is still unidentified. However, ryanodine receptors (RyR) open in a low probability state (Hernandez-Cruz *et al.*, 1995 and Armisen *et al.*, 1996) could mediate this Ca^{2+} leak. Since, cADPr was proposed as the endogenous agonist for RyR (see Galione, 1993; Bak *et al.*, 1999 and Petersen & Cancela, 1999), one could suggest that a basal activation of RyR *via* cADPr could underlie the observed Ca^{2+} leak. The Ca^{2+} released into the cytosol would finally be extruded into the extracellular medium through a PMCA working under basal condition. It can be further suggested that in SCG neurones, this basal Ca^{2+} extrusion might be carried out *via* PMCA-1 and/or 4 since both Ca^{2+}-ATPases are expressed in these neurones and considered as the 'house keeping' isoforms (see Carafoli 1994). The PMCA activity would compensate both the leak from the ER and the Ca^{2+} influx across the plasma membrane (*figure 53*, top panel left). In SCG neurones, this observation is supported by the rise in $[Ca^{2+}]_i$ following PMCA inhibition (see *figures* in Results sections 5 and 7). Of course, one has to consider that all these mechanisms are simultaneously active so that as a result resting $[Ca^{2+}]_i$ would be maintained ≈ 100 nM and $[Ca^{2+}]_L$ ≈ 100 μM (see Pozzan *et al.*, 1994).

Such a system would allow a steady $[Ca^{2+}]_L$ and provide a Ca^{2+} source to compensate for the Ca^{2+} leak from the ER. This process would enable both the maintenance of resting $[Ca^{2+}]_i$ ≈ 100 nM and ensure that the Ca^{2+} store remain in a filled state ready to release Ca^{2+} when stimulated by an intracellular messenger or a rise in $[Ca^{2+}]_i$. The model presented also propose a strong interaction between resting $[Ca^{2+}]_i$ and $[Ca^{2+}]_L$ so that both cellular compartments would be in equilibrium with each other and changes in one of them would be compensated by variation in the Ca^{2+} regulation in

the other. The fact that PMCA overexpression resulted in a decrease in $[Ca^{2+}]_L$ (Brini *et al.*, 2000) and therefore modified the equilibrium between Ca^{2+} content in the cytosol and ER further support the idea of an interaction between cytosol and ER.

Thus, a decrease in $[Ca^{2+}]_L$ is known to activate SOCC (Usachev & Thayer, 1999b, Garaschuk *et al.*, 1997 and Putney & MacKay, 1999) and would as a consequence induce an increase in $[Ca^{2+}]_i$ (*figures 30 and 53,* panel 1). However, the Ca^{2+} influx would primarily serve the refilling of the Ca^{2+} store by the upregulation of SERCA and one would expect only minimal changes in $[Ca^{2+}]_i$ and therefore no increase in the activation of PMCA (Mogami *et al.*, 1998). Moreover, Mogami and colleagues (1998) suggested that the Ca^{2+} refilling of the ER was triggered by an intra-luminal signal and could occur without elevation of $[Ca^{2+}]_i$ to avoid a prolonged upregulation of PMCA. On the other hand, the Ca^{2+} leak through intracellular store could be inhibited to promote stores refilling (*figure 53*, panel 1). This hypothesis would be further supported if one consider that Ca^{2+} leak from the intracellular stores is mediated through RyR since these channels have been shown to be inhibited following a decrease in $[Ca^{2+}]_L$ (Pozzan *et al.*, 1994 and Mogami *et al.*, 1998). Finally, as a consequence, $[Ca^{2+}]_L$ would be brought back to basal value without significantly affecting resting $[Ca^{2+}]_i$ and the equilibrium between cytosolic and luminal $[Ca^{2+}]$ that existed at rest would be progressively restored.

On the other hand, to compensate a decrease in $[Ca^{2+}]_i$ both the activity of PMCA and the rate of Ca^{2+} uptake *via* SERCA could be reduced (*figure 53*, panel 2). This process would induce a larger net Ca^{2+} influx through SOCC related Ca^{2+} channels in parallel with the Ca^{2+} leak from the ER (*figure 53*, panel 2) and would result in an increase in $[Ca^{2+}]_i$ back to resting values. With the restoration of resting $[Ca^{2+}]_i$ the different systems involved in the regulation of resting $[Ca^{2+}]_i$ would then progressively return to their basal activity (*figure 53*, top panel).

Although, several features in the regulation of resting $[Ca^{2+}]_i$ presented in this study (see Results section 7) are in agreement with Usachev and Thayer (1999b), the proposed model is still speculative since supporting evidence for some of the proposed aspects are still missing. Further experiments would be necessary to determine the nature of the Ca^{2+} influx and to demonstrate if it corresponds to a basal activation of SOCC. It would be necessary to characterise the channel type involved in the Ca^{2+} leak

from the ER. Experiments in which combined recording of $[Ca^{2+}]_i$ and $[Ca^{2+}]_L$ with Ca^{2+} indicators targeted to specific cellular compartments would provide valuable clues for a better understanding of this issue. Finally, molecular biological experiments would enable the characterisation of the proteins underlying the passive Ca^{2+} influx.

3. Mechanisms involved in the clearance of calcium

In order to determine the rates of Ca^{2+} clearance for the major systems involved in the regulation of $[Ca^{2+}]_i$, Ca^{2+} transients with similar peak values in control and in experimental conditions were compared. *Figure 54* summarises the Ca^{2+} clearance rate as a function of $[Ca^{2+}]_i$ for PMCA, NCX and SERCA. The clearance rate in control was obtained from the best fit of the experimental data pooled from all Ca^{2+} transients recorded in control. For each clearance system the experimental data obtained in the presence of a particular inhibitor were pooled and fitted and the curves presented in *figure 54* correspond to the inhibitor-sensitive component obtained after subtraction of the best fit in the presence of the inhibitor to the best fit in control.

In the present study the role of mitochondria in the regulation of rises in $[Ca^{2+}]_i$ was also determined and appears to be an important component of Ca^{2+} homeostasis particularly following large increase in $[Ca^{2+}]_i$ (see *figures 24* and *27*). However, because the analysis of the recovery from large rises in $[Ca^{2+}]_i$ was complicated by the multiphasic recovery induced by a functional mitochondrial Ca^{2+} release, the study was carried out in the absence of intracellular Na^+ to reduce the contribution of mitochondria in the overall recovery process. Although in the absence of intracellular Na^+, mitochondrial Ca^{2+} release was mostly inhibited, mitochondria still appear to be capable of sequestering Ca^{2+} and presumably to slowly release it at lower $[Ca^{2+}]_i$ when the net mitochondrial Ca^{2+} flux would be outward (see *figure 28*). Therefore, one needs to bear in mind that the overall clearance rate presented in *figure 54* is mostly qualitative and might be underestimated since the mitochondrial contribution is not represented. The data collected in the present study would indicate that mitochondria have a dual effect, by releasing Ca^{2+} at low $[Ca^{2+}]_i$ and therefore delaying the recovery and sequestering Ca^{2+} at higher $[Ca^{2+}]_i$ and therefore accelerating the Ca^{2+} clearance.

At the lowest range of $[Ca^{2+}]_i$ and up to $\approx$ 300 nM, PMCA appears to be the major extrusion mechanism and to represent 75% of the overall Ca^{2+} clearance (see *figures* in

A

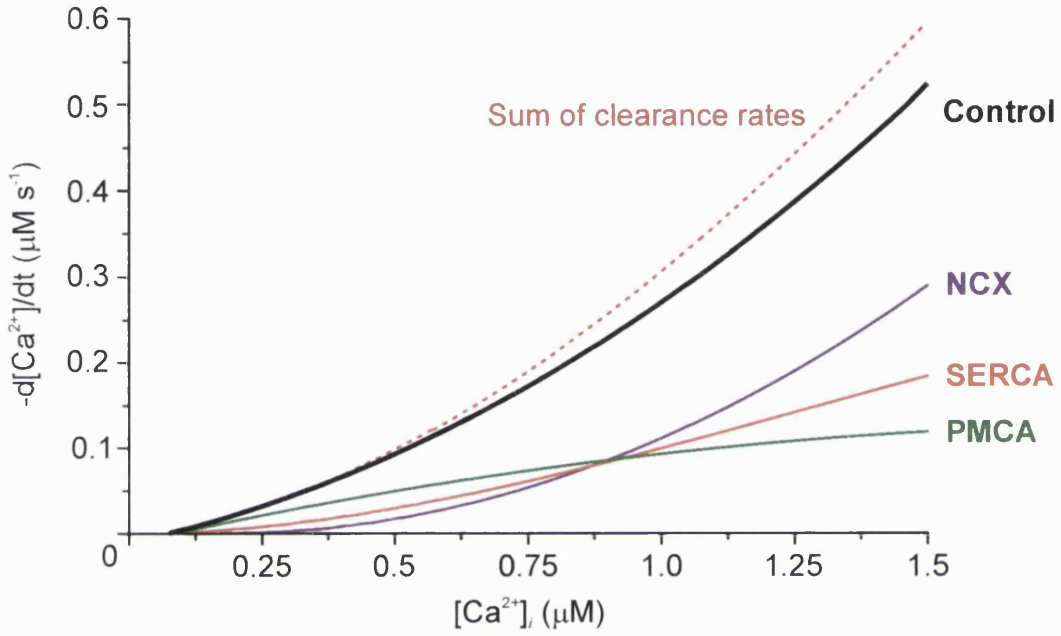

B

$[Ca^{2+}]_i$ (μM)	0.25	0.5	0.75	1.0	1.25	1.5
PMCA	75%	55%	45%	34%	32%	23%
SERCA	25%	36%	35%	38%	37%	36%
NCX	0%	18%	30%	44%	56%	57%

Figure 54: Summary of the calcium clearance in rat SCG neurones

(A) Plot of the clearance rate in control (black line) and for PMCA, SERCA and NCX as characterised in this study (see Results sections). The sum of the clearance rates is also represented (red dashed line) for comparison. The different curves represent the respective contribution of each clearance process (see Results sections for more details) and are represented against $[Ca^{2+}]_i$ (B) Summary of the respective contribution of each clearance mechanism at particular $[Ca^{2+}]_i$ (in percentage).

Results section 5 and *figure 54*). Surprisingly, the determination of the clearance rate for SERCA indicates that even close to rest, 25% of the overall Ca^{2+} removal from the cytosol is carried out *via* SERCA (see *figure 54* and Table). However, after SERCA inhibition the decay time constant from small rises in $[Ca^{2+}]_i$ ($\approx$ 300 nM) was not significantly modified (see Tables 11 and 12 in Results section 4). One could suggest that this discrepancy arise from the activation of a Ca^{2+} influx following SERCA inhibition that might prolong the recovery compared to the control situation. On the other hand, following SERCA inhibition especially with CPA, the slow component of biexponential recoveries was prolonged compared with control ($\approx$ 23 s in control *versus* 34 s in CPA see Table 11 in Results section 4) and could suggest Ca^{2+} sequestration at low $[Ca^{2+}]_i$.

With the increase in $[Ca^{2+}]_i$, the contribution of PMCA was still predominant (see Table in *figure 54*) but the contribution of both NCX and SERCA increased. Thus, at $\approx$ 800 nM, NCX and SERCA respectively account for $\approx$ 30% and 35% of the Ca^{2+} removal from the cytosol whereas PMCA contribute by $\approx$ 45% to the Ca^{2+} clearance (see *figure 54*). The rate of Ca^{2+} transport through PMCA is maximal and remains constant $\approx$ 100 nM s^{-1} for any further increase in $[Ca^{2+}]_i$. The plot of the clearance rate for PMCA suggests a half-maximal activation at $[Ca^{2+}]_i \approx$ 500 nM that is in agreement with the reported Ca^{2+} affinity for PMCA ($K_d \approx$ 500 nM). The Ca^{2+} extrusion through PMCA observed at higher $[Ca^{2+}]_i$, could be explained by the involvement of two different PMCA isoforms with different affinity for Ca^{2+}. Since, CaM binding to PMCA increases the Ca^{2+} affinity from 10-20 μM to 0.5 μM (Carafoli, 1994 and Carafoli & Stauffer, 1994), one could suggest the presence in SCG neurones of a PMCA isoform that would be active at higher $[Ca^{2+}]_i$ because of their lower affinity for Ca^{2+} and possibly in a CaM-independent manner. The predominant role for PMCA at low $[Ca^{2+}]_i$ in SCG neurones (see *Figure* 35) is also in agreement with previous reports in other cell types (*e.g.* Benham *et al.*, 1992 and Park *et al.*, 1996). Interestingly this major role for PMCA in SCG neurones contrasts with the observation by Fierro and colleagues (1998) in rat cerebellar Purkinje neurones. These authors suggested that even for small increases in $[Ca^{2+}]_i$, the Ca^{2+} clearance would involve, to the same extent, both SERCA and NCX along with PMCA. It is surprising to consider that PMCA play only a minor role in the Ca^{2+} extrusion in rat Purkinje neurones, since immunocytochemical studies

have demonstrated a high level of expression of several PMCA isoforms (see Discussion in Fierro *et al.*, 1998). This difference in the regulation of $[Ca^{2+}]_i$ could be explained by the type of neurones, since functional differences in the regulation of $[Ca^{2+}]_i$ were suggested between neurones from the central and the peripheral nervous system (see Kostyuck & Verkhratsky, 1995c for review).

Above $[Ca^{2+}]_i \approx 800$ nM, the PMCA contribution to the overall Ca^{2+} clearance decreases to represent only ≈ 23% at $[Ca^{2+}]_i \approx 1.5$ μM (see *Table* in *figure 54*). The determination of the role of SERCA in the regulation of $[Ca^{2+}]_i$ indicates that Ca^{2+} store might be partially filled (≈ 80 % in sensory neurones, Shmigol *et al.*, 1994b) and that above ≈ 300 nM the clearance rate increases linearly with the rise in $[Ca^{2+}]_i$, since the SERCA contribution remains constant ≈ 36% (see *figure 54*). Such a result would imply that the net ER Ca^{2+} transport is constant and that SERCA are not saturated for $[Ca^{2+}]_i$ up to 1.5 μM. This observation in SCG neurones is in agreement with the previously reported activity of SERCA in rat cerebellar Purkinje neurones that suggested no SERCA saturation in the micromolar range (Fierro *et al.*, 1998). The determination of the Ca^{2+} handling by the intracellular stores suggested that, most of the Ca^{2+} released through RyR was re-sequestered into the ER and that there was a constant Ca^{2+} leak into the cytosol (see *figures 29* and *30*). Furthermore, the Ca^{2+} store is thought to be, at least, partially filled with Ca^{2+} (Pozzan *et al.*, 1994; Garaschuk *et al.*, 1997 and Usachev & Thayer, 1999b) and the SERCA activity to be inhibited by a high $[Ca^{2+}]_L$ (Inesi & de Meis, 1989; Favre *et al.*, 1996 and Mogami *et al.*, 1998) presumably by the direct binding of calreticulin (John *et al.*, 1998) or calnexin (Roderick *et al.*, 2000). Therefore, it is tempting to consider that the constant clearance rate observed for $[Ca^{2+}]_i \geq 500$ nM is the result of Ca^{2+} being released from and subsequently re-sequestered into Ca^{2+} store before being progressively extruded *via* NCX at high $[Ca^{2+}]_i$ and through PMCA when $[Ca^{2+}]_i$ decreases to lower levels.

In contrast, NCX becomes the predominant Ca^{2+} extrusion system for high $[Ca^{2+}]_i$ and its contribution increases with $[Ca^{2+}]_i$ (see *figure 42*). Thus ≈ 60% of the Ca^{2+} clearance rate appears to be mediated through this exchanger at $[Ca^{2+}]_i \approx 1.5$ μM (see Table in *figure 54*). The increased contribution of NCX with the rise in $[Ca^{2+}]_i$ is both in agreement with the reported Ca^{2+} affinity of the exchanger ($K_d \approx 750$ nM; Philipson and Nicoll, 2000) and with the properties of an exchanger since the increase in $[Ca^{2+}]_i$ is

expected to promote the efflux mode of NCX. Similar observations were reported in several other cell types and suggested that NCX activity is non-saturable at least in the range of physiological $[Ca^{2+}]_i$ (Herrington *et al.*, 1996; Fierro *et al.*, 1998). The plot of the clearance rate suggests that PMCA and NCX work in parallel between 500 and 800 nM. This results is further supported by the observations that following PMCA inhibition, the rise in $[Ca^{2+}]_i$ is limited *via* NCX activity whereas a Ca^{2+} influx forced by NCX working in the reverse mode is counter-balanced by Ca^{2+} extrusion through PMCA (see Results section 6 *figure 43*). These observations firstly indicate that NCX is capable, even at a slow rate, to extrude Ca^{2+} at $[Ca^{2+}]_i$ as low as 300-400 nM and secondly emphasise the co-operativity of the different system involved in the regulation of $[Ca^{2+}]_i$. Thus, for a $[Ca^{2+}]_i \approx 500$ nM the control of $[Ca^{2+}]_i$ is the most efficient since several system are simultaneously active (*figure 54*).

4. Clearance of depolarisation-induced calcium transients

The determination of the regulation of $[Ca^{2+}]_i$ following depolarisation-induced Ca^{2+} transients has indicated that the mechanisms involved in the recovery would depend on the amplitude of the rise in $[Ca^{2+}]_i$. Since the critical $[Ca^{2+}]_i$, *i.e.* $[Ca^{2+}]_i$ at which the recovery switches from a monoexponential to a biexponential decay, appears to be $\approx$ 500 nM, two different models are proposed to described the mechanisms involved in the regulation of $[Ca^{2+}]_i$. Although, $[Ca^{2+}]_i$ is increased by the plasma membrane depolarisation, one might consider that the processes described for the maintenance of resting $[Ca^{2+}]_i$ (see *figure 53* above) might still be active in parallel to the processes involved in the recovery from Ca^{2+} transients.

4.1. Calcium clearance of small rises in intracellular calcium

Following a short depolarisation (60 ms in the presented experiments) that might correspond to a short train of action potentials, Ca^{2+} would enter the cytosol through VACCs and would be strongly buffered by cytosolic CaBPs so that only 1 out of 1000 Ca^{2+} ions would remain in the ionised form (see *figure 21* and blue arrow in *figure 55*). With the rise in $[Ca^{2+}]_i$, the PMCA activity would be stimulated and Ca^{2+} extruded back into the extracellular medium (see *figure 35*, green arrow in *figure 55* and in inset). Since, studies of the tissue distribution for PMCA suggested that isoform 1

and 4 would be responsible for the house keeping Ca^{2+} regulation whereas isoform 2 and 3 would exhibit more specialised functions, one could proposed that the latter PMCA isoforms might be responsible for extrusion of Ca^{2+} following the depolarisation. At this low $[Ca^{2+}]_i$, as supported from the plot of the clearance rate illustrated in *figure 54*, PMCA appears to be the major clearance mechanism involved in the control of $[Ca^{2+}]_i$ (see *figure 35*). It was further suggested that Ca^{2+} extrusion through PMCA would start in parallel with the rise in $[Ca^{2+}]_i$ (Tepikin *et al.*, 1991, 1992). Since the mitochondrial uncoupling with protonophores accelerated the recovery from small Ca^{2+} transients (see *figure 26*), one could suggest that at this low $[Ca^{2+}]_i$ mitochondria might be active in the regulation of $[Ca^{2+}]_i$. Thus, following the rise in $[Ca^{2+}]_i$, Ca^{2+} would be sequestered into the mitochondria *via* *m*CU (see 1 in *figure 55* and inset) and since at this low $[Ca^{2+}]_i$ the net mitochondrial Ca^{2+} flux is close to the set-point (≈ 200 nM as suggested from *figure 24-A*), Ca^{2+} would be released from the mitochondrial matrix. With the Ca^{2+} extrusion through PMCA, $[Ca^{2+}]_i$ would decrease and less Ca^{2+} would be sequestered into the mitochondria so that the $[Ca^{2+}]$ in the matrix would progressively return to the resting level. Surprisingly, the removal of intracellular Na^+ in SCG neurones did not affect the recovery of these small Ca^{2+} transients suggesting the involvement of a Na^+-independent mechanism (see *figure 28*). Murchison and colleagues (2000) as well as Montero and colleagues (2000) suggested that Ca^{2+} could be released under physiological condition either *via* *m*CU working in the reverse mode (Murchison *et al.*, 2000) or the MPTP (see 2 in *figure 55*). It is therefore tempting to propose that such a mitochondrial Ca^{2+} release might occur in SCG neurones. However, this is only speculative since further experiments using selective inhibitors for *m*CU and/or MPTP would be necessary to confirm this assumption.

4.2. Calcium clearance of large rises in intracellular calcium

For larger rise in $[Ca^{2+}]_i$ that would correspond to prolonged cellular stimulation, $[Ca^{2+}]_i$ would rise in the micromolar range and invade the cytosol. Since the Ca^{2+} influx through VACCs is larger, the endogenous buffer might be partially saturated and therefore the amount of free cytosolic Ca^{2+} would increase (4/1000 from *figure 21*; blue arrow in *figure 56*). During the rising phase of the Ca^{2+} transient, Ca^{2+} would be

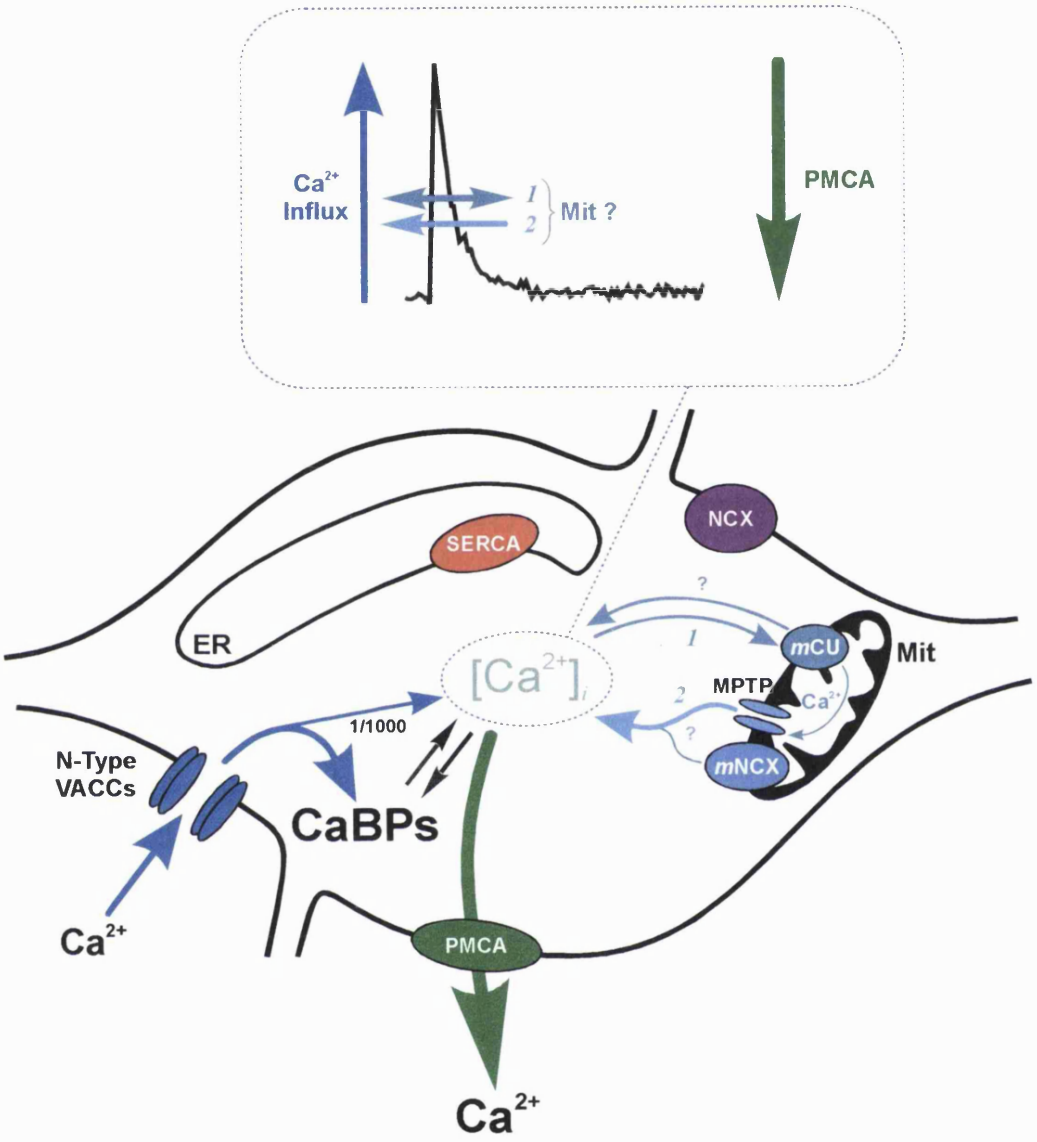

Figure 55: A model for the calcium clearance from small rises in intracellular calcium

Representation of the different mechanisms involved in the recovery from small Ca^{2+} transients (<500 nM). The inset represents a typical Ca^{2+} transient elicited by a 60 ms depolarisation step from -60 mV to 0 mV. The arrows symbolise either Ca^{2+} influx/release (upward arrows) or Ca^{2+} clearance (downward arrows).

N-Type voltage-activated Ca^{2+} channels (N-Type VACCs); cytosolic Ca^{2+} binding proteins (CaBPs); cytosolic free Ca^{2+} concentration ($[Ca^{2+}]_i$); plasma membrane Ca^{2+}-ATPase (PMCA, endoplasmic reticulum (ER); sarco/endoplasmic Ca^{2+}-ATPase (SERCA); mitochondria (Mit); Ca^{2+} uniporter (*m*CU); mitochondrial permeability transition pore (MPTP); mitochondrial Na^{+}/Ca^{2+} exchanger (*m*NCX) and plasma membrane Na^{+}/Ca^{2+} exchanger (NCX).

primarily sequestered into mitochondria *via* the *m*CU activated through the rise in $[Ca^{2+}]_i$ (see *figure 24, 23* and 1 in *figure 56*) that would both limit the rise in $[Ca^{2+}]_i$ and promote Ca^{2+} clearance. The high $[Ca^{2+}]_i$ would activate both Ca^{2+} extrusion through NCX (*figure 42*-C and violet arrow in *figure 56*) and Ca^{2+} sequestration into the ER *via* SERCA (*figures 31-C, 32-C* and orange arrow in *figure 56*). At these high $[Ca^{2+}]_i$, PMCA would only play a minor role in the Ca^{2+} extrusion. (*figures 37, 38* and green arrow in *figure 56*). Since SCG neurones posses functional ryanodine-sensitive stores that have been shown to be at least partially filled, one might suggest that the Ca^{2+} influx or the high $[Ca^{2+}]_i$ would trigger a Ca^{2+} release, also known as CICR, from the intracellular stores *via* ryanodine receptors (RyR). However, from the experimental data there is no evidence for such a mechanism. Nevertheless, one could propose that, although Ca^{2+} store contain Ca^{2+}, the intracellular stores need to be saturated with Ca^{2+} in order to enable Ca^{2+} release similarly to the situation observed in most central neurones (Shmigol *et al.*, 1994b). The fact that SERCA or RyR inhibition had only little effect on the properties of large Ca^{2+} transients (see *figure 37 and 38*) suggesting the absence of CICR-like process in SCG neurones is surprising since in rat sensory neurones CICR was triggered for rise in $[Ca^{2+}]_i \approx 200$ nM (Usachev & Thayer, 1997). With the decrease in $[Ca^{2+}]_i$ the NCX contribution in the overall Ca^{2+} clearance would be progressively reduced to be close to zero for $[Ca^{2+}]_i$ below 500 nM (see *figures 42, 43* and *54*). On the other hand, PMCA would progressively become the major Ca^{2+} extrusion system (see *figures 35* and *54*) while SERCA would still take part in the reduction of $[Ca^{2+}]_i$ by sequestering Ca^{2+} (see *figures 31, 32* and *54*). As $[Ca^{2+}]_i$ reaches $\approx$ 200-300 nM, NCX would be inactive, SERCA at its basal activity and PMCA would be the only Ca^{2+} clearance system in operation (see inset in *figure 56*). However, the net mitochondrial Ca^{2+} flux would now be outward (see *figure 24* and *25*) and Ca^{2+} would be primarily released from mitochondria through the mitochondrial NCX (*m*NCX; 2 in *figure 56*). Typically, this mitochondrial Ca^{2+} release would induce a prolonged plateau phase that would delay the recovery as PMCA progressively extrude the Ca^{2+} released from the mitochondrial matrix. The recovery from small Ca^{2+} transients suggested the involvement of a Na^+-independent mitochondrial Ca^{2+} release (see General Discussion section 4.1), therefore one might propose that at low $[Ca^{2+}]_i$ a similar mechanism

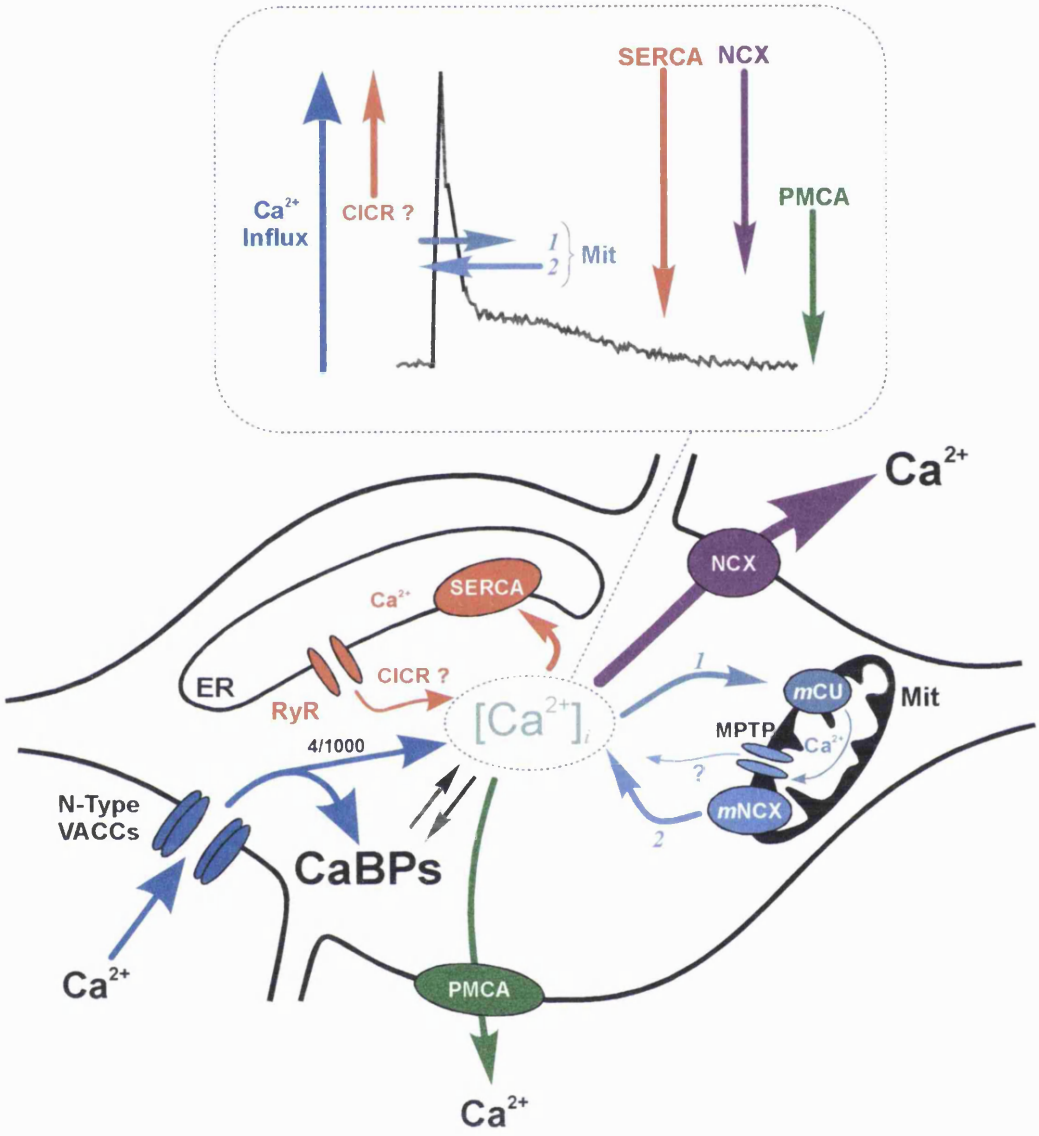

Figure 56: A model for the calcium clearance from large rises in intracellular calcium

Representation of the different mechanisms involved in the recovery from a large Ca^{2+} transients (>500 nM). The inset represents a typical Ca^{2+} transient elicited by a 500 ms depolarisation step from -60 mV to 0 mV. The arrows symbolise either Ca^{2+} influx/release (upward arrows) or Ca^{2+} clearance (downward arrows).

N-Type voltage-activated Ca^{2+} channels (N-Type VACCs); cytosolic Ca^{2+} binding protein (CaBPs); cytosolic free Ca^{2+} concentration ($[Ca^{2+}]_i$); plasma membrane Ca^{2+}-ATPase (PMCA); endoplasmic reticulum (ER); sarco/endoplasmic Ca^{2+}-ATPase (SERCA); ryanodine receptor (RyR); Ca^{2+} induced Ca^{2+} release (CICR); mitochondria (Mit); Ca^{2+} uniporter (*m*CU); mitochondrial permeability transition pore (MPTP); mitochondrial Na^{+}/Ca^{2+} exchanger (*m*NCX) and plasma membrane Na^{+}/Ca^{2+} exchanger (NCX).

might exist during the recovery of larger Ca^{2+} transients. With $[Ca^{2+}]_i$ close to its resting value all the components of Ca^{2+} homeostasis would be back to their basal activity.

5. Conclusion

For more simplicity, two separate Ca^{2+} clearance processes depending on the amplitude of the rise in $[Ca^{2+}]_i$ have been considered and the involvement of each mechanism has been described sequentially. However, Ca^{2+} homeostasis is a dynamic process and the different systems would operate simultaneously and only the net effect would be observed.

One of the major results described in the present study is the predominant role for PMCA in both the regulation of resting $[Ca^{2+}]_i$ but more importantly in the Ca^{2+} clearance for $[Ca^{2+}]_i$ rises as high as 500 nM. Another important observation is the presence in SCG neurones of an passive Ca^{2+} influx that appears to be both involved in the maintenance of resting $[Ca^{2+}]_i$ and in the 'refilling' of the Ca^{2+} store. This result appears even more important since, in neurones, only one other study has described such a passive Ca^{2+} influx at rest (Usachev & Thayer, 1999b). In agreement with numerous studies in peripheral neurones, the characterisation of the Ca^{2+} clearance *via* NCX confirms that this exchanger is only substantially active for rises in the micromolar range (≥1 μM). However, the characterisation of the NCX contribution to the Ca^{2+} clearance has indicated that this exchanger is capable of substantial Ca^{2+} extrusion at low $[Ca^{2+}]_i$ (< 500 nM) particularly when PMCA is inhibited. Such a result supports the concept that a system normally inactive at a particular $[Ca^{2+}]_i$ could be activated to compensate the inactivation of another. Finally, the determination of $[Ca^{2+}]_i$ regulation by mitochondria further supports the growing evidence for a primordial mitochondrial role in Ca^{2+} homeostasis in neurones at physiological $[Ca^{2+}]_i$.

In conclusion, this study emphasises the complexity of Ca^{2+} homeostasis and demonstrates the co-operativity and complementarity of the mechanisms involved in the regulation of $[Ca^{2+}]_i$ to ensure the strict control of the level of free Ca^{2+} in a cell. Such a precise control and regulation of $[Ca^{2+}]_i$ would be a prerequisite for allowing a cell to integrate the relevant information from its environment and to relay them into the different intracellular organelles to enable an adequate cellular response. The idea of a

tight regulation of $[Ca^{2+}]_i$ appears even more relevant in neurones where Ca^{2+} responses need to be restricted to specialised compartment in order to provided efficient coding of the synaptic inputs. Disturbances in the Ca^{2+} handling are known to have dramatic consequences for the cellular activity and on a larger scale to impair the normal functions of an organism (see Missiaen *et al.*, 2000 for review). The characterisation of the different actors involved in Ca^{2+} homeostasis and the better understanding of their interaction to control $[Ca^{2+}]_i$ would probably result in a better comprehension of the pathology caused by a deficient regulation of Ca^{2+} homeostasis.

6. Future directions

From the results presented throughout the present study, the major components of Ca^{2+} homeostasis involved in the regulation of $[Ca^{2+}]_i$ have been described. The overall recovery process can be dissected into three principal components: one representing the Ca^{2+} buffering, the second corresponding to the extrusion processes mainly through PMCA and the third involving intracellular organelles (mitochondria and Ca^{2+} store). Using experimental data describing the clearance rates of the different Ca^{2+} regulatory processes, a mathematical model could be developed to determine if they are sufficient to account for the time course of the recovery from weak and strong stimuli. Further, such analytical study would enable a better understanding of the interactions between the mechanisms that control $[Ca^{2+}]_i$ and also to describe how the defect of one of these systems would perturb Ca^{2+} homeostasis.

From the present work, several questions have arisen, which focuses firstly on the regulation of the expression of the systems involved in Ca^{2+} homeostasis and in the involvement of intracellular organelles in the control of $[Ca^{2+}]_i$.

- Regulation of PMCA expression and activity?

The level of expression of PMCAs has been shown to change during development (Guerini *et al.*, 1999). Therefore, it would be interesting to determine, in SCG neurones, how the expression of PMCA varies during cellular activity and with ageing and how eventual modifications would affect the regulation of $[Ca^{2+}]_i$. Such a study could be carried out by combining functional recording of $[Ca^{2+}]_i$ regulation with molecular biological experiments and particularly single cell PCR. Since, numerous

neurodegenerative diseases, especially motoneurones diseases, are caused by perturbations of Ca^{2+} homeostasis. The results obtained in such investigation might help to understand the modifications that occur during neurodegeneration and could allow the development of new therapy.

PMCA is a highly regulated protein particularly through acidic phospholipids and long-chain polyunsaturated fatty acid as well as by phosphorylation processes and CaM. The mechanisms underlying such a regulation of PMCA activity could be determined by investigating how intracellular transducing pathways would modify Ca^{2+} clearance through PMCA-dependent mechanisms. Preliminary results (Marsh & Wanaverbecq, unpublished observations and see Benham *et al.*, 1992) have indicated that CaM inhibition with calmidazolium induced both a rise in $[Ca^{2+}]_i$ and a delay in the Ca^{2+} clearance. Further, experiments would allow determining which mechanisms are involved in this regulatory process with a particular attention given to the activation of muscarinic receptor expressed in SCG neurones.

- Calcium clearance through the mitochondria at low $[Ca^{2+}]_i$?

The results presented for the mitochondrial regulation of $[Ca^{2+}]_i$ suggested the involvement of a Na^+-independent Ca^{2+}release at low $[Ca^{2+}]_i$. This result would be in agreement with earlier work (Petronilli *et al.*, 1999; Murchison & Griffith, 2000 and Montero *et al.*, 2000). It would be interesting to investigate further this mechanism especially by using specific inhibitors of *m*CU and of PMTP to demonstrate their possible involvement in the observed Ca^{2+}release.

- Calcium-induced Ca^{2+} release?

Although SCG neurones posses strong caffeine-sensitive response and have been shown to express functional RyR, no experimental evidence are available for a CICR mechanism. Cyclic ADPr has been proposed to correspond to the endogenous agonist of RyR and to be able to potentiate Ca^{2+} release from intracellular stores. Higashida and colleagues showed in neuroblastoma cells NG108-15 that adrenergic and muscarinic receptors were capable of activating ADP-rybosyl cyclase and to potentiate CICR (Hashii *et al.*, 2000 and Higashida *et al.*, 2000). Since SCG neurones express both muscarinic and adrenergic receptors along with functional RyR, it would be interesting to study the role of cADPr in Ca^{2+} regulation. Firstly, the effects on Ca^{2+} release of

cADPr injection into the neurones cytoplasm could be determined. Secondly, the presence of a functional transducing pathway from the receptor activation to the production of cADPr could be investigated. Finally, it has been suggested that neurones in culture would exhibit different properties than *in situ* that might explain the absence of CICR process in dissociated SCG neurones. Therefore, a study using recording from neurones in SCG slices could be carried out to determine if the absence of CICR in the presented data might be due to the down regulation of functional transducing pathways by lack of synaptic input.

- Resting free Ca^{2+} concentration?

The data presented in Results section 7 indicated that resting $[Ca^{2+}]_i$ is partly maintained by a Ca^{2+} influx through the plasma membrane that exhibit characteristic related to SOCC. Therefore, further experiments would be necessary to determine the nature of the channel mediating the observed passive Ca^{2+} influx and the mechanisms involved in their regulation. Members of the TRP channels (TRP3, Boulay *et al.*, 1999; Kiselyov *et al.*, 2000) have been suggested to mediate a store-operated Ca^{2+} influx but also to be activated by several other messengers (see Clapham *et al.*, 2001 for review). Therefore, it would be interesting to determine using PCR analysis if TRP channels are expressed in SCG neurones and if they are involved in the passive Ca^{2+}influx observed at rest. Secondly, the mechanisms by which these channels are regulated would be investigated.

The work presented in this thesis was supported by
the *UK Medical Research Council* and the *Wellcome Trust.*

Chapter V

References

AARHUS, R., DICKEY, D.M., GRAEFF, R.M., GEE, K.R., WALSETH, T.F. & LEE, H.C. (1996). Activation and inactivation of Ca^{2+} release by $NAADP^{+}$. *J. Biol. Chem.* **271**, 8513-8516.

ADKINS, C.E. & TAYLOR, C.W. (1999). Lateral inhibition of inositol 1,4,5-trisphosphate receptors by cytosolic Ca^{2+}. *Curr. Biol.* **9**, 1115-1118.

ADUNYAH, E.S., NIGGLI, V. & CARAFOLI, E. (1982). The anticalmodulin drugs trifluoperazine and R24571 remove the activation of the purified erythrocyte Ca^{2+}-ATPase by acidic phospholipids and by controlled proteolysis. *FEBS Lett.* **143**, 65-68.

AGARD, D.A., HIRAOKA, Y., SHAW, P. & SEDAT, J.W. (1989). Fluorescence microscopy in three dimensions. *Methods Cell Biol.* **30**, 353-377.

AHMED, Z. & CONNOR, J.A. (1988). Calcium regulation by and buffer capacity of molluscan neurons during calcium transients. *Cell Calcium* **9**, 57-69.

AIRAKSINEN, M.S., EILERS, J., GARASCHUK, O., THOENEN, H., KONNERTH, A. & MEYER, M. (1997). Ataxia and altered dendritic calcium signaling in mice carrying a targeted null mutation of the calbindin D_{28k} gene. *Proc. Natl. Acad. Sci. U.S.A* **94**, 1488-1493.

AKERMAN, K.E. (1978). Measurements of membrane potentials using the dye safranine. *Microsc. Acta* **81**, 147-153.

AKITA, T. & KUBA, K. (2000). Functional triads consisting of ryanodine receptors, Ca^{2+} channels, and Ca^{2+}-activated K^{+} channels in bullfrog sympathetic neurons. Plastic modulation of action potential. *J. Gen. Physiol.* **116**, 697-720.

AL SHAIKHALY, M.H., NEDERGAARD, J. & CANNON, B. (1979). Sodium-induced calcium release from mitochondria in brown adipose tissue. *Proc. Natl. Acad. Sci. U.S.A* **76**, 2350-2353.

ALBRECHT, M.A., COLEGROVE, S.L., HONGPAISAN, J., PIVOVAROVA, N.B., ANDREWS, S.B. & FRIEL, D.D. (2001). Multiple modes of calcium-induced calcium release in sympathetic neurons I: attenuation of endoplasmic reticulum Ca^{2+} accumulation at low $[Ca^{2+}]_i$ during weak depolarization. *J. Gen. Physiol.* **118**, 83-100.

ALLEN, T.J. & BAKER, P.F. (1985). Intracellular Ca indicator Quin-2 inhibits Ca^{2+} inflow via Na^{+}/Ca^{2+} exchange in squid axon. *Nature* **315**, 755-756.

ALLEN, T.J. & BAKER, P.F. (1986). Influence of membrane potential on calcium efflux from giant axons of Loligo. *J. Physiol. Lond.* **378**, 77-96.

ANDERSEN, J.P. & VILSEN, B. (1998). Structure-function relationships of the calcium binding sites of the sarcoplasmic reticulum Ca^{2+}-ATPase. *Acta Physiol. Scand. Suppl.* **643**, 45-54.

ANDREEVA, N., KHODOROV, B., STELMASHOOK, E., CRAGOE, E. & VICTOROV, I. (1991). Inhibition of Na^{+}/Ca^{2+} exchange enhances delayed neuronal death elicited by glutamate in cerebellar granule cell cultures. *Brain Res.* **548**, 322-325.

ARMISEN, R., SIERRALTA, J., VELEZ, P., NARANJO, D. & SUAREZ-ISLA, B.A. (1996). Modal gating in neuronal and skeletal muscle ryanodine-sensitive Ca^{2+} release channels. *Am. J. Physiol.* **271**, C144-C153

ASHBY, M.C. & TEPIKIN, A.V. (2001). ER calcium and the functions of intracellular organelles. *Semin. Cell Dev. Biol.* **12**, 11-17.

ASHLEY, R.H. (1989). Activation and conductance properties of ryanodine-sensitive calcium channels from brain microsomal membranes incorporated into planar lipid bilayers. *J. Membr. Biol.* **111**, 179-189.

AUBIER, M. & VIIRES, N. (1998). Calcium ATPase and respiratory muscle function. *Eur. Respir. J.* **11**, 758-766.

BABCOCK, D.F., HERRINGTON, J., GOODWIN, P.C., PARK, Y.B. & HILLE, B. (1997). Mitochondrial participation in the intracellular Ca^{2+} network. *J. Cell. Biol.* **136**, 833-844.

BADING, H., GINTY, D.D. & GREENBERG, M.E. (1993). Regulation of gene expression in hippocampal neurons by distinct calcium signaling pathways. *Science* **260**, 181-186.

BAIMBRIDGE, K.G., CELIO, M.R. & ROGERS, J.H. (1992). Calcium-binding proteins in the nervous system. *Trends Neurosci.* **15**, 303-308.

BAK, J., WHITE, P., TIMAR, G., MISSIAEN, L., GENAZZANI, A.A. & GALIONE, A. (1999). Nicotinic acid adenine dinucleotide phosphate triggers Ca^{2+} release from brain microsomes. *Curr. Biol.* **9**, 751-754.

BAKEEVA, L.E., CHENTSOV, Y. & SKULACHEV, V.P. (1978). Mitochondrial framework (reticulum mitochondriale) in rat diaphragm muscle. *Biochim. Biophys. Acta* **501**, 349-369.

BAKER, P.F., BLAUSTEIN, M.P., HODGKIN, A.L. & STEINHARDT, R.A. (1969). The influence of calcium on sodium efflux in squid axons. *J. Physiol. Lond.* **200**, 431-458.

BAKER, P.F. & GLITSCH, H.G. (1973). Does metabolic energy participate directly in the Na^+-dependent extrusion of Ca^{2+} ions from squid giant axons? *J. Physiol. Lond.* **233**, 44P-46P.

BAKER, P.F. & DIPOLO, R. (1984). Axonal calcium and magnesium homeostasis. *Curr. Topics Membr. Transp.* **22**, 95-147.

BAKER, P.F. & UMBACH, J.A. (1987). Calcium buffering in axons and axoplasm of Loligo. *J. Physiol. Lond.* **383**, 369-394.

BAKER, A.J., BRANDES, R., SCHREUR, J.H., CAMACHO, S.A. & WEINER, M.W. (1994). Protein and acidosis alter calcium-binding and fluorescence spectra of the calcium indicator indo-1. *Biophys. J.* **67**, 1646-1654.

BALSHAW, D.M., XU, L., YAMAGUCHI, N., PASEK, D.A. & MEISSNER, G. (2001). Calmodulin binding and inhibition of cardiac muscle calcium release channel (ryanodine receptor). *J. Biol. Chem.* **276**, 20144-20153.

BARON, K.T. & THAYER, S.A. (1997). CGP37157 modulates mitochondrial Ca^{2+} homeostasis in cultured rat dorsal root ganglion neurons. *Eur J.Pharmacol* **340**, 295-300.

BASSANI, R.A., BASSANI, J.W. & BERS, D.M. (1995). Relaxation in ferret ventricular myocytes: role of the sarcolemmal Ca^{2+}-ATPase. *Pflugers Arch.* **430**, 573-578.

BEAN, B.P. (1989). Classes of calcium channels in vertebrate cells. *Annual Reviews in Physiology* **51**, 367-384.

BEATRICE, M.C., STIERS, D.L. & PFEIFFER, D.R. (1982). Increased permeability of mitochondria during Ca^{2+} release induced by t-butyl hydroperoxide or oxalacetate. the effect of ruthenium red. *J.Biol. Chem.* **257**, 7161-7171.

BELAN, P., KOSTYUK, P., SNITSAREV, V. & TEPIKIN, A. (1993a). Calcium clamp in isolated neurones of the snail Helix pomatia. *J. Physiol. Lond.* **462**, 47-58.

BELAN, P.V., KOSTYUK, P.G., SNITSAREV, V.A. & TEPIKIN, A.V. (1993b). Calcium clamp in single nerve cells. *Cell Calcium* **14**, 419-425.

BENHAM, C.D. (1989). Voltage-gated and agonist-mediated rises in intracellular Ca^{2+} in rat clonal pituitary cells (GH3) held under voltage clamp. *J. Physiol. Lond.* **415**, 143-158.

BENHAM, C.D., EVANS, M.L. & McBAIN, C.J. (1992). Ca^{2+} efflux mechanisms following depolarization evoked calcium transients in cultured rat sensory neurones. *J. Physiol. Lond.* **455**, 567-583.

BERNARDI, P. & AZZONE, G.F. (1979). delta pH induced calcium fluxes in rat liver mitochondria. *Eur. J. Biochem.* **102**, 555-562.

BERNARDI, P. & PETRONILLI, V. (1996). The permeability transition pore as a mitochondrial calcium release channel: a critical appraisal. *J. Bioenerg. Biomembr.* **28**, 131-138.

BERNARDI, P. (1999). Mitochondrial transport of cations: channels, exchangers, and permeability transition. *Physiol. Rev.* **79**, 1127-1155.

BERRIDGE, M.J. (1993). Cell signalling. A tale of two messengers. *Nature* **365**, 388-389.

BERRIDGE, M.J. (1995). Capacitative calcium entry. *Biochem. J.* **312(1)**, 1-11.

BERRIDGE, M.J. (1998). Neuronal calcium signaling. *Neuron* **21**, 13-26.

BERRIDGE, M.J., LIPP, P. & BOOTMAN, M.D. (2000). Signal transduction. The calcium entry pas de deux. *Science* **287**, 1604-1605.

BEZPROZVANNY, I., WATRAS, J. & EHRLICH, B.E. (1991). Bell-shaped calcium-response curves of Ins(1,4,5)P3- and calcium-gated channels from endoplasmic reticulum of cerebellum. *Nature* **351**, 751-754.

BIRDSALL, W.J., LEVINE, B.A., WILLIAMS, R.J., DEMAILLE, J.G., HAIECH, J. & PECHERE, J.F. (1979). Calcium and magnesium binding by parvalbumin. A proton magnetic resonance spectral study. *Biochimie* **61**, 741-750.

BIRNBAUMER, L., CAMPBELL, K.P., CATTERALL, W.A., HARPOLD, M.M., HOFMANN, F., HORNE, W.A., MORI, Y., SCHWARTZ, A., SNUTCH, T.P., TANABE, T. & TSIEN, R.W. (1994). The naming of voltage-gated calcium channels. *Neuron* **13**, 505-506.

BLAUSTEIN, M.P. & SANTIAGO, E.M. (1977). Effects of internal and external cations and of ATP on sodium-calcium and calcium-calcium exchange in squid axons. *Biophys. J.* **20**, 79-111.

BLAUSTEIN, M.P. (1988a). Calcium transport and buffering in neurons. *Trends.Neurosci* **11**, 438-443.

BLAUSTEIN, M.P. (1988b). Sodium/calcium exchange and the control of contractility in cardiac muscle and vascular smooth muscle. *J.Cardiovasc.Pharmacol* **12(5)**, S56-S68.

BLAUSTEIN, M.P. & LEDERER, W.J. (1999). Sodium/calcium exchange: its physiological implications. *Physiol.Rev.* **79**, 763-854.

BOOTMAN, M.D. & LIPP, P. (1999). Ringing changes to the 'bell-shaped curve'. *Curr.Biol.* **9**, R876-R878

BOOTMAN, M.D., COLLINS, T.J., PEPPIATT, C.M., PROTHERO, L.S., MACKENZIE, L., DE SMET, P., TRAVERS, M., TOVEY, S.C., SEO, J.T., BERRIDGE, M.J., CICCOLINI, F. & LIPP, P. (2001). Calcium signalling--an overview. *Semin.Cell Dev.Biol.* **12**, 3-10.

BORKE, J.L., CARIDE, A., VERMA, A.K., KELLEY, L.K., SMITH, C.H., PENNISTON, J.T. & KUMAR, R. (1989). Calcium pump epitopes in placental trophoblast basal plasma membranes. *Am. J. Physiol.* **257**, C341-C346.

BORST, J.G., HELMCHEN, F. & SAKMANN, B. (1995). Pre- and postsynaptic whole-cell recordings in the medial nucleus of the trapezoid body of the rat. *J. Physiol. Lond.* **489(3)**, 825-840.

BOULAY, G., BROWN, D.M., QIN, N., JIANG, M., DIETRICH, A., ZHU, M.X., CHEN, Z., BIRNBAUMER, M., MIKOSHIBA, K. & BIRNBAUMER, L. (1999). Modulation of Ca^{2+} entry by polypeptides of the inositol 1,4, 5-trisphosphate receptor (IP_3R) that bind transient receptor potential (TRP): evidence for roles of TRP and IP3R in store depletion-activated Ca^{2+} entry. *Proc. Natl. Acad. Sci. U.S.A* **96**, 14955-14960.

BRAND, M.D. & de SELINCOURT, C. (1980). Effects of glucagon and Na^+ on the control of extramitochondrial free Ca^{2+} concentration by mitochondrial from liver and heart. *Biochem. Biophys. Res. Commun.* **92**, 1377-1382.

BRAND, M.D. (1985). The stoichiometry of the exchange catalysed by the mitochondrial calcium/sodium antiporter. *Biochem. J.* **229**, 161-166.

BRANDL, C.J., GREEN, N.M., KORCZAK, B. & McLENNAN, D.H. (1986). Two Ca^{2+}-ATPase genes: homologies and mechanistic implications of deduced amino acid sequences. *Cell* **44**, 597-607.

BRANDT, P. & NEVE, R.L. (1992). Expression of plasma membrane calcium-pumping ATPase mRNAs in developing rat brain and adult brain subregions: evidence for stage-specific expression. *J.Neurochem* **59**, 1566-1569.

BRINI, M., BANO, D., MANNI, S., RIZZUTO, R. & CARAFOLI, E. (2000). Effects of PMCA and SERCA pump overexpression on the kinetics of cell Ca^{2+} signalling. *EMBO J.* **19**, 4926-4935.

BROWN, D.A. (1990). Regulation of cell excitability. *Curr. Opin. Cell Biol.* **2**, 221-230.

BRUNS, D.E., KRISHNAN, A.V., FELDMAN, D., GRAY, R.W., CHRISTAKOS, S., HIRSCH, G.N. & BRUNS, M.E. (1989). Epidermal growth factor increases intestinal calbindin-D9k and 1,25-dihydroxyvitamin D receptors in neonatal rats. *Endocrinology* **125**, 478-485.

BRUSTOVETSKY, N. & KLINGENBERG, M. (1996). Mitochondrial ADP/ATP carrier can be reversibly converted into a large channel by Ca^{2+}. *Biochemistry* **35**, 8483-8488.

BUDD, S.L. (1998). Mechanisms of neuronal damage in brain hypoxia/ischemia: focus on the role of mitochondrial calcium accumulation. *Pharmacol. Ther.* **80**, 203-229.

BURK, S.E. & SHULL, G.E. (1992). Structure of the rat plasma membrane Ca^{2+}-ATPase isoform 3 gene and characterization of alternative splicing and transcription products. Skeletal muscle-specific splicing results in a plasma membrane Ca^{2+}-ATPase with a novel calmodulin-binding domain. *J. Biol. Chem.* **267**, 19683-19690.

BURK, S.E., LYTTON, J., MACLENNAN, D.H. & SHULL, G.E. (1989). cDNA cloning, functional expression, and mRNA tissue distribution of a third organellar Ca^{2+} pump. *J. Biol. Chem.* **264** , 18561-18568.

BUSH, K.T., STUART, R.O., LI, S.H., MOURA, L.A., SHARP, A.H., ROSS, C.A. & NIGAM, S.K. (1994). Epithelial inositol 1,4,5-trisphosphate receptors. Multiplicity of localization, solubility, and isoforms. *J. Biol. Chem.* **269**, 23694-23699.

CAILLARD, O., MORENO, H., SCHWALLER, B., LLANO, I., CELIO, M.R. & MARTY, A. (2000). Role of the calcium-binding protein parvalbumin in short-term synaptic plasticity. *Proc. Natl. Acad. Sci. U.S.A* **97**, 13372-13377.

CARAFOLI, E. & SOTTOCASA, G.L. (1974). *Dynamics of energy-transducing membranes.* Amsterdam: Elseveir.

CARAFOLI, E., TIOZZO, R., LUGLI, G., CROVETTI, F. & KRATZING, C. (1974). The release of calcium from heart mitochondria by sodium. *J. Mol. Cell. Cardiol.* **6(4)**, 361-371.

CARAFOLI, E. (1975). Mitochondria, Ca^{2+} transport and the regulation of heart contraction and metabolism. *J. Mol. Cell Cardiol.* **7**, 83-87.

CARAFOLI, E. (1979). The calcium cycle of mitochondria. *FEBS Lett* **104**, 1-5.

CARAFOLI, E. (1982). The transport of calcium across the inner membrane of mitochondria. In *Membrane transport of calcium*, ed. CARAFOLI, E., pp. 107-139. New York: Academic Press.

CARAFOLI, E. (1987). Intracellular calcium homeostasis. *Annu.Rev.Biochem.* **56**, 395-433.

CARAFOLI, E. (1988). Intracellular calcium regulation, with special attention to the role of the plasma membrane calcium pump. *J. Cardiovasc. Pharmacol.* **12(3)**, S77-S84

CARAFOLI, E. & STAUFFER, T. (1994). The plasma membrane calcium pump: functional domains, regulation of the activity, and tissue specificity of isoform expression. *Neurobiol.* **25**, 312-324.

CARAFOLI, E. (1994). Biogenesis: plasma membrane calcium ATPase: 15 years of work on the purified enzyme. *FASEB J.* **8**, 993-1002.

CARAFOLI, E., GARCIA, M.E. & GUERINI, D. (1996). The plasma membrane calcium pump: recent developments and future perspectives. *Experientia* **52**, 1091-1100.

CARAFOLI, E. (2002). Calcium signaling: a tale for all seasons. *Proc. Natl. Acad. Sci. U S A* **99**, 1115-1122.

CARBONE, E. & SWANDULLA, D. (1989). Neuronal calcium channels: kinetics, blockade and modulation. *Prog. Biophys. Mol. Biol.* **54**, 31-58.

CARONI, P. & CARAFOLI, E. (1981). Regulation of Ca^{2+}-pumping ATPase of heart sarcolemma by a phosphorylation-dephosphorylation Process. *J. Biol. Chem.* **256**, 9371-9373.

CASSARINO, D.S., SWERDLOW, R.H., PARKS, J.K., PARKER, W.D. & BENNETT, J.P. (1998). Cyclosporin A increases resting mitochondrial membrane potential in SY5Y cells and reverses the depressed mitochondrial membrane potential of Alzheimer's disease cybrids. *Biochem. Biophys. Res. Commun.* **248**, 168-173.

CASTELEMAN, K.R. (1996). *Digital image processing.* Prentice Hall.

CAVIERES, J.D. (1984). Calmodulin and the target size of the (Ca^{2+}-Mg^{2+})-ATPase of human red-cell ghosts. *Biochim. Biophys. Acta* **771**, 241-244.

CELIO, M.R. (1990). Calbindin D_{28k} and parvalbumin in the rat nervous system. *Neuroscience* **35**, 375-475.

CHARD, P.S., BLEAKMAN, D., CHRISTAKOS, S., FULLMER, C.S. & MILLER, R.J. (1993). Calcium buffering properties of calbindin D_{28k} and parvalbumin in rat sensory neurones. *J. Physiol. Lond.* **472**, 341-357.

CHEN, S.R., ZHANG, L. & MACLENNAN, D.H. (1992). Characterization of a Ca^{2+} binding and regulatory site in the Ca^{2+} release channel (ryanodine receptor) of rabbit skeletal muscle sarcoplasmic reticulum. *J. Biol. Chem.* **267**, 23318-23326.

CHESLER, M. & KAILA, K. (1992). Modulation of pH by neuronal activity. *Trends. Neurosci.* **15**, 396-402.

CHEUNG, W.Y. (1970). Cyclic 3',5'-nucleotide phosphodiesterase. Demonstration of an activator. *Biochem. Biophys. Res. Commun.* **38**, 533-538.

CHIESI, M., SCHWALLER, R. & EICHENBERGER, K. (1988). Structural dependency of the inhibitory action of benzodiazepines and related compounds on the mitochondrial Na^{+}/Ca^{2+} exchanger. *Biochem. Pharmacol.* **37**, 4399-4403.

CHIN, D. & MEANS, A.R. (2000). Calmodulin: a prototypical calcium sensor. *Trends. Cell Biol.* **10**, 322-328.

CHINI, E.N., BEERS, K.W. & DOUSA, T.P. (1995). Nicotinate adenine dinucleotide phosphate (NAADP) triggers a specific calcium release system in sea urchin eggs. *J. Biol. Chem.* **270**, 3216-3223.

CHINI, E.N. & DOUSA, T.P. (1996). Nicotinate-adenine dinucleotide phosphate-induced Ca^{2+}-release does not behave as a Ca^{2+}-induced Ca^{2+}-release system. *Biochem. J.* **316 (3)**, 709-711.

CLAPHAM, D.E. & SNEYD, J. (1995). Intracellular calcium waves. *Adv. Second Messenger Phosphoprotein Res.* **30**, 1-24.

CLAPHAM, D.E., RUNNELS, L.W. & STRUBING, C. (2001). The TRP ion channel family. *Nat. Rev. Neurosci.* **2**, 387-396.

COCHILLA, A.J. & ALFORD, S. (1998). Metabotropic glutamate receptor-mediated control of neurotransmitter release. *Neuron* **20**, 1007-1016.

COLEGROVE, S.L., ALBRECHT, M.A. & FRIEL, D.D. (2000). Dissection of mitochondrial Ca^{2+} uptake and release fluxes in situ after depolarization-evoked $[Ca^{2+}]_i$ elevations in sympathetic neurons. *J. Gen. Physiol* **115**, 351-370.

COLL, K.E., JOSEPH, S.K., CORKEY, B.E. & WILLIAMSON, J.R. (1982). Determination of the matrix free Ca^{2+} concentration and kinetics of Ca^{2+} efflux in liver and heart mitochondria. *J. Biol. Chem.* **257**, 8696-8704.

CONDRESCU, M., GARDNER, J.P., CHERNAYA, G., ACETO, J.F., KROUPIS, C. & REEVES, J.P. (1995). ATP-dependent regulation of sodium-calcium exchange in Chinese hamster ovary cells transfected with the bovine cardiac sodium-calcium exchanger. *J. Biol. Chem.* **270**, 9137-9146.

COOK, O., LOW, W. & RAHAMIMOFF, H. (1998). Membrane topology of the rat brain Na^{+}-Ca^{2+} exchanger. *Biochim. Biophys. Acta* **1371**, 40-52.

COVERNTON, P.J., KOJIMA, H., SIVILOTTI, L.G., GIBB, A.J. & COLQUHOUN, D. (1994). Comparison of neuronal nicotinic receptors in rat sympathetic neurones with subunit pairs expressed in Xenopus oocytes. *J. Physiol. Lond.* **481(1)**, 27-34.

COX, D.A., CONFORTI, L., SPERELAKIS, N. & MATLIB, M.A. (1993). Selectivity of inhibition of Na^{+}/Ca^{2+} exchange of heart mitochondria by benzothiazepine CGP-37157. *J. Cardiovasc. Pharmacol.* **21**, 595-599.

CROMPTON, M., CAPANO, M. & CARAFOLI, E. (1976). The sodium induced efflux of calcium from heart mitochondria. A possible mechanism for the regulation of mitochondrial calcium. *Eur. J. Biochem.* **69**, 453-462.

CROMPTON, M. & HEID, I. (1978). The cycling of calcium, sodium, and protons across the inner membrane of cardiac mitochondria. *Eur. J. Biochem.* **91**, 599-608.

CROMPTON, M., MOSER, R., LUDI, H. & CARAFOLI, E. (1978). The interrelations between the transport of sodium and calcium in mitochondria of various mammalian tissues. *Eur. J. Biochem.* **82**, 25-31.

CROMPTON, M. & ROOS, I. (1985). On the hormonal control of heart mitochondrial Ca^{2+}. *Biochem. Soc. Trans.* **13**, 667-669.

CROMPTON, M. & COSTI, A. (1990). A heart mitochondrial Ca^{2+}-dependent pore of possible relevance to re-perfusion-induced injury. Evidence that ADP facilitates pore interconversion between the closed and open states. *Biochem. J.* **266**, 33-39.

CROMPTON, M. & ANDREEVA, L. (1994). On the interactions of Ca^{2+} and cyclosporin A with a mitochondrial inner membrane pore: a study using cobaltammine complex inhibitors of the Ca^{2+} uniporter. *Biochem. J.* **302(1)**, 181-185.

CROMPTON, M., VIRJI, S., DOYLE, V., JOHNSON, N. & WARD, J.M. (1999). The mitochondrial permeability transition pore. *Biochem. Soc. Symp.* **66**, 167-79.

CSORDAS, G., THOMAS, A.P. & HAJNOCZKY, G. (1999). Quasi-synaptic calcium signal transmission between endoplasmic reticulum and mitochondria. *EMBO J.* **18**, 96-108.

CURRIE, K.P., SWANN, K., GALIONE, A. & SCOTT, R.H. (1992). Activation of Ca^{2+}-dependent currents in cultured rat dorsal root ganglion neurones by a sperm factor and cyclic ADP-ribose. *Mol. Biol. Cell* **3**, 1415-1425.

DAUGIRDAS, J.T., ARRIETA, J., YE, M., FLORES, G. & BATTLE, D.C. (1995). Intracellular acidification associated with changes in free cytosolic calcium. Evidence for Ca^{2+}/H^{+} exchange via a plasma membrane Ca^{2+}-ATPase in vascular smooth muscle cells. *J. Clin. Invest.* **95**, 1480-1489.

DAVID, G., BARRETT, J.N. & BARRETT, E.F. (1998). Evidence that mitochondria buffer physiological Ca^{2+} loads in lizard motor nerve terminals. *J. Physiol. Lond.* **509(1)**, 59-65.

DAVIES, P.J., IRELAND, D.R. & McLACHLAN, E.M. (1996). Sources of Ca^{2+} for different Ca^{2+}-activated K^{+} conductances in neurones of the rat superior cervical ganglion. *J. Physiol. Lond.* **495**, 353-366.

DE WAARD, M., GURNETT, C.A. & CAMPBELL, K.P. (1996). Structural and functional diversity of voltage-activated calcium channels. *Ion. Channels.* **4**, 41-87.

DEDMAN, J.R., POTTER, J.D., JACKSON, R.L., JOHNSON, J.D. & MEANS, A.R. (1977). Physicochemical properties of rat testis Ca^{2+}-dependent regulator protein of cyclic nucleotide phosphodiesterase. Relationship of Ca^{2+}-binding, conformational changes, and phosphodiesterase activity. *J. Biol.Chem.* **252**, 8415-8422.

DELMAS, P., ABOGADIE, F.C., DAYRELL, M., HALEY, J.E., MILLIGAN, G., CAULFIELD, M.P., BROWN, D.A. & BUCKLEY, N.J. (1998a). G-proteins and G-protein subunits mediating cholinergic inhibition of N-type calcium cuirrents in sympathetic neurons. *Eur. J. Neurosci.* **10**, 1654-1666.

DELMAS, P., BROWN, D.A., DAYRELL, M., ABOGADIE, F.C., CAULFIELD, M.P. & BUCKLEY, N.J. (1998b). On the role of endogenous G-protein beta gamma subunits in N- type Ca^{2+} current inhibition by neurotransmitters in rat sympathetic neurones. *J. Physiol. Lond.* **506**, 319-329.

DELMAS, P., ABOGADIE, F.C., BUCKLEY, N.J. & BROWN, D.A. (2000). Calcium channel gating and modulation by transmitters depend on cellular compartmentalization. *Nat. Neurosci.* **3**, 670-678.

DEMAUREX, N., LEW, D.P. & KRAUSE, K.H. (1992). Cyclopiazonic acid depletes intracellular Ca^{2+} stores and activates an influx pathway for divalent cations in HL-60 cells. *J. Biol. Chem.* **267**, 2318-2324.

de TALAMONI, N., SMITH, C.A., WASSERMAN, R.H., BELTRAMINO, C., FULLMER, C.S. & PENNISTON, J.T. (1993). Immunocytochemical localization of the plasma membrane calcium pump, calbindin-D28k, and parvalbumin in Purkinje cells of avian and mammalian cerebellum. *Proc. Natl. Acad. Sci. U.S.A* **90**, 11949-11953.

DI LISA, F., GAMBASSI, G., SPURGEON, H. & HANSFORD, R.G. (1993). Intramitochondrial free calcium in cardiac myocytes in relation to dehydrogenase activation. *Cardiovasc. Res.* **27**, 1840-1844.

DIPOLO, R. (1973). Calcium efflux from internally dialyzed squid giant axons. *J. Gen. Physiol.* **62**, 575-589.

DIPOLO, R. (1974). Effect of ATP on the calcium efflux in dialyzed squid giant axons. *J. Gen. Physiol.* **64**, 503-517.

DIPOLO, R. (1978). Ca^{2+}-pump driven by ATP in squid axons. *Nature* **274**, 390-392.

DIPOLO, R. & BEAUGE, L. (1982). The effect of pH on Ca^{2+} extrusion mechanisms in dialyzed squid axons. *Biochim. Biophys. Acta* **688**, 237-245.

DIPOLO, R., ROJAS, H. & BEAUGE, L. (1982). Ca^{2+} entry at rest and during prolonged depolarization in dialyzed squid axons. *Cell Calcium* **3**, 19-41.

DIPOLO, R. & BEAUGE, L. (1983). The calcium pump and sodium-calcium exchange in squid axons. *Annual Reviews in Physiology* **45**, 313-324.

DIPOLO, R. & BEAUGE, L. (1984). Interactions of physiological ligands with the Ca^{2+} pump and Na^{+}/Ca^{2+} exchange in squid axons. *J. Gen. Physiol.* **84**, 895-914.

DIPOLO, R. & BEAUGE, L. (1987). In squid axons, ATP modulates Na^{+}-Ca^{2+} exchange by a Ca^{2+}-dependent phosphorylation. *Biochim. Biophys. Acta* **897**, 347-354.

DIPOLO, R. & BEAUGE, L. (1988). Ca^{2+} transport in nerve fibers. *Biochim. Biophys. Acta* **947**, 549-569.

DIPOLO, R. & BEAUGE, L. (1991). Regulation of Na^{+}-Ca^{2+} exchange. An overview. *Ann. N.Y. Acad. Sci.* **639**, 100-111.

DIPOLO, R. & BEAUGE, L. (1998). Differential up-regulation of Na^{+}-Ca^{2+} exchange by phosphoarginine and ATP in dialysed squid axons. *J. Physiol. Lond.* **507**, 737-747.

DOLPHIN, A.C. (1996). Facilitation of Ca^{2+} current in excitable cells. *Trends. Neurosci.* **19**, 35-43.

DOLPHIN, A.C. (1998). Mechanisms of modulation of voltage-dependent calcium channels by G proteins. *J. Physiol. Lond.* **506**, 3-11.

DONAHUE, B.S. & ABERCROMBIE, R.F. (1987). Free diffusion coefficient of ionic calcium in cytoplasm. *Cell Calcium* **8**, 437-448.

DOWNES, P. & MICHELL, R.H. (1981). Human erythrocyte membranes exhibit a cooperative calmodulin-dependent Ca^{2+}-ATPase of high calcium sensitivity. *Nature* **290**, 270-271.

DRUMMOND, R.M. & FAY, F.S. (1996). Mitochondria contribute to Ca^{2+} removal in smooth muscle cells. *Pflugers Arch.* **431**, 473-482.

DUBYAK, G.R. & EL-MOATASSIM, C. (1993). Signal transduction via P2-purinergic receptors for extracellular ATP and other nucleotides. *Am. J. Physiol. Lond.* **265**, C577-C606

DUCHEN, M.R., VALDEOLMILLOS, M., O'NEILL, S.C. & EISNER, D.A. (1990). Effects of metabolic blockade on the regulation of intracellular calcium in dissociated mouse sensory neurones. *J. Physiol. Lond.* **424**, 411-426.

DUCHEN, M.R. (1992). Ca^{2+}-dependent changes in the mitochondrial energetics in single dissociated mouse sensory neurons. *Biochem. J.* **283(1)**, 41-50.

DUCHEN, M.R. (1999). Contributions of mitochondria to animal physiology: from homeostatic sensor to calcium signalling and cell death. *J. Physiol. Lond.* **516**, 1-17.

DUNLAP, K., LUEBKE, J.I. & TURNER, T.J. (1995). Exocytotic Ca^{2+} channels in mammalian central neurons. *Trends. Neurosci.* **18**, 89-98.

EBASHI, S. (1961) *J. Biochem.* **234**, 2764-2769.

EBASHI, S. & LIPMANN (1962) *J. Cell. Biol.* **14**, 389-400.

EDWARDS, F.A. (1994). ATP receptors. *Curr. Opin. Neurobiol.* **4**, 347-352.

EHRLICH, B.E., KAFTAN, E., BEZPROZVANNAYA, S. & BEZPROZVANNY, I. (1994). The pharmacology of intracellular Ca^{2+}-release channels. *Trends. Pharmacol. Sci.* **15**, 145-149.

EMPSON, R.M. & GALIONE, A. (1997). Cyclic ADP-ribose enhances coupling between voltage-gated Ca^{2+} entry and intracellular Ca^{2+} release. *J. Biol. Chem.* **272**, 20967-20970.

ENGLAND, P.J. (1986). Intracellular calcium receptor mechanisms. *Br. Med. Bull.* **42**, 375-383.

ERTEL, E.A., CAMPBELL, K.P., HARPOLD, M.M., HOFMANN, F., MORI, Y., PEREZ-REYES, E., SCHWARTZ, A., SNUTCH, T.P., TANABE, T., BIRNBAUMER, L., TSIEN, R.W. & CATTERALL, W.A. (2000). Nomenclature of voltage-gated calcium channels. *Neuron* **25**, 533-535.

FABIATO, A. (1983). Calcium-induced release of calcium from the cardiac sarcoplasmic reticulum. *Am. J. Physiol. Lond.* **245(1)**, C1-C14.

FALCHETTO, R., VORHERR, T., BRUNNER, J. & CARAFOLI, E. (1991). The plasma membrane Ca^{2+} pump contains a site that interacts with its calmodulin-binding domain. *J. Biol. Chem.* **266**, 2930-2936.

FAN, J., SHUBA, Y.M. & MORAD, M. (1996). Regulation of cardiac sodium-calcium exchanger by beta-adrenergic agonists. *Proc. Natl. Acad. Sci. U.S.A* **93**, 5527-5532.

FANG, Y., CONDRESCU, M. & REEVES, J.P. (1998). Regulation of Na^+/Ca^{2+} exchange activity by cytosolic Ca^{2+} in transfected Chinese hamster ovary cells. *Am. J. Physiol.* **275**, C50-C55

FAVRE, C.J., SCHRENZEL, J., JACQUET, J., LEW, D.P. & KRAUSE, K.H. (1996). Highly supralinear feedback inhibition of Ca^{2+} uptake by the Ca^{2+} load of intracellular stores. *J. Biol. Chem.* **271**, 14925-14930.

FEIN, A. & TSACOPOULOS, M. (1988). Activation of mitochondrial oxidative metabolism by calcium ions in Limulus ventral photoreceptor. *Nature* **331**, 437-440.

FERNANDEZ-FERNANDEZ, J.M., WANAVERBECQ, N., HALLEY, P., CAULFIELD, M.P. & BROWN, D.A. (1999). Selective activation of heterologously expressed G protein-gated K^+ channels by M2 muscarinic receptors in rat sympathetic neurones. *J. Physiol. Lond.* **515(3)**, 631-637.

FERRIS, C.D. & SNYDER, S.H. (1992). Inositol 1,4,5-trisphosphate-activated calcium channels. *Annu. Rev. Physiol.* **544**, 469-488.

FIEBER, L.A. & ADAMS, D.J. (1991). Acetylcholine-evoked currents in cultured neurones dissociated from rat parasympathetic cardiac ganglia. *J. Physiol. Lond.* **434**, 215-237.

FIERRO, L. & LLANO, I. (1996). High endogenous calcium buffering in Purkinje cells from rat cerebellar slices. *J. Physiol. Lond.* **496(3)**, 617-625.

FIERRO, L., DIPOLO, R. & LLANO, I. (1998). Intracellular calcium clearance in Purkinje cell somata from rat cerebellar slices. *J. Physiol. Lond.* **510**, 499-512.

FILOTEO, A.G., ELWESS, N.L., ENYEDI, A., CARIDE, A., AUNG, H.H. & PENNISTON, J.T. (1997). Plasma membrane Ca^{2+} pump in rat brain. Patterns of alternative splices seen by isoform-specific antibodies. *J. Biol. Chem.* **272**, 23741-23747.

FISKUM, G. & COCKRELL, R.S. (1978). Ruthenium red sensitive and insensitive calcium transport in rat liver and Ehrlich ascites tumor cell mitochondria. *FEBS Lett.* **92**, 125-128.

FISKUM, G. & LEHNINGER, A.L. (1979). Regulated release of Ca^{2+} from respiring mitochondria by $Ca^{2+}/2H^+$ antiport. *J. Biol.Chem.* **254**, 6236-6239.

FOX, A.P., NOWYCKY, M.C. & TSIEN, R.W. (1987). Kinetic and pharmacological properties distinguishing three types of calcium currents in chick sensory neurones. *J. Physiol. Lond.* **394**, 149-172.

FREY, T.G. & MANNELLA, C.A. (2000). The internal structure of mitochondria. *Trends. Biochem. Sci.* **25**, 319-324.

FRIEL, D.D. & TSIEN, R.W. (1992). A caffeine- and ryanodine-sensitive Ca^{2+} store in bullfrog sympathetic neurones modulates effects of Ca^{2+} entry on $[Ca^{2+}]i$. *J. Physiol. Lond.* **450** , 217-246.

FRIEL, D.D. & TSIEN, R.W. (1994). An FCCP-sensitive Ca^{2+} store in bullfrog sympathetic neurons and its participation in stimulus-evoked changes in $[Ca^{2+}]_i$. *J. Neurosci* **14**, 4007-4024.

FULLMER, C.S. & WASSERMAN, R.H. (1987). Chicken intestinal 28-kilodalton calbindin-D: complete amino acid sequence and structural considerations. *Proc. Natl. Acad. Sci. U.S.A* **84**, 4772-4776.

GALIONE, A. (1992). Ca^{2+}-induced Ca^{2+} release and its modulation by cyclic ADP-ribose. *Trends Pharmacol. Sci.* **13**, 304-306.

GALIONE, A. (1993). Cyclic ADP-ribose: a new way to control calcium. *Science* **259**, 325-326.

GALIONE, A. (1994). Cyclic ADP-ribose, the ADP-ribosyl cyclase pathway and calcium signalling. *Mol. Cell Endocrinol.* **98**, 125-131.

GALIONE, A., WHITE, A., WILLMOTT, N., TURNER, M., POTTER, B.V. & WATSON, S.P. (1993). cGMP mobilizes intracellular Ca^{2+} in sea urchin eggs by stimulating cyclic ADP-ribose synthesis. *Nature* **365**, 456-459.

GARASCHUK, O., YAARI, Y. & KONNERTH, A. (1997). Release and sequestration of calcium by ryanodine-sensitive stores in rat hippocampal neurones. *J. Physiol. Lond.* **502**, 13-30.

GARRAHAM, P.J. & REGA, A.F. (1990). Plasma membrane calcium pump. In *Intracellular calcium regulation*, ed. BRONNER, F., pp. 272-303. New York: Alan R. Liss, Inc.

GASSNER, B., LUTERBACHER, S., SCHATZMANN, H.J. & WUTHRICH, A. (1988). Dependence of the red blood cell calcium pump on the membrane potential. *Cell Calcium* **9**, 95-103.

GATTO, C. & MILANICK, M.A. (1993). Inhibition of the red blood cell calcium pump by eosin and other fluorescein analogues. *Am. J. Physiol.* **264**, C1577-C1586

GATTO, C., HALE, C.C., XU, W. & MILANICK, M.A. (1995). Eosin, a potent inhibitor of the plasma membrane Ca^{2+}-pump, does not inhibit the cardiac Na-Ca exchanger. *Biochemistry* **34**, 965-972.

GATTO, C., XU, W.Y., DENISON, H.A., HALE, C.C. & MILANICK, M.A. (1996). Modifications of XIP, the autoinhibitory region of the Na-Ca exchanger, alter its ability to inhibit the Na^{+}-Ca^{2+} exchanger in bovine sarcolemmal vesicles. *Ann. N.Y. Acad. Sci.* **779**, 284-285.

GENAZZANI, A.A. & GALIONE, A. (1996). Nicotinic acid-adenine dinucleotide phosphate mobilizes Ca^{2+} from a thapsigargin-insensitive pool. *Biochem. J.* **315**, 721-725.

GENAZZANI, A.A., EMPSON, R.M. & GALIONE, A. (1996). Unique inactivation properties of NAADP-sensitive Ca^{2+} release. *J. Biol. Chem.* **271**, 11599-11602.

GENAZZANI, A.A. & GALIONE, A. (1997). A Ca^{2+} release mechanism gated by the novel pyridine nucleotide, NAADP. *Trends Pharmacol. Sci.* **18**, 108-110.

GERDAY, C. & GILLIS, J.M. (1976). Proceedings: The possible role of parvalbumins in the control of contraction. *J. Physiol. Lond.* **258**, 96P-97P.

GIETZEN, K. (1983). Comparison of the calmodulin antagonists compound 48/80 and calmidazolium. *Biochem. J.* **216**, 611-616.

GILCHRIST, J.S., BELCASTRO, A.N. & KATZ, S. (1992). Intraluminal Ca^{2+} dependence of Ca^{2+} and ryanodine-mediated regulation of skeletal muscle sarcoplasmic reticulum Ca^{2+} release. *J. Biol. Chem.* **267**, 20850-20856.

GLENNEY, J.R. & GLENNEY, P. (1985). Comparison of Ca^{2+}-regulated events in the intestinal brush border. *J. Cell Biol.* **100**, 754-763.

GMAJ, P., MURER, H. & CARAFOLI, E. (1982). Localization and properties of a high-affinity (Ca^{2+}-Mg^{2+})-ATPase in isolated kidney cortex plasma membranes. *FEBS Lett.* **144**, 226-230.

GOMEZ, T.M., SNOW, D.M. & LETOURNEAU, P.C. (1995). Characterization of spontaneous calcium transients in nerve growth cones and their effect on growth cone migration. *Neuron* **14**, 1233-1246.

GOPINATH, R.M. & VINCENZI, F.F. (1977). Phosphodiesterase protein activator mimics red blood cell cytoplasmic activator of (Ca^{2+}-Mg^{2+})-ATPase. *Biochem. Biophys. Res. Commun.* **77**, 1203-1209.

GRAEFF, R.M., PODEIN, R.J., AARHUS, R. & LEE, H.C. (1995). Magnesium ions but not ATP inhibit cyclic ADP-ribose-induced calcium release. *Biochem. Biophys. Res. Commun.* **206**, 786-791.

GRAF, E. & PENNISTON, J.T. (1981). Equimolar interaction between calmodulin and the Ca^{2+}-ATPase from human erythrocyte membranes. *Arch. Biochem. Biophys.* **210**, 257-262.

GRAY, M.W. & LANG, B.F. (1998). Transcription in chloroplasts and mitochondria: a tale of two polymerases. *Trends. Microbiol.* **6**, 1-3.

GREEB, J. & SHULL, G.E. (1989). Molecular cloning of a third isoform of the calmodulin-sensitive plasma membrane Ca^{2+}-transporting ATPase that is expressed predominantly in brain and skeletal muscle. *J. Biol. Chem.* **264**, 18569-18576.

GRIFFITHS, E.J. & HALESTRAP, A.P. (1995). Mitochondrial non-specific pores remain closed during cardiac ischaemia, but open upon reperfusion. *Biochem. J.* **307(1)**, 93-98.

GRYNKIEWICZ, G., POENIE, M. & TSIEN, R.Y. (1985). A new generation of Ca^{2+} indicators with greatly improved fluorescence properties. *J. Biol. Chem.* **260**, 3440-3450.

GUERINI, D., GARCIA, M.E., ZECCA, A., GUIDI, F. & CARAFOLI, E. (1998). The calcium pump of the plasma membrane: membrane targeting, calcium binding sites, tissue-specific isoform expression. *Acta Physiol. Scand. Suppl.* **643**, 265-273.

GUERINI, D., GARCIA, M.E., GERBER, A., VOLBRACHT, C., LEIST, M., MERINO, C.G. & CARAFOLI, E. (1999). The expression of plasma membrane Ca^{2+} pump isoforms in cerebellar granule neurons is modulated by Ca^{2+} *J. Biol. Chem.* **274**, 1667-1676.

GUILLEMETTE, G., BALLA, T., BAUKAL, A.J. & CATT, K.J. (1988). Characterization of inositol 1,4,5-trisphosphate receptors and calcium mobilization in a hepatic plasma membrane fraction. *J. Biol. Chem.* **263**, 4541-4548.

GUNTER, T.E. & PFEIFFER, D.R. (1990). Mechanisms by which mitochondria transport calcium. *Am. J. Physiol.* **258**, C755-C786

GUNTER, T.E., CHACE, J.H., PUSKIN, J.S. & GUNTER, K.K. (1983). Mechanism of sodium independent calcium efflux from rat liver mitochondria. *Biochemistry* **22**, 6341-6351.

GUNTESKI-HAMBLIN, A.M., GREEB, J. & SHULL, G.E. (1988). A novel Ca^{2+} pump expressed in brain, kidney, and stomach is encoded by an alternative transcript of the slow-twitch muscle sarcoplasmic reticulum Ca^{2+}-ATPase gene. Identification of cDNAs encoding Ca^{2+} and other cation-transporting ATPases using an oligonucleotide probe derived from the ATP-binding site. *J. Biol. Chem.* **263**, 15032-15040.

GYORKE, S. & FILL, M. (1993). Ryanodine receptor adaptation: control mechanism of Ca^{2+}-induced Ca^{2+} release in heart. *Science* **260**, 807-809.

HAGIWARA, S. & TAKAHASHI, K. (1967). Surface density of calcium ions and calcium spikes in the barnacle muscle fiber membrane. *J. Gen. Physiol.* **50**, 583-601.

HAJNOCZKY, G., ROBB-GASPERS, L.D., SEITZ, M.B. & THOMAS, A.P. (1995). Decoding of cytosolic calcium oscillations in the mitochondria. *Cell* **82**, 415-424.

HALASZOVICH, C.R., ZITT, C., JUNGLING, E. & LUCKHOFF, A. (2000). Inhibition of TRP3 channels by lanthanides. Block from the cytosolic side of the plasma membrane. *J. Biol. Chem.* **275**, 37423-37428.

HALL, A.K. & NORMAN, A.W. (1991). Vitamin D-independent expression of chick brain calbindin-D28K. *Brain Res. Mol. Brain Res.* **9**, 9-14.

HAMILL, O.P., MARTY, A., NEHER, E., SAKMANN, B. & SIGWORTH, F.J. (1981). Improved patch-clamp techniques for high-resolution current recording from cells and cell-free membrane patches. *Pflugers Arch.* **391**, 85-100.

HANSFORD, R.G. & CASTRO, F. (1981). Effects of micromolar concentrations of free calcium ions on the reduction of heart mitochondrial NAD(P) by 2-oxoglutarate. *Biochem. J.* **198**, 525-533.

HANSFORD, R.G. (1985). Relation between mitochondrial calcium transport and control of energy metabolism. *Rev. Physiol. Biochem. Pharmacol.* **102**, 1-72.

HARDINGHAM, G.E., CHAWLA, S., JOHNSON, C.M. & BADING, H. (1997). Distinct functions of nuclear and cytoplasmic calcium in the control of gene expression. *Nature* **385**, 260-265.

HASHII, M., MINABE, Y. & HIGASHIDA, H. (2000). cADP-ribose potentiates cytosolic Ca^{2+} elevation and Ca^{2+} entry via L-type voltage-activated Ca^{2+} channels in NG108-15 neuronal cells. *Biochem. J.* **345(2)**, 207-215.

HASSELBACH, W. & MAKINOSE, M. (1961) *Biochem. Z.* **333**, 518-528.

HAUG, L.S., JENSEN, V., HVALBY, O., WALAAS, S.I. & OSTVOLD, A.C. (1999). Phosphorylation of the inositol 1,4,5-trisphosphate receptor by cyclic nucleotide-dependent kinases in vitro and in rat cerebellar slices in situ. *J. Biol. Chem.* **274**, 7467-7473.

HAWORTH, R.A. & HUNTER, D.R. (1979). The Ca^{2+}-induced membrane transition in mitochondria. II. Nature of the Ca^{2+} trigger site. *Arch. Biochem. Biophys.* **195**, 460-467.

HEHL, S., GOLARD, A. & HILLE, B. (1996). Involvement of mitochondria in intracellular calcium sequestration by rat gonadotropes. *Cell Calcium* **20**, 515-524.

HEIM, R., IWATA, T., ZVARITCH, E., ADAMO, H.P., RUTISHAUSER, B., STREHLER, E.E., GUERINI, D. & CARAFOLI, E. (1992). Expression, purification, and properties of the plasma membrane Ca^{2+} pump and of its N-terminally truncated 105-kDa fragment. *J. Biol. Chem.* **267**, 24476-24484.

HEIZMANN, C.W. & BERCHTOLD, M.W. (1987). Expression of parvalbumin and other Ca^{2+}-binding proteins in normal and tumor cells: a topical review. *Cell Calcium* **8**, 1-41.

HEIZMANN, C.W. & HUNZIKER, W. (1990). Intracellular calcium-binding molecules. In *Intracellular calcium regulation*, ed. BRONNER, F., pp. 211-248. New York: Alan R. Liss, Inc.

HEIZMANN, C.W. (1984). Parvalbumin, an intracellular calcium-binding protein; distribution, properties and possible roles in mammalian cells. *Experientia* **40**, 910-921.

HELMCHEN, F., IMOTO, K. & SAKMANN, B. (1996). Ca^{2+} buffering and action potential-evoked Ca^{2+} signaling in dendrites of pyramidal neurons. *Biophys. J.* **70**, 1069-1081.

HENZI, V. & MACDERMOTT, A.B. (1992). Characteristics and function of Ca^{2+}- and inositol 1,4,5-trisphosphate-releasable stores of Ca^{2+} in neurons. *Neuroscience* **46**, 251-273.

HERNANDEZ-CRUZ, A., DIAZ-MUNOZ, M., GOMEZ-CHAVARIN, M., CANEDO-MERINO, R., PROTTI, D.A., ESCOBAR, A.L., SIERRALTA, J. & SUAREZ-ISLA, B.A. (1995). Properties of the ryanodine-sensitive release channels that underlie caffeine-induced Ca^{2+} mobilization from intracellular stores in mammalian sympathetic neurons. *Eur. J. Neurosci.* **7**, 1684-1699.

HERNANDEZ-CRUZ, A., ESCOBAR, A.L. & JIMENEZ, N. (1997). Ca^{2+}-induced Ca^{2+} release phenomena in mammalian sympathetic neurons are critically dependent on the rate of rise of trigger Ca^{2+}. *J. Gen. Physio.l* **109**, 147-167.

HERRINGTON, J., PARK, Y.B., BABCOCK, D.F. & HILLE, B. (1996). Dominant role of mitochondria in clearance of large Ca^{2+} loads from rat adrenal chromaffin cells. *Neuron* **16**, 219-228.

HIGASHIDA, H., BROWN, D.A. & ROBBINS, J. (2000). Both linopirdine- and WAY123,398-sensitive components of I K(M,ng) are modulated by cyclic ADP ribose in NG108-15 cells. *Pflugers Arch.* **441**, 228-234.

HILGEMANN, D.W., MATSUOKA, S., NAGEL, G.A. & COLLINS, A. (1992). Steady-state and dynamic properties of cardiac sodium-calcium exchange. Sodium-dependent inactivation. *J. Gen. Physiol.* **100**, 905-932.

HILL, T.D., BERGGREN, P.O. & BOYNTON, A.L. (1987). Heparin inhibits inositol trisphosphate-induced calcium release from permeabilized rat liver cells. *Biochem. Biophys. Res. Commun.* **149**, 897-901.

HILLE, B. (1992). Calcium Channels. In *Ionic channels of excitable membranes*, ed. HILLE, B. Sunderland, Massachusetts: Sinauer Associates Inc.

HILLE, B. (1994). Modulation of ion-channel function by G-protein-coupled receptors. *Trends. Neurosci.* **17**, 531-536.

HINDS, T.R. & ANDREASEN, T.J. (1981). Photochemical cross-linking of azidocalmodulin to the (Ca^{2+}-Mg^{2+})-ATPase of the erythrocyte membrane. *J. Biol. Chem.* **256**, 7877-7882.

HIRNING, L.D., FOX, A.P., McCLESKEY, E.W., OLIVERA, B.M., THAYER, S.A., MILLER, R.J. & TSIEN, R.W. (1988). Dominant role of N-type Ca^{2+} channels in evoked release of norepinephrine from sympathetic neurons. *Science* **239**, 57-61.

HONGPAISAN, J., PIVOVAROVA, N.B., COLEGROVE, S.L., LEAPMAN, R.D., FRIEL, D.D. & ANDREWS, S.B. (2001). Multiple modes of calcium-induced calcium release in sympathetic neurons II: a $[Ca^{2+}]_i$- and location-dependent transition from endoplasmic reticulum Ca accumulation to net Ca release. *J. Gen. Physiol.* **118**, 101-112.

HORN, R. & MARTY, A. (1988). Muscarinic activation of ionic currents measured by a new whole-cell recording method. *J. Gen. Physiol.* **92**, 145-159.

HOTH, M., FANGER, C.M. & LEWIS, R.S. (1997). Mitochondrial regulation of store-operated calcium signaling in T lymphocytes. *J. Cell Biol.* **137**, 633-648.

HUA, S.Y., NOHMI, M. & KUBA, K. (1993). Characteristics of Ca^{2+} release induced by Ca^{2+} influx in cultured bullfrog sympathetic neurones. *J. Physiol. Lond.* **464**, 245-272.

HUA, S.Y., TOKIMASA, T., TAKASAWA, S., FURUYA, Y., NOHMI, M., OKAMOTO, H. & KUBA, K. (1994). Cyclic ADP-ribose modulates Ca^{2+} release channels for activation by physiological Ca^{2+} entry in bullfrog sympathetic neurons. *Neuron* **12**, 1073-1079.

HUNTER, D.R. & HAWORTH, R.A. (1979a). The Ca^{2+}-induced membrane transition in mitochondria. I. The protective mechanisms. *Arch. Biochem. Biophys.* **195**, 453-459.

HUNTER, D.R. & HAWORTH, R.A. (1979b). The Ca^{2+}-induced membrane transition in mitochondria. III. Transitional Ca^{2+} release. *Arch. Biochem. Biophys.* **195**, 468-477.

HUNZIKER, W. & SCHRICKEL, S. (1988). Rat brain calbindin D28: six domain structure and extensive amino acid homology with chicken calbindin D_{28k}. *Mol. Endocrinol.* **2**, 465-473.

IACOPINO, A.M. & CHRISTAKOS, S. (1990). Specific reduction of calcium-binding protein (28-kilodalton calbindin-D) gene expression in aging and neurodegenerative diseases. *Proc. Natl. Acad. Sci. U.S.A* **87**, 4078-4082.

ICHAS, F., JOUAVILLE, L.S., SIDASH, S.S., MAZAT, J.P. & HOLMUHAMEDOV, E.L. (1994). Mitochondrial calcium spiking: a transduction mechanism based on calcium-induced permeability transition involved in cell calcium signalling. *FEBS Lett.* **348**, 211-215.

ICHAS, F., JOUAVILLE, L.S. & MAZAT, J.P. (1997). Mitochondria are excitable organelles capable of generating and conveying electrical and calcium signals. *Cell* **89**, 1145-1153.

ICHIMIYA, Y., EMSON, P.C., MOUNTJOY, C.Q., LAWSON, D.E. & IIZUKA, R. (1989). Calbindin-immunoreactive cholinergic neurones in the nucleus basalis of Meynert in Alzheimer-type dementia. *Brain Res.* **499**, 402-406.

IINO, M. & TSUKIOKA, M. (1994). Feedback control of inositol trisphosphate signalling bycalcium. *Mol.Cell Endocrinol.* **98**, 141-146.

IKEDA, S.R. & SCHOFIELD, G.G. (1989). Somatostatin blocks a calcium current in rat sympathetic ganglion neurones. *J. Physiol.Lond.* **409**, 221-240.

INESI, G. & de MEIS, L. (1989). Regulation of steady state filling in sarcoplasmic reticulum. Roles of back-inhibition, leakage, and slippage of the calcium pump. *J. Biol. Chem.* **264**, 5929-5936.

IRVINE, R.F. (1990). 'Quantal' Ca^{2+} release and the control of Ca^{2+} entry by inositol phosphates: a possible mechanism. *FEBS Lett.* **263**, 5-9.

IWAMOTO, T., WAKABAYASHI, S. & SHIGEKAWA, M. (1995). Growth factor-induced phosphorylation and activation of aortic smooth muscle Na^{+}/Ca^{2+} exchanger. *J. Biol. Chem.* **270**, 8996-9001.

IWAMOTO, T., PAN, Y., WAKABAYASHI, S., IMAGAWA, T., YAMANAKA, H.I. & SHIGEKAWA, M. (1996). Phosphorylation-dependent regulation of cardiac Na^{+}/Ca^{2+} exchanger via protein kinase C. *J. Biol. Chem.* **271**, 13609-13615.

IWAMOTO, T., NAKAMURA, T.Y., PAN, Y., UEHARA, A., IMANAGA, I. & SHIGEKAWA, M. (1999). Unique topology of the internal repeats in the cardiac Na^{+}/Ca^{2+} exchanger. *FEBS Lett.* **446**, 264-268.

JAFFE, D.B. & BROWN, T.H. (1994). Confocal imaging of dendritic Ca^{2+} transients in hippocampal brain slices during simultaneous current- and voltage-clamp recording. *Microsc. Res. Tech.* **29**, 279-289.

JAMES, P.H., PRUSCHY, M., VORHERR, T.E., PENNISTON, J.T. & CARAFOLI, E. (1989). Primary structure of the cAMP-dependent phosphorylation site of the plasma membrane calcium pump. *Biochemistry* **28**, 4253-4258.

JARRETT, H.W. & PENNISTON, J.T. (1977). Partial purification of the (Ca^{2+}-Mg^{2+})-ATPase activator from human erythrocytes: its similarity to the activator of 3':5' - cyclic nucleotide phosphodiesterase. *Biochem. Biophys. Res. Commun.* **77**, 1210-1216.

JENG, A.Y. & SHAMOO, A.E. (1980). The electrophoretic properties of a Ca^{2+} carrier isolated from calf heart inner mitochondrial membrane. *J. Biol. Chem.* **255**, 6904-6912.

JENSEN, J., LYNCH, G. & BAUDRY, M. (1990). Regional differences in the activation of synaptosomal mitochondrial Ca^{2+} uptake by spermine in rat brain. *Brain Res.* **523**, 313-315.

JOHN, L.M., LECHLEITER, J.D. & CAMACHO, P. (1998). Differential modulation of SERCA2 isoforms by calreticulin. *J. Cell. Biol.* **142**, 963-973.

JONAS, P., RACCA, C., SAKMANN, B., SEEBURG, P.H. & MONYER, H. (1994). Differences in Ca^{2+} permeability of AMPA-type glutamate receptor channels in neocortical neurons caused by differential GluR-B subunit expression. *Neuron* **12**, 1281-1289.

JONES, E.G. & HENDRY, S.H. (1990). Differential calcium binding protein immunoreactivity distinguishes classes of relay neurons in monkey thalamic nuclei. *Eur. J. Neurosci.* **1**, 222-246

JOSEPH, S.K. & RYAN, S.V. (1993). Phosphorylation of the inositol trisphosphate receptor in isolated rat hepatocytes. *J. Biol. Chem.* **268**, 23059-23065.

JOSEPH, S.K., LIN, C., PIERSON, S., THOMAS, A.P. & MARANTO, A.R. (1995). Heteroligomers of type-I and type-III inositol trisphosphate receptors in WB rat liver epithelial cells. *J. Biol. Chem.* **270**, 23310-23316.

JOUAVILLE, L.S., ICHAS, F., HOLMUHAMEDOV, E.L., CAMACHO, P. & LECHLEITER, J.D. (1995). Synchronization of calcium waves by mitochondrial substrates in Xenopus laevis oocytes. *Nature* **377**, 438-441.

JUHASZOVA, M., SHIMIZU, H., BORIN, M.L., YIP, R.K., SANTIAGO, E.M., LINDENMAYER, G.E. & BLAUSTEIN, M.P. (1996). Localization of the Na^{+}-Ca^{2+} exchanger in vascular smooth muscle, and in neurons and astrocytes. *Ann. NY. Acad. Sci.* **779**, 318-335.

JUHASZOVA, M., CHURCH, P., BLAUSTEIN, M.P. & STANLEY, E.F. (2000). Location of calcium transporters at presynaptic terminals. *Eur J. Neurosci* **12**, 839-846.

JUNG, D.W., BAYSAL, K. & BRIERLEY, G.P. (1995). The sodium-calcium antiport of heart mitochondria is not electroneutral. *J. Biol. Chem.* **270**, 672-678.

JURKOWITZ, M.S., ALTSCHULD, R.A., BRIERLEY, G.P. & CRAGOE, E.J. (1983). Inhibition of Na^{+}-dependent Ca^{2+} efflux from heart mitochondria by amiloride analogues. *FEBS Lett.* **162**, 262-265.

KAKIUCHI, S. & YAMAZAKI, R. (1970). Calcium dependent phosphodiesterase activity and its activating factor (PAF) from brain studies on cyclic 3',5'-nucleotide phosphodiesterase (3). *Biochem. Biophys. Res. Commun.* **41**, 1104-1110.

KANO, M., GARASCHUK, O., VERKHRATSKY, A. & KONNERTH, A. (1995). Ryanodine receptor-mediated intracellular calcium release in rat cerebellar Purkinje neurones. *J. Physiol. Lond.* **487**, 1-16.

KARLIN, A. (1993). Structure of nicotinic acetylcholine receptors. *Curr. Opin. Neurobiol.* **3**, 299-309.

KARLISH, S.J., BEAUGE, L.A. & GLYNN, I.M. (1979). Vanadate inhibits (Na^{+}-K^{+})-ATPase by blocking a conformational change of the unphosphorylated form. *Nature* **282**, 333-335.

KAWAGUCHI, Y., KATSUMARU, H., KOSAKA, T., HEIZMANN, C.W. & HAMA, K. (1987). Fast spiking cells in rat hippocampus (CA1 region) contain the calcium-binding protein parvalbumin. *Brain Res.* **416**, 369-374.

KEETON, T.P., BURK, S.E. & SHULL, G.E. (1993). Alternative splicing of exons encoding the calmodulin-binding domains and C termini of plasma membrane Ca^{2+}-ATPase isoforms 1, 2, 3, and 4. *J. Biol. Chem.* **268**, 2740-2748.

KEINANEN, K., WISDEN, W., SOMMER, B., WERNER, P., HERB, A., VERDOORN, T.A., SAKMANN, B. & SEEBURG, P.H. (1990). A family of AMPA-selective glutamate receptors. *Science* **249**, 556-560.

KEITH, C., DIPAOLA, M., MAXFIELD, F.R. & SHELANSKI, M.L. (1983). Microinjection of Ca^{2+}-calmodulin causes a localized depolymerization of microtubules. *J. Cell Biol.* **97**, 1918-1924.

KENNEDY, H.J. & THOMAS, R.C. (1995). Intracellular calcium and its sodium-independent regulation in voltage-clamped snail neurones. *J. Physiol. Lond.* **484**, 533-548.

KHODOROV, B., PINELIS, V., VERGUN, O., STOROZHEVYKH, T., FAJUK, D., VINSKAYA, N., ARSENJEVA, E., KHASPEKOV, L., LYZIN, A., ISAEV, N. & ET, A. (1995). Dramatic effects of external alkalinity on neuronal calcium recovery following a short-duration glutamate challenge: the role of the plasma membrane Ca^{2+}/H^{+} pump. *FEBS Lett.* **371**, 249-252.

KIEDROWSKI, L., WROBLEWSKI, J.T. & COSTA, E. (1994). Intracellular sodium concentration in cultured cerebellar granule cells challenged with glutamate. *Mol. Pharmacol.* **45**, 1050-1054.

KISELYOV, K., MIGNERY, G.A., ZHU, M.X. & MUALLEM, S. (1999). The N-terminal domain of the IP_3 receptor gates store-operated hTrp3 channels. *Mol. Cell* **4**, 423-429.

KISELYOV, K., XU, X., MOZHAYEVA, G., KUO, T., PESSAH, I., MIGNERY, G., ZHU, X., BIRNBAUMER, L. & MUALLEM, S. (1998). Functional interaction between InsP3 receptors and store-operated Htrp3 channels. *Nature* **396**, 478-482.

KISELYOV, K.I., SHIN, D.M., WANG, Y., PESSAH, I.N., ALLEN, P.D. & MUALLEM, S. (2000). Gating of store-operated channels by conformational coupling to ryanodine receptors. *Mol. Cell* **6**, 421-431.

KOHLER, M., BURNASHEV, N., SAKMANN, B. & SEEBURG, P.H. (1993). Determinants of Ca^{2+} permeability in both TM1 and TM2 of high affinity kainate receptor channels: diversity by RNA editing. *Neuron* **10**, 491-500.

KORKOTIAN, E. & SEGAL, M. (1998). Fast confocal imaging of calcium released from stores in dendritic spines. *Eur. J. Neurosci.* **10**, 2076-2084.

KOSK-KOSICKA, D. & BZDEGA, T. (1988). Activation of the erythrocyte Ca^{2+}-ATPase by either self-association or interaction with calmodulin. *J. Biol. Chem.* **263**, 18184-18189.

KOSTYUK, P. & VERKHRATSKY, A. (1995a). Calcium influx through the plasmalemma. In *Calcium signalling in the nervous system*, eds. KOSTYUK, P. & VERKHRATSKY, A., pp. 1-38. New York: John Wiley & Son,Inc.

KOSTYUK, P. & VERKHRATSKY, A. (1995b). Calcium stores and calcium release channels. In *Calcium signalling in the nervous system*, eds. KOSTYUK, P. & VERKHRATSKY, A., pp. 39-57. New York: John Wiley & Son,Inc.

KOSTYUK, P. & VERKHRATSKY, A. (1995c). Temporal and spatial organization of calcium signal in nerve cells. In *Calcium signalling in the nervous system*, eds. KOSTYUK, P. & VERKHRATSKY, A., pp. 58-109. New York: John Wiley & Son,Inc.

KRETSINGER, R.H. (1980). Structure and evolution of calcium-modulated proteins. *CRC Crit.Rev Biochem.* **8**, 119-174.

KRETSINGER, R.H. (1987). Calcium coordination and the calmodulin fold: divergent versus convergent evolution. *Cold Spring Harb. Symp. Quant. Biol.* **5(2)**, 499-510.

KRETSINGER, R.H. (1990). Why cells must export calcium. In *Intracellular calcium regulation*, ed. BRONNER, F., pp. 439-457. New York: Alan R. Liss, Inc.

KROEMER, G., DALLAPORTA, B. & RESCHE-RIGON, M. (1998). The mitochondrial death/life regulator in apoptosis and necrosis. *Annu. Rev. Physiol.* **60**, 619-642.

KRZYWKOWSKI, P., POTIER, B., BILLARD, J.M., DUTAR, P. & LAMOUR, Y. (1996). Synaptic mechanisms and calcium binding proteins in the aged rat brain. *Life Sci.* **59**, 421-428.

KUBA, K. (1980). Release of calcium ions linked to the activation of potassium conductance in a caffeine-treated sympathetic neurone. *J. Physiol. Lond.* **298**, 251-269.

KUBA, K. (1994). Ca^{2+}-induced Ca^{2+} release in neurones. *Jpn. J. Physiol. Lond.* **44**, 613-650.

KUWAJIMA, G., FUTATSUGI, A., NIINOBE, M., NAKANISHI, S. & MIKOSHIBA, K. (1992). Two types of ryanodine receptors in mouse brain: skeletal muscle type exclusively in Purkinje cells and cardiac muscle type in various neurons. *Neuron* **9**, 1133-1142.

KWAN, C.Y. & PUTNEY, J.W. (1990). Uptake and intracellular sequestration of divalent cations in resting and methacholine-stimulated mouse lacrimal acinar cells. Dissociation by Sr^{2+} and Ba^{2+} of agonist-stimulated divalent cation entry from the refilling of the agonist-sensitive intracellular pool. *J. Biol. Chem.* **265**, 678-684.

KWAN, C.Y., TAKEMURA, H., OBIE, J.F., THASTRUP, O. & PUTNEY, J.W. (1990). Effects of MeCh, thapsigargin, and La^{3+} on plasmalemmal and intracellular Ca^{2+} transport in lacrimal acinar cells. *Am. J. Physiol.* **258**, C1006-C1015

LECHLEITER, J.D. & CLAPHAM, D.E. (1992). Spiral waves and intracellular calcium signalling. *J. Physiol. Paris.* **86**, 123-128.

LEE, H.C., WALSETH, T.F., BRATT, G.T., HAYES, R.N. & CLAPPER, D.L. (1989). Structural determination of a cyclic metabolite of NAD^+ with intracellular Ca^{2+}-mobilizing activity. *J. Biol. Chem.* **264**, 1608-1615.

LEE, S.L., YU, A.S. & LYTTON, J. (1994). Tissue-specific expression of Na^+/Ca^{2+} exchanger isoforms. *J. Biol Chem* **269**, 14849-14852.

LEE, H.C., AARHUS, R., GRAEFF, R., GURNACK, M.E. & WALSETH, T.F. (1994). Cyclic ADP ribose activation of the ryanodine receptor is mediated by calmodulin. *Nature* **370**, 307-309.

LEE, H.C. & AARHUS, R. (1995). A derivative of NADP mobilizes calcium stores insensitive to inositol trisphosphate and cyclic ADP-ribose. *J. Biol. Chem.* **270**, 2152-2157.

LEE, S.H., SCHWALLER, B. & NEHER, E. (2000). Kinetics of Ca^{2+} binding to parvalbumin in bovine chromaffin cells: implications for $[Ca^{2+}]$ transients of neuronal dendrites. *J. Physiol. Lond.* **525(2)**, 419-432.

LEE, A.G. & EAST, J.M. (2001). What the structure of a calcium pump tells us about its mechanism. *Biochem. J.* **356**, 665-683.

LEHNINGER, A.L., CARAFOLI, E. & ROSSI, C.S. (1967). Energy-linked ion movements in mitochondrial systems. *Adv. Enzymol. Relat. Areas. Mol. Biol.* **29**, 259-320.

LENZEN, S., MUNSTER, W. & RUSTENBECK, I. (1992). Dual effect of spermine on mitochondrial Ca^{2+} transport. *Biochem. J.* **286**, -602

LI, Z., MATSUOKA, S., HRYSHKO, L.V., NICOLL, D.A., BERSOHN, M.M., BURKE, E.P., LIFTON, R.P. & PHILIPSON, K.D. (1994). Cloning of the NCX2 isoform of the plasma membrane Na^+-Ca^{2+} exchanger. *J. Biol.Chem.* **269**, 17434-17439.

LIN, Y.Q., BRAIN, K.L. & BENNETT, M.R. (1998). Calcium in sympathetic boutons of rat superior cervical ganglion during facilitation, augmentation and potentiation. *J. Auton. Nerv. Syst.* **73**, 26-37.

LIU, Q.Y., LAI, F.A., ROUSSEAU, E., JONES, R.V. & MEISSNER, G. (1989). Multiple conductance states of the purified calcium release channel complex from skeletal sarcoplasmic reticulum. *Biophys. J.* **55**, 415-424.

LLANO, I., DIPOLO, R. & MARTY, A. (1994). Calcium-induced calcium release in cerebellar Purkinje cells. *Neuron* **12**, 663-673.

LLEDO, P.M., SOMASUNDARAM, B., MORTON, A.J., EMSON, P.C. & MASON, W.T. (1992). Stable transfection of calbindin-D28k into the GH3 cell line alters calcium currents and intracellular calcium homeostasis. *Neuron* **9**, 943-954.

LU, F.M. & KUBA, K. (2001). Synchronized Ca^{2+} signals mediated by Ca^{2+} action potentials in the hippocampal neuron network in vitro. *Cell Calcium* **29**, 379-394.

LUETJE, C.W. & PATRICK, J. (1991). Both alpha- and beta-subunits contribute to the agonist sensitivity of neuronal nicotinic acetylcholine receptors. *J. Neurosci.* **11**, 837-845.

LUKACS, G.L. & KAPUS, A. (1987). Measurement of the matrix free Ca^{2+} concentration in heart mitochondria by entrapped fura-2 and quin2. *Biochem. J.* **248**, 609-613.

LUKYANENKO, V., GYORKE, I. & GYORKE, S. (1996). Regulation of calcium release by calcium inside the sarcoplasmic reticulum in ventricular myocytes. *Pflugers Arch.* **432**, 1047-1054.

LUTERBACHER, S. & SCHATZMANN, H.J. (1983). The site of action of La^{3+} in the reaction cycle of the human red cell membrane Ca^{2+}-pump ATPase. *Experientia* **39**, 311-312.

LUTHER, P.W., YIP, R.K., BLOCH, R.J., AMBESI, A., LINDENMAYER, G.E. & BLAUSTEIN, M.P. (1992). Presynaptic localization of sodium/calcium exchangers in neuromuscular preparations. *J. Neurosci.* **12**, 4898-4904.

LYTTON, J. & McLENNAN, D.H. (1988). Molecular cloning of cDNAs from human kidney coding for two alternatively spliced products of the cardiac Ca^{2+}-ATPase gene. *J. Biol. Chem.* **263** , 15024-15031.

LYTTON, J., WESTLIN, M. & HANLEY, M.R. (1991). Thapsigargin inhibits the sarcoplasmic or endoplasmic reticulum Ca^{2+}-ATPase family of calcium pumps. *J. Biol. Chem.* **266**, 17067-17071.

MA, H.T., PATTERSON, R.L., VAN ROSSUM, D.B., BIRNBAUMER, L., MIKOSHIBA, K. & GILL, D.L. (2000). Requirement of the inositol trisphosphate receptor for activation of store-operated Ca^{2+} channels. *Science* **287**, 1647-1651.

MAEDA, H., ELLIS-DAVIES, G.C., ITO, K., MIYASHITA, Y. & KASAI, H. (1999). Supralinear Ca^{2+} signaling by cooperative and mobile Ca^{2+} buffering in Purkinje neurons. *Neuron* **24**, 989-1002.

MANNELLA, C.A., BUTTLE, K., RATH, B.K. & MARKO, M. (1998). Electron microscopic tomography of rat-liver mitochondria and their interaction with the endoplasmic reticulum. *Biofactors* **8**, 225-228.

MARGULIS, L., OLENDZENSKI, L., DOLAN, M. & MACINTYRE, F. (1996). Diversity of eukaryotic microorganisms: computer-based resources, "The Handbook of Protoctista" and its "Glossary". *Microbiologia.* **12**, 29-42.

MARIE, V. & SILVA, J.E. (1998). Calcium pool size modulates the sensitivity of the ryanodine receptor channel and calcium-dependent ATPase of heavy sarcoplasmic reticulum to extravesicular free calcium concentration. *J. Cell Physiol.* **175**, 283-294.

MARRION, N.V., SMART, T.G. & BROWN, D.A. (1987). Membrane currents in adult rat superior cervical ganglia in dissociated tissue culture. *Neurosci. Lett.* **77**, 55-60.

MARSH, S.J., TROUSLARD, J., LEANEY, J.L. & BROWN, D.A. (1995). Synergistic regulation of a neuronal chloride current by intracellular calcium and muscarinic receptor activation: a role for protein kinase C. *Neuron* **15**, 729-737.

MARSH, S.J., WANAVERBECQ, N., SELYANKO, A.A. & BROWN, D.A. (2000). Calcium signalling in neurons exemplified by rat symapthetic ganglion cells. In *Calcium: the molecular basis of calcium action in biology and medicine*, eds. POCHET, R., DONATO, R., HAIECH, J., HEIZMANN, C. & GERKE, V., pp. 27-44. Netherlands: Kluver Academic Publishers.

MARSHALL, I.C. & TAYLOR, C.W. (1993). Regulation of inositol 1,4,5-trisphosphate receptors. *J. Exp. Biol.* **184(1)**, 61-82.

MASSARI, S., BALBONI, E. & AZZONE, G.F. (1972). Distribution of permeant cations in rat liver mitochondria under steady-state conditions. *Biochim. Biophys. Acta* **283**, 16-22.

MATSUOKA, S. & HILGEMANN, D.W. (1994). Inactivation of outward Na^{+}/Ca^{2+} exchange current in guinea-pig ventricular myocytes. *J. Physiol. Lond.* **476**, 443-458.

MATTSON, M.P., GUTHRIE, P.B. & KATER, S.B. (1989). A role for Na^{+}-dependent Ca^{2+} extrusion in protection against neuronal excitotoxicity. *FASEB J* **3**, 2519-2526.

MATTSON, M.P., RYCHLIK, B., CHU, C. & CHRISTAKOS, S. (1991). Evidence for calcium-reducing and excito-protective roles for the calcium-binding protein calbindin-D_{28k} in cultured hippocampal neurons. *Neuron* **6**, 41-51.

McGEHEE, D.S. & ROLE, L.W. (1995). Physiological diversity of nicotinic acetylcholine receptors expressed by vertebrate neurons. *Annu. Rev. Physiol.* **57521-46**, -46

McGREW, S.G., WOLLEBEN, C., SIEGL, P., INUI, M. & FLEISCHER, S. (1989). Positive cooperativity of ryanodine binding to the calcium release channel of sarcoplasmic reticulum from heart and skeletal muscle. *Biochemistry* **28**, 1686-1691.

McLENNAN, D.H. (1970). Purification and properties of an adenosine triphosphatase from sarcoplasmic reticulum. *J. Biol. Chem.* **245**, 4508-4518.

McLENNAN, D.H., BRANDL, C.J., KORCZAK, B. & GREEN, N.M. (1985). Amino-acid sequence of a (Ca^{2+}-Mg^{2+})-dependent ATPase from rabbit muscle sarcoplasmic reticulum, deduced from its complementary DNA sequence. *Nature* **316**, 696-700.

McPHERSON, P.S., KIM, Y.K., VALDIVIA, H., KNUDSON, C.M., TAKEKURA, H., FRANZINI-ARMSTRONG, C., CORONADO, R. & CAMPBELL, K.P. (1991). The brain ryanodine receptor: a caffeine-sensitive calcium release channel. *Neuron* **7**, 17-25.

McPHERSON, P.S. & CAMPBELL, K.P. (1993). The ryanodine receptor/Ca^{2+} release channel. *J. Biol. Chem.* **268**, 13765-13768.

MEISSNER, G. & HENDERSON, J.S. (1987). Rapid calcium release from cardiac sarcoplasmic reticulum vesicles is dependent on Ca^{2+} and is modulated by Mg^{2+}, adenine nucleotide, and calmodulin. *J. Biol. Chem.* **262**, 3065-3073.

MEISSNER, G. (1994). Ryanodine receptor/Ca^{2+} release channels and their regulation by endogenous effectors. *Annu. Rev. Physiol.* **56**, 485-508.

MELDOLESI, J. & POZZAN, T. (1998). The endoplasmic reticulum Ca^{2+} store: a view from the lumen. *Trends Biochem. Sci.* **23**, 10-14.

MESZAROS, L.G., BAK, J. & CHU, A. (1993). Cyclic ADP-ribose as an endogenous regulator of the non-skeletal type ryanodine receptor Ca^{2+} channel. *Nature* **364**, 76-79.

MIGNERY, G.A., NEWTON, C.L., ARCHER, B.T. & SUDHOF, T.C. (1990). Structure and expression of the rat inositol 1,4,5-trisphosphate receptor. *J. Biol. Chem.* **265**, 12679-12685.

MILANICK, M.A. (1990). Proton fluxes associated with the Ca^{2+} pump in human red blood cells. *Am. J. Physiol.* **258**, C552-C562

MILLER, R.J. (1991). The control of neuronal Ca^{2+} homeostasis. *Prog. Neurobiol.* **37**, 255-285.

MINGHETTI, P.P., CANCELA, L., FUJISAWA, Y., THEOFAN, G. & NORMAN, A.W. (1988). Molecular structure of the chicken vitamin D-induced calbindin-D_{28k} gene reveals eleven exons, six Ca^{2+}-binding domains, and numerous promoter regulatory elements. *Mol. Endocrinol.* **2**, 355-367.

MINTZ, I.M., ADAMS, M.E. & BEAN, B.P. (1992). P-type calcium channels in rat central and peripheral neurons. *Neuron* **9**, 85-95.

MIRONOV, S.L. & HERMANN, A. (1996). Ethanol actions on the mechanisms of Ca^{2+} mobilization in rat hippocampal cells are mediated by protein kinase C. *Brain Res.* **714**, 27-37.

MISSIAEN, L., de SMEDT, H., PARYS, J.B. & CASTEELS, R. (1994). Co-activation of inositol trisphosphate-induced Ca^{2+} release by cytosolic Ca^{2+} is loading-dependent. *J. Biol. Chem.* **269**, 7238-7242.

MISSIAEN, L., TAYLOR, C.W. & BERRIDGE, M.J. (1992). Luminal Ca^{2+} promoting spontaneous Ca^{2+} release from inositol trisphosphate-sensitive stores in rat hepatocytes. *J. Physiol. Lond.* **455**, 623-640.

MITCHELL, P. & MOYLE, J. (1967). Chemiosmotic hypothesis of oxidative phosphorylation. *Nature* **213** , 137-139.

MIURA, Y. & KIMURA, J. (1989). Sodium-calcium exchange current. Dependence on internal Ca^{2+} and Na^+ and competitive binding of external Na^+ and Ca^{2+}. *J. Gen. Physiol.* **93**, 1129-1145.

MIYATA, H., SILVERMAN, H.S., SOLLOTT, S.J., LAKATTA, E.G., STERN, M.D. & HANSFORD, R.G. (1991). Measurement of mitochondrial free Ca^{2+} concentration in living single rat cardiac myocytes. *Am. J. Physiol.* **261**, H1123-H1134

MIYAWAKI, A., FURUICHI, T., RYOU, Y., YOSHIKAWA, S., NAKAGAWA, T., SAITOH, T. & MIKOSHIBA, K. (1991). Structure-function relationships of the mouse inositol 1,4,5-trisphosphate receptor. *Proc. Natl. Acad. Sci. U.S.A* **88**, 4911-4915.

MOGAMI, H., TEPIKIN, A.V. & PETERSEN, O.H. (1998). Termination of cytosolic Ca^{2+} signals: Ca^{2+} reuptake into intracellular stores is regulated by the free Ca^{2+} concentration in the store lumen. *EMBO J.* **17**, 435-442.

MOLINARI, S., BATTINI, R., FERRARI, S., POZZI, L., KILLCROSS, A.S., ROBBINS, T.W., JOUVENCEAU, A., BILLARD, J.M., DUTAR, P., LAMOUR, Y., BAKER, W.A., COX, H. & EMSON, P.C. (1996). Deficits in memory and hippocampal long-term potentiation in mice with reduced calbindin D_{28k} expression. *Proc. Natl. Acad. Sci. U.S.A* **93**, 8028-8033.

MONKAWA, T., HAYASHI, M., MIYAWAKI, A., SUGIYAMA, T., YAMAMOTO-HINO, M., HASEGAWA, M., FURUICHI, T., MIKOSHIBA, K. & SARUTA, T. (1998). Localization of inositol 1,4,5-trisphosphate receptors in the rat kidney. *Kidney Int.* **53**, 296-301.

MONTERO, M., ALONSO, M.T., CARNICERO, E., CUCHILLO-IBANEZ, I., ALBILLOS, A., GARCIA, A.G., GARCIA-SANCHO, J. & ALVAREZ, J. (2000). Chromaffin-cell stimulation triggers fast millimolar mitochondrial Ca^{2+} transients that modulate secretion. *Nat. Cell Biol.* **2**, 57-61.

MOORE, C.L. (1971). Specific inhibition of mitochondrial Ca^{2+} transport by ruthenium red. *Biochem. Biophys. Res. Commun.* **42**, 298-305.

MULLER, T.H., PARTRIDGE, L.D. & SWANDULLA, D. (1993). Calcium buffering in bursting Helix pacemaker neurons. *Pflugers Arch.* **425**, 499-505.

MURCHISON, D. & GRIFFITH, W.H. (2000). Mitochondria buffer non-toxic calcium loads and release calcium through the mitochondrial permeability transition pore and sodium/calcium exchanger in rat basal forebrain neurons. *Brain Res.* **854**, 139-151.

NAGASAKI, K. & FLEISCHER, S. (1988). Ryanodine sensitivity of the calcium release channel of sarcoplasmic reticulum. *Cell Calcium* **9**, 1-7.

NAKADE, S., MAEDA, N. & MIKOSHIBA, K. (1991). Involvement of the C-terminus of the inositol 1,4,5-trisphosphate receptor in Ca^{2+} release analysed using region-specific monoclonal antibodies. *Biochem. J.* **277**(1), 125-131.

NARAYANAN, N. & XU, A. (1997). Phosphorylation and regulation of the Ca^{2+}-pumping ATPase in cardiac sarcoplasmic reticulum by calcium/calmodulin-dependent protein kinase. *Basic. Res. Cardiol.* **92(1)**, 25-35

NARITA, K., AKITA, T., OSANAI, M., SHIRASAKI, T., KIJIMA, H. & KUBA, K. (1998). A Ca^{2+}-induced Ca^{2+} release mechanism involved in asynchronous exocytosis at frog motor nerve terminals. *J. Gen. Physiol.* **112**, 593-609.

NAVAZIO, L., BEWELL, M.A., SIDDIQUA, A., DICKINSON, G.D., GALIONE, A. & SANDERS, D. (2000). Calcium release from the endoplasmic reticulum of higher plants elicited by the NADP metabolite nicotinic acid adenine dinucleotide phosphate. *Proc. Natl. Acad. Sci. U.S.A* **97**, 8693-8698.

NEERING, I.R. & McBURNEY, R.N. (1984). Role for microsomal Ca storage in mammalian neurones? *Nature* **309**, 158-160.

NEHER, E. & AUGUSTINE, G.J. (1992). Calcium gradients and buffers in bovine chromaffin cells. *J. Physiol. Lond.* **450**, 273-301.

NEHER, E. (1995). The use of fura-2 for estimating Ca^{2+} buffers and Ca^{2+} fluxes. *Neuropharmacology* **34** , 1423-1442.

NICHOLLS, D.G. (1978a). The regulation of extramitochondrial free calcium ion concentration by rat liver mitochondria. *Biochem. J.* **176**, 463-474.

NICHOLLS, D.G. (1978b). Calcium transport and porton electrochemical potential gradient in mitochondria from guinea-pig cerebral cortex and rat heart. *Biochem. J.* **170**, 511-522.

NICHOLLS, D.G. & SCOTT, I.D. (1980). The regulation of brain mitochondrial calcium-ion transport. The role of ATP in the discrimination between kinetic and membrane-potential-dependent calcium-ion efflux mechanisms. *Biochem. J.* **186**, 833-839.

NICHOLLS, D.G. (1986). Intracellular calcium homeostasis. *Br. Med. Bull.* **42**, 353-358.

NICOLL, D.A., LONGONI, S. & PHILIPSON, K.D. (1990). Molecular cloning and functional expression of the cardiac sarcolemmal Na^{+}-Ca^{2+} exchanger. *Science* **250**, 562-565.

NICOLL, D.A., QUEDNAU, B.D., QUI, Z., XIA, Y.R., LUSIS, A.J. & PHILIPSON, K.D. (1996). Cloning of a third mammalian Na^{+}-Ca^{2+} exchanger, NCX3. *J. Biol. Chem.* **271**, 24914-24921.

NICOLL, D.A., OTTOLIA, M., LU, L., LU, Y. & PHILIPSON, K.D. (1999). A new topological model of the cardiac sarcolemmal Na^{+}-Ca^{2+} exchanger. *J. Biol. Chem.* **274**, 910-917.

NIEMINEN, A.L., SAYLOR, A.K., TESFAI, S.A., HERMAN, B. & LEMASTERS, J.J. (1995). Contribution of the mitochondrial permeability transition to lethal injury after exposure of hepatocytes to t-butylhydroperoxide. *Biochem. J.* **307(1)**, 99-106.

NIGGLI, V., RONNER, P., CARAFOLI, E. & PENNISTON, J.T. (1979). Effects of calmodulin on the (Ca^{2+}-Mg^{2+})-ATPase partially purified from erythrocyte membranes. *Arch. Biochem. Biophys.* **198**, 124-130.

NIGGLI, V., ADUNYAH, E.S. & CARAFOLI, E. (1981). Acidic phospholipids, unsaturated fatty acids, and limited proteolysis mimic the effect of calmodulin on the purified erythrocyte Ca^{2+}-ATPase. *J. Biol. Chem.* **256**, 8588-8592.

NIGGLI, V., SIGEL, E. & CARAFOLI, E. (1982). Inhibition of the purified and reconstituted calcium pump of erythrocytes by micro M levels of DIDS and NAP-taurine. *FEBS Lett.* **138**, 164-166.

NISHIMURA, T., AKASU, T. & TOKIMASA, T. (1991). A slow calcium-dependent chloride current in rhythmic hyperpolarization in neurones of the rabbit vesical pelvic ganglia. *J. Physiol. Lond.* **437**, 673-690.

NITSCH, R., BERGMANN, I., KUPPERS, K., MUELLER, G. & FROTSCHER, M. (1990). Late appearance of parvalbumin-immunoreactivity in the development of GABAergic neurons in the rat hippocampus. *Neurosci. Lett.* **118**, 147-150.

NITSCH, R., BERGMANN, I., KUPPERS, K., MUELLER, G. & FROTSCHER, M. (1990). Late appearance of parvalbumin-immunoreactivity in the development of GABAergic neurons in the rat hippocampus. *Neurosci. Lett.* **118**, 147-150.

NOONEY, J.M., LAMBERT, R.C. & FELTZ, A. (1997). Identifying neuronal non-L Ca^{2+} channels--more than stamp collecting? *Trends. Pharmacol. Sci.* **18**, 363-371.

NORMAN, A.W., ROTH, J. & ORCI, L. (1982). The vitamin D endocrine system. Steroid metabolism, hormon receptors, and biological response. *Endocrinology Review* **3**, 331-366.

NUNN, D.L. & TAYLOR, C.W. (1992). Luminal Ca^{2+} increases the sensitivity of Ca^{2+} stores to inositol 1,4,5-trisphosphate. *Mol. Pharmacol.* **41**, 115-119.

OLDERSHAW, K.A. & TAYLOR, C.W. (1993). Luminal Ca^{2+} increases the affinity of inositol 1,4,5-trisphosphate for its receptor. *Biochem. J.* **292(3)**, 631-633.

OTSU, K., WILLARD, H.F., KHANNA, V.K., ZORZATO, F., GREEN, N.M. & MACLENNAN, D.H. (1990). Molecular cloning of cDNA encoding the Ca^{2+} release channel (ryanodine receptor) of rabbit cardiac muscle sarcoplasmic reticulum. *J. Biol. Chem.* **265**, 13472-13483.

PALECEK, J., LIPS, M.B. & KELLER, B.U. (1999). Calcium dynamics and buffering in motoneurones of the mouse spinal cord. *J. Physiol. Lond.* **520(2)**, 485-502.

PARK, Y.B., HERRINGTON, J., BABCOCK, D.F. & HILLE, B. (1996). Ca^{2+} clearance mechanisms in isolated rat adrenal chromaffin cells. *J. Physiol. Lond.* **492**, 329-346.

PATEL, S., CHURCHILL, G.C. & GALIONE, A. (2001). Coordination of Ca^{2+} signalling by NAADP. *Trends Biochem. Sci.* **26**, 482-489.

PEERSEN, O.B., MADSEN, T.S. & FALKE, J.J. (1997). Intermolecular tuning of calmodulin by target peptides and proteins: differential effects on Ca^{2+} binding and implications for kinase activation. *Protein Sci.* **6**, 794-807.

PELLEGRINI-GIAMPIETRO, D.E., BENNETT, M.V. & ZUKIN, R.S. (1992). Are Ca^{2+}-permeable kainate/AMPA receptors more abundant in immature brain? *Neurosci. Lett.* **144**, 65-69.

PENG, Y. (1996). Ryanodine-sensitive component of calcium transients evoked by nerve firing at presynaptic nerve terminals. *J. Neurosci.* **16**, 6703-6712.

PERSECHINI, A., MONCRIEF, N.D. & KRETSINGER, R.H. (1989). The EF-hand family of calcium-modulated proteins. *Trends. Neurosci.* **12**, 462-467.

PETERSEN, O.H. & CANCELA, J.M. (1999). New Ca^{2+}-releasing messengers: are they important in the nervous system? *Trends Neurosci.* **22**, 488-495.

PETRONILLI, V., MIOTTO, G., CANTON, M., BRINI, M., COLONNA, R., BERNARDI, P. & DI LISA, F. (1999). Transient and long-lasting openings of the mitochondrial permeability transition pore can be monitored directly in intact cells by changes in mitochondrial calcein fluorescence. *Biophys. J.* **76**, 725-734.

PHILIPSON, K.D., LONGONI, S. & WARD, R. (1988). Purification of the cardiac Na^+/Ca^{2+} exchange protein. *Biochim. Biophys. Acta* **945**, 298-306.

PHILIPSON, K.D. & NICOLL, D.A. (2000). Sodium-calcium exchange: a molecular perspective. *Annu. Rev. Physiol.* **62**, 111-133.

PIVOVAROVA, N.B., HONGPAISAN, J., ANDREWS, S.B. & FRIEL, D.D. (1999). Depolarization-induced mitochondrial Ca^{2+} accumulation in sympathetic neurons: spatial and temporal characteristics. *J. Neurosci.* **19**, 6372-6384.

PLUMMER, M.R., LOGOTHETIS, D.E. & HESS, P. (1989). Elementary properties and pharmacological sensitivities of calcium channels in mammalian peripheral neurons. *Neuron* **2**, 1453-1463.

POTIER, B., KRZYWKOWSKI, P., LAMOUR, Y. & DUTAR, P. (1994). Loss of calbindin-immunoreactivity in CA1 hippocampal stratum radiatum and stratum lacunosum-moleculare interneurons in the aged rat. *Brain Res.* **661**, 181-188.

POZZAN, T., RIZZUTO, R., VOLPE, P. & MELDOLESI, J. (1994). Molecular and cellular physiology of intracellular calcium stores. *Physiol. Rev.* **74**, 595-636.

PUSKIN, J.S., GUNTER, T.E., GUNTER, K.K. & RUSSELL, P.R. (1976). Evidence for more than one Ca^{2+} transport mechanism in mitochondria. *Biochemistry* **15**, 3834-3842.

PUTNEY, J.W. (1986). A model for receptor-regulated calcium entry. *Cell Calcium* **7**, 1-12.

PUTNEY, J.W. & BIRD, G.S. (1993). The signal for capacitative calcium entry. *Cell* **75**, 199-201.

PUTNEY, J.W. (1997). Type 3 inositol 1,4,5-trisphosphate receptor and capacitative calcium entry. *Cell Calcium* **21**, 257-261.

PUTNEY, J.W. & McKAY, R.R. (1999). Capacitative calcium entry channels. *Bioessays* **21**, 38-46.

PUTNEY, J.W. (1999a). "Kissin' cousins": intimate plasma membrane-ER interactions underlie capacitative calcium entry. *Cell* **99**, 5-8.

PUTNEY, J.W. (1999b). TRP, inositol 1,4,5-trisphosphate receptors, and capacitative calcium entry. *Proc. Natl. Acad. Sci. U.S.A* **96**, 14669-14671.

RAE, J., COOPER, K., GATES, P. & WATSKY, M. (1991). Low access resistance perforated patch recordings using amphotericin B. *J. Neurosci Methods* **37**, 15-26.

REED, K.C. & BYGRAVE, F.L. (1974a). A low molecular weight ruthenium complex inhibitory to mitochondrial Ca^{2+} transport. *FEBS Lett.* **46**, 109-114.

REED, K.C. & BYGRAVE, F.L. (1974b). The inhibition of mitochondrial calcium transport by lanthanides and ruthenium red. *Biochem. J.* **140**, 143-155.

REEVES, J.P. & SUTKO, J.L. (1983). Competitive interactions of sodium and calcium with the sodium-calcium exchange system of cardiac sarcolemmal vesicles. *J. Biol. Chem.* **258**, 3178-3182.

REEVES, J.P. & HALE, C.C. (1984). The stoichiometry of the cardiac sodium-calcium exchange system. *J. Biol.Chem.* **259**, 7733-7739.

REGAN, L.J., SAH, D.W. & BEAN, B.P. (1991). Ca^{2+} channels in rat central and peripheral neurons: high- threshold current resistant to dihydropyridine blockers and omega- conotoxin. *Neuron* **6**, 269-280.

REGEHR, W.G. & TANK, D.W. (1994). Dendritic calcium dynamics. *Curr. Opin. Neurobiol.* **4**, 373-382.

REGEHR, W.G. & ATLURI, P.P. (1995). Calcium transients in cerebellar granule cell presynaptic terminals. *Biophys. J.* **68**, 2156-2170.

REILANDER, H., ACHILLES, A., FRIEDEL, U., MAUL, G., LOTTSPEICH, F. & COOK, N.J. (1992). Primary structure and functional expression of the $Na^+/Ca^{2+},K^+$-exchanger from bovine rod photoreceptors. *EMBO J.* **11**, 1689-1695.

REUTER, H. & SEITZ, N. (1968). The dependence of calcium efflux from cardiac muscle on temperature and external ion composition. *J. Physiol. Lond.* **195**, 451-470.

REUTER, H. & PORZIG, H. (1995). Localization and functional significance of the Na^+/Ca^{2+}-exchanger in presynaptic boutons of hippocampal cells in culture. *Neuron* **15**, 1077-1084.

REYES, M. & STANTON, P.K. (1996). Induction of hippocampal long-term depression requires release of Ca^{2+} from separate presynaptic and postsynaptic intracellular stores. *J. Neurosci.* **16**, 5951-5960.

RICHMAN, P.G. & KLEE, C.B. (1978). Interaction of 125I-labeled Ca^{2+}-dependent regulator protein with cyclic nucleotide phosphodiesterase and its inhibitory protein. *J. Biol. Chem.* **253**, 6323-6326.

RINK, T.J., TSIEN, R.Y. & POZZAN, T. (1982). Cytoplasmic pH and free Mg^{2+} in lymphocytes. *J. Cell Biol.* **95**, 189-196.

RIOS, E. & PIZARRO, G. (1991). Voltage sensor of excitation-contraction coupling in skeletal muscle. *Physiol. Rev.* **71**, 849-908.

RIOS, E., PIZARRO, G. & STEFANI, E. (1992). Charge movement and the nature of signal transduction in skeletal muscle excitation-contraction coupling. *Annu. Rev. Physiol.* **54**, 109-133.

RIZZUTO, R., SIMPSON, A.W., BRINI, M. & POZZAN, T. (1992). Rapid changes of mitochondrial Ca^{2+} revealed by specifically targeted recombinant aequorin. *Nature* **358**, 325-327.

RIZZUTO, R., BRINI, M., MURGIA, M. & POZZAN, T. (1993). Microdomains with high Ca^{2+} close to IP3-sensitive channels that are sensed by neighboring mitochondria. *Science* **262**, 744-747.

RIZZUTO, R., BRINI, M. & POZZAN, T. (1994). Targeting recombinant aequorin to specific intracellular organelles. *Methods Cell Biol.* **40**, 339-358.

RIZZUTO, R., PINTON, P., CARRINGTON, W., FAY, F.S., FOGARTY, K.E., LIFSHITZ, L.M., TUFT, R.A. & POZZAN, T. (1998). Close contacts with the endoplasmic reticulum as determinants of mitochondrial Ca^{2+} responses. *Science* **280**, 1763-1766.

RIZZUTO, R., PINTON, P., BRINI, M., CHIESA, A., FILIPPIN, L. & POZZAN, T. (1999). Mitochondria as biosensors of calcium microdomains. *Cell Calcium* **26**, 193-199.

ROBB-GASPERS, L.D., BURNETT, P., RUTTER, G.A., DENTON, R.M., RIZZUTO, R. & THOMAS, A.P. (1998). Integrating cytosolic calcium signals into mitochondrial metabolic responses. *EMBO J.* **17**, 4987-5000.

RODERICK, H.L., LECHLEITER, J.D. & CAMACHO, P. (2000). Cytosolic phosphorylation of calnexin controls intracellular Ca^{2+} oscillations via an interaction with SERCA2b. *J. Cell Biol.* **149**, 1235-1248.

ROGERS, M. & DANI, J.A. (1995). Comparison of quantitative calcium flux through NMDA, ATP, and ACh receptor channels. *Biophys. J.* **68**, 501-506.

ROGERS, M., COLQUHOUN, L.M., PATRICK, J.W. & DANI, J.A. (1997). Calcium flux through predominantly independent purinergic ATP and nicotinic acetylcholine receptors. *J. Neurophysiol.* **77**, 1407-1417.

ROMERO, P.J. & ORTIZ, C.E. (1988). Electrogenic behavior of the human red cell Ca^{2+} pump revealed by disulfonic stilbenes. *J. Membr. Biol.* **101**, 237-246.

ROM-GLAS, A., SANDLER, C., KIRSCHFELD, K. & MINKE, B. (1992). The nss mutation or lanthanum inhibits light-induced Ca^{2+} influx into fly photoreceptors. *J. Gen. Physiol.* **100**, 767-781.

RONNER, P., GAZZOTTI, P. & CARAFOLI, E. (1977). A lipid requirement for the (Ca^{2+}-Mg^{2+})-activated ATPase of erythrocyte membranes. *Arch. Biochem. Biophys.* **179**, 578-583.

RORSMAN, P., AMMALA, C., BERGGREN, P.O., BOKVIST, K. & LARSSON, O. (1992). Cytoplasmic calcium transients due to single action potentials and voltage-clamp depolarizations in mouse pancreatic B-cells. *EMBO J.* **11**, 2877-2884.

ROSSI, J.P. & SCHATZMANN, H.J. (1982). Is the red cell calcium pump electrogenic? *J. Physiol. Lond.* **327**, 1-15.

ROUSSEAU, E., SMITH, J.S. & MEISSNER, G. (1987). Ryanodine modifies conductance and gating behavior of single Ca^{2+} release channel. *Am. J. Physiol.* **253**, C364-C368

RUTTER, G.A. & RIZZUTO, R. (2000). Regulation of mitochondrial metabolism by ER Ca^{2+} release: an intimate connection. *Trends. Biochem. Sci.* **25**, 215-221.

SACKETT, D.L. & KOSK-KOSICKA, D. (1996). The active species of plasma membrane Ca^{2+}-ATPase are a dimer and a monomer-calmodulin complex. *J. Biol. Chem.* **271**, 9987-9991.

SADOSHIMA, J. & AKAIKE, N. (1991). Kinetic properties of the caffeine-induced transient outward current in bull-frog sympathetic neurones. *J. Physiol. Lond.* **433**, 341-355.

SAH, P. (1996). Ca^{2+}-activated K^+ currents in neurones: types, physiological roles and modulation. *Trends. Neurosci.* **19**, 150-154.

SAH, P. & BEKKERS, J.M. (1996). Apical dendritic location of slow afterhyperpolarization current in hippocampal pyramidal neurons: implications for the integration of long-term potentiation. *J. Neurosci.* **16**, 4537-4542.

SALAMINO, F., SPARATORE, B., MELLONI, E., MICHETTI, M., VIOTTI, P.L., PONTREMOLI, S. & CARAFOLI, E. (1994). The plasma membrane calcium pump is the preferred calpain substrate within the erythrocyte. *Cell Calcium* **15**, 28-35.

SALVADOR, J.M., INESI, G., RIGAUD, J.L. & MATA, A.M. (1998). Ca^{2+} transport by reconstituted synaptosomal ATPase is associated with H^+ countertransport and net charge displacement. *J. Biol. Chem.* **273**, 18230-18234.

SANCHEZ-VIVES, M.V. & GALLEGO, R. (1993). Effects of axotomy or target atrophy on membrane properties of rat sympathetic ganglion cells. *J. Physiol* **471**, 801-815.

SANCHEZ-VIVES, M.V. & GALLEGO, R. (1994a). Calcium-dependent chloride current induced by axotomy in rat sympathetic neurons. *J. Physiol* **475**, 391-400.

SANCHEZ-VIVES, M.V., VALDEOLMILLOS, M., MARTINEZ, S. & GALLEGO, R. (1994b). Axotomy-induced changes in Ca^{2+} homeostasis in rat sympathetic ganglion cells. *Eur. J. Neurosci.* **6**, 9-17.

SARIS, N.E. (1987). Non-respiring rat liver mitochondria do not have a $Ca^{2+}/2H^+$ antiporter. *Acta Chem. Scand. B.* **41**, 79-82.

SARKADI, B., ALIFIMOFF, J.K., GUNN, R.B. & TOSTESON, D.C. (1978). Kinetics and stoichiometry of Na-dependent Li transport in human red blood cells. *J. Gen. Physiol.* **72**, 249-265.

SCHATZMANN, H.J. (1966). ATP-dependent Ca^{2+}-extrusion from human red cells. *Experientia* **22**, 364-365.

SCHATZMANN, H.J. & VINCENZI, F.F. (1969). Calcium movements across the membrane of human red cells. *J. Physiol. Lond.* **201**, 369-395.

SCHATZMANN, H.J. (1982). The plasma membrane calcium pump of erythrocytes and other animal cells. In *Membrane transport of calcium*, ed. CARAFOLI, E., pp. 41-108. New York: Academic Press.

SCHNETKAMP, P.P., BASU, D.K. & SZERENCSEI, R.T. (1989). Na^+-Ca^{2+} exchange in bovine rod outer segments requires and transports K^+. *Am. J. Physiol.* **257**, C153-C157

SCHWARZ, E.M. & BENZER, S. (1997). Calx, a Na^+/Ca^{2+} exchanger gene of Drosophila melanogaster. *Proc. Natl. Acad. Sci. U S A* **94**, 10249-10254.

SCHWIENING, C.J., KENNEDY, H.J. & THOMAS, R.C. (1993). Calcium-hydrogen exchange by plasma membrane Ca^{2+}-ATPase of voltage-clamped snail neurons. *Proceeding of the Royal Society, London* **253**, 285-289.

SCOTT, R.H., PEARSON, H.A. & DOLPHIN, A.C. (1991). Aspects of vertebrate neuronal voltage-activated calcium currents and their regulation. *Prog. Neurobiol.* **36**, 485-520.

SEGAL, M. & MANOR, D. (1992). Confocal microscopic imaging of $[Ca^{2+}]_i$ in cultured rat hippocampal neurons following exposure to N-methyl-D-aspartate. *J. Physiol. Lond.* **448**, 655-676.

SELYANKO, A.A. (1996). Single apamin-sensitive, small-conductance calcium-activated potassium channels (SKCa) in membranes patches from rat sympathetic neurones. *J. Physiol. Lond.***494P**, 52P

SELYANKO, A.A. & BROWN, D.A. (1996). Intracellular calcium directly inhibits potassium M channels in excised membrane patches from rat sympathetic neurons. *Neuron* **16**, 151-162.

SEYMOUR-LAURENT, K.J. & BARISH, M.E. (1995). Inositol 1,4,5-trisphosphate and ryanodine receptor distributions and patterns of acetylcholine- and caffeine-induced calcium release in cultured mouse hippocampal neurons. *J. Neurosci.* **15**, 2592-2608.

SHIGEKAWA, M. & IWAMOTO, T. (2001). Cardiac Na^+/Ca^{2+} exchange: molecular and pharmacological aspects. *Circ. Res.* **88**, 864-876.

SHMIGOL, A., KIRISCHUK, S., KOSTYUK, P. & VERKHRATSKY, A. (1994a). Different properties of caffeine-sensitive Ca^{2+} stores in peripheral and central mammalian neurones. *Pflugers Arch.* **426**, 174-176.

SHMIGOL, A., KOSTYUK, P. & VERKHRATSKY, A. (1994b). Role of caffeine-sensitive Ca^{2+} stores in Ca^{2+} signal termination in adult mouse DRG neurones. *Neuroreport.* **5**, 2073-2076.

SHMIGOL, A., VERKHRATSKY, A. & ISENBERG, G. (1995). Calcium-induced calcium release in rat sensory neurons. *J. Physiol. Lond.* **489**, 627-636.

SHULL, G.E. & GREEB, J. (1988). Molecular cloning of two isoforms of the plasma membrane Ca^{2+}-transporting ATPase from rat brain. Structural and functional domains exhibit similarity to Na^+/K^+- and other cation transport ATPases. *J. Biol. Chem.* **263**, 8646-8657.

SIMMERMAN, H.K., COLLINS, J.H., THEIBERT, J.L., WEGENER, A.D. & JONES, L.R. (1986). Sequence analysis of phospholamban. Identification of phosphorylation sites and two major structural domains. *J. Biol. Chem.* **261**, 13333-13341.

SITSAPESAN, R. & WILLIAMS, A.J. (1990). Mechanisms of caffeine activation of single calcium-release channels of sheep cardiac sarcoplasmic reticulum. *J. Physiol. Lond.* **423**, 425-439.

SITSAPESAN, R., McGARRY, S.J. & WILLIAMS, A.J. (1995a). Cyclic ADP-ribose, the ryanodine receptor and Ca^{2+} release. *Trends. Pharmacol. Sci.* **16**, 386-391.

SITSAPESAN, R. & WILLIAMS, A.J. (1995b). Cyclic ADP-ribose and related compounds activate sheep skeletal sarcoplasmic reticulum Ca^{2+} release channel. *Am. J. Physiol.* **268**, C1235-C1240

SITSAPESAN, R. & WILLIAMS, A.J. (1997). Regulation of current flow through ryanodine receptors by luminal Ca^{2+}. *J. Membr. Biol.* **159**, 179-185.

SITSAPESAN, R. & WILLIAMS, A.J. (2000). Do inactivation mechanisms rather than adaptation hold the key to understanding ryanodine receptor channel gating? *J. Gen. Physiol.* **116**, 867-872.

SIVILOTTI, L.G., McNEIL, D.K., LEWIS, T.M., NASSAR, M.A., SCHOEPFER, R. & COLQUHOUN, D. (1997). Recombinant nicotinic receptors, expressed in Xenopus oocytes, do not resemble native rat sympathetic ganglion receptors in single-channel behaviour. *J. Physiol. Lond.* **500(1)**, 123-138.

SLOVITER, R.S. (1989). Calcium-binding protein (calbindin-D28k) and parvalbumin immunocytochemistry: localization in the rat hippocampus with specific reference to the selective vulnerability of hippocampal neurons to seizure activity. *J. Comp. Neurol.* **280**, 183-196.

SMALLWOOD, J.I., WAISMAN, D.M., LAFRENIERE, D. & RASMUSSEN, H. (1983). Evidence that the erythrocyte calcium pump catalyzes a Ca^{2+}:nH^+ exchange. *J. Biol. Chem.* **258**, 11092-11097.

SMART, T.G. (1987). Single calcium-activated potassium channels recorded from cultured rat sympathetic neurones. *J. Physiol. Lond.* **389**, 337-360.

SMITH, A.B. & CUNNANE, T.C. (1996). Ryanodine-sensitive calcium stores involved in neurotransmitter release from sympathetic nerve terminals of the guinea-pig. *J. Physiol. Lond.* **497(3)**, 657-664.

SNUTCH, T.P. & REINER, P.B. (1992). Ca^{2+} channels: diversity of form and function. *Curr. Opin. Neurobiol.* **2**, 247-253.

SORIMACHI, M. (1993). Caffeine- and muscarinic receptor agonist-sensitive Ca^{2+} stores in chick ciliary ganglion cells. *Brain Res.* **627**, 34-40.

SORRENTINO, V. & VOLPE, P. (1993). Ryanodine receptors: how many, where and why? *Trends. Pharmacol. Sci.* **14**, 98-103.

SOTTOCASA, G., SANDRI, G., PANFILI, E., DE-BERNARD, B., GAZZOTTI, P., VASINGTON, F.D. & CARAFOLI, E. (1972). Isolation of a soluble Ca^{2+} binding glycoprotein from ox liver mitochondria. *Biochem. Biophys. Res. Commun.* **47**, 808-813.

STAUFFER, T.P., HILFIKER, H., CARAFOLI, E. & STREHLER, E.E. (1993). Quantitative analysis of alternative splicing options of human plasma membrane calcium pump genes [published erratum appears in J Biol Chem 1994 Dec 16;269(50):32022]. *J. Biol. Chem.* **268**, 25993-26003.

STAUFFER, T.P., GUERINI, D. & CARAFOLI, E. (1995). Tissue distribution of the four gene products of the plasma membrane Ca^{2+} pump. A study using specific antibodies. *J. Biol. Chem.* **270**, 12184-12190.

STAUFFER, T.P., GUERINI, D., CELIO, M.R. & CARAFOLI, E. (1997). Immunolocalization of the plasma membrane Ca^{2+}-pump isoforms in the rat brain. *Brain Res.* **748**, 21-29.

STEIN, P. & PALADE, P. (1988). Sarcoballs: direct access to sarcoplasmic reticulum Ca^{2+}-channels in skinned frog muscle fibers. *Biophys. J.* **54**, 357-363.

STREHLER, E.E., STREHLER, P.M., VOGEL, G. & CARAFOLI, E. (1989). mRNAs for plasma membrane calcium pump isoforms differing in their regulatory domain are generated by alternative splicing that involves two internal donor sites in a single exon. *Proc. Natl. Acad. Sci. U.S.A.* **86**, 6908-6912.

STREHLER, E.E., JAMES, P., FISCHER, R., HEIM, R., VORHERR, T., FILOTEO, A.G., PENNISTON, J.T. & CARAFOLI, E. (1990). Peptide sequence analysis and molecular cloning reveal two calcium pump isoforms in the human erythrocyte membrane. *J. Biol. Chem.* **265**, 2835-2842.

STREHLER, E.E., HEIM, R. & CARAFOLI, E. (1991). Molecular characterization of plasma membrane calcium pump isoforms. *Adv. Exp. Med. Biol.* **307**, 251-261.

STUENKEL, E.L. (1994). Regulation of intracellular calcium and calcium buffering properties of rat isolated neurohypophysial nerve endings. *J. Physiol. Lond.* **481(1)**, 251-271.

SUKO, J., HELLMANN, G. & DROBNY, H. (2000). Modulation of the calmodulin-induced inhibition of sarcoplasmic reticulum calcium release channel (ryanodine receptor) by sulfhydryl oxidation in single channel current recordings and [(3)H]ryanodine binding. *J. Membr. Biol.* **174**, 105-120.

TAGLIALATELA, M., DI-RENZO, G. & ANNUNZIATO, L. (1990a). Na^{+}/Ca^{2+} exchange activity in central nerve endings. I. Ionic conditions that discriminate $^{45}Ca^{2+}$ uptake through the exchanger from that occurring through voltage-operated Ca^{2+} channels. *Mol. Pharmacol.* **38**, 385-392.

TAGLIALATELA, M., CANZONIERO, L.M., CRAGOE, E.J., DI-RENZO, G. & ANNUNZIATO, L. (1990b). Na^{+}/Ca^{2+} exchange activity in central nerve endings. II. Relationship between pharmacological blockade by amiloride analogues and dopamine release from tuberoinfundibular hypothalamic neurons. *Mol. Pharmacol.* **38**, 393-400.

TAKASAWA, S., NATA, K., YONEKURA, H. & OKAMOTO, H. (1993). Cyclic ADP-ribose in insulin secretion from pancreatic beta cells. *Science* **259**, 370-373.

TAKESHIMA, H., NISHIMURA, S., MATSUMOTO, T., ISHIDA, H., KANGAWA, K., MINAMINO, N., MATSUO, H., UEDA, M., HANAOKA, M., HIROSE, T. & ET, A. (1989). Primary structure and expression from complementary DNA of skeletal muscle ryanodine receptor. *Nature* **339**, 439-445.

TANG, Y. & ZUCKER, R.S. (1997). Mitochondrial involvement in post-tetanic potentiation of synaptic transmission. *Neuron* **18**, 483-491.

TATSUMI, H. & KATAYAMA, Y. (1993). Regulation of the intracellular free calcium concentration in acutely dissociated neurones from rat nucleus basalis. *J. Physiol. Lond.* **464**, 165-181.

TAYLOR, C.W. & MARSHALL, I.C. (1992). Calcium and inositol 1,4,5-trisphosphate receptors: a complex relationship. *Trends. Biochem. Sci.* **17**, 403-407.

TAYLOR, C.W. (1998). Inositol trisphosphate receptors: Ca^{2+}-modulated intracellular Ca^{2+} channels. *Biochim. Biophys. Acta* **1436**, 19-33.

TAYLOR, C.W. & BROAD, L.M. (1998). Pharmacological analysis of intracellular Ca^{2+} signalling: problems and pitfalls. *Trends. Pharmacol. Sci.* **19**, 370-375.

TEPIKIN, A.V., KOSTYUK, P.G., SNITSAREV, V.A. & BELAN, P.V. (1991). Extrusion of calcium from a single isolated neuron of the snail Helix pomatia. *J. Membr. Biol.* **123**, 43-47.

TEPIKIN, A.V. & PETERSEN, O.H. (1992). Mechanisms of cellular calcium oscillations in secretory cells. *Biochim. Biophys. Acta* **1137**, 197-207.

THATCHER, D.R. & PECHERE, J.F. (1977). The amino-acid sequence of the major parvalbumin from thornback-ray muscle. *Eur. J. Biochem.* **75**, 121-132.

THAYER, S.A. & MILLER, R.J. (1990). Regulation of the intracellular free calcium concentration in single rat dorsal root ganglion neurones in vitro. *J. Physiol. Lond.* **425**, 85-115.

THAYER, S.A., HIRNING, L.D. & MILLER, R.J. (1988). The role of caffeine-sensitive calcium stores in the regulation of the intracellular free calcium concentration in rat sympathetic neurons in vitro. *Mol. Pharmacol.* **34**, 664-673.

TOKIMASA, T., CHERUBINI, E. & NORTH, R.A. (1983). Nicotinic depolarization activates calcium dependent gK in myenteric neurons. *Brain Res.* **263**, 57-62.

TOKIMASA, T. & NORTH, R.A. (1984). Calcium entry through acetylcholine-channels can activate potassium conductance in bullfrog sympathetic neurons. *Brain Res.* **295**, 364-367.

TOUTENHOOFD, S.L. & STREHLER, E.E. (2000). The calmodulin multigene family as a unique case of genetic redundancy: multiple levels of regulation to provide spatial and temporal control of calmodulin pools? *Cell Calcium* **28**, 83-96.

TOYOFUKU, T., KURZYDLOWSKI, K., TADA, M. & MACLENNAN, D.H. (1993). Identification of regions in the Ca^{2+}-ATPase of sarcoplasmic reticulum that affect functional association with phospholamban. *J. Biol. Chem.* **268**, 2809-2815.

TOYOSHIMA, C., NAKASAKO, M., NOMURA, H. & OGAWA, H. (2000). Crystal structure of the calcium pump of sarcoplasmic reticulum at 2.6 A resolution. *Nature* **405**, 647-655.

TRAPP, S., LUCKERMANN, M., KAILA, K. & BALLANYI, K. (1996). Acidosis of hippocampal neurones mediated by a plasmalemmal Ca^{2+}/H^{+} pump. *Neuroreport.* **7**, 2000-2004.

TREIMAN, M., CASPERSEN, C. & CHRISTENSEN, S.B. (1998). A tool coming of age: thapsigargin as an inhibitor of sarco-endoplasmic reticulum Ca^{2+}-ATPases. *Trends. Pharmacol. Sci.* **19** , 131-135.

TROUSLARD, J., MARSH, S.J. & BROWN, D.A. (1993). Calcium entry through nicotinic receptor channels and calcium channels in cultured rat superior cervical ganglion cells. *J. Physiol. Lond.* **468**, 53-71.

TSE, A., TSE, F.W. & HILLE, B. (1994). Calcium homeostasis in identified rat gonadotrophs. *J. Physiol. Lond.* **477**, 511-525.

TSIEN, R.W., HESS, P., McCLESKEY, E.W. & ROSENBERG, R.L. (1987). Calcium channels: mechanisms of selectivity, permeation, and block. *Annu. Rev. Biophys. Biophys.Chem.* **16**, -1990

TSIEN, R.W. & TSIEN, R.Y. (1990). Calcium channels, stores, and oscillations. *Annu. Rev. Cell Biol.* **6**, 715-760.

TSIEN, R.W., ELLINOR, P.T. & HORNE, W.A. (1991). Molecular diversity of voltage-dependent Ca^{2+} channels. *Trends. Pharmacol. Sci.* **12**, 349-354.

TSOI, M., RHEE, K.H., BUNGARD, D., LI, X.F., LEE, S.L., AUER, R.N. & LYTTON, J. (1998). Molecular cloning of a novel potassium-dependent sodium-calcium exchanger from rat brain. *J. Biol. Chem.* **273**, 4155-4162.

TURNER, T.J. & GOLDIN, S.M. (1985). Calcium channels in rat brain synaptosomes: identification and pharmacological characterization. High affinity blockade by organic Ca^{2+} channel blockers. *J. Neurosci.* **5**, 841-849.

USACHEV, Y., SHMIGOL, A., PRONCHUK, N., KOSTYUK, P. & VERKHRATSKY, A. (1993). Caffeine-induced calcium release from internal stores in cultured rat sensory neurons. *Neuroscience* **57**, 845-859.

USACHEV, Y.M. & THAYER, S.A. (1997). All-or-none Ca^{2+} release from intracellular stores triggered by Ca^{2+} influx through voltage-gated Ca^{2+} channels in rat sensory neurons. *J. Neurosci.* **17**, 7404-7414.

USACHEV, Y.M. & THAYER, S.A. (1999a). Controlling the urge for a Ca^{2+} surge: all-or-none Ca^{2+} release in neurons. *Bioessays* **21**, 743-750.

USACHEV, Y.M. & THAYER, S.A. (1999b). Ca^{2+} influx in resting rat sensory neurones that regulates and is regulated by ryanodine-sensitive Ca^{2+} stores. *J. Physiol. Lond.* **519(1),** 115-130.

USACHEV, Y.M., TOUTENHOOFD, S.L., GOELLNER, G.M., STREHLER, E.E. & THAYER, S.A. (2001). Differentiation induces up-regulation of plasma membrane Ca^{2+}-ATPase and concomitant increase in Ca^{2+} efflux in human neuroblastoma cell line IMR-32. *J. Neurochem.* **76** , 1756-1765.

VACA, L. & KUNZE, D.L. (1994). Depletion of intracellular Ca^{2+} stores activates a Ca^{2+}-selective channel in vascular endothelium. *Am. J. Physiol.* **267**, C920-C925

VALDIVIA, H.H., KAPLAN, J.H., ELLIS-DAVIES, G.C. & LEDERER, W.J. (1995). Rapid adaptation of cardiac ryanodine receptors: modulation by Mg^{2+} and phosphorylation. *Science* **267**, 1997-2000.

VAN ROSSUM, D.B. (1998). Modulation of the cytoskeletal architecture by calcium. In *Integrative aspects of calcium signaling* , eds. VERKHRATSKY, A. & TOESCU, E.C., pp. 177-196. New York: Plenum Press.

VANSELOW, B.K. & KELLER, B.U. (2000). Calcium dynamics and buffering in oculomotor neurones from mouse that are particularly resistant during amyotrophic lateral sclerosis (ALS)-related motoneurone disease. *J. Physiol. Lond.* **525(2),** 433-445.

VERKHRATSKY, A. & SHMIGOL, A. (1996). Calcium-induced calcium release in neurones. *Cell Calcium* **19**, 1-14.

VERKHRATSKY, A. & TOESCU, E.C. (1998). Principles of calcium signaling. In *Integrative aspects of calcium signaling*, eds. VERKHRATSKY, A. & TOESCU, E.C., pp. 1-19. New York: Plenum Press.

VERMA, A.K., FILOTEO, A.G., STANFORD, D.R., WIEBEN, E.D., PENNISTON, J.T., STREHLER, E.E., FISCHER, R., HEIM, R., VOGEL, G., MATHEWS, S. & ET, A. (1988). Complete primary structure of a human plasma membrane Ca^{2+} pump. *J. Biol. Chem.* **263**, 14152-14159.

VERNALLIS, A.B., CONROY, W.G. & BERG, D.K. (1993). Neurons assemble acetylcholine receptors with as many as three kinds of subunits while maintaining subunit segregation among receptor subtypes. *Neuron* **10**, 451-464.

VILLA, A., PODINI, P., PANZERI, M.C., RACCHETTI, G. & MELDOLESI, J. (1994). Cytosolic Ca^{2+} binding proteins during rat brain ageing: loss of calbindin and calretinin in the hippocampus, with no change in the cerebellum. *Eur. J. Neurosci.* **6**, 1491-1499.

VORHERR, T., KESSLER, T., HOFMANN, F. & CARAFOLI, E. (1991). The calmodulin-binding domain mediates the self-association of the plasma membrane Ca^{2+} pump. *J. Biol. Chem.* **266**, 22-27.

WAISMAN, D.M., GIMBLE, J.M., GOODMAN, D.B. & RASMUSSEN, H. (1981a). Studies of the Ca^{2+} transport mechanism of human erythrocyte inside-out plasma membrane vesicles. I. Regulation of the Ca^{2+} pump by calmodulin. *J. Biol. Chem.* **256**, 409-414.

WAISMAN, D.M., GIMBLE, J.M., GOODMAN, D.B. & RASMUSSEN, H. (1981b). Studies of the Ca^{2+} transport mechanism of human erythrocyte inside-out plasma membrane vesicles. II. Stimulation of the Ca^{2+} pump by phosphate. *J. Biol. Chem.* **256**, 415-419.

WAISMAN, D.M., GIMBLE, J.M., GOODMAN, D.B. & RASMUSSEN, H. (1981c). Studies of the Ca^{2+} transport mechanism of human erythrocyte inside-out plasma membrane vesicles. III. Stimulation of the Ca^{2+} pump by anions. *J. Biol. Chem.* **256**, 420-424.

WANG, K.K., ROUFOGALIS, B.D. & VILLALOBO, A. (1988). Further characterization of calpain-mediated proteolysis of the human erythrocyte plasma membrane Ca^{2+}-ATPase. *Arch. Biochem. Biophys* **267**, 317-327.

WANG, K.K., DU, Y.S., DIGLIO, C., TSANG, W. & KUO, T.H. (1991). Hormone-induced phosphorylation of the plasma membrane calcium pump in cultured aortic endothelial cells. *Arch. Biochem. Biophys.* **289**, 103-108.

WANG, Y., ROWAN, M.J. & ANWYL, R. (1997). Induction of LTD in the dentate gyrus in vitro is NMDA receptor independent, but dependent on Ca^{2+} influx via low-voltage-activated Ca^{2+} channels and release of Ca^{2+} from intracellular stores. *J. Neurophysiol.* **77**, 812-825.

WANG, H.J., GUAY, G., POGAN, L., SAUVE, R. & NABI, I.R. (2000). Calcium regulates the association between mitochondria and a smooth subdomain of the endoplasmic reticulum. *J. Cell Biol.* **150**, 1489-1498.

WEGENER, A.D., SIMMERMAN, H.K., LINDEMANN, J.P. & JONES, L.R. (1989). Phospholamban phosphorylation in intact ventricles. Phosphorylation of serine 16 and threonine 17 in response to beta-adrenergic stimulation. *J. Biol. Chem.* **264**, 11468-11474.

WERTH, J.L. & THAYER, S.A. (1994). Mitochondria buffer physiological calcium loads in cultured rat dorsal root ganglion neurons. *J. Neurosci.* **14**, 348-356.

WESTBROOK, G.L. & MAYER, M.L. (1984). Glutamate currents in mammalian spinal neurons: resolution of a paradox. *Brain Res.* **301**, 375-379.

WHITE, A.M., WATSON, S.P. & GALIONE, A. (1993). Cyclic ADP-ribose-induced Ca^{2+} release from rat brain microsomes. *FEBS Lett.* **318**, 259-263.

WHITE, R.J. & REYNOLDS, I.J. (1997). Mitochondria accumulate Ca^{2+} following intense glutamate stimulation of cultured rat forebrain neurones. *J. Physiol. Lond.* **498(1)**, 31-47.

WICTOME, M., MICHELANGELI, F., LEE, A.G. & EAST, J.M. (1992). The inhibitors thapsigargin and 2,5-di(tert-butyl)-1,4-benzohydroquinone favour the E2 form of the (Ca^{2+}-Mg^{2+})-ATPase. *FEBS Lett.* **304**, 109-113.

WIER, W.G. (1990). Cytoplasmic [Ca^{2+}] in mammalian ventricle: dynamic control by cellular processes. *Annu. Rev. Physiol.* **52**, 467-485.

WILLIAMS, D.A. & FAY, F.S. (1990). Intracellular calibration of the fluorescent calcium indicator Fura-2. *Cell Calcium* **11**, 75-83.

WILLIAMS, M.E., BRUST, P.F., FELDMAN, D.H., PATTHI, S., SIMERSON, S., MAROUFI, A., McCUE, A.F., VELICELEBI, G., ELLIS, S.B. & HARPOLD, M.M. (1992). Structure and functional expression of an omega-conotoxin- sensitive human N-type calcium channel. *Science* **257**, 389-395.

WILLOUGHBY, D., THOMAS, R. & SCHWIENING, C. (2001). The effects of intracellular pH changes on resting cytosolic calcium in voltage-clamped snail neurones. *J. Physiol. Lond.* **530**, 405-416.

WISDEN, W. & SEEBURG, P.H. (1993). Mammalian ionotropic glutamate receptors. *Curr. Opin. Neurobiol.* **3**, 291-298.

WOMACK, M.D., WALKER, J.W. & KHODAKHAH, K. (2000). Impaired calcium release in cerebellar Purkinje neurons maintained in culture. *J. Gen. Physiol.* **115**, 339-346.

XU, W., WILSON, B.J., HUANG, L., PARKINSON, E.L., HILL, B.J. & MILANICK, M.A. (2000). Probing the extracellular release site of the plasma membrane calcium pump. *Am. J. Physiol.* **278**, C965-C972

YAMAGUCHI, N., XIN, C. & MEISSNER, G. (2001). Identification of apocalmodulin and Ca^{2+}-calmodulin regulatory domain in skeletal muscle Ca^{2+} release channel, ryanodine receptor. *J. Biol. Chem.* **276**, 22579-22585.

YAMOAH, E.N., LUMPKIN, E.A., DUMONT, R.A., SMITH, P.J., HUDSPETH, A.J. & GILLESPIE, P.G. (1998). Plasma membrane Ca^{2+}-ATPase extrudes Ca^{2+} from hair cell stereocilia. *J. Neurosci.* **18**, 610-624.

YOSHIDA, S., SENBA, E., KUBOTA, Y., HAGIHIRA, S., YOSHIYA, I., EMSON, P.C. & TOHYAMA, M. (1990). Calcium-binding proteins calbindin and parvalbumin in the superficial dorsal horn of the rat spinal cord. *Neuroscience* **37**, 839-848.

YU, X., HAO, L. & INESI, G. (1994). A pK change of acidic residues contributes to cation countertransport in the Ca^{2+}-ATPase of sarcoplasmic reticulum. Role of H^+ in Ca^{2+}-ATPase countertransport. *J. Biol. Chem.* **269**, 16656-16661.

YUE, L., PENG, J.B., HEDIGER, M.A. & CLAPHAM, D.E. (2001). CaT1 manifests the pore properties of the calcium-release-activated calcium channel. *Nature* **410**, 705-709.

ZHOU, Z. & NEHER, E. (1993). Mobile and immobile calcium buffers in bovine adrenal chromaffin cells. *J. Physiol. Lond.* **469**, 245-273.

ZHOU, Z., MATLIB, M.A. & BERS, D.M. (1998). Cytosolic and mitochondrial Ca^{2+} signals in patch clamped mammalian ventricular myocytes. *J. Physiol. Lond.* **507(2)**, 379-403.

ZOCCARATO, F. & NICHOLLS, D. (1982). The role of phosphate in the regulation of the independent calcium-efflux pathway of liver mitochondria. *Eur. J. Biochem.* **127**, 333-338.

ZORATTI, M. & SZABO, I. (1995). The mitochondrial permeability transition. *Biochim. Biophys. Acta* **1241**, 139-176.

ZORZATO, F., FUJII, J., OTSU, K., PHILLIPS, M., GREEN, N.M., LAI, F.A., MEISSNER, G. & McLENNAN, D.H. (1990). Molecular cloning of cDNA encoding human and rabbit forms of the Ca^{2+} release channel (ryanodine receptor) of skeletal muscle sarcoplasmic reticulum. *J. Biol. Chem.* **265**, 2244-2256.

ZUBOV, A.I., KAZNACHEEVA, E.V., NIKOLAEV, A.V., ALEXEENKO, V.A., KISELYOV, K., MUALLEM, S. & MOZHAYEVA, G.N. (1999). Regulation of the miniature plasma membrane Ca^{2+} channel I(min) by inositol 1,4,5-trisphosphate receptors. *J. Biol. Chem.* **274**, 25983-25985.

ZUCCHI, R. & RONCA-TESTONI, S. (1997). The sarcoplasmic reticulum Ca^{2+} channel/ryanodine receptor: modulation by endogenous effectors, drugs and disease states. *Pharmacol. Rev.* **49(1)**, 1-51.

ZVARITCH, E., JAMES, P., VORHERR, T., FALCHETTO, R., MODYANOV, N. & CARAFOLI, E. (1990). Mapping of functional domains in the plasma membrane Ca^{2+} pump using trypsin proteolysis. *Biochemistry* **29**, 8070-8076.

ZVARITCH, E., VELLANI, F., GUERINI, D. & CARAFOLI, E. (1995). A signal for endoplasmic reticulum retention located at the carboxyl terminus of the plasma membrane Ca^{2+}-ATPase isoform 4CI. *J. Biol.Chem.* **270**, 2679-2688.